



The University of
Nottingham

UNITED KINGDOM · CHINA · MALAYSIA

Faculty of Engineering, Division of Materials,
Mechanics and Structure

**Thermo-physical Properties
and High-temperature Durability
of Reactive Powder Concrete (RPC)**

Masdar Helmi, ST., DEA

Supervisors: Prof Matthew R Hall, Prof Sean P Rigby

Thesis submitted to the University of Nottingham for
the degree of Doctor of Philosophy

December 2015

FOR MY BIG FAMILY
WHO ALWAYS SUPPORT AND PRAY
FOR ME TO STRUGGLE IN THIS LIFE
ESPECIALLY 'ALMARHUMAH MOTHER'

Abstract

The popular use of concrete, particularly in the construction industry, has continually challenged researchers to advance its performance to new levels. Research in this area has led to substantial ideas of reactive powder concrete (RPC) which is developed by controlling three main variables: composition, pressure during setting period, and post-set heat curing. A growing community of research has emerged to define the physical and mechanical properties of RPC, but to date few have focussed on the high temperature behaviour and aging effects after exposure to fire and that influence the durability of concrete.

This research aimed to characterise the thermo-physical properties of RPC and to quantify the microstructural transformation caused by (i) high temperature curing, and (ii) fixed and cyclic high temperature exposure (at 28-day strength). The experimental work mainly used a RPC mixture and involved three defined stages. Firstly, the optimisation of RPC was investigated by analysing the mix composition and measuring the corresponding mechanical properties of RPC with variables such as heating rate, heating duration, and starting time of heating. Secondly, the transformation of microstructural properties was investigated with respect to the pre- and post-treatment conditions and included pore network evolution, elemental composition, and image analysis of the interfacial transition zone (ITZ). Thirdly, the response to high temperature exposure was analysed by focussing on the residual compressive strength and alteration of microstructural properties (after both static and cyclic temperature exposure of varying levels).

The main findings are summarised as follows: (1) heat curing appears to have optimum impact (after casting) at a ramp rate of 50 °C/hr for 48 hours; (2) heat curing treatment induced some effects such as pore filling by tobermorite and xonotlite, with some dehydroxilation of C-S-H gel and Ca (OH)₂; (3) the thermo-physical properties of RPC were all reduced following heat treatment/ exposure due to crack network progression; (4) after elevated temperature exposure, the compressive strength of RPC decreases due to differential shrinkage between the matrix and aggregate phases.

Publications

Parts of this study have been published in both a conference article and a journal article, as follows:

1. M. Helmi, M.R. Hall, S.P. Rigby, Treatment effects on the compressive strength of reactive powder concrete (RPC) at 7 days, In Proceeding of 33rd Cement and Concrete Science Conference, University of Portsmouth UK., 2013, pp. 288-233.
2. M. Helmi, M.R. Hall, L.A. Stevens, S.P. Rigby, Effect of high-pressure / temperature curing on reactive powder concrete microstructure formation, *Construction and Building Materials Journal*. Volume 105, 15 February 2016, Pages 554–562.

Acknowledgment

Firstly I would like to thank to my supervisors Prof Matthew R Hall and Prof Sean P Rigby for their constructive guidance and their full support throughout my study. In this point, I have to mention here that Matthew is the best supervisor that I have ever met in the University of Nottingham. His passion to motivate others and to solve problems during the study were very helpful and became valuable experiences in my life.

I am also grateful to the Government of Indonesia through the Directorate General of Higher Education (DIKTI) for financial support and the University of Nottingham for its welcome and all services to finish my PhD.

Thanks are also due to the Civil Engineering Laboratory technical staff: Mike, Bal, Mark, Gary, Nigel, Jim. In addition thanks to staffs in Wolfson Building: Keith, Martin, Nigel, and Tom for helping in MIP, TGA, SEM, and XRD tests. I would also like to express my sincere thanks to friends: Max, Wisnu, Wahyudin, Peni, Muklason, their family and other Indonesian students in Nottingham.

I also would like to thank to examiners, Dr Christopher Goodier and Dr Nicholas Thom for their acceptance to review my thesis and give valuable suggestions to improve the writing of my thesis.

Lastly, thanks to my big family and those whom I love for your great patience.

Declaration

I declare that the results written in this thesis are my own work conducted at Department of Civil Engineering University of Nottingham between October 2011 and December 2015. No part of this thesis has been submitted for a degree of another university.

December 2015

Masdar Helmi

Contents

1	CHAPTER 1- INTRODUCTION	1
1.1	BACKGROUND	1
1.2	RESEARCH SIGNIFICANCE	2
1.3	AIM AND OBJECTIVES	7
1.4	SCOPE OF STUDY	8
1.5	ANTICIPATED CONTRIBUTIONS	9
2	CHAPTER 2- LITERATURE REVIEW	10
2.1	INTRODUCTION	10
2.2	MATERIAL OF CONCRETE	10
2.2.1	Cement	10
2.2.2	Aggregate	14
2.2.3	Admixtures	16
2.2.4	Pozzolan Materials	17
2.2.5	Fibre	18
2.3	THERMAL PROPERTIES OF CONCRETE	19
2.3.1	Thermal Conductivity	19
2.3.2	Thermal Diffusivity	21
2.3.3	Thermal Expansion Coefficient	22
2.4	REACTIVE POWDER CONCRETE (RPC)	23
2.4.1	Factors Influencing RPC Performance	24
2.4.2	Treatments on RPC	29
2.4.3	Mechanical Properties of RPC	34
2.4.4	RPC Application	39
2.5	DURABILITY OF CONCRETE UNDER HIGH TEMPERATURE EXPOSURE	41
2.5.1	Effect of High Temperature on Mechanical Properties	42
2.5.2	Effect of High Temperature Exposure on Physical and Chemical Properties	46
2.5.3	Effect of High Temperature on Thermo-Physical Properties	47
2.6	MICROSTRUCTURE CHARACTERISATION	49
2.6.1	Microscopy	49
2.6.2	Porosity	50
2.6.3	Thermogravimetry	52
2.6.4	Mineralogy and Chemical Composition	53
2.6.5	Microcracks Progression	56
2.7	INTERFACIAL TRANSITION ZONE (ITZ)	57
2.7.1	Wall effect (porosity)	57
2.7.2	Chemical Composition	59
2.8	SUMMARY	62
3	CHAPTER 3- EXPERIMENTAL PROGRAM	64
3.1	EXPERIMENT METHODS IN BRIEF	64
3.2	MATERIALS	64
3.2.1	Binder	64
3.2.2	Sand	65
3.2.3	Fibre reinforcement	66
3.2.4	Chemical Admixtures	67
3.3	SAMPLE FABRICATION AND EARLY TREATMENTS	67
3.3.1	Composition of RPC Mixture	67
3.3.2	Mixing Process	68
3.3.3	Pressure Treatment	69
3.3.4	Heat Curing Treatment	71
3.4	METHOD OF TESTING	72
3.4.1	Properties in Fresh Mixture	72
3.4.2	Properties in Hardened Condition	74

3.4.3	<i>Microstructure Test</i>	78
3.5	HIGH TEMPERATURE EXPOSURE ON RPC SPECIMENS	86
3.5.1	<i>Fixed Temperature</i>	86
3.5.2	<i>Cyclic Heating and Cooling</i>	88
3.6	SUMMARY.....	90
4	CHAPTER 4- OPTIMISING CONDITIONS AND MECHANICAL PROPERTIES OF RPC	91
4.1	INTRODUCTION	91
4.2	PROPERTIES OF FRESH MIXTURES	92
4.2.1	<i>Setting Time</i>	92
4.2.2	<i>Workability</i>	93
4.3	OPTIMISATION OF CEMENT CURE.....	94
4.3.1	<i>Heating Rate</i>	94
4.3.2	<i>Heating Duration</i>	97
4.3.3	<i>Heating Start Time</i>	98
4.3.4	<i>Significance Analysis</i>	100
4.4	EFFECT OF CONDITION ON PHYSICAL PROPERTIES	101
4.4.1	<i>Compressive Strength</i>	101
4.4.2	<i>Density</i>	104
4.4.3	<i>Correlation between porosity and compressive strength</i>	107
4.4.4	<i>Preliminary Model Proposed</i>	108
4.5	MECHANICAL PROPERTIES OF RPC WITH CARBON FIBRE.....	110
4.5.1	<i>Flexure Strength</i>	111
4.5.2	<i>Toughness and Flexural Modulus</i>	112
4.5.3	<i>Compressive Strength</i>	115
4.5.4	<i>Correlation between Compressive and Flexural Strength</i>	117
4.6	SUMMARY.....	118
5	CHAPTER 5- MICROSTRUCTURE OF RPC	121
5.1	INTRODUCTION	121
5.2	MORPHOLOGY OF CEMENT PASTE BASED ON SEM TEST	121
5.2.1	<i>Entrapped Air Pores</i>	122
5.2.2	<i>Anhydrous and Hydrated Materials Formed after Treatments</i>	123
5.2.3	<i>Microcracks Appearance</i>	129
5.2.4	<i>Pore Filling after Heat Curing</i>	133
5.3	CHEMICAL COMPOSITION OF HYDRATED MATERIALS	136
5.3.1	<i>Crystalline Phase Based on Mass Loss</i>	136
5.3.2	<i>Crystalline Phase Based on XRD spectrum</i>	138
5.4	INTERFACIAL TRANSITION ZONE PROPERTIES.....	140
5.4.1	<i>Hydrated Materials in the ITZ</i>	140
5.4.2	<i>ITZ Thickness</i>	144
5.5	PORE SIZE DISTRIBUTION AND POROSITY	149
5.5.1	<i>Pore Distribution</i>	149
5.5.2	<i>Physical Pore Properties</i>	152
5.5.3	<i>Porosity in ITZ</i>	153
5.5.4	<i>Effect of Hydrate Transformation on Porosity</i>	154
5.6	CONCEPTUAL MODEL PROPOSED FOR RPC MICRO STRUCTURE	156
5.7	INTERFACIAL BINDING WITH CARBON FIBRES.....	160
5.8	SUMMARY.....	161
6	CHAPTER 6- DURABILITY OF HARDENED RPC UNDER HIGH TEMPERATURE EXPOSURE	164
6.1	INTRODUCTION	164
6.2	PROPERTIES OF RPC IN FIXED TEMPERATURE EXPOSURE.....	165
6.2.1	<i>Appearance and Colour Change</i>	165
6.2.2	<i>Thermal Properties</i>	168
6.2.3	<i>Mechanical Properties</i>	171

6.2.4	<i>Microstructural Properties</i>	175
6.2.5	<i>Micro Crack Progression</i>	180
6.3	PROPERTIES OF RPC AFTER EXPOSURE AT 500 °C WITH VARIABLE HEATING DURATION.....	185
6.3.1	<i>Residual Compressive Strength</i>	185
6.3.2	<i>Pore Size Distribution</i>	186
6.3.3	<i>Alteration of Cement Paste Composition</i>	188
6.4	PROPERTIES OF RPC AFTER CYCLIC EXPOSURE AT 500 °C.....	189
6.4.1	<i>Compressive Strength</i>	189
6.4.2	<i>Pore Network Evolution</i>	190
6.4.3	<i>Compositional Changes by TGA after Cyclic Exposure</i>	192
6.5	PROPERTIES OF RPC FOLLOWING WATER QUENCHING AFTER HEATING AT 500 °C	193
6.5.1	<i>Compressive Strength</i>	193
6.5.2	<i>Pore Size Distribution</i>	194
6.6	SUMMARY.....	196
7	CHAPTER 7- CONCLUSIONS AND RECOMMENDATIONS	198
7.1	CONCLUSIONS.....	198
7.1.1	<i>(Obj.1) Optimising Heat Curing Treatment</i>	198
7.1.2	<i>(Obj. 2) Analysing Microstructure Properties to Develop a Basic Model of RPC Affected by Treatments</i>	199
7.1.3	<i>(Obj. 3) Quantifying the Properties of RPC after Fixed-term Exposure to Heat</i>	200
7.1.4	<i>(Obj. 4) Quantifying the Properties of RPC after Cyclical Heat Exposure with Different Cooling Regimes</i>	201
7.1.5	<i>(Obj. 5) Characterising the Correlation between Mechanical Properties and Crack Progression</i>	202
7.2	RECOMMENDATIONS FOR FUTURE RESEARCH	202
8	REFERENCES	204
	JOHNSTON, C.D. 2006. FIBER-REINFORCED CEMENTS AND CONCRETES (ADVANCES IN CONCRETE TECHNOLOGY;V:3). TAYLOR&FRANCIS-NY. 364P	207
9	APPENDIXES.....	213
	APPENDIX A: PHYSICAL AND MECHANICAL PROPERTIES.....	213
	APPENDIX B: EXAMPLE ELEMENT ANALYSIS FROM EDS	218
	APPENDIX C: CURVE OF TGA TEST (FILE: WORDS FORMAT)	219
	APPENDIX D: SEM IMAGES (FILE: TIF FORMAT)	219
	APPENDIX E: ANALYSIS OF PORE DISTRIBUTION FROM MIP (FILE: EXCEL FORMAT)	219
	APPENDIX F: ANALYSIS OF ELEMENT FROM EDS (FILE: EXCEL FORMAT)	219

List of Figures

Figure 2.1 Typical rate of heat output from Portland cement during hydration (Domone, 1996).....	13
Figure 2.2 Schematic of the development of the microstructure of hydrating cement paste: (a) fresh cement and water; (b) initial set; (c) two to three days old; (d) mature paste (Domone, 1996).	13
Figure 2.3 Grading of sand fraction (BS 1881-131, 1998).....	16
Figure 2.4 Sketch of thermal conductivity changes at high temperature exposure (Neville, 2011).	21
Figure 2.5 Effect of quartz size on compressive strength of RPC (Tam <i>et al.</i> 2010)	25
Figure 2.6 Pullout fibre surface (a) without SF; (b) with 30% SF (Chan & Chu, 2004)	26
Figure 2.7 Graph of released power evolutions with time (Morin <i>et al.</i> , 2001) ...	29
Figure 2.8 Effect of pressure on compressive strength (Yazici <i>et al.</i> , 2008).....	30
Figure 2.9 Effect of curing method on compressive strength (Yazici <i>et al.</i> , 2009).	32
Figure 2.10 Compressive strength values measured for samples exposed to different temperature and duration of curing (Tam & Tam, 2012).	33
Figure 2.11 Effect of pressure and heating on compressive strength (Sadrekarimi, 2004).	36
Figure 2.12 Effect of curing method on flexural strength (Yazici <i>et al.</i> , 2009)....	37
Figure 2.13 Load-displacement relationship of steaming curing (Yazici <i>et al.</i> , 2009)	39
Figure 2.14 Sherbrooke pedestrian/bikeway bridge (Blais & Couture, 1999)	40
Figure 2.15 Train station roof supported by a single line of columns (Vicenzino <i>et al.</i> , 2005)	41
Figure 2.16 Residual compressive strengths with respect to different fire durations at a constant temperature of 500 ± 50 °C (Liu & Huang, 2009).	44
Figure 2.17 Residual compressive strength of RPC (Tai <i>et al.</i> , 2011).....	45
Figure 2.18 Typical BSE image of a Portland cement mortar (Scrivener, 2004)..	49
Figure 2.19 Standard mercury intrusion/extrusion volumes as a function of pore sizes (Y-Leon, 1998).	51
Figure 2.20 Curves of TGA and DTG measurements (Cheyrezy <i>et al.</i> , 1995)	53
Figure 2.21 Microstructural features of hydrated paste in a 3-day (Diamond, 2004)	55
Figure 2.22 Illustration of wall effect (Peng <i>et al.</i> , 2011)	58
Figure 2.23 Typical inhomogeneity of ITZ (Scrivener <i>et al.</i> , 2004)	59
Figure 2.24 Representation of the microstructure of Portland cement paste (Scrivener <i>et al.</i> , 2004).....	60
Figure 2.25 Microstructure of the aggregate-paste interfacial zone in UHPC samples (Peng <i>et al.</i> , 2011).....	61
Figure 3.1 Binder material	65
Figure 3.2 Quartz sand grades	66
Figure 3.3 Carbon fibre 12 mm long and 7 μ m individual diameter	66
Figure 3.4 Small concrete mixer with adjustable speed setting.....	69
Figure 3.5 Mould with and without pressure.....	70
Figure 3.6 Cross section of mould with pressure.....	70
Figure 3.7 Oven for heat treatment	71
Figure 3.8 Setting time apparatus	72
Figure 3.9 Spreading test to measure the mixture consistency	74
Figure 3.10 Setting up the span in flexural test (BS EN 196-1, 2011)	75
Figure 3.11 Setting up the LVDT on two sides of a prism.....	75
Figure 3.12 Setting out of sample for compressive test	77

Figure 3.13 Setting up thermal conductivity test	78
Figure 3.14 SEM equipment fixed with EDS	79
Figure 3.15 Placing the mounted and coated sample in vacuum chamber	79
Figure 3.16 MIP equipment and sample dimension	82
Figure 3.17 TGA test (a) Instruments SDT Q500, (b) Sample on aluminium pans	84
Figure 3.18 Principal Bragg's Law	85
Figure 3.19 Setting up XRD test	86
Figure 3.20 Heating scenario for temperature increments.....	87
Figure 3.21 Heating scenarios for duration exposure.....	88
Figure 3.22 Heating scenarios for cooling in air	89
Figure 3.23 Heating scenarios for cooling in water.....	90
Figure 4.1 Fresh mixture and consistency measurement	94
Figure 4.2 Compressive strength-heating rate curves for a heating duration of 48 hours after 2 days of casting.....	96
Figure 4.3 Compressive strength-heat duration curves for a heat rate of 50 °C/hr after 2 days of casting.	98
Figure 4.4 Compressive strength-heated starting time curve for heating rate of 50 °C/hr and duration of 48 h	100
Figure 4.5 Normal failure mode of RPC in compression forming a double pyramid shape	102
Figure 4.6 Compressive strengths for conditions A - D at 7-d and 28-d (Helmi <i>et al.</i> , 2013).	102
Figure 4.7 Bulk densities for all conditions at 7-d (Helmi <i>et al.</i> , 2013).....	105
Figure 4.8 Apparent porosities for all conditions (Helmi <i>et al.</i> , 2013)	106
Figure 4.9 Correlation between porosity and compressive strength under each set of conditions (Helmi <i>et al.</i> , 2013)	108
Figure 4.10 Entrapped air appearances on sample surface without heat curing: (a) for conditions A and (b) for conditions C.....	109
Figure 4.11 Conceptual model of curing condition effects on spherical entrapped air pores in RPC: (a) standard curing, (b) pressurized setting, (c) pressurized setting followed by heat condition during hardening (Helmi <i>et al.</i> , 2013)	110
Figure 4.12 Comparison of flexural strength between RPC non-fibre (NF) and with carbon fibre (CF) for all conditions.....	112
Figure 4.13 Load and deflection curves for NF and CF with condition D showing immediate rupture after peak load.....	113
Figure 4.14 Compressive strength NF and CF for all conditions showing the overlapping of error bars between both.....	116
Figure 4.15 Correlation between compressive and flexural strength of RPC, data in this study merged with Yazici <i>et al.</i> (2009).....	118
Figure 5.1 Secondary electron micrographs of polished cross-sections through RPC samples following (a) no treatment, (b) heat treatment during hardening, (c) static pressure treatment during setting, and (d) combined pressure and heat treatment. The diameter and volume of entrapped air pores have been reduced by around one order of magnitude.	123
Figure 5.2 Backscattered electron micrographs of polished cross-sections through RPC samples following (a) no treatment, and (b) heat treatment during hardening. The intensity of anhydrous grains has been increased by heat curing due to quick evaporation.	125
Figure 5.3 Backscattered electron micrographs of polished cross-sections through RPC samples following (a) static pressure treatment during setting, and (b) combined pressure and heat treatment. The intensity of anhydrous	

grains and microcracks have been increased by pressure due to lowering free water content and much more after heat curing.	127
Figure 5.4 Higher magnifications by 2000x of BSE micrographs describing microcracks (red circles) and hydrated formed for (a) no treatment, (b) and heat treatment during hardening. The microcracks exist in paste have been increased by heat curing surrounding pores due to small explosions mechanism.	131
Figure 5.5 Higher magnifications of BSE micrographs describing microcracks and hydrated formed (a) static pressure treatment during setting, and (b) combined pressure and heat treatment. Small explosions also occur in treatment D.	132
Figure 5.6 SE micrographs on surface of a fracture specimen describing pore filling mechanism (a) no treatment, (b) heat treatment. Insert A: group of ettringite crystal located in pores; insert B: groups of tobermorite (platy-shape) and xonotlite (needle-shape) filled in pores. Heat curing induces pore filling mechanism.	135
Figure 5.7 Mass loss of hydrate formed for all treatments: no-treatment (A); heat curing only (B); pressure only (C); both pressure and heat curing (D). Treatments decrease the hydrate formed which indicates the increase of anhydrous grains.	137
Figure 5.8 XRD diffractograms of RPC bulk powder samples following treatments A – D. Heat curing produces xonotlite and reduces portlandite which indicate the transformation of C-S-H and pozzolanic reaction.	140
Figure 5.9 Atomic ratios between (Al+Fe)/Ca and Ca/Si for all treatments.	143
Figure 5.10 Atomic ratios between S/Ca and (Al+Fe)/Ca for all treatments.	143
Figure 5.11 Spatial distribution of atomic ratio across the ITZ as a function of distance from an aggregate grain boundary determined using quantitative EDS.	144
Figure 5.12 Example plot of 15 grids area @5x50 μm in treatment D.	145
Figure 5.13 Bulk porosity as a function of distance from an aggregate grain boundary determined using segmentation image analysis of BSE micrographs.	146
Figure 5.14 Example plot of mean porosity as a function of distance (treatment D) with interpolated ITZ distance.	147
Figure 5.15 MIP cumulative intrusion-pore diameter plot. Cement pore size range classification is interpolated from Domone (1996) for a w/c of 0.22.	150
Figure 5.16 Conceptual model of RPC microstructural alterations resulting from all treatments (A-D).	159
Figure 5.17 Interfacial carbon fibre for treatment A and D: (a) and (b) are surface of carbon fibre and cement paste in treatment A; (c) and (d) are surface of carbon fibre and cement paste in treatment D.	161
Figure 6.1 The appearance and colour on the surface and cross section of RPC specimens for four temperature conditions: ambient, 400 $^{\circ}\text{C}$, 500 $^{\circ}\text{C}$ and 800 $^{\circ}\text{C}$. The colours changes are mostly affected by chemical reactions or transformation of hydrates.	167
Figure 6.2 Thermal conductivity of RPC after high temperature exposure.	170
Figure 6.3 Residual compressive strength of RPC after high temperature exposure.	173
Figure 6.4 Ratio of residual compressive strength after exposure compared to the results of other scholars.	175
Figure 6.5 Mass loss-temperature plots showing the main hydrate content after high temperature exposure.	177
Figure 6.6 Distribution and proportion of pores in different temperature of exposure.	180

Figure 6.7 Micro crack appearance on the fracture surface of specimen core (a) at 20 °C showing dense matrix with initial micro crack(b) 400 °C showing micro crack progression on paste due to small explosion and ITZ. ...	181
Figure 6.8 Micro crack appearance on fracture surface of specimen core (a) at 500 °C showing more micro crack in paste and wider cracks in ITZ (b) 800 °C showing micro crack in a whole of paste, ITZ and even in the quartz aggregate.	184
Figure 6.9 Residual compressive strength after different durations of exposure at 500 °C and comparison the results of Liu & Huang (2009) with the present study.....	186
Figure 6.10 MIP cumulative intrusion vs. pore diameter after different duration of exposure at 500 °C for treatment D samples	187
Figure 6.11 TGA mass loss for treatment D samples after exposure for different durations.....	188
Figure 6.12 Residual compressive strength after cyclic exposure at 500 °C.....	190
Figure 6.13 MIP pore size distribution after cyclic exposure at 500 °C	191
Figure 6.14 TGA mass loss for RPC after cyclic exposure at 500 °C.....	192
Figure 6.15 Residual compressive strength after controlled and water (quench) cooling, following initial exposure at 500 °C.....	194
Figure 6.16 MIP pore size distribution after air and water (quench) cooling following exposure at 500 °C	195

List of Tables

Table 2.1 Major phases present in Portland cement clinker (Ghani, 1997)	11
Table 2.2: Classification of cement based on the content (EN BS 197-1:2011)..	14
Table 2.3: Grading of aggregates (BS EN 12620:2002)	15
Table 2.4: Classification of admixtures	17
Table 2.5: Typical properties of PFA, GGBS and SF (Taylor, 1991).....	17
Table 2.6: Thermal expansion coefficients of concrete at high temperature (Neville, 2011)	23
Table 2.7: Composition per 1 m ³ of RPC and compressive strength (Yazici <i>et al.</i> , 2008)	27
Table 3.1: Composition of RPC per cubic meter	68
Table 4.1: Composition of mixtures and the average of setting time taken from three samples	93
Table 4.2: Analysis Student's t-test of compressive strength for all factors	101
Table 4.3: Toughness and flexural modulus result for NF and CF with condition D	114
Table 5.1 : The average of mass loss (wt%) for key temperature ranges determined by TGA analysis.....	138
Table 5.2: Atom ratio average of three measurements in ITZ	141
Table 5.3: Thickness and porosity in ITZ	147
Table 5.4: Equation of porosity up to ITZ thickness according to equation (5.6)	149
Table 5.5: Volume fraction distribution (%) of pore diameters	151
Table 5.6: Summary of experimental data from MIP	153
Table 5.7: Calculation of PITZ	154
Table 5.8: Summary of TGA inferred mineral transformations with corresponding density increase (per 1 g specimen)	155
Table 6.1: The average result of bulk density, thermal conductivity, thermal effusivity and specific heat capacity after high temperature exposure	168
Table 6.2: Pore properties after high temperature exposure	178
Table 6.3: Physical properties of pores after different duration of exposure at 500 °C	187
Table 6.4: Physical properties of pore network after cyclic exposure at 500 °C	191
Table 6.5: Physical properties of pore network after air and water (quench) cooling following exposure at 500 °C	196

Nomenclature

q	: heat flow ($\text{J s}^{-1} \text{m}^{-2}$)
λ	: thermal conductivity ($\text{J s}^{-1} \text{m}^{-1} \text{K}^{-1}$)
β	: thermal effusivity ($\text{W s}^{1/2} \text{cm}^{-3} \text{K}^{-1}$)
T	: temperature (K)
$\frac{dT}{dx}$: differential temperature to length
δ	: diffusivity (m^2/h)
C_p	: specific heat ($\text{J kg}^{-1} \text{C}^{-1}$)
ρ_d	: dry density of concrete (kg m^{-3})
l	: length of the liquid column at time t (m)
r	: radius of the capillary (m)
γ_L	: liquid vapour interfacial tension (N m^{-2})
θ	: contact angle between mercury and the specimen surface ($^\circ$)
η	: viscosity of the liquid (dynes cm^{-2})
d_p	: pore diameter (μm)
σ^{Hg}	: surface tension of mercury (dynes cm^{-2})
p	: press pressure in MIP test (psi)
k	: transfer constant ($10^{-4} \text{cm}/\mu\text{m} \times 68947 \text{psi}/\text{dynes cm}^{-2}$)
n	: an integer
λ	: wavelength of the incident X-ray beam
d	: distance between atomic layers in crystal (mm)
θ	: angle of incidence of X-ray ($^\circ$)
ρ	: porosity (%)
f'_c	: compressive strength (MPa)
$f'_{c,0}$: strength of paste at zero porosity (MPa)
E_f	: flexural Modulus of elasticity, (MPa)
L	: support span, (mm)
b	: width of test beam, (mm)
d	: depth of tested beam, (mm)
m	: gradient of the initial straight-line portion of the load deflection
f_t	: tensile strength (MPa)
$\varphi(x)$: porosity value at distance x from to the aggregate surface (%)
φ_{if}	: porosity value at the closest aggregate surface (%)
φ_{bulk}	: porosity value of bulk paste (%)
d	: ITZ thickness (μm)
β	: gradient of porosity profile within the ITZ
P_{total}	: total mercury intrusion for mortar (mL/g)
P_a	: total mercury intrusion for cement paste (mL/g)
V_a	: aggregate proportion in volume
P_{ITZ}	: mercury spelling in ITZ (mL/g).
f'_{cT}	: compressive strengths of RPC after high temperature exposure
v_f	: fibre volume fraction (%)

Chapter 1- Introduction

1.1 Background

Concrete has become the predominant construction material in a large variety of structures around the world (Neville, 2011). Its widespread use can be attributed to the low cost of the materials, construction process, and low maintenance. Another important requirement of a concrete structure is also durability, which is related to the mechanical properties and the environmental resistance of the concrete (Gani, 1997). Currently, the application of concrete with high durability faces some challenges particularly in the construction industry. Therefore, researchers seek to advance concrete technology in order to fulfil the demand for high performance concrete (HPC) or even ultra-high performance concrete (UHPC).

The development of HPC commonly can be achieved by adding into the concrete mixture some mineral additives, such as silica fume (SF), pulverised fly ash (PFA), ground granulated blast-furnace slag (GGBS), and natural pozzolans (De Larrard & Sedran, 2002; Liu *et al.*, 2000; Long *et al.*, 2002). HPC has a low water-binder ratio, typically <0.4 , and a compressive strength of a concrete cylinder of at least 60 MPa at 28 days (De Larrard & Sedran, 2002). However, Neville (2011) defines that it has certain unique features such as compressive strength of typically between 80 – 140 MPa, an ultimate strain of about 0.003, and a modulus of elasticity of about 40 GPa.

Reactive powder concrete (RPC), which also is categorised as UHPC due to having compressive strength > 140 MPa, can be developed by controlling three main variables: composition, pressure during setting period, and post-set heat curing (Richard & Cheyrezy, 1995). Firstly, composition can be improved through a microstructural engineering approach by using fine aggregate only (no coarse

aggregate), reducing water-binder ratio, lowering the CaO–SiO₂ ratio through the introducing of silica-rich pozzolona (Bonneau *et al.*, 2000; Matte & Moranville, 1999), and adding fibre reinforcement to increase ductility (Chan & Chu, 2004). Secondly, pressure applied during the setting period also influences the strength of concrete. Pressure induces three main effects: reducing the entrapped air, removing the excess water, and eliminating the porosity caused by chemical shrinkage (Richard & Cheyrezy, 1995).

Meanwhile, heat curing induces the acceleration of the pozzolanic reaction between amorphous silica and calcium hydroxide as well as the silicate and aluminate hydration reaction, and also the modification of hydrate microstructure (Zanni *et al.*, 1996; Cwirzen, 2007). By implementing these techniques, the performance of RPC properties is better than HPC in relation to a number of characteristics such as: (i) a compressive strength ranging between 200 and 800 MPa, (ii) a fracture energy of up to 40,000 J/m², and (iii) an ultimate elongation of up to 0.007 m/m⁻¹ (Richard & Cheyrezy, 1995).

RPC has the potential to be applied in several types of precast structures, such as pre-stressed structures, pressure precast pipes, or impermeable containers for hazardous fluid or nuclear waste (Sadrekarimi, 2004; Vodak *et al.*, 1997). Most RPC structures are produced by the precast method. This can increase the productivity of structural elements and construction application due to the ability to reach high strength concrete at early age (Blais & Couture, 1999; Vicenzino *et al.*, 2005; Rebenstrot & Cavill, 2006; Helmi *et al.*, 2013).

1.2 Research Significance

An RPC mixture typically contains a high amount of cement at a dosage of 800-1000 kg/m³ (Yazici *et al.*, 2008). The use of cement in a high amount impacts on

the heat of hydration and leads to potential risks associated with shrinkage and creep-induced strain problems, and also the production cost. The addition of fibre reinforcement in a RPC mixture is common solution to the problem of shrinkage and creep-induced strain; this also contributes to ultra-high mechanical properties and strain capacity which allows the production of very thin structural components (Richard & Cheyrezy, 1995; Yazici *et al.*, 2009). To solve the second problems related to cost, Yazici *et al.*, (2008) conducted research on the composition of RPC mixtures to find the optimal amount of finer materials from industrial waste (SF, PFA, and GGBS) as cement replacement. They suggested that RPC comprising 35wt% SF and up to 40 % GGBS (as cement replacement) could result in a compressive strength of more than 200 MPa.

Most scholars have argued that the strength of RPC is mainly developed by the pozzolanic reaction and hydrate transformation after heat curing. Heat curing, which is one of the most important treatments in RPC, can be applied by various methods. Yazici *et al* (2008) applied heat curing on RPC prism specimens (after demoulding) in an autoclave at 2.0 MPa and 210 °C. These conditions were achieved within a 2.5 h heating period, and the heat curing was then applied for 8 hours. Cwirzen (2007) used a method of steam curing (95 %RH, 90 °C) to optimise the conditions for heat curing by varying two factors: the starting time of heating after demoulding, and the duration of heating. Heat curing was applied to the RPC cube specimens with durations of 24, 48 and 168 hours, and starting times at 1, 2, and 4 days after casting the samples. He suggests that the optimal conditions of heating can be reached after 2 days of casting with a total duration of 48 hours producing the highest degree of hydration. Another heat curing method was applied by Sadrekarimi (2004) and Tam *et al.* (2010) in drying oven equipment with different rates and maximum temperatures. Sadrekarimi (2004) placed samples in the oven with a constant heat rate of 10 °C/hr until it reached a temperature of 240 °C. Tam *et al.* (2010) set first a

drying oven at 100 °C then placed samples into the oven with a temperature rate of 50 °C/hr until it reached 250 °C. It should be noted that the duration and heating rate are important factors in heat curing since they affect the crystallisation of hydrates, pozzolanic reaction, microstructure development and associated bulk mechanical properties (Tam & Tam, 2012).

Heat curing treatment, which is generally applied after final set of cement at a temperature between 90 °C and 250 °C, contributes to both the progression of cement hydration and the acceleration of pozzolanic reaction between silica fume (amorphous) and quartz flour (crystalline) (Cheyrezy *et al.*, 1995; Zanni *et al.*, 1996; Cwirzen, 2007; Tam & Tam, 2012). Heat curing also modifies the micro structure of hydrates by changing the C-S-H chain length from trimer to pentamer (Cwirzen, 2007). When the temperature of curing increases to more than 200 °C, this condition leads to the transformation of crystalline hydrates and dehydration of the hardened paste. The transformation hydrate will be formed spontaneously when water extracted from hydrates is trapped in the centre of samples during transient heating (Cheyrezy *et al.*, 1995) becoming tobermorite at a temperature of 150 °C and xonotlite at temperatures of both 200 and 250 °C (Tam & Tam, 2012).

Although heat curing has a positive influence on the compressive strength of RPC mixtures containing steel fibres, it has a different impact on the flexural strength (Sadrekarimi, 2004). He found that the flexural strength of RPC cured by standard curing (in fresh water) was higher than one cured by heat curing. This could be due to the formation of microcracks surrounding the steel fibres because of the wide differences in thermal coefficient between steel fibres and cement paste.

Pressure is another treatment in RPC which is often applied to fresh mixtures to improve the density (Sadrekarimi, 2004). The pressure can be generated by a

static load or by air compression with various durations which influences RPC properties in fresh and hardened conditions (Richard & Cheyrezy, 1995; Yazıcı *et al.*, 2008; Cwirzen, 2007; Cheyrezy *et al.*, 1995). When it is applied before or during setting, pressure has three main effects: reducing the entrapped air, removing the excess water, and eliminating the porosity caused by chemical shrinkage (Richard & Cheyrezy, 1995). The combination of pressure and heat curing during processing may result in higher strengths than by heat treatment alone because the addition of pressure treatment to the fresh concrete increases the density and in turn decreases the porosity (Neville, 2011; Chen & Kwan, 2012)

High temperature can change the chemical composition and physical structure of hardened concrete, which also relates to the durability of concrete structures. The chemical changes are commonly evaluated in terms of colour (Arioz, 2007; Poon *et al.*, 2004a; Liu & Huang, 2009; Tai *et al.*, 2011) and composition of oxide content (Shin *et al.*, 2002). The physical effects that have been analysed in past research include weight loss (Arioz, 2007; Liu & Huang, 2009), residual porosity (Poon *et al.*, 2001; Xu *et al.*, 2001), spalling phenomena (Chen & Liu, 2004; Peng *et al.*, 2006), residual strength (Arioz, 2007; Poon *et al.*, 2004a; Peng *et al.*, 2006; Khaliq & Khodur, 2011; Dos Santos, 2003), fracture energy (Poon *et al.*, 2004a; Peng *et al.*, 2006), crack width (Poon *et al.*, 2001), microstructural properties (Tai *et al.*, 2011) and thermo-physical properties (Shin *et al.*, 2002).

During exposure at high temperature, the phenomenon of gas transport will influence the thermo-physical properties of concrete such as viscosity, thermal conductivity and diffusion (Blundell & Blundell, 2011). Thermal conductivity and diffusion are important factors to evaluate the durability of concrete under different temperature regimes (Najim, 2012). After exposure, both thermal

conductivity and thermal diffusivity decrease due to the increase of porosity in concrete (Hall *et al.*, 2012a). In addition, the volumetric heat capacity increases in line with the increase of porosity (Hall *et al.*, 2012b). For a high risk structure, such as a nuclear reactor for example, both mechanical and thermo-physical properties of concrete have to be evaluated over a wide range of temperature and moisture levels to prevent structural failure caused by non-standardised conditions (Vodak *et al.*, 1997). There are fewer scholars reporting the effects of high temperature on thermo-physical properties of RPC. It appears that this area is open for further exploration mainly due to its complex factors, which differ from those of common concrete. They also influence several types of behaviour seen in RPC such as entrapped air pressure, microcrack progression, pozzolanic reaction and dehydration of cement hydrates.

Heat and fire-resistant concrete requires a properly designed mixture in order to ensure a dense, well-consolidated, and high strength mix since the strength of the hydraulic bond decreases at about 400 °C (Neville, 2011). The densest cement gel structure can be achieved when it uses a very fine fraction of less than 0.06 mm particle diameter at a content of between 30 and 100% of the cement content (Liu *et al.*, 2012). Ultrafine powder from mineral admixtures, such as SF and GGBS, play an important role in the density and workability of fresh RPC mixtures (Long *et al.*, 2002). Although the use of a high amount of SF can reduce density of RPC, pressure treatment during setting may control this condition (Cwirzen, 2007). Therefore, it is important to quantify the effect of high temperature on the microstructural properties of RPC containing different amounts of ultrafine powder.

The composition of RPC mixtures studied by Yazici *et al.* (2008) is interesting because it removed the problem of a high cement content in RPC by using GGBS as partial replacement, which resulted in compressive strength >200 MPa. As this

mixture uses a lot of ultrafine powders to make very dense concrete, it also has the potential to be implemented as one type of fire-resistant concrete with a good durability in terms of residual compressive strength. Therefore, it is necessary to reproduce their work with some modifications. These may include reduction of SF content to increase the workability, applied static pressure during the setting period to get a denser matrix, and applying heat curing in an oven after hardening. Although many scholars have reported findings relating to the microstructural properties of RPC, it is important to evaluate the evolution of these properties following treatment by pressure, heat curing, or combined treatments.

Although the properties of RPC under elevated temperature have been studied by several scholars, they have focused mostly on physical properties and less on thermo-physical properties (Liu & Huang, 2009; Tai *et al.*, 2011). Moreover, they have used a monotonic heat exposure by heating the specimens in a furnace only once. In fact, the RPC structure may face multiple cyclic conditions of heating and cooling, sometimes slowly and other times suddenly, for example in a fire (Hertz, 2005). These heating cycles are likely to affect both the microstructural properties and durability of RPC due to fatigue loading.

1.3 Aim and Objectives

This research aims to define the characteristics of thermo-physical properties of RPC and quantify the microstructure changes caused by high temperature curing during the setting period and fixed-cyclic high temperature exposure after 28-days.

In order to meet this aim, the research developed a number of objectives:

1. To optimise the heat curing treatment related to rate, duration, and starting time of heating, which were evaluated based on the compressive strength values.
2. To analyse the effects of both pressure and heat curing treatments on microstructural properties in order to develop a conceptual model that describes post-treatment RPC.
3. To quantify the effects of fixed-term exposure in high temperature treatments on the physical, mechanical, and thermo-physical properties of RPC.
4. To quantify and compare the relative effects of high temperature treatment on the mechanical properties of RPC with variations in heating duration, number of heating cycles, and cooling conditions.
5. To define the characteristics of RPC before and after heat treatment, including its composition, microstructure, degree of crack propagation, and alterations in macro-scale physical and mechanical properties.

1.4 Scope of Study

This research focuses on RPC characteristics which include a number of important aspects. Therefore, this research focuses on RPC characteristics which include a number of features important aspects that link to the following issues:

1. This study focuses on a composition that uses GGBS 40 wt.% cement replacement and carbon fibre reinforcement. Since this mixture has a compressive strength >200 MPa and carbon fibre has lower thermal expansion than steel fibre, this was deemed to produce a mix with suitable performance for testing in high temperature exposure. This research just need a typical RPC mixture because the aim is to explore a broad issue rather than investigating the difference between different mixtures. The reason for the inclusion of fibres will be explained in Chapter 3.

2. Pressure treatment applied before and during the setting period could change the sample dimension. However, the density of samples affected by pressure treatment was evaluated before compression testing or in microstructure analysis.
3. The high temperature curing could affect the cement hydration rate during the setting period. The effect during this period was not evaluated because the study focused on the properties of samples after compressive testing. Therefore, samples were cured in water in order to continue hydration after heat curing until the day of testing.
4. The high temperature exposure on hardened specimens could induce many alterations in RPC behaviour such as mechanical, shrinkage, elastic moduli, and spalling. Due to the limited time for this study, the durability properties of RPC were evaluated only in terms of residual compressive strength and thermo-physical properties, along with corresponding microstructural changes.

1.5 Anticipated Contributions

It was hypothesised that the alteration of microstructural properties in RPC following monotonic or cyclic high temperature exposure would have a significant effect on the durability of rigid RPC structures. The published information in this area is limited and there is no detailed information currently available on the residual properties of RPC following cyclic high temperature exposure. Following the proposed testing, the recommendations from this study could be applied to the design of concrete structures that are at risk of fire. It is hoped that the findings of this research could enrich overall knowledge of RPC properties, particularly in relation to the correlation between microstructural alterations and macro structural physical properties.

Chapter 2- Literature Review

2.1 Introduction

Concrete is one of the most widely used construction materials and is made by mixing cement, water, aggregate and admixtures. The quality of concrete is determined by its properties in one of two possible states: hardened and fresh (*i.e.* Bingham fluid) (Neville, 2011). Hardened concrete has a well-known set of correlations between mechanical properties and durability, while the fresh state is defined by the consistency of properties when mixed, transported, compacted, and finished.

This chapter presents a review of current knowledge in concrete technology, particularly with respect to reactive powder concrete (RPC) and thermal properties. The discussion of RPC presents recent research containing some factors influencing the mechanical and microstructure properties, the behaviour under high temperature, and the potential application for real construction projects.

2.2 Material of Concrete

2.2.1 Cement

Cement is arguably the most important component in concrete construction. Its role is to bond the mineral aggregates into a solid composite having certain characteristics. Cement is hydraulic and so sets and hardens during an exothermic hydration reaction with water. Ordinary Portland cement (OPC) consists of lime, silica, alumina, and iron oxide which are finely ground, mixed and heated together to a temperature of about 1500 °C in a rotary kiln. This

process involves decomposition of the calcium carbonate into four main compounds (Gani, 1997; Domone, 1996; Neville, 2011; Taylor, 1991), as shown in Table 2.1.

The function and amount of each compound are different when they are mixed with water. C₃A (about 10 % of OPC) mixes rapidly with water and is mostly responsible for the initial setting. C₄AF (around 8%) contributes little to long-term strength and is responsible for the grey colour of cements. C₃S (around 52%) hydrates quickly on adding water and is responsible for early strength. C₂S (19%) hydrates slowly and is responsible for the ultimate strength. The remaining percentages are C_SH₂, N and K which influence the setting action of cement (Taylor, 1991).

Table 2.1 Major phases present in Portland cement clinker (Ghani, 1997)

Real phases in clinker	Idealized chemical composition		Code
Alite	3CaO.SiO ₂	Tricalcium silicate	C ₃ S
Belite	2CaO.SiO ₂	Dicalcium silicate	C ₂ S
C ₃ A-alkali solid solution	3CaO. Al ₂ O ₃	Tricalcium aluminate	C ₃ A
Ferrite phase solid solution	4CaO. Al ₂ O ₃ .Fe ₂ O ₃	Tetracalcium alluminoferrite	C ₄ AF

Cement hydration is a complex process and sees gradual chemical reactions between cement and water. It becomes solid after setting and then stiff and strong after hardening (Taylor, 1991). During the mixing process, the consistency of the cement-water paste is relatively constant then gradually loses its fluidity. At a certain time, called the initial set, the rate of gain in stiffness is faster but it has little strength. After several hours, it reaches the final set stage and begins to gain strength. The strength increases quickly for one or two days and then continuously rises for a few months. The hydration reactions are exothermic which release heat during setting and hardening.

Hydration results in a complex microstructure with a large surface area due to the very small size of crystals formed. These can be analysed by various methods of scanning, transmission and analytical electron microscopy. Several studies state that the hydration reaction changes the condition of the mixture from liquid to solid. The changing stages are described in Figure 2.1 and Figure 2.2. The anhydrous cement particles are dispersed through the water where the spacing of particles depends on the water/cement ratio. During a dormant period, C_3A and $CaSO_4 \cdot 2H_2O$ (gypsum) hydrate to form calcium sulphoaluminate (called ettringite) in the form of sharp needles or rods which interlock the weak C-S-H product. At the end of the dormant period the ettringite from nearby particles begins to affect the solid layers of C-S-H hydrate with a spicular (cigar-shaped) crumpled-foil form. A continuous gel of C-S-H hydrate is then produced around the $Ca(OH)_2$ crystals which increases the strength. At two or three days, there are some unhydrated (anhydrous) cement regions and gel voids in the centre of the cement grains (Illston, 1996).

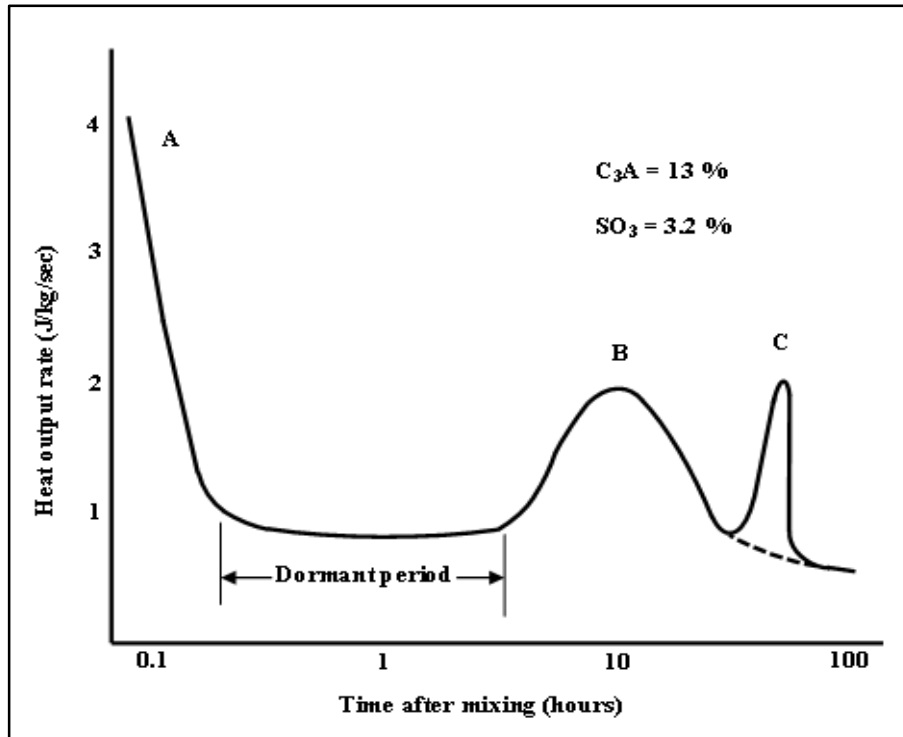


Figure 2.1 Typical rate of heat output from Portland cement during hydration (Domone, 1996)

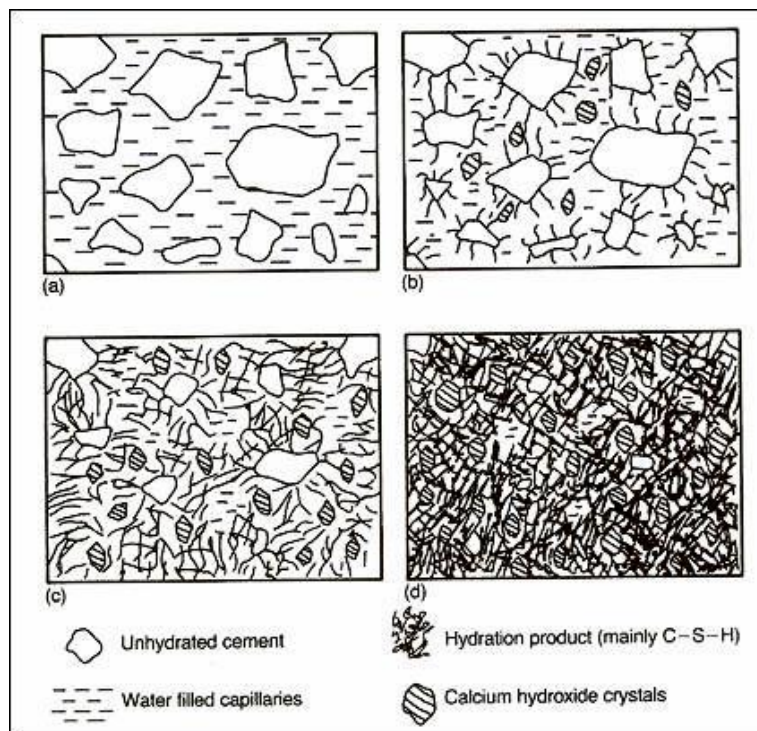


Figure 2.2 Schematic of the development of the microstructure of hydrating cement paste: (a) fresh cement and water; (b) initial set; (c) two to three days old; (d) mature paste (Domone, 1996).

EN BS 197-1 (2011) classifies Portland cement based on its content in terms of CEM cement in five categories and 27 variants, mainly as shown in Table 2.2.

Table 2.2: Classification of cement based on the content (EN BS 197-1:2011)

Type	Designation		Mass as percentage of mass of cementitious material			
			PC clinker	Pozzolana or fly ash	Silica fume	GGBS
CEM I	Portland	I	95-100	-	-	-
CEM II	Portland slag	II/A	80-94	-	-	6-20
		II/B	65-79	-	-	21-35
	Portland pozzolona or Portland fly ash	II/A	80-94	6-20	-	-
		II/B	65-79	21-35	-	-
	Portland silica fume	II/A	90-94	-	6-10	-
	Portland composite	II/A	80-94	← 6-20 →		
II/B		65-79	← 21-35 →			
CEM III	Blast furnace	III/A	35-64	-	-	36-65
		III/B	20-34	-	-	66-80
		III/C	5-19	-	-	81-95
CEM IV	Pozzolonic	IV/A	65-89	← 11-35 →		-
		IV/B	45-64	← 36-55 →		-
CEM V	Composite	V/A	40-64	18-30	-	18-30
		V/B	20-38	31-49	-	31-49

2.2.2 Aggregate

Aggregates used in construction consist of coarse and fine granular materials from natural resources, manufacturing, or re-cycling (EN BS 12620, 2002). The use of aggregates in all concrete types can reduce the construction cost and control the concrete properties in terms of shrinkage, thermal movement, and abrasion-resistance (Taylor, 1991). The properties of aggregates that are considered to be the most important for concrete are density, size, shape, texture, and grading.

Grading describes the relative proportions of various particle sizes, from the nominal maximum aggregate size to the smallest material present. Grading of aggregate is essential in order to produce concrete with satisfactory plastic properties (workability, cohesion and resistance to bleeding), as well as satisfactory hardened properties (strength, voids content, durability and surface finish), using as little cement as possible. Aggregate will be well-graded if the small particles can fill the voids continuously until the smallest one.

BS EN 12620 (2002) classifies the grading of aggregates according to the ratio of lower (d) and upper (D) sieve sizes as presented in Table 2.3. Furthermore, BS 1881-131 (1998) divides fine aggregates into five fractions: A (2.36 – 1.18 mm), B (1.18 – 0.6 mm), C (600 – 300 μm), D (300 – 150 μm) and E (150 – 90 μm) as described in Figure 2.3.

Table 2.3: Grading of aggregates (BS EN 12620:2002)

Aggregate	Size	Percentage passing by mass					Category G^d
		$2D$	$1,4D^{a\&b}$	D^c	d^b	$d/2^{a\&b}$	
Coarse	$D/d \leq 2$ or $D \leq 11,2$ mm	100 100	98 to 100 98 to 100	85 to 99 80 to 99	0 to 20 0 to 20	0 to 5 0 to 5	$G_{C85/20}$ $G_{C80/20}$
	$D/d > 2$ and $D > 11,2$ mm	100	98 to 100	90 to 99	0 to 15	0 to 5	$G_{C90/15}$
Fine	$D \leq 4$ mm and $d = 0$	100	95 to 100	85 to 99	–	–	G_F85
Natural graded 0/8	$D = 8$ mm and $d = 0$	100	98 to 100	90 to 99	–	–	G_{NG90}
All-in	$D \leq 45$ mm and $d = 0$	100 100	98 to 100 98 to 100	90 to 99 85 to 99	–	–	G_A90 G_A85

^a Where the sieves calculated are not exact sieve numbers in the ISO 565:1990 R 20 series then the next nearest sieve size shall be adopted.
^b For gap graded concrete or other special uses additional requirements may be specified.
^c The percentage passing D may be greater than 99 % by mass but in such cases the producer shall document and declare the typical grading including the sieves D , d , $d/2$ and sieves in the basic set plus set 1 or basic set plus set 2 intermediate between d and D . Sieves with a ratio less than 1,4 times the next lower sieve may be excluded.
^d Other aggregate product standards have different requirements for categories.

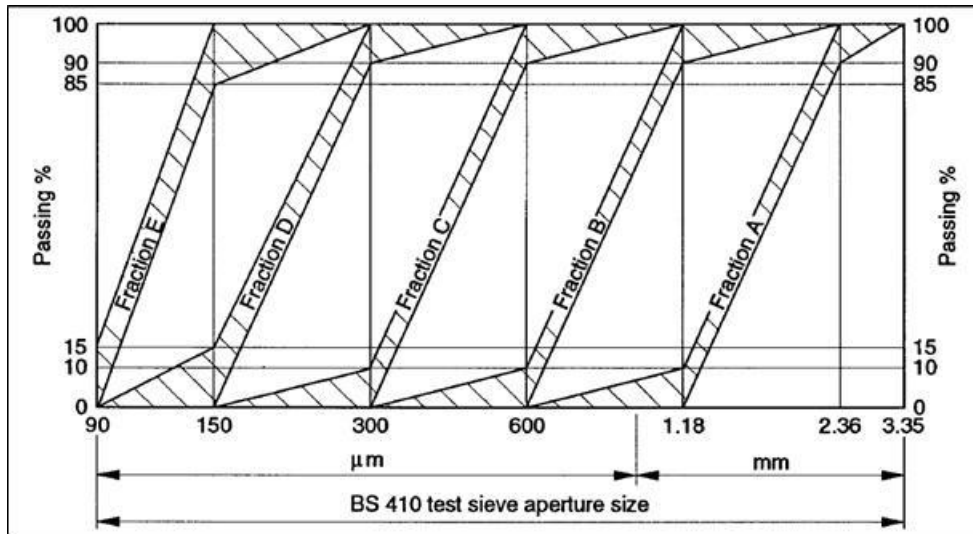


Figure 2.3 Grading of sand fraction (BS 1881-131, 1998)

2.2.3 Admixtures

Admixtures produced from sulphated melamine formaldehyde condensate and modified lignosulphonates can enhance the properties of fresh mixtures in terms of making them highly fluid, self-levelling and self-compacting (Mehta & Monteiro, 2006; Taylor, 1991). This can increase workability to about three times that of normal concrete for a short time, *i.e.* less than 60 minutes. In mixtures with normal workability, water content can be reduced by up to 30%, producing high-strength concrete. The classification of admixtures generally is based on their intended purpose in the field, as shown in Table 2.4.

Table 2.4: Classification of admixtures

Neville (2011)	BS EN 934-2;2009
1. Type A Water-reducing	1. Water reducing/plasticizing
2. Type B Retarding	2. High range water reducing/super plasticizing
3. Type C Accelerating	3. Water retaining
4. Type D Water-reducing and retarding	4. Air entraining
5. Type E Water-reducing and accelerating	5. Set accelerating
6. Type F High-range water-reducing or superplasticizing	6. Hardening accelerating
7. Type G High-range water-reducing and retarding or superplasticizing and retarding	7. Set retarding
	8. Water resisting
	9. Set retarding/water reducing/plasticizing
	10. Set retarding/high range water reducing/plasticizing
	11. Set accelerating/water reducing/plasticizing

2.2.4 Pozzolanic Materials

BS EN 197-1 (2011) defines pozzolans as materials containing natural substances of silica or silico-aluminium or a combination which cannot harden themselves in water, but if finely ground they can react with water and dissolved calcium hydroxide to produce strength-developing compounds of calcium silicate and calcium aluminate. Neville (2011) simplifies it as a natural or artificial material containing silica in reactive and amorphous form (glassy). The most common natural pozzolanic materials are volcanic ash, pumicite, calcined diatomaceous earth and burnt clay, while common synthetic pozzolans are pulverised fuel ash (PFA), ground granulated blast-furnace slag (GGBS) and micro silica or silica fume (SF) (Taylor, 1991). The properties of the latter materials are presented in Table 2.5.

Table 2.5: Typical properties of PFA, GGBS and SF (Taylor, 1991)

Type	Silica content (%)	Lime content (%)	Relative density (g/cm ³)	Fineness	Particle shape
PFA	50	3	2.3	6 % retained on 45 µm sieve	spherical
GGBS	38	40	2.9	specific surface 400 m ² /kg	irregular
SF	92	0.1	2.2	specific surface 15,000 m ² /kg	hollow or solid spheres

2.2.5 Fibre

The presence of fibre in mixtures can change the strength, durability and failure mode of concrete (Johnston, 2006). The commonly used fibres are steel, carbon, glass, aramid, and organic fibres. Steel fibres are made from carbon or stainless steel and are mostly used in concrete mixtures to give increased toughness and post-crack load carrying (Taylor, 1991). BS EN 14889-1 (2000) classifies steel fibres for mixing with concrete based on the method of fabrication into five groups that are: (i) cold-drawn wire, (ii) cut sheet, (iii) melt extracted, (iv) shaved cold drawn wire and (v) milled from blocks.

Carbon fibre or graphite fibre is a solid semi-crystalline organic material containing the atomic level of planar two-dimensional arrays of carbon atoms (Bank, 2006). Carbon fibre has good durability performance in hot or moist environments, even under cyclical loads. The thermal coefficient of this fibre in the longitudinal direction is very low and they do not absorb moisture; its dimensional stability is excellent. Despite some property advantages, this material is thermally and electrically conductive. Carbon fibre has a charcoal-black colour with a diameter of about 5 to 10 µm and is produced at high temperatures of around 1200 to 2400 °C. The heat treatment applied during production develops the atomic structure more of the sheet like planar graphitic array and results in carbon fibre with higher longitudinal modulus. The standard grade of carbon fibre has some properties such as a density of 1.7 g/cm³, tensile

modulus of 250 GPa, tensile strength of 3700 MPa, and maximum elongation of 1.2% (Bank, 2006).

2.3 Thermal Properties of Concrete

The term thermal physics generally includes two components: classical thermodynamics related to the conversion of heat into work and statistical mechanics concerned with the behaviour of the principal microstates of the system (Blundell & Blundell, 2011). Heat is energy in transit which transfers from hot to cold sources. The factors generally considered in thermodynamic theory are specific heat capacity, thermal conductivity, thermal diffusivity and coefficient of thermal expansion.

Specific heat (C_p) is the quantity of heat needed to increase temperature by one degree per unit mass of material. Specific heat is generally less influenced by type of aggregate and temperature (Mehta & Monteiro, 1997), but it is significantly affected by moisture (Neville, 2011) due to the higher C_p of liquid water (4150 J/kg.K at temperature of 293 K). The specific heat capacity of concrete is not a constant and rises as a function of temperature along with decreasing density due to thermal expansion. This property can be measured by elementary methods of physics, such as hot disk sensors. For ordinary concrete, C_p is between 840 and 1170 J/kg °C (Neville, 2011) or 0.9 to 1.0 kJ/kg °C (Mehta & Monteiro, 1997).

2.3.1 Thermal Conductivity

The ability of material to conduct heat is measured as a coefficient called the thermal conductivity which is defined as the ratio of the heat flux to temperature gradient per unit length (Neville, 2011). According to Blundell & Blundell (2011)

thermal conductivity can be considered in one direction such that the heat flows from a hot part to a cold part in a material, and so it flows against the temperature gradient.

Fourier's law of thermal conductivity gives a linear relationship between the heat flow and the temperature gradient. If this law is applied, in particular, to a system in contact with two heat reservoirs at different temperatures, the heat flowing through the steady state system is constant. The equation is given as:

$$q = \lambda(T) \frac{dT}{dx} \quad (2.1)$$

Where q is heat flow ($\text{J s}^{-1} \text{m}^{-2}$); λ is conductivity ($\text{J s}^{-1} \text{m}^{-1} \text{K}^{-1}$); and T is temperature (K).

Thermal conductivity of normal concrete typically in a range 2.15 – 2.51 W/m K is more greatly affected by its composition than its density (Neville, 2011). However, Mehta & Monteiro (1997) take a different point of view that conductivity is affected not only by minerals in the aggregates but also by other factors such as moisture, density, and temperature of concrete.

The temperature fluctuation at values close to ambient room temperature has little effect on thermal conductivity. However, the value of conductivity can vary significantly at elevated temperatures (Neville, 2011). It increases slowly at temperatures up to 50 to 60 °C. Conductivity decreases sharply until water is totally lost at 120 °C, and tends to stabilise at a temperature of 120 to 140 °C. The value reaches one-half of that at room temperature when it is at 800 °C. This behaviour is illustrated in Figure 2.4.

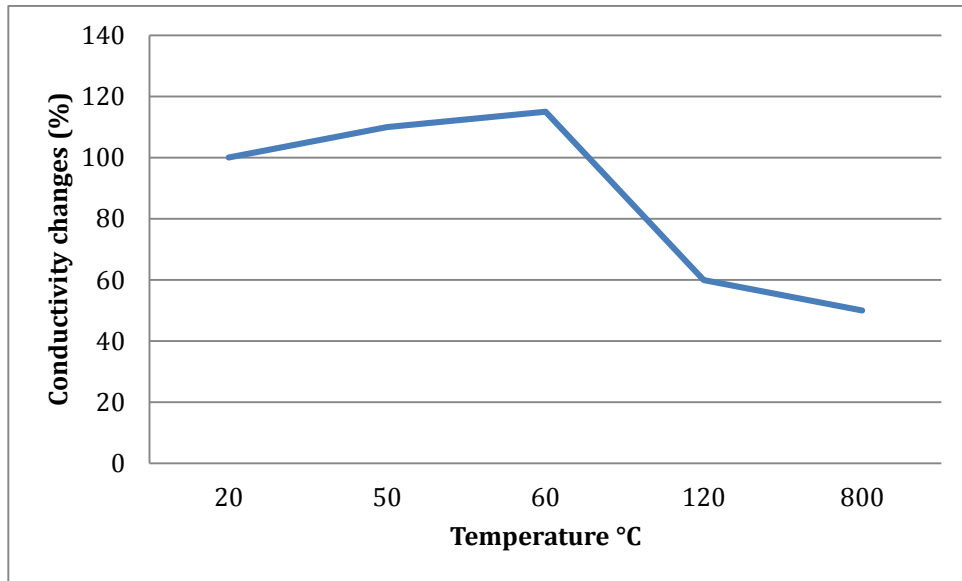


Figure 2.4 Sketch of thermal conductivity changes at high temperature exposure (Neville, 2011).

This property is normally calculated from the diffusivity, but it is possible to measure it directly. The steady-state method (hot plate and guarded hot box) is commonly used to test thermal conductivity under dry conditions. The most preferable method to test moist concrete is by using the transient method (Neville, 2011). The effect of moisture on heat transfer in materials can principally be measured using the guarded hot plate method and procedure according to ISO8302 and the supporting standards for a moist porous material in EN12664 and ISO10051 (Salmon & Tye, 2005).

2.3.2 Thermal Diffusivity

Thermal diffusivity is an important property in for transient heat flow and represents the rate of diffusion of energy through a material (m^2/s), which is calculated by the equation:

$$\alpha = \frac{\lambda}{\rho_d c_p} \quad (2.2)$$

Where: α is thermal diffusivity (m^2/h); λ is thermal conductivity ($\text{J s}^{-1} \text{m}^{-1} \text{K}^{-1}$); C_p is specific heat ($\text{J kg}^{-1} \text{C}^{-1}$); ρ_d is density of concrete (kg m^{-3}).

In equation 2.2, thermal diffusivity linearly depends on thermal conductivity which is also influenced by the moisture condition. Concrete has high thermal diffusivity causing heat to diffuse quite rapidly (Mehta & Monteiro, 1997).

Concrete generally has a diffusivity in a range of 0.002 - 0.006 m^2/h and the exact value is influenced by the type of aggregates, density, porosity, thermal conductivity and moisture content (Neville, 2011; Mehta & Monteiro, 1997).

2.3.3 Thermal Expansion Coefficient

Thermal expansion of concrete depends on two factors: on mix composition and hygric state at the time of the temperature change (Neville, 2011). The composition of concrete mainly consists of aggregate and hydrated paste both of which have different thermal coefficients. The linear thermal coefficient of paste is between 11×10^{-6} and $20 \times 10^{-6} \text{ s/}^\circ\text{C}$ which is higher than that of most aggregate.

These variations induce differential movement between paste and aggregate while concrete is undergoing a large change in temperature. Failure will happen at the bond between aggregate particles and the surrounding paste. When the change of temperature is between 4 and 60 $^\circ\text{C}$, this movement may not disturb the concrete. However, thermal shock caused by a differential of more than 50 $^\circ\text{C}$ between the surface and the core of the concrete may induce cracking. A differential coefficient of more than $5.5 \times 10^{-6} \text{ s/}^\circ\text{C}$ between two materials will affect concrete subjected to freezing and thawing (Neville, 2011).

The linear thermal expansion coefficient of cement paste is normally maximum at a relative humidity of about 70 %. Cement paste cured in high-pressure steam has no such variation in the coefficient of thermal expansion. High temperature has a large effect on cement paste; the coefficient decreases at temperatures above 150 °C and becomes negative between 200 °C and 500 °C. It happens probably because of the internal collapse of cement paste. Meanwhile in concrete, this phenomenon does not happen because the aggregate continuously expands during concrete expansion (Neville, 2011). Aggregates which have a positive coefficient at all temperatures and expand with an increase of temperature mainly contribute to the overall expansion of concrete, as shown in Table 2.6.

Table 2.6: Thermal expansion coefficients of concrete at high temperature (Neville, 2011)

Curing condition	Water/cement ratio	Cement content (kg/m ³)	Aggregate type	Linear coefficient of expansion (10 ⁻⁶ s/°C)			
				28 days		90 days	
				<260 °C	>430 °C	<260 °C	>430 °C
Moist	0.4	435	Calcareous gravel	7.6	20.3	6.5	11.2
	0.6	310		12.8	20.5	8.4	22.5
	0.8	245		11.0	21.1	16.7	32.8
Air, 50% relative humidity	0.4	435	Calcareous gravel	7.7	18.9	12.2	20.7
	0.6	310		7.7	21.1	8.8	20.2
	0.8	245		9.6	20.7	11.7	21.6
Moist air	0.68	355	Expanded shale	6.1	7.5	-	-
Air dried	0.68	355		4.7	9.7	5.0	8.8

2.4 Reactive Powder Concrete (RPC)

Research into Reactive powder concrete (RPC), categorized as a type of ultra-high performance concrete (UHPC), began with studies on pressure treatment of fresh concrete by Eugene Freyssinet in the 1930s. This resulted in a compressive strength of 650 MPa in the 1960s (Richard & Cheyrezy, 1995). RPC mixtures are

different from ordinary concrete in terms of material content. RPC has no coarse aggregate and contains a lot of fine particles (<600 µm) comprising silica fume, quartz sand and other admixtures. Although BS EN 196-1 (2005) categorizes a mixture without coarse aggregate, most scholars refer to this as reactive powder concrete (RPC) because all the aggregate components are a powder and react chemically, e.g. hydration from cement particles; pozzolonic reaction of silicate oxide from silica fume; formation of tobermorite or xonotlite from C-S-H after heat curing (Cheyrezy *et al.*, 1995).

2.4.1 Factors Influencing RPC Performance

2.4.1.1 Cement

The main binder component of RPC is cement, which is commonly characterised by chemical composition, particle size and mechanical performance. The best type of cement for RPC has low wt% C₃A content, low Blaine fineness, and high silica content (Richard & Cheyrezy, 1995). Researchers most frequently use CEM1 type cement in RPC research due to the lowest Blaine fineness and high clinker content (>95wt%), as it is usually used for high strength concrete (Matte & Moranville, 1999; Yazici *et al.*, 2008; Sadrekarimi, 2004). Although Bonneau *et al.* (2000) used four types of cement (CEM1, CEM2, CEM3, and CEM4), the effect of cement types to characterize the granular packing and percolation threshold of RPC have not been explained clearly.

2.4.1.2 Aggregate

RPC uses quartz sand as the only aggregate component which induces: an increase of mix homogeneity, a reduction of aggregate/matrix ratio; and

reduction in the size of equatorial cracking around aggregates. Fine aggregate has more angular asperities leading to a higher friction angle, if it is artificially produced by crushing stones or more spherical shapes through natural decay. Quartz is regarded as one of the best types of sand due to the hardness, interface bonding with paste, availability, and cost (Richard & Cheyrezy, 1995). In addition, quartz can react with cement paste at the cement/ aggregate interface at high temperature (Yazici *et al.*, 2008). The size of sand particles is favourable between 150 and 600 μm , to avoid interference with the largest cement particles (80 – 100 μm) (Cwirzen, 2007; Cheyrezy *et al.*, 1995; Tam *et al.*, 2010). However, using a maximum aggregate size of 3.0 mm it is still possible to produce RPC with a compressive strength of more than 200 MPa (Sadrekarimi, 2004; Yazici *et al.*, 2008). The effect of quartz size is illustrated in Figure 2.5.

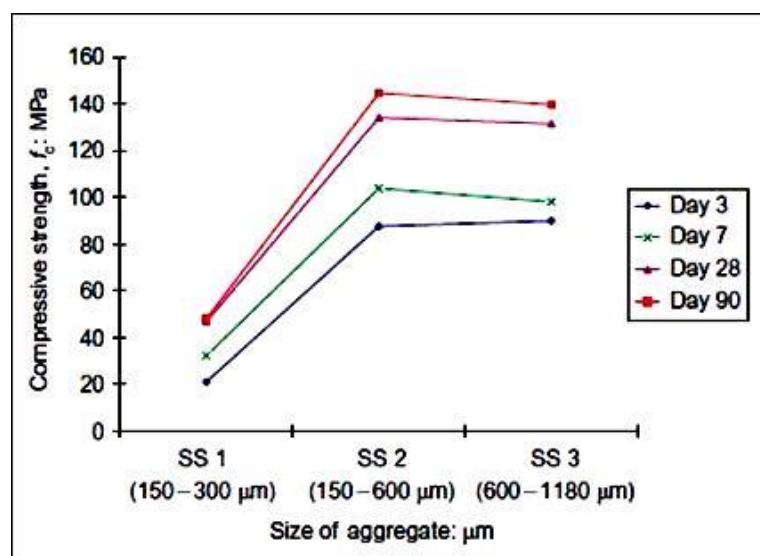


Figure 2.5 Effect of quartz size on compressive strength of RPC (Tam *et al.* 2010)

2.4.1.3 Silica Fume

Silica fume in the form of amorphous silica is a highly reactive material and, due to its high Blaine fineness, high temperature curing can accelerate the chemical

reaction of silica fume with the calcium hydroxide produced during calcium silicate hydration (Neville, 2011). On the other hand, silica fume particles can redistribute to fill the voids between cement particles and improve the rheological characteristics by a lubrication effect resulting from the high sphericity of the basic particles (Richard & Cheyrezy, 1995). A study of the effect of silica fume on the durability of RPC has been done by Matte & Moranville (1999). This focused on calcium leaching, degradation depth, and tritium diffusion. The results showed that silica fume had a positive effect on durability and the leaching process caused the disappearance of the anhydrous compounds in the altered zone. Chan & Chu (2004) studied its effect on fibre bonding and showed that the presence of silica fume increased the interfacial-toughening effect upon fibre slip due to contribution of friction and resistance during the fibre pullout process, as shown in Figure 2.6.

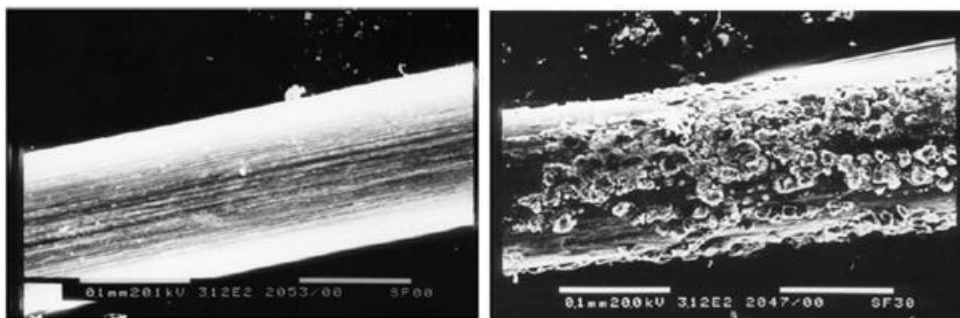


Figure 2.6 Pullout fibre surface (a) without SF; (b) with 30% SF (Chan & Chu, 2004)

2.4.1.4 Mineral admixtures

The use of mineral admixtures in RPC allows reduced cement content and has been studied by Yazici *et al.* (2008). They used PFA and GGBS for cement replacement at up to 60 wt.%, with a constant amount of additional silica fume at 35 wt.%. The list of compositions that resulted in compressive strengths of at least 200 MPa is presented in Table 2.7. The average compressive strength of

RPC is still over 200 MPa while cement content is replaced by PFA and/or GGBS with total amounts of 40 wt.%, or even by GGBS alone at 60 wt.%. The presence of PFA and/or GGBS can modify the microstructure of hardened pastes by filling the capillary pores with low density C-S-H gel (Sadrekarimi, 2004).

The results concerning the reduction of cement quantity in RPC mixtures with an amount less than 500 kg/m³ is an important one which was deemed reasonable to examine in this study. However, the use of silica fume was higher than suggested by the previous studies and needs to be reduced closer to 25% of cement weight in order to reduce surface area of finer grains as this may improve workability. It is necessary to try using a smaller size of aggregate combined with pressure.

Table 2.7: Composition per 1 m³ of RPC and compressive strength (Yazici *et al.*, 2008)

Material	Ctrl	F40	F30 G10	F20 G20	F10 G30	G40	G60
Cement (kg/m ³)	830	498	498	498	498	498	332
Silica fume (kg/m ³)	291	291	291	291	291	291	291
Fly ash (F) (kg/m ³)	-	332	249	166	83	-	-
GGBS (G) (kg/m ³)	-	-	83	166	289	332	498
1-3mm quartz (kg/m ³)	489	431	441	452	462	473	465
0.5-1mm quartz (kg/m ³)	244	215	221	226	231	236	232
0-0.4mm quartz (kg/m ³)	244	215	221	226	231	236	232
Water (kg/m ³)	151	151	151	151	151	151	151
SP (kg/m ³)	55	62	62	60	58	55	55
Steel fibre (kg/m ³)	234	234	234	234	234	234	234
Compressive strength (MPa)	262	229	234	240	230	244	202

2.4.1.5 Superplasticizer

The use of superplasticizer is essential in RPC mixtures with a low water/cement ratio to produce flowing concrete. Superplasticizer has the capability of reducing the water requirements of the mixture without affecting the workability. The ability of superplasticizer to increase the slump of concrete depends on such factors as the type, dosage, and time of addition of superplasticizer; w/c; and the nature or amount of cement.

Morin *et al.* (2001) stated that one problem associated with using superplasticizer in concrete is the effect on setting time. In small quantities superplasticizer can influence particles chemically and structurally; however, in excess of a critical amount it makes the concrete setting very difficult, as shown in Figure 2.7. Label of DE/C in figure is the ratio of superplasticizer dry extract and cement in weight. In their study they found that the presence of superplasticizer enlarged the screening layer by reducing the positive ion concentration in the vicinity of the negatively charged solid particles. Superplasticizer induced air entrapment and micro bubble formation during the mixing due to lowering the surface tension of the interstitial fluid. However, increasing the amount of superplasticizer prolonged the setting time and decreased the released power in hydration reaction. In addition, high superplasticizer content caused larger shrinkage.

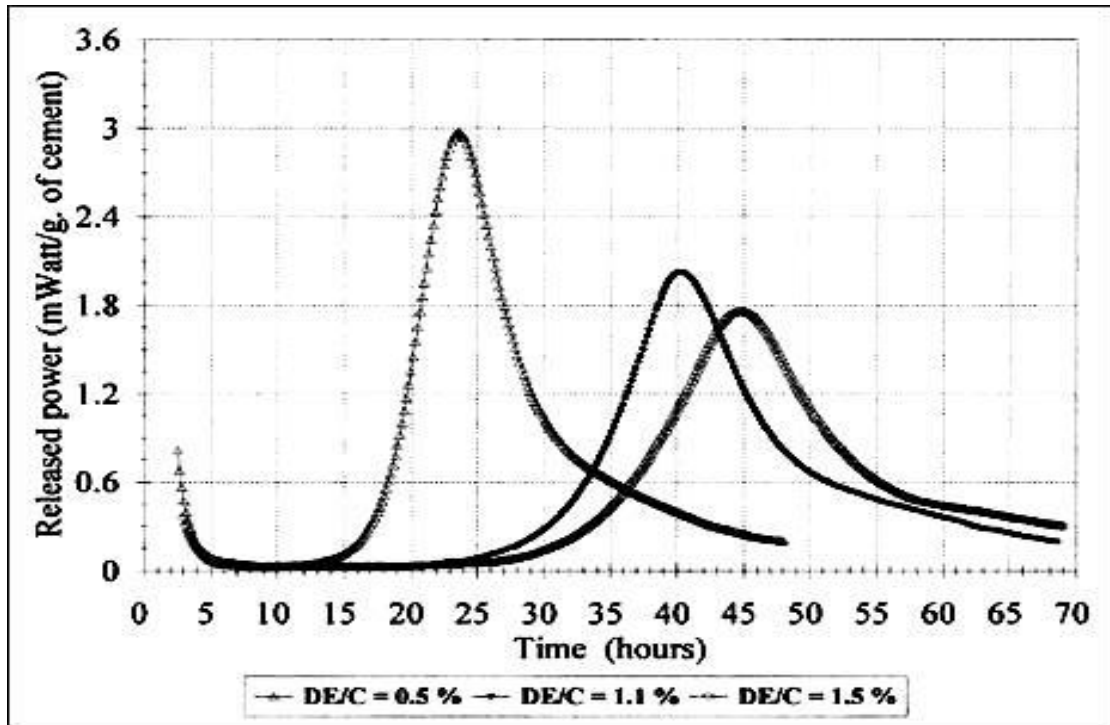


Figure 2.7 Graph of released power evolutions with time (Morin *et al.*, 2001)

2.4.2 Treatments on RPC

2.4.2.1 Pressure

The purpose of applying pressure to fresh RPC mixtures is to improve the compacted density. Static pressure can affect the mixture in three ways: reduction or even elimination of entrapped air voids; extraction of free water content; and elimination of macro porosity that appears as a result of chemical shrinkage (Richard & Cheyrezy, 1995). Duration and value of pressure are different for each study, such as: 50 MPa for 6 to 12 h (Richard & Cheyrezy, 1995); 30 MPa for 8 h (Yazici *et al.*, 2008); 40 MPa for 24 h (Cwirzen, 2007); 625 atm (Cheyrezy *et al.*, 1995); and without any pressure (Yazici *et al.*, 2009; Yazici *et al.*, 2010).

Yazici *et al.* (2008) concluded that pressure applied on a fresh mixture had a significant effect on compressive strength, as shown in Figure 2.8. Compressive

strength increased between 15% and 36% with levels of at least 300 MPa. The other important point is the highest increase happened in mixtures with the lowest cement content or highest mineral admixture replacement (G10F30 and G40).

A study on the effect of pressure on the RPC microstructure under various pressures (between 1 and 625 atm) and temperatures (between 20 and 400 °C) was analysed by using thermogravimetry (Cheyrezy *et al.*, 1995). The result showed three points:

1. the pressure had little influence on the distribution of total water content
2. pressure had the role of eliminating the trapped air and compacting the concrete
3. a combination of pressure and heating between 150 and 200 °C produced nil porosity

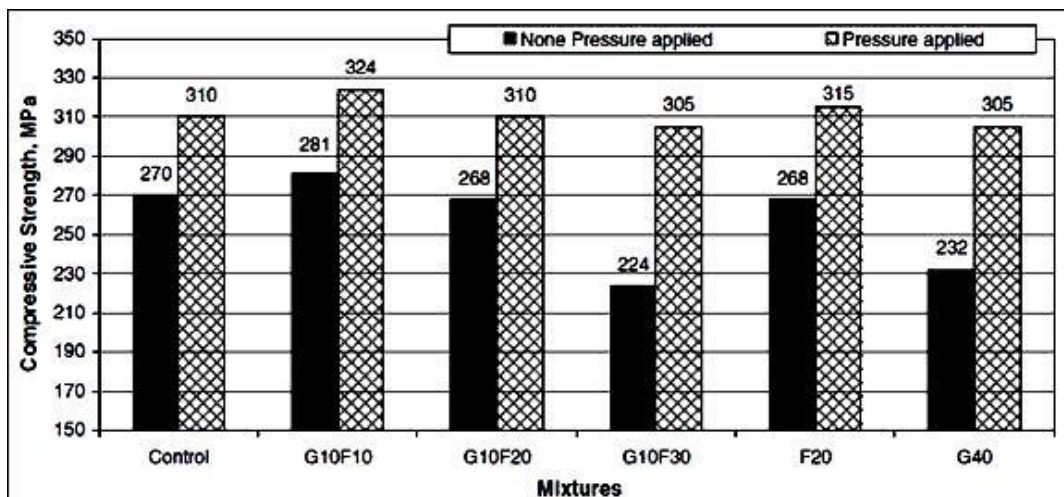


Figure 2.8 Effect of pressure on compressive strength (Yazici *et al.*, 2008).

2.4.2.2 Heat Curing

RPC is commonly heated to temperatures between 90 and 200 °C which affects the microstructure and mechanical properties. The most important effect is better crystallisation of the hydrates and activation of the pozzolanic reaction of the filler (Cwirzen, 2007). Heat curing applied by different scholars varies in terms of temperature level, duration and method, *e.g.* 210 °C for 8 h with pressure 2 MPa in autoclave (Yazici *et al.*, 2008); 240 °C in dry oven for 24 h (Cwirzen, 2007); 400 °C with pressure 625 atm (Cheyrezy *et al.*, 1995); 100 °C for 3 days in oven (Yazici *et al.*, 2009; Sadrekarimi, 2004); and 90 °C for 24 h and 48 h (Yazici *et al.*, 2010).

Yazici *et al.* (2009) studied the effect of heat curing on RPC performance. In this study, pressure was not applied on fresh RPC mixtures. Prism samples (40 x 40 x 160 mm) were kept in the mouldings at a room temperature of about 20 °C for 16 h. After demoulding, the samples were then cured by three methods: in water 20 °C for 28 days, in an autoclave with a temperature of 210 °C with pressure of 2 MPa for 8 h, and in a steam room with a temperature of 100 °C for 3 days. After heating in an autoclave or by steam, the specimens were kept in the laboratory until testing. The results are shown in Figure 2.9.

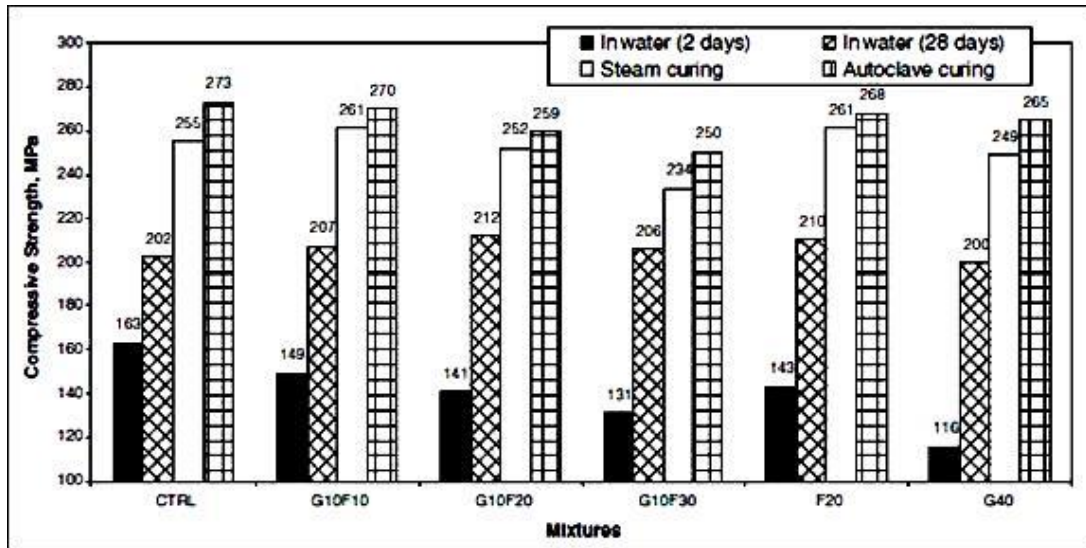


Figure 2.9 Effect of curing method on compressive strength (Yazici *et al.*, 2009).

Both methods of heat curing had a significant effect on compressive strength for all types of mixtures. The mixtures with low cement content, which are replaced by a high mineral admixture, had strength close to the control RPC mixture (100 % cement content). Compared to the control RPC at 28 days, the compressive strength of RPC increased around 21 % to 35 % for autoclaving and 14 % to 26 % for steaming. The ratio of steam/autoclave was over 93 %.

The improvement in strength is caused by increasing the pozzolanic reaction at elevated temperature, with it normally being much less reactive under standard curing. Moreover, the presence of mineral admixtures can slow down the hydration reaction, lower the heat of hydration, and decrease shrinkage. This is often a difficult problem to overcome in mixtures with high cement content and low water/cement ratios (Yazici *et al.*, 2009). Generally, the first two advantages have an impact on the setting time in slowing down the hardening process. Even though the authors succeeded to carry out the demoulding after 16 h, the method that they used to solve this problem has not been included in their

paper. In fact, demoulding of concrete with high silica fume can take at least 24 h (Tam *et al.*, 2010).

The effect of heating duration on RPC microstructure properties has been studied by Cwirzen (2007) by maintaining a constant temperature of 90 °C and varying the start and duration of heating. In this study, heating was applied at 24 h, 48 h and 168 h after demoulding for durations of 24 h, 48 h and 96 h. The results showed that longer heating times increased the degree of hydration, gave better microstructure and higher compressive strength. He found that heat curing applied for 96 h decreased the total porosity compared to that for 24 h or 48 h. More recent studies by Tam & Tam (2012) focused on microstructural behaviour of RPC under different heating regimes. They used two variables: temperature between 100 and 250 °C; and duration between 8 and 24 h. The results showed that compressive strength increased following increased duration and temperature as described in Figure 2.10. Although both studies have shown the advantages of heating in terms of time to start and duration, the correlation of both has not been explained clearly.

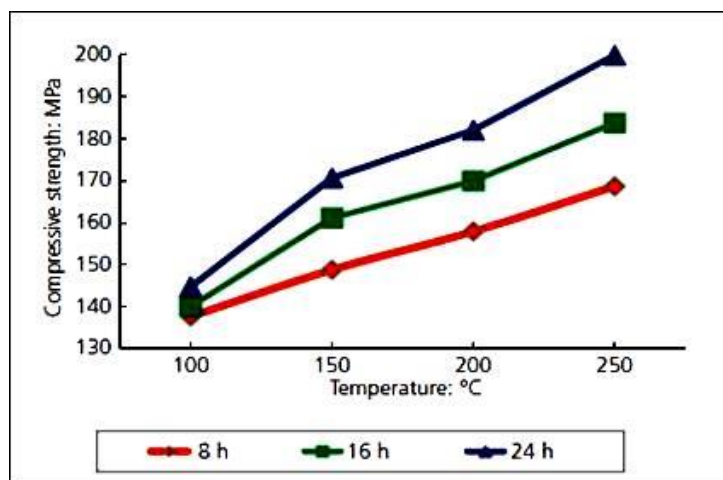


Figure 2.10 Compressive strength values measured for samples exposed to different temperature and duration of curing (Tam & Tam, 2012).

2.4.3 Mechanical Properties of RPC

The compressive strength of RPC can reach up to 800 MPa when composition and treatments are properly applied. Including steel fibres can improve the tensile strength and the level of ductility (Richard & Cheyrezy, 1995). Every variation of composition and treatment has an effect on the mechanical properties of RPC, as has been proven in many cases.

2.4.3.1 Compressive Strength

Compressive strength has been tested using RPC samples in a variety of types and sizes, such as cylindrical (Richard & Cheyrezy, 1995; Yazici *et al.*, 2008), pure cube (Cwirzen, 2007; Tam & Tam, 2012) or cubes extracted from tested prism samples (Yazici *et al.*, 2009; Yazici *et al.*, 2010). The procedure of testing followed various standards as well, such as ASTM C 116, BS1881, or BS EN 12390-3.

Tam *et al.* (2010) studied the compressive strength behaviour of RPC affected by: water/binder ratio, SP dosage, aggregate size, curing regime and heating regime. The results show that compressive strength increased continuously and linearly with age. Heating was found to have a significant effect on compressive strength in terms of temperature but not for duration. When considering practical and economic factors, the optimum composition was found to be RPC with a water/binder ratio of 0.2, SP dosage of 2.5 %, quartz particle diameter of 150 - 600 μm , and cured in water. However, this study was not complete in terms of the heating effect for 28 days or more, so the heating duration seemed to have little impact on compressive strength. This result has been improved upon in a subsequent study which came to a different conclusion; that the total duration in fact had a significant effect on the mechanical properties (Tam & Tam, 2012).

A combination of pressure and heating applied in the fresh state and curing process showed the best results of compressive strength for any condition of mixtures (Richard & Cheyrezy, 1995; Yazici *et al.*, 2008; Cwirzen, 2007). Sadrekarimi (2004) applied both treatments in a study about modified RPC in order to produce an economical material with a high ratio of strength/weight. The materials used were PC type I, silica fume with a bulk density of 0.12, superplasticizer of polycarboxylate base, quartz sand of 0.125-0.500 mm, and without fibres. The pressure applied was 40 MPa for 24 h while maximum curing temperatures were 90 and 240 °C. Samples were kept in the mould for at least 24 h. After demoulding, they were put in about 20 °C water for a week, followed by 18 days in 90 °C water. Heat curing was continued in a dry oven with a heating ramp rate of 10 °C/h until a final temperature of either 90 °C or 240 °C was reached and then held for 24 hours. Samples were tested after 28 days of treatment and curing. The results in Figure 2.11 show that compressive strength increased linearly with the percentage of silica fume used, and with the applied temperature. The increase was significant when combined with pressure. However, using silica fume in high quantities to produce RPC might be more expensive, so then this concept becomes less effective.

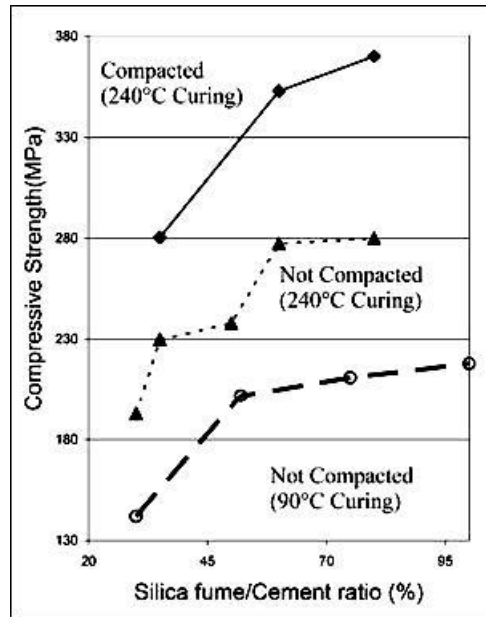


Figure 2.11 Effect of pressure and heating on compressive strength (Sadrekarimi, 2004).

2.4.3.2 Flexural strength

In general, the flexural properties of concrete have a direct correlation with the compressive strength; as compressive strength increases and flexural strength will increase as well. However, this correlation does not appear to be valid for RPC that incorporates steel fibre in the mixture and after heat curing has been applied. Yazici *et al.* (2009) studied the mechanical properties of RPC affected by the curing process and found that steam and high pressure steam curing increased the compressive strength significantly but decreased the flexural strength. Flexure tests used prismatic specimens (40 x 40 x 160 mm) loaded at the mid prism of a 130 mm span with a loading rate 0.1 mm/min. The result is presented in Figure 2.12. Flexural strength of RPC cured by steaming or autoclave generally was lower than that for 28 days standard curing. Steam curing significantly decreased flexural strength by between 11 % and 33 %. However, the autoclave only decreased the flexural strength slightly. This decrease could be explained by the fact that both curing methods induced a

weaker bond between the fibres and the matrix. This is probably due to differences in thermal properties between the fibres and matrix at high temperature.

If the result in Figure 2.12 is compared to Figure 2.9, the ratio of flexural/compressive was about 14 % for standard cured Portland cement RPC and increased to between 15 and 19 % according to mineral admixture replacement levels in the same curing regime. However, both heat curing methods decreased the flexural/compressive ratio for mixtures G10F30 and G40, which contained the lowest amount of cement replaced by maximum mineral admixtures. Cwirzen *et al.* (2008) studied the effect of steel fibre content on flexural strength of RPC with variables of 10, 20 and 30 % of cement weight. They summarized that addition of fibres from 10 % to 20 and 30 % significantly increased flexural strength from 13 MPa to 25 MPa and 36 MPa, respectively. However, a 10 % addition of fibre provided a small increase in flexural strength. Steel fibres function by restricting the initiation and the propagation of microcracks.

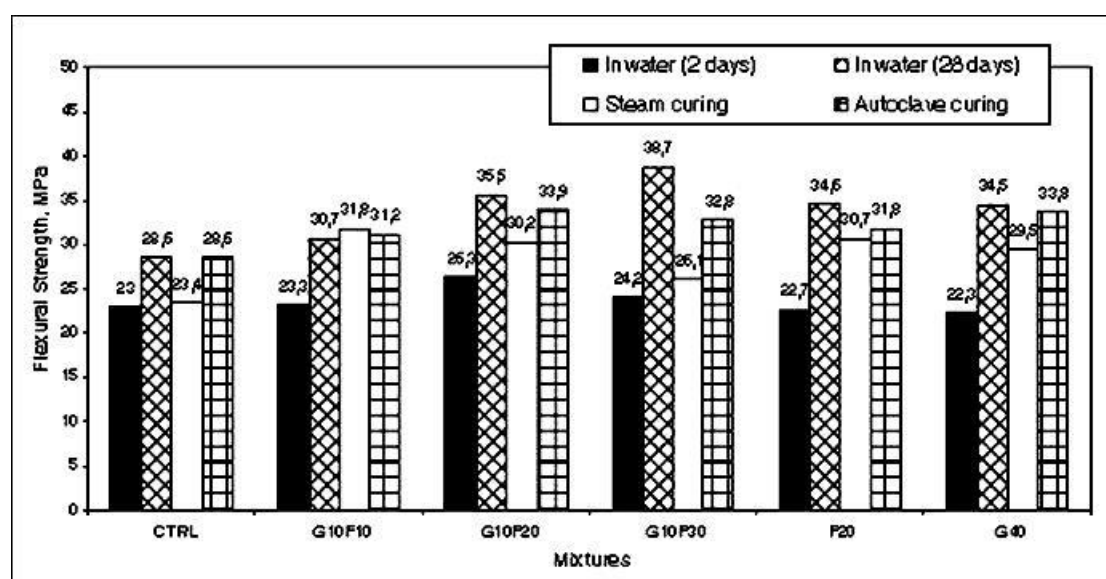


Figure 2.12 Effect of curing method on flexural strength (Yazici *et al.*, 2009)

The summary of mechanical properties from several scholars is presented in Table 2.8. It is shown that both pressure and heat curing treatments have significant effects on the mechanical properties. RPC treated with heat curing only (no pressure) may result in a high compressive strength, *i.e.* > 140 MPa. Higher temperature curing generally results in a higher compressive strength. When pressure treatment is also applied during the setting period, the compressive strength increases. On the other hand, treatments seemingly have less effect on the flexural strength as shown in Yazici *et al.* (2009). It is likely that fibre content has a significant role in determining the flexural strength.

Table 2.8: Comparison mechanical properties from several scholars

References	Heat curing (°C)	Pressure (MPa)	Compressive strength (MPa)	Flexural strength (MPa)
Richard&Cheyrezy (1995)	20 - 90	-	170 - 230	30 - 60
	240 - 400	50	490 - 680	45 - 141
Cwirjen <i>et al.</i> (2008)	90	-	181	14
Sadrekarimi (2004)	90	-	142	-
	240	-	193	-
	240	40	280	-
Tam&Tam (2012)	90	-	145	
	150	-	168	
	200	-	180	
	250	-	200	
Yazici <i>et al.</i> (2008)	210		232	
	210	30	305	
Yazici <i>et al.</i> (2009)	In water	-	200	34.5
	90	-	249	29.5
	210	2	265	33.8

2.4.3.3 Toughness

Previous studies have shown that heat curing may lower the flexural strength of RPC, but that the presence of mineral admixtures may increase it (Yazici *et al.*, 2010). The load-deflection curves recorded from flexural tests indicate the toughness of RPC, as presented in Figure 2.13.

The presence of mineral admixtures influenced the rupture behaviour in heat cured samples. This improvement indicated that heat curing contributed to the bond strength between matrix phase and fibres. The toughness of concrete containing mineral admixtures increased by between 24 and 44 % for steam curing and between 23 and 39 % for autoclaving compared to a plain mixture (Yazici *et al.*, 2009). In another study, GGBS generally affected the flexural strength, toughness and fracture energy in RPC when the quartz was totally replaced by bauxite or in some part by granite (Yazici *et al.*, 2010).

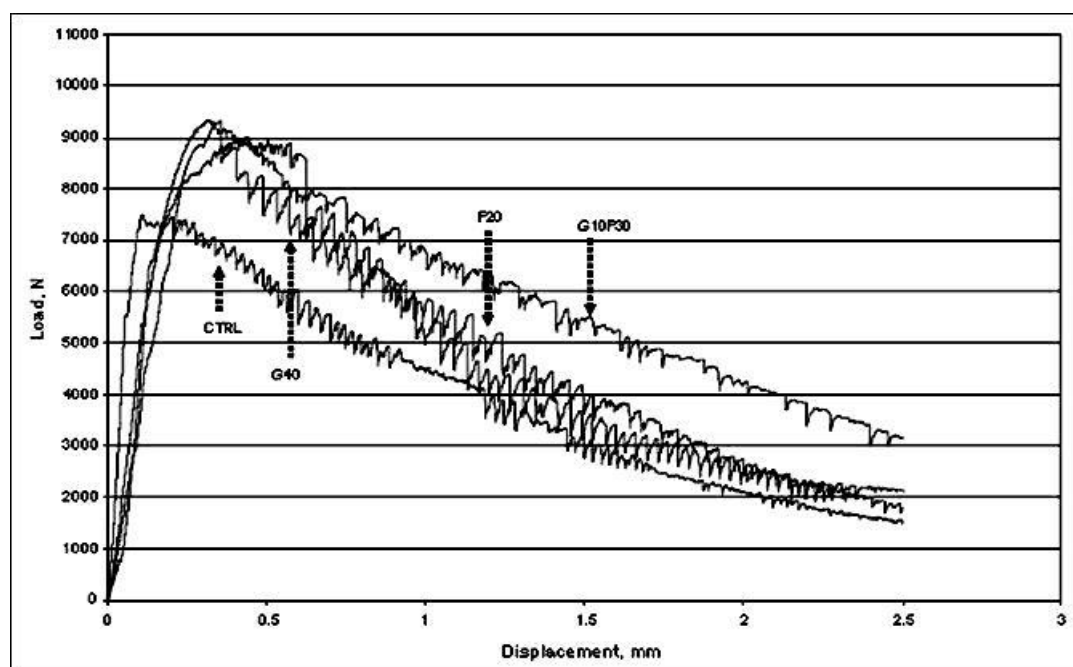


Figure 2.13 Load-displacement relationship of steaming curing (Yazici *et al.*, 2009)

2.4.4 RPC Application

The world's first major structure built with RPC is the Sherbrooke pedestrian/bikeway bridge in Canada (see Fig. 2.14) having a span of 60 m and with a compressive strength of 150 MPa and without steel bar reinforcement (Blais & Couture, 1999). The main beam of the bridge was treated by heat curing at 90 °C for two days in a vapour-saturated atmosphere. The diagonal stiffeners

of this bridge were cast in a 75 mm tube metal frame to which static pressure treatment at 2 MPa was immediately applied, followed by heat curing after one day.

Other RPC bridges have since been developed around the world such as the Sunyudo (Peace) Footbridge with a single span of 120 m (Seoul, Korea), the Sakata-Mirai Footbridge with no reinforcement and lighter by 80% than common reinforced concrete bridge (Sakata, Japan), the Shepherds Creek Road Bridge with thin permanent precast RPC formwork panels (Australia), and the Wapello Country Bridge with no reinforcement and used for a highway (USA) (Rebenstrot & Cavill, 2006). The thinnest precast concrete structure achieved using RPC is 20 mm thick and area dimensions 5 x 6 m (see Fig. 2.15), a train station roof supported by a single line of columns (150 MPa) (Vicenzino *et al.*, 2005). Its potential for even greater mechanical properties gives RPC the opportunity for many applications beyond those of conventional concrete, *e.g.* advanced lightweight composites (Sadrekarimi, 2004) or impermeable containers for hazardous fluids or nuclear waste (Vodak *et al.*, 2005).

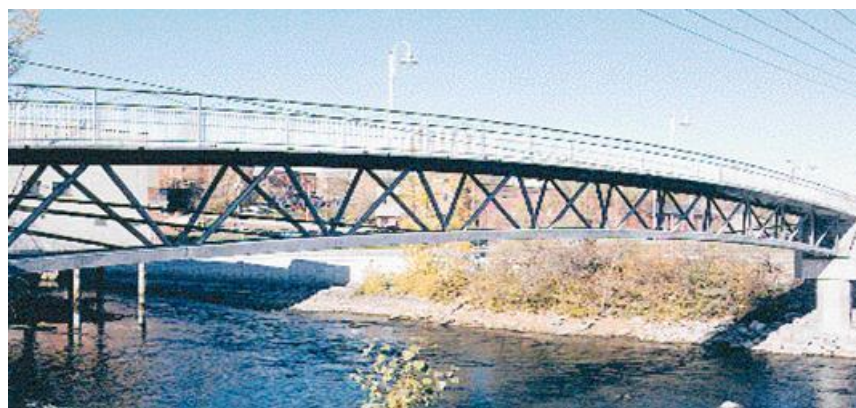


Figure 2.14 Sherbrooke pedestrian/bikeway bridge (Blais & Couture, 1999)



Figure 2.15 Train station roof supported by a single line of columns (Vicenzino *et al.*, 2005)

2.5 Durability of Concrete Under High Temperature Exposure

Durability of concrete is the ability of concrete to limit the contaminants which may permeate the porous body through liquids or air (Neville, 2011) or heat (Poon *et al.*, 2001), and therefore still to withstand the conditions of exposure. Durability depends on two factors; mechanical damage relating to the loss of integrity of concrete, and chemical damage related to chemical changes of concrete elements, which leads to strength loss over time (Domone & Illston, 2010).

Elevated temperatures have significant effects on the properties of concrete when applied during the setting process, curing period or post-hardening. Concrete can often maintain adequate residual strength after several hours of burning (Xu *et al.*, 2001; Arioiz, 2007; Poon *et al.*, 2004a; Liu & Huang, 2009; Tai *et al.*, 2011; Chen & Liu, 2004). This is mainly affected by paste chemical composition and aggregate properties, which can decompose at different temperatures during heating. Gases arise from the decomposition of both paste and aggregate minerals, leading to a build-up of internal pressures that are influenced by several factors, e.g. permeability, size of elements, and the rate of

temperature rise (Mehta & Monteiro, 1997). However, the mechanisms of property changes are very complex because they are induced by chemical and physical processes in the hardened cement paste, in aggregates, and at the interfacial transition zone (Peng, 2006).

2.5.1 Effect of High Temperature on Mechanical Properties

Studies on the effects of high temperatures on the mechanical properties of concrete mainly focus on the residual strength (Xu *et al.*, 2001; Arioiz, 2007; Poon *et al.*, 2001; Poon *et al.*, 2004a; Liu & Huang, 2009; Chen & Liu, 2004; Peng *et al.*, 2006). These are often accompanied by other tests, for example on chloride resistance (Xu *et al.*, 2001; Poon *et al.*, 2001), toughness (Poon *et al.*, 2004a; Peng *et al.*, 2006) or modulus of elasticity (Tai *et al.*, 2011). Most of these studies were predominantly focused on compressive strength although several also were concerned with indirect tensile strength in splitting (Chen & Liu, 2004) or in flexure (Peng *et al.*, 2006).

Xu *et al.* (2001) exposed PFA concrete to temperatures up to 800 °C. They found that at 450 °C the compressive strength decreased by around 15% compared to unheated samples. Furthermore, residual strengths were about 50% and 30 % of the original 28-day value at temperatures of 650 °C and 800 °C, respectively. Another study determined that PFA improved the concrete's performance significantly when exposed to temperatures of less than 600 °C (Poon *et al.*, 2001). Arioiz (2007) applied elevated temperature treatment ranging from 200 °C to 1200 °C for two hours to plain concrete samples having different types of aggregate. The results demonstrated that the compressive strength of concrete with limestone aggregate decreased by about 10% at 600 °C, and then sharply reduced as the temperature was raised to 800 °C. Residual strengths after two

hours exposure were 13 % and 6 % at temperatures of 1000 and 1200 °C, respectively.

Poon *et al.* (2004a) continued to evaluate the high temperature impact on fibre reinforced high-performance concrete using two different steel and polypropylene fibre reinforced mixtures. They concluded that steel fibre significantly contributed to the residual compressive strength where it retained more than 50 % after exposure to 600 °C, and about 30 % after exposure to 800 °C. Chen & Liu (2004) used three types of fibre in their study: steel, polypropylene and carbon with 0.6 volume fraction for each fibre type (or for a combination of fibres). This study summarised that carbon fibre increased the compressive strength of the concrete slightly more than steel or polypropylene fibre before exposure. Carbon and steel fibre could maintain the compressive strength until temperatures reached 400 °C after which strength gradually decreased and was below 40 % at temperatures above 800 °C. The behaviour of residual splitting strength was similar to compressive strength. The fibres have a high elasticity modulus and can bridge cracking inside the concrete which could control the volume changes of concrete due to rapid changes in environmental temperature.

The behaviour of RPC exposed to high temperatures has been studied by many scholars. Liu & Huang (2009) evaluated the behaviour of RPC (75.2 MPa) at elevated temperature which was compared to high performance concrete (45.4 MPa) and ordinary concrete (27.7 MPa). They demonstrated the testing of fire endurance by placing samples in heavy-oil burning and heating, according to the JIS A1304 method. Other tests investigated fire duration by setting the temperature at a fixed level of 500 ± 50 °C and heating for different durations of 30, 60, 90 and 120 min.

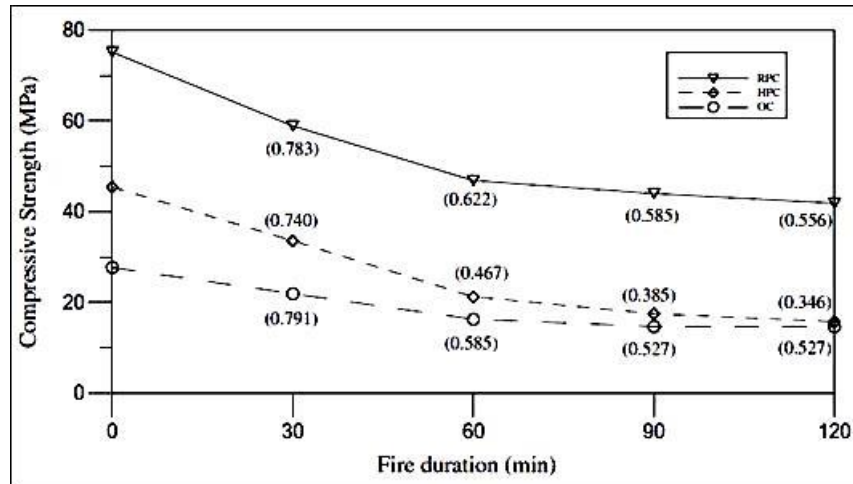


Figure 2.16 Residual compressive strengths with respect to different fire durations at a constant temperature of 500 ± 50 °C (Liu & Huang, 2009).

The result shows that compressive strength significantly reduced with increasing fire exposure duration and the residual compressive strength of RPC was higher than other concretes, as shown in Figure 2.16. However, the RPC samples used in this study were unrepresentative because the compressive strength was much lower than values recorded for RPC samples in previous studies.

Tai *et al.* (2011) evaluated the mechanical properties of RPC by placing samples in a high temperature electric furnace and heating them, according to the ASTM E119 method. Because all of the samples were destroyed after heating within a range of 400-500 °C, the heating rate was decreased to 2 °C/min and maintained for 30 min at 200 °C before increasing incrementally up to 800 °C. They summarized that compressive strength increased gradually and linearly with temperature until 300 °C, then decreased slowly to 700 °C, and finally dropped sharply at 800 °C. The residual compressive strength was about 20% after exposure at 800 °C, as shown in Figure 2.17. Based on this figure, they presented a regression expression for the compressive strength as follows:

$$\frac{f'_{cT}}{f'_c} = \begin{cases} 0.946 + 2.855 \times 10^{-3} T - 8.375 \times 10^{-6} T^2 + 4.648 \times 10^{-9} T^3, & v_f = 0.01 \\ 1.059 + 1.053 \times 10^{-3} T - 4.223 \times 10^{-6} T^2 + 2.066 \times 10^{-9} T^3, & v_f = 0.02 \\ 0.984 + 9.782 \times 10^{-3} T - 3.923 \times 10^{-6} T^2 + 1.919 \times 10^{-9} T^3, & v_f = 0.03 \end{cases} \quad (2.3)$$

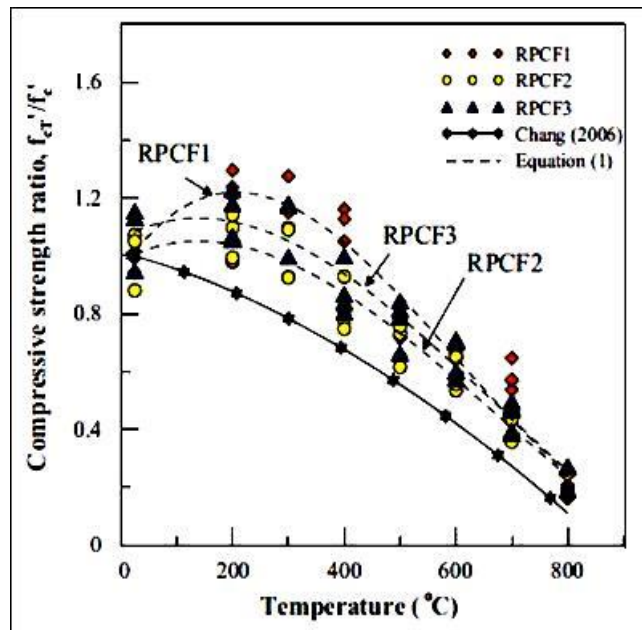


Figure 2.17 Residual compressive strength of RPC (Tai *et al.*, 2011)

Even though the heating process applied by the authors was not in accordance with the standard, by using a longer time to reach the temperature target they succeeded in showing a modification of high temperature testing on RPC by lowering and holding the heating rate.

Residual toughness of fibre reinforced concrete after exposure has been studied by Peng *et al.* (2006) based on flexural testing. Concrete was mixed with steel and polypropylene fibres and heated to 400 °C. A prism sample with a notch at the middle was subjected to one-point loading at a rate of 0.05 mm/min. They found that the toughness of steel fibre concrete increased by about double at a temperature 400 °C, compared to samples without heat exposure. The fracture energy was increased because the process of fibre pull out could take place during fracture by preventing the crack from being wider and longer.

2.5.2 Effect of High Temperature Exposure on Physical and Chemical Properties

Various other factors have been studied together with mechanical properties of concrete under high temperature such as mass loss (Arioz, 2007; Liu & Huang, 2009), appearance and colour (Arioz, 2007; Liu & Huang, 2009; Thai *et al.*, 2011), spalling (Peng *et al.*, 2006), composition change (Shin *et al.*, 2002) and microstructure (Thai *et al.*, 2011). All of these factors generally are studied together with the mechanical properties of concrete after exposure.

High temperature exposure can reduce the mass of concrete which impacts then on the loss of concrete strength. The level of loss is proportional to the decrease of weight loss (Cheyrezy *et al.*, 1995). Total weight loss of RPC is less than HPC and ordinary concrete (OC) at the same temperature or duration of heating (Liu & Huang, 2009). For instance, these authors report that at temperatures between 600 and 800 °C, the mass loss was 2.37 and 6.15 % for RPC and HPC, respectively. Mass loss of RPC cured at elevated temperature and pressure was found to be lower than when cured in water at 27 °C. Pressure can densify the microstructure and high temperature curing can accelerate the chemical reaction between quartz sand and silica fume. Moreover, both treatments increase the bond of particles in RPC.

Elevated temperature has an effect on the cracks appearance and colour which can be observed on the surface of concrete. In HPC no change to the surface has yet been observed at temperatures below 400 °C, but cracks appear when temperatures reach 600 °C (Arioz, 2007). Meanwhile in RPC, there is no effect on the surface when temperatures are below 300 °C. Small cracks appear at 400 °C and the colour becomes greyish brown. At 600 °C, cracks expand progressively and the colour changes to a darkish grey colour. At temperatures

of 700-800 °C, RPC becomes brittle and contains more pores and large cracks and becomes a darkish brown colour (Tai *et al.*, 2011).

Elevated temperature also produces an impermeable wall as a result of higher temperature outside of the specimen (Anderberg, 1997). The water vapour and air are evacuated during the heat curing process. When there are no net macroscopic flows of mass or energy, either within a system or between systems, then thermodynamic equilibrium conditions are satisfied. Furthermore, the vapour condenses again and results in a quasi-saturated layer between the dehydrating and initial state elements, which forms as an impermeable barrier for gas diffusion.

2.5.3 Effect of High Temperature on Thermo-Physical Properties

Thermo-physical properties fundamentally contain three factors (thermal conductivity, thermal diffusivity and specific heat capacity) that are needed in heat transfer calculations (Dos Santos, 2003) and to predict material behaviour after exposure to elevated temperatures (Shin *et al.*, 2002; Zhou & Hao, 2008). After exposure, the density decreases because of the evaporation of free water, and decomposition of chemically bound water, calcium oxide and carbon dioxide. This means that increasing temperature causes a decrease of density, conductivity and diffusivity (Shin *et al.*, 2002). This decrease is related to the thermal expansion coefficient, *i.e.* volumetric expansion during heating.

Khaliq & Kodur (2011) studied the effect of temperature on the thermal properties of high-strength concrete (HSC), self-consolidating concrete (SCC) and fly ash concrete (FAC). Two types of fibres (steel and polypropylene) were mixed in fibre-reinforced HSC and SCC. The temperatures applied varied in the range of 20 - 800 °C for conductivity and specific heat measurements, and of 20-

1000 °C for thermal expansion. This study concluded that thermal properties were affected by the type of concrete and the temperature range. At temperatures up to 800 °C, thermal conductivity decreased and thermal expansion increased. Specific heat capacity was approximately constant at temperatures up to 400 °C, then increased slightly and was relatively constant in the range 600-800 °C. The addition of steel or PP fibres had little effect on thermal conductivity, but increased the specific heat and thermal expansion of SSC, and decreased for HSC. The SSC containing higher chemical and mineral admixtures produces a lower permeability concrete. At temperatures above 600 °C, the loss of chemically bound water in hydrates causes shrinkage which may depend on fly ash content. The presence of fibre may also contribute to differential thermal expansion.

A similar study has been done by Liu *et al.* (2012) on RPC with variable volume fraction of shear-type, extra-fine short steel fibres. The fibres were 0.2-0.22 mm in diameter, 13 mm in length and with a direct tensile strength of 2900 MPa. Heating rate was 5 °C/min with a maximum temperature of 250 °C. The study found that at a given temperature, fibre volume fraction significantly increased the thermal diffusivity and decreased the heat capacity. Steel fibre as a good heat conductor contributes to these properties. If more fibre is used in the mixture, the heat will spread easier. Meanwhile temperature level increased the heat capacity; decreased thermal conductivity and thermal diffusivity; and had less effect on linear expansion and bulk density. However, this study applied lower temperatures than previous references and the information about compressive strength of RPC has not been presented yet. Therefore, a study on RPC thermo-physical properties at higher temperatures is still needed.

2.6 Microstructure Characterisation

Hardened concrete at micro scale focuses on the cement paste in terms of its constituents and where chemistry and thermodynamic actually begin to play a role (Dolado & Breugel, 2011). The microstructure of concrete develops by hydration reaction between the anhydrous cement grains and water to produce hydrates and to increase the solid volume of the system. This additional solid connects the spaces between cement particles which leads to the formation of a solid mass (Scrivener, 2004).

2.6.1 Microscopy

The characteristics of hardened paste taken from concrete samples are often not very different from those of pure cement paste (Diamond, 2004). The key features of paste microstructures can be captured by back scattered electron detector mode using SEM (Yazici *et al.*, 2008; Yazici *et al.*, 2009; Yazici *et al.*, 2010; Scrivener, 2004; Diamond, 2004; Scrivener *et al.*, 2004) as shown in Figure 2.18.

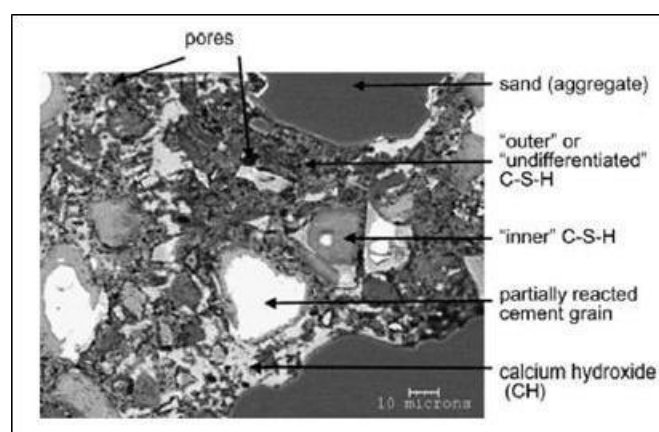


Figure 2.18 Typical BSE image of a Portland cement mortar (Scrivener, 2004)

2.6.2 Porosity

Porosity is defined as the volume of all voids in concrete which is expressed as a percentage of the overall volume of the hydrated cement paste (Neville, 2011). The voids content consists of: entrapped air, capillary pores, gel pore, and entrained air. The expression of diameter in terms of pore size represents a sphere with the same ratio of volume to surface area as the totality of the pores. The strength of hydrated cement fundamentally depends on its porosity and on the pore size distribution (Neville, 2011).

The methods to define the porosity are various and do not have the same values because the process of porosimetry measurement (especially if it involves removal or addition of water) affects the structure of hydrated cement. Mercury intrusion porosimetry (MIP) is a common method applied to analyse the porosity of hardened cement because of its relative ease and simplicity (Cwirzen, 2007; Abell *et al.*, 1999; Diamond, 2000).

It assumes that pores become narrower with depth while, in fact, some pores have a constricted entrance (Neville, 2011). Cylindrical pores which can entirely and equally be intruded by mercury are used as the pore network model assumption upon which pore size distribution can be calculated using the Washburn equation. The pore size distribution is defined with respect to the volume of mercury intruded at each pressure increment, while total porosity is from the total volume intruded. The largest differential intruded volume where percolation has occurred is known as the effective or threshold diameter (Abell *et al.*, 1999).

Washburn equation clearly provides a simple and convenient relationship between applied pressure and pore size. Pore size distributions are therefore generated by monitoring the amount of non-wetting mercury intruded into pores

as a function of increasing applied pressure (Leon, 1998), and the equation is given as:

$$l^2 = \frac{r \gamma_L \cos \theta}{2\eta} t \quad (2.4)$$

l is the length of the liquid column at time t (m)

r is the radius of the capillary (m)

γ_L is the liquid vapour interfacial tension (N m⁻²)

θ is the contact angle between the liquid and the capillary wall (°)

η is viscosity of the liquid (dynes cm⁻²)

A typical result of MIP measurement is shown in Figure 2.19.

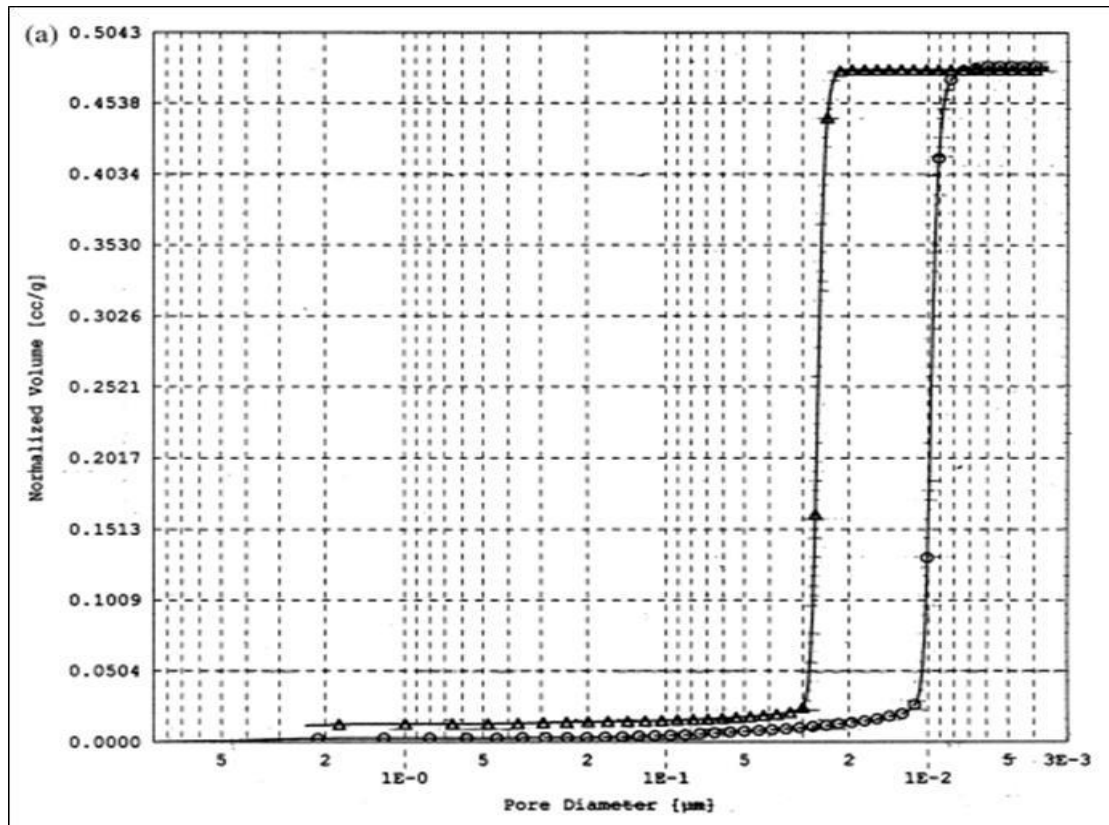


Figure 2.19 Standard mercury intrusion/extrusion volumes as a function of pore sizes (Y-Leon, 1998).

Figure 2.19 shows that mercury extrusion curves do not overlap intrusion curves.

Y-Leon (1998) stated that there are three typical explanations for this

phenomenon: i) the ink-bottle pore assumption; (ii) network effects, i.e. an

extension of the ink-bottle concept which is substantiated by complex computer simulations; and (iii) pore potential theory whereby mercury is not subjected to pore wall interactions during its initial intrusion but is partly held in pores upon extrusion as a function of wall interactions.

2.6.3 Thermogravimetry

Thermogravimetry is the continuous measurement of a material's mass changes, as a function of a combination of temperature with time, and additionally of pressure and gas composition. The process to conduct thermogravimetric analyses (TGA) on concrete has been explained by Liu & Huang (2009). Samples are taken from the inner core of the concrete and then ground to powder. TGA measurements were carried out by employing a Pyris 6 thermogravimetric analyser. The total weight of sample was set to be within the range of 38–48 mg and placed in a chamber of the thermogravimetric analyser. Then, the chamber of the thermogravimetric analyser is heated up from room temperature to 1000 °C at a constant heating rate of 25 °C/min under nitrogen atmosphere.

The weight losses obtained from TGA samples subjected to temperatures that represent different fire conditions and durations, and can provide some physical insights about the changes of microstructure and mechanical properties of concrete after fire. Thermogravimetry of RPC has been done by Cheyrezy *et al.* (1995) and their result is shown in Figure 2.20.

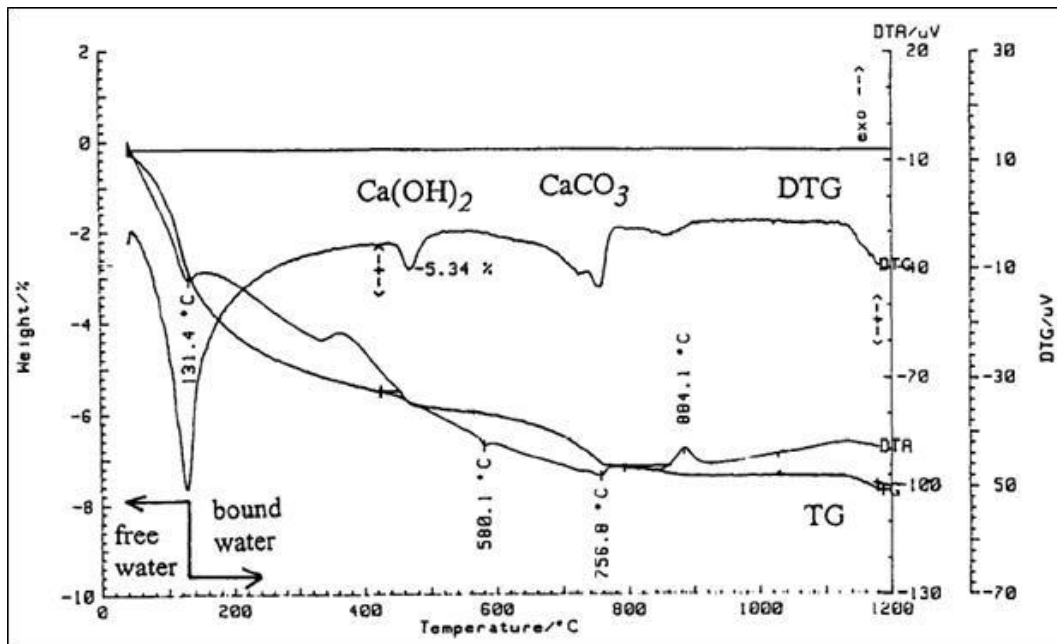


Figure 2.20 Curves of TGA and DTG measurements (Cheyrezy *et al.*, 1995)

The figure shows that the derivative thermogravimetric (DTG) fluctuates as a function of temperature. The weight loss between 20 °C and the temperature of the first DTG peak is due to loss of water not chemically bound in hydrates (free water). The next water losses at temperatures higher than that of the first DTG peak are due to structural water (dehydration of CSH, dihydroxylation of portlandite): between 420 and 500 °C the effect was identified as dihydroxylation of portlandite $\text{Ca}(\text{OH})_2$; between 750 and 850 °C it was attributed to decarbonation of calcite CaCO_3 .

2.6.4 Mineralogy and Chemical Composition

The hydration reaction in Portland cement paste is mainly governed by the reaction of the tricalcium silicate (C_3S) which produces calcium hydroxide (CH) and calcium silicate hydrate (C-S-H). The position of these two is very different; CH is deposited in the water-filled pores and C-S-H is predominantly around the

cement grains. In fact, Portland cement contains not only C₃S (alite), but also C₂S (belite), C₃A (aluminate) and Ca₂S(Al,Fe) (ferrite solid solution) (Scrivener, 2004).

Among these four main compounds, the biggest contributor to strength in Portland cements are C₂S and C₃S which finally produce C₃S₂H₃ (Neville, 2011; Illston, 1996). The physical properties of the calcium silicate hydrates characterize the behavior of setting and hardening of cement. The C-S-H formed in extremely small interlocking crystals grows out from the cement grains to occupy previously water-filled spaces (Illston, 1996). By electron microscopy these hydrates reveal a crystalline nature (Neville, 2011). The chemical reaction of both is illustrated as follows:



Figure 2.21 illustrates the content of the microstructure of hardened concrete which contains: unhydrated cement remnants (A), inner product C-S-H (B), calcium hydroxide (C), and a large amount of porous groundmass containing many Hadley grains, both fully hollow fine grain shells (D) and partly hollowed out larger grains (E) (Scrivener, 2004; Diamond, 2004).

The unhydrated cement fragments (A) have a much higher electron backscatter coefficient than the hydrated product. The variations in the grey level may be observed in C-S-H phase which contains variable composition, such as: ettringite, monosulfate, etc. The degree of microscopy may also affect these variations (Scrivener, 2004), the brighter zone being less porous (Diamond, 2004). Therefore, they appear in backscatter SEM images as high *H* intensity regions or artefacts. Most of these are surrounded by smooth textured uniformly grey hydration product shells of varying thickness.

The complete hydration cement or inner product C-S-H appears non-porous and lacks the presence of a bright core. Most of these particles are slightly smaller than unhydrated particles. However, this appearance does not guarantee that they have completely hydrated on the plane of observation; there may exist unhydrated core below the plane.

The calcium hydroxide (C-S-H gel) constitutes a convenient collective term for a range of quasi-amorphous particles containing calcium, silica, and water that have been produced by hydration of the C_3S and C_2S in cement. These products are deposited within the hardened cement paste structure, and appear smooth-textured and at a uniformly grey level.

The groundmass or 'outer product' which is deposited in the originally water-filled space is irregularly textured. These areas appear mostly darker overall than the inner product hydration shells, contain many individually recognizable pores, host extensive deposits of CH and the minor hydration products (ettringite, monosulfate, etc) (Scrivener, 2004). In contrast, the outer product may be slightly brighter than the inner product when C-S-H is formed earlier in the hydration sequence (Diamond, 2004).

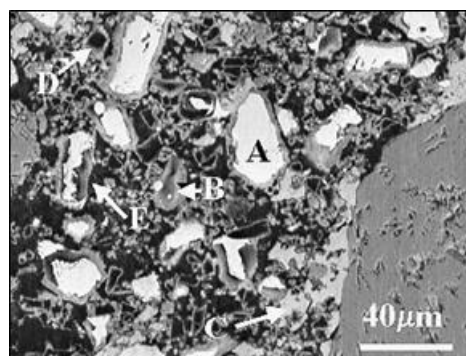


Figure 2.21 Microstructural features of hydrated paste in a 3-day (Diamond, 2004)

2.6.5 Microcracks Progression

The actual strength of hydrated cement paste is very much lower than the theoretical strength estimated on the basis of molecular cohesion, and calculated from the surface energy of a homogeneous and flawless solid material. In fact there are defects which lead to high stress concentration in material under load and microcracks (Neville, 2011).

Hydrated cement has numerous non-homogeneous discontinuities such as pores, microcracks and voids, but the exact nature of their effect on the strength is not known. The voids themselves need not act as flaws, but the flaws may be cracks in individual crystals associated with the voids or caused by shrinkage or poor bond. The pores in the cement paste are not the only possible critical flaws. So the mechanism of concrete rupture is probably related to the bond within the hydrated cement paste and between the paste and the aggregate (Neville, 2011).

In general, there are very fine cracks at the interface between coarse aggregate and cement paste, even before loading. These are probably caused by the differences of mechanical properties and modulus of elasticity in terms of shrinkage and thermal movement between aggregate and paste. Microcracks appear not only in normal concrete but also in wet-cured concrete with a water/cement ratio as low as 0.25 without any load. The existing microcracks are assumed to be responsible for the low tensile strength of concrete (Neville, 2011). Under compressive loading, the increase of microcracks mostly contributes to the non-linear stress-strain behaviour of concrete (Scrivener *et al.*, 2004).

2.7 Interfacial Transition Zone (ITZ)

The Interfacial Transition Zone (ITZ) is the narrow region between the cement paste and the aggregate, and is very important in terms of controlling the bulk physical properties and performance of concrete (Scrivener *et al.*, 2004). This region is structurally the weakest zone in concrete because it contains the most pores, a high quantity of CH, and fewer cement particles compared to the bulk region (Mehta & Monteiro, 2006). The ITZ microstructure properties are generally defined by analysis of BSE images near the aggregate (Gao *et al.*, 2014). In ordinary concrete, the ITZ contains large pores in a region with a total width typically between 0.05 to 0.1 mm (Neville, 2011). Although RPC generally contains sand only, with a particle diameter range of 150 – 600 μm , a measureable ITZ can usually be found (Tam *et al.*, 2010).

Regarding the microstructure of concrete at meso scale, the interfacial transition zone (ITZ) between cement paste and aggregate is one of the features that is commonly characterised (Zhou & Hao, 2008; Dolado & Breugel, 2011). The ITZ is the weak part in concrete due to development of multiple microcracks predominantly after the peak load. The origin of the ITZ lies in the so-called “wall” effect of packing of cement grains against the relatively flat aggregate surface. This is directly responsible for the features of the ITZ, particularly its higher porosity (Peng *et al.*, 2011).

2.7.1 Wall effect (porosity)

“A wall effect” is formed by the large difference of size between aggregate and cement particles that disrupts the packing of the cement grains, resulting in the “wall” effect as described in Figure 2.22 (Peng *et al.*, 2011). The result is that a zone closest to the aggregate contains predominately small grains and has a significantly higher porosity, while larger grains are found further out.

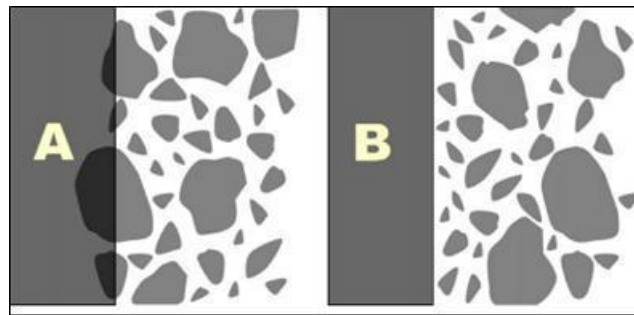


Figure 2.22 Illustration of wall effect (Peng *et al.*, 2011)

Cement grains have grain diameters typically between 2 – 70 μm , and it is difficult to consolidate them with the same efficiency around the much larger aggregate particles due to the “wall effect”. This imposes packing constraints and creates a region that has higher porosity and smaller grains (Scrivener *et al.*, 2004). ITZ thickness depends on the median size of cement grains, not on the aggregate size, because the aggregate surface is assumed locally flat due to a huge difference between the size of the two (Bents *et al.*, 1992).

The size of the ITZ is comparable with the size of the cement grains and each individual region of ITZ will be different. Therefore the average effects may not be immediately apparent in images of concrete microstructure. However, even in good quality concretes, it is quite usual to observe heterogeneities in the microstructure on a scale of several hundred microns as shown in Figure 2.23. In area “1” the microstructure has a significantly higher porosity, while in area in “2” there is a concentration of calcium hydroxide along the lower edge of the aggregate, but such concentrations are not observed around all aggregates.

Porosity is the volume not filled by cement grains or hydration products. The hydrate redistribution has an important role to modify the excess porosity in the ITZ. On mixing the porosity adjacent to the interface is some 40% higher than

that in the bulk. After the first day this difference is reduced to only 10–20 % and the gradient is less steep. At greater ages the porosity in the ITZ reduces by about the same amount as it is reduced in the bulk. As there is much less anhydrous material remaining in the ITZ, this reduction must be attributed to the deposition of hydrates from the migration of ions from the reaction of cement further from the interface.

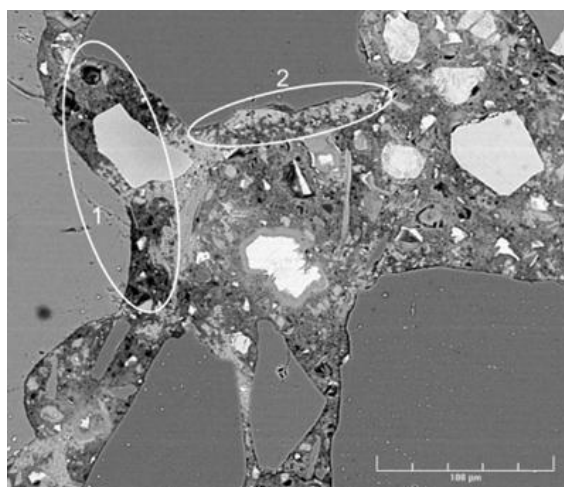


Figure 2.23 Typical inhomogeneity of ITZ (Scrivener *et al.*, 2004)

2.7.2 Chemical Composition

The ITZ is formed by the packing of the anhydrous cement grains which is eventually affected by the way of depositing of hydration products in this region. There are two major hydrate phases, calcium silicate hydrate (C-S-H) and calcium hydroxide (CH) which are formed during the hydration process. The C-S-H phase is mostly deposited directly around the cement grains whilst the calcium hydroxide is mainly deposited in the open pores. Furthermore, silica prevents the nucleation of calcium hydroxide and helps to move the nucleation process away from the cement grains. The microstructure formed in this phase is shown in Figure 2.24.

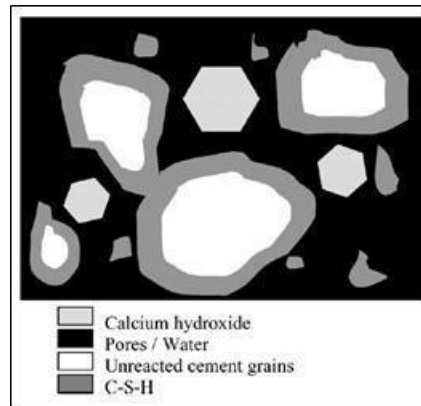


Figure 2.24 Representation of the microstructure of Portland cement paste (Scrivener *et al.*, 2004)

As the quantity of anhydrous material in this region is low, most of this calcium hydroxide must form from calcium ions coming from the reaction of anhydrous cement outside the interfacial region. The zone of increased calcium hydroxide corresponds very closely to the zone which is deficient in anhydrous material on mixing, *i.e.* has excess porosity. The ITZ contains excess calcium hydroxide compared to the bulk because the wall effect packing forms zones: a porosity zone containing 'bigger' grains and placed far away from the aggregate; a dense zone containing 'smaller' grains close to the aggregate.

The other hydrate product whose distribution is found in the ITZ is ettringite (Scrivener, 2004). Ettringite can be found as a secondary product in sulphate attack, often in air voids, and in cracks and rims surrounding aggregates in concretes subject to delayed ettringite formation (DEF) (Diamond, 2004). The small crystals of ettringite cannot be easily resolved in BSE images, so X-ray diffraction is used and progressive polishing on model specimens (Scrivener, 2004; Diamond, 2004). The ions forming ettringite are highly mobile in cement pastes, as witnessed by the recrystallisation of ettringite into pores and voids in mature concretes (Scrivener, 2004).

Peng *et al.* (2011) studied the ITZ properties of RPC containing fly ash and steel slag in the mixture. The microstructure of the ITZ was investigated by utilization of a JSM 5610 electron microscope (SEM) with an accelerating voltage of 20 kV. The result is shown in Figure 2.25. They found that sand-paste ITZ has a low porosity and the bond between the sand and paste is quite close. There is no obvious pore or crack existing in the ITZ and the boundary of the sand becomes blurred. This blur means that quartz sand had reacted with cement paste because of heat curing.

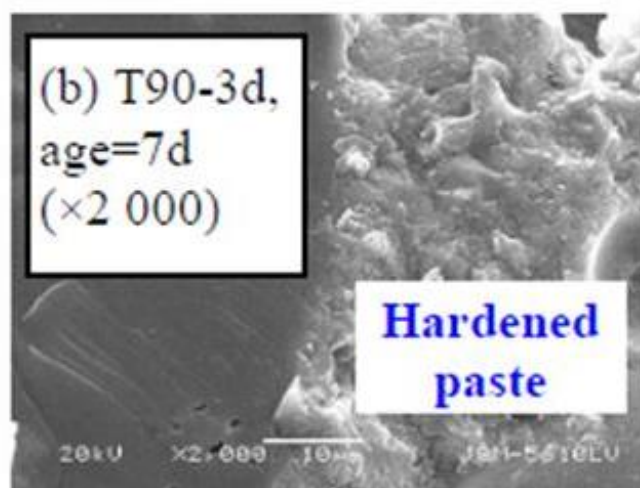


Figure 2.25 Microstructure of the aggregate-paste interfacial zone in UHPC samples (Peng *et al.*, 2011)

The chemical composition of hydrated materials in cement paste can be detected by energy-dispersive spectroscopy (EDS) which is connected together with an SEM instrument. Hydrated cement contains around 60-70% of C-S-H and is the main component of concrete strength, having a Ca/Si ratio between 0.7 and 2.3 (Dolado *et al.*, 2007). As heat curing can transform the crystallized product, the ratio of Ca/Si may indicate the type of C-S-H, *i.e.* whether tobermorite (in the range of 0.6 - 0.9) or xonotlite (around 1) (Diez & Bohnemann, 2000).

2.8 Summary

Reactive powder concrete (RPC) has no coarse aggregate and contains a lot of fine particles ($<600\ \mu\text{m}$) from silica fume, quartz sand and other admixtures. It is labelled 'reactive' because all the components may react chemically such as: hydration from cement particles; pozzolanic reaction of silicate oxide from silica fume; formation tobermorite or xonotlite from C-S-H after heat curing.

Heat curing can be applied by various methods, such as: placing demoulded samples in an autoclave, steaming fresh mixture in the mould, or heating demoulded samples in a dry oven. Heat curing at a low temperature up to $90\ ^\circ\text{C}$ contributes to both the progression of cement hydration and the acceleration of pozzolanic reaction. When it increases higher than $90\ ^\circ\text{C}$, the hydrate transforms to become tobermorite at a temperature of $150\ ^\circ\text{C}$ and xonotlite at temperatures between 200 and $250\ ^\circ\text{C}$.

Properties of RPC are influenced by three factors: composition, pressure during setting period, and heat curing. Since GGBS can be used as a partial cement replacement and this results in positive mechanical and microstructural properties, the problem of high cement content in RPC due to high shrinkage and cost has been solved. The use of a lot of ultrafine powders results in very dense concrete which has the potential to be implemented as a type of fire-resistant concrete.

High temperatures exposure of RPC produces significant effects on the durability, that is the ability of concrete to limit the contaminants which may permeate the porous body through liquids or air or heat but no rupture after exposure. Its durability may be indicated by physical, mechanical or chemical alterations which lead to strength loss over time depending on the temperature exposure level. This decrease is commonly affected by paste chemical composition and

aggregate properties which can decompose at different temperatures during heating. RPC has a better performance than HPC and can often maintain adequate residual strength after several hours of burning.

Evaluation of the effects of high temperature on durability of RPC at micro scale has mostly been focused on the cement paste. Its effect on paste morphology such as unhydrated cement grains, inner product C-S-H, calcium hydroxide (C), other hydrates and pores can be captured by back scattered electron detector mode using an SEM instrument. In addition, the SEM images can also be used to analyse crack progression and ITZ properties. When SEM instruments are used with energy-dispersive spectroscopy (EDS), the chemical composition of hydrated materials can also be evaluated. Porosity changes can be detected by MIP which describes the evolution of pore size and the pore distribution. The differences in hydrates formed can also be measured by TGA based on the material's mass changes, as a function of a combination of temperature and time.

Chapter 3- Experimental Program

3.1 Experiment Methods in Brief

In order to assess the thermo-physical and durability properties of RPC, this research has conducted a set of laboratory experiments. This chapter presents the general information on the experiments which includes material type, sample fabrication and the initial treatments, method of testing, and finally the response to high temperature exposure on RPC.

3.2 Materials

3.2.1 Binder

The main binder was CEM1 52.5 cement (Rugby, Cemex UK), in accordance with BS EN 197-1:2011. The silica fume was used along with microsilica grade 940-D (Elkem, Switzerland) and Ground Granulated Blastfurnace Slag (GGBS) (Hanson, UK) was used as a partial cement replacement. The colour of materials is shown in Figure 3.1 and their properties are presented in Table 3.1.



Figure 3.1 Binder material

Table 3.1: Chemical and physical properties of cement, silica fume and GGBS

Properties	Cement ^a wt.%	Silica fume ^a wt.%	GGBS ^b wt.%
SiO ₂	20.09	>90	35.00
Al ₂ O ₃	4.84	-	12.00
Fe ₂ O ₃	3.87	-	0.20
CaO	64.02	-	40.00
MgO	1.15	-	10.00
SO ₃	2.83	-	-
Loss on ignition %	2.36	<3	-
Specific gravity	3.15	2.2	2.9
Blaine finesse (m ² /kg)	395	22400	450

^a (Mohammed *et al.*, 2014)

^b (Hanson, 2009)

3.2.2 Sand

Quartz sand (David Ball Ltd. UK) was used where, $G = 2.65$ and water absorption = 1.5 %, with gradation conforming to BS 1881-131. This study used three grades of sand: A (2.36 mm - 1.18 mm), C (0.60 mm - 0.30 mm) and E (0.15 mm - 0.09 mm). These grades were mixed in a ratio of 2A:1C:1E (by mass) to produce a suitable particle size distribution as suggested in Yazici *et al.*, (2008).



Figure 3.2 Quartz sand grades

3.2.3 Fibre reinforcement

The experiment used high performance carbon fibre T700SC-120000-50C with grade L, produced by Tora and distributed by Soficar S.A. France. The factory data sheets present the physical properties as follows: diameter = 7 μm ; tensile strength = 4.9 GPa; tensile modulus = 230 GPa; elongation = 2.10%; density = 1.8 g/cm^3 (Torayca, 2016). The fibre was originally in thin bundle form and cut by an automatic cutting machine in 12 mm length as shown in Figure 3.3.

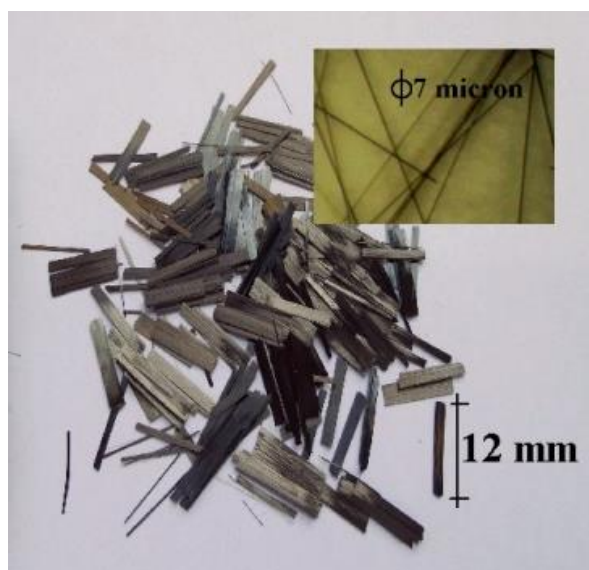


Figure 3.3 Carbon fibre 12 mm long and 7 μm individual diameter

3.2.4 Chemical Admixtures

A high range water-reducing admixture based on a polycarboxylate polymer, namely ADVA Flow 411 (GRACE construction product Ltd., UK), was used to increase the workability. The use of this plasticizer should not exceed 5 wt.% of cement. The properties of this admixture are as follows: $G = 1.08$ kg/l; freezing temperature at 0 °C; chloride content <0.1 %; and alkali content 0.5 % by mass.

3.3 Sample Fabrication and Early Treatments

3.3.1 Composition of RPC Mixture

In general, the homogeneity and granular compacted density of RPC has become the main concern of current studies in this area (for example Richard and Cheyrezy, 1995; Bonneau *et al.*, 2000; Chen & Kwan, 2012). In response, some researchers have used additional materials to change the properties of RPC, for example to reduce the weight (Sadrekarimi, 2004; Long *et al.*, 2002), to increase the bonding between fibre and paste (Chan & Chu, 2004), and to reduce the cement content by replacing it with industrial waste (Yazici *et al.*, 2008). In this study, the composition followed the research conducted by Yazici *et al.* (2008) by using industrial waste due to the fact that this technique can reduce the use of cement by up to 40 % while giving compressive strength of more than 200 MPa. The experiments covered various mixture compositions to get an appropriate and acceptable workability and the steel fibre used by Yazici *et al.* (2008) was replaced by carbon fibre.

The present study uses carbon fibre with 7 μm diameter and 12 mm length which means there are many more fibres per unit volume than for steel fibre with 120 μm diameter and 60 mm length. In terms of their numbers per cm^3 , carbon fibre

has a higher total surface area by about 21 times than steel fibre. It means that the friction surface area of steel fibre 1.0.v_f% is equal to carbon fibre at 0.05 %v_f. Lower fibre content may be used to improve the flexural performance while reducing cost and to improving the mixture workability (Wang *et al*, 2013).

A trial mix was done three times in order to get enough workability of fresh RPC mixture with carbon fibre and a content of 0.1 v_f% was chosen, will an equivalent area to steel fibre at 2.0 v_f%. Table 3.1 presents the result of the final composition, showing where it differs from that of Yazici *et al.* (2008). It has more water and less fibre content. The additional water is needed to keep workability level high because the reduction of SF content, from 35 to 25 % by the weight of cement, decreases the number of finer grains; therefore, this will increase workability due to lower surface area, increasing cement coating, and reducing friction between grains.

Table 3.1: Composition of RPC per cubic meter

PC (kg)	SF (kg)	GGBS (kg)	Quartz (kg)			Water (kg)	SP (litre)	fibre (kg)	Note
			A	C	E				
498	208	332	488	244	244	200	55	1.8 (carbon) (v _f =0.1%)	Present study
498	291	332	488	244	244	151	55	234 (steel) (v _f =3.0%)	Yazici et al. (2008)

3.3.2 Mixing Process

The mixing procedure is an important factor in the laboratory works to ensure the consistency of the mixture. The mixing of RPC containing very fine materials and low water-cement ratio is different from a conventional concrete mixing process. The process of mixing in this study was adopted from Yazici *et. al* (2008). Initially, dry materials, including binder and quartz sand, were put in a stainless mixer bowl (Figure 3.4), mixed at a speed of ~120 rpm for 2 minutes

and then followed by mixing with a speed of up to ~ 450 rpm for another 2 minutes. The half volume of water and SP premixed were then added and mixed for about 5 minutes until the mixture had a consistent look. The fibre was added incrementally into the mixture at a lower speed with the rest of the water, and then the speed was increased to ~ 450 rpm again. The entire process of mixing took about 12-16 minutes. After the mixture became consistent, it was cast into oiled steel moulding which contained three prisms with dimension of 40 x 40 x 160 mm (see in Fig. 3.5). The use of oil helps to reduce the friction at the interface between the moulding and hardened RPC.



Figure 3.4 Small concrete mixer with adjustable speed setting.

3.3.3 Pressure Treatment

Pressure treatment was used to compact RPC samples in the setting period. Static pressure was applied on the top of fresh mixtures using a compressive machine for about 5 hours after casting. The load was increased and controlled by a computer at a rate 1 kN/s to reach at 150 kN, which resulted in a stress of 8 MPa for each sample. The compressive machine was held in this load position for about 2 minutes in order to tighten four corner bolts in the moulding. Using this

method will allow the load to continue pressing the samples during the setting period. Releasing the pressure and demoulding the samples was done after 48 hours of casting in order to let the mixture harden properly and not stick to the moulding (Tam *et al.*, 2010). Figure 3.5 and 3.6 present the appearance of the mould and the samples.



Figure 3.5 Mould with and without pressure

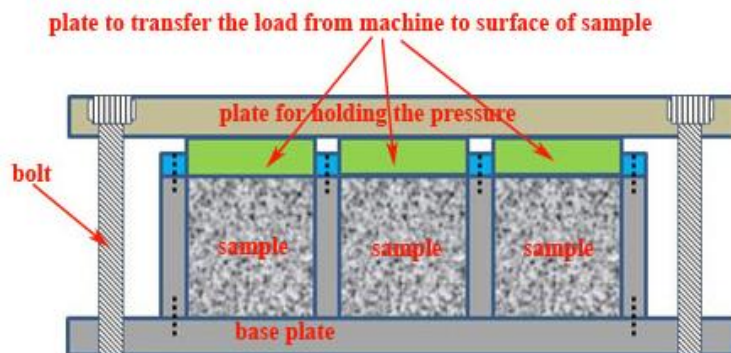


Figure 3.6 Cross section of mould with pressure

3.3.4 Heat Curing Treatment

Heating the sample in the setting period is a unique treatment for RPC, which is different from treatments in common concrete. The heat curing process in this study uses a drying oven (Figure 3.7) similar to an experiment by Tam *et al.* (2010). The samples are put on a rack and preheated at 40 °C for 2 hours, and then increased to 240 °C. The rate, durations, and starting time of heating were used as variables in the preliminary study to get the optimum condition which were indicated by compressive strength. There were three different levels in every set; rates were 10, 50, and 100 °C/hour; durations were 12, 24, and 48 hours; and starting times were 1, 2, and 3 days. After heat curing finished, the temperatures of the oven was decreased at 2 °C/min rate to 40 °C, then samples were cooled at room temperature. The samples were then submerged in water at a temperature of 10 °C until the day of testing, either 7-d or 28-d.



Figure 3.7 Oven for heat treatment

3.4 Method of Testing

3.4.1 Properties in Fresh Mixture

3.4.1.1 Setting Time

The setting of a concrete mixture is indicative of a transition process from a fluid phase to a rigid state (Pinto & Hover, 1999). The process of transformation commences when a mixture loses its plasticity, becoming unworkable, and is complete when the mixture has enough strength to support loads. At the end of the setting period, concrete continuously gains strength with time in the subsequent hardening period (Reinhardt & Grosse, 2004).

A setting test measures the time of cement particles becoming set after mixing with water. The measurement is determined by recording the time needed for the needle to penetrate into the paste until it reaches a specified depth (BS EN 196-3:2005). To test the setting time of concrete, BS EN 480-2:2006 suggests to measure two indicators: initial setting with a needle penetration of 5 to 7 mm from the bottom of the mould and final setting with a penetration at 1 mm from surface. The equipment of the setting test is shown in Figure 3.8.



Figure 3.8 Setting time apparatus

3.4.1.2 Workability

The workability of concrete or mortar is important to control to ensure the homogeneity of fresh concrete mixtures and make them easy to be mixed, placed, flowed, consolidated and finished (ACI 116R-90). Workability is influenced by several properties, such as consistency, plasticity and cohesion (Panarese *et al.*, 1991). The consistency is often used to describe the workability property because plasticity and cohesion are difficult to measure *in situ* (Panarese *et al.*, 1991).

Workability relates to factors such as handling, placing, compacting, and finishing. In general, the workability of concrete is measured by a slump test using an Abrams cone; a metal cone with openings at both ends (Neville, 2011). This measurement can be used to indicate the consistency of mixtures in every batch. A flow table test is usually used to define this property in mortar; and this is also ideal for RPC which contains no coarse aggregate in its mixture. Although RPC has very low water-cement ratio, a workable mixture can be made by adding superplasticizer in large doses (Richard *et al.*, 1995).

Due to lack of flow test equipment, the spreadability of the mixture was applied, instead of a workability test, to indicate the consistency. This test follows the method used by Nambiar & Ramamurthy (2008) to simplify the manner and evaluate the effect of fibre mixture spreading. The distribution was measured using a tube with inner diameter of 75 mm and height of 150 mm, as shown in Figure 3.9. When the tube is lifted, the mixture spreads due to self-weight. The consistency was defined by the spreading value as a mean average from transverse and longitudinal diameter measurements.

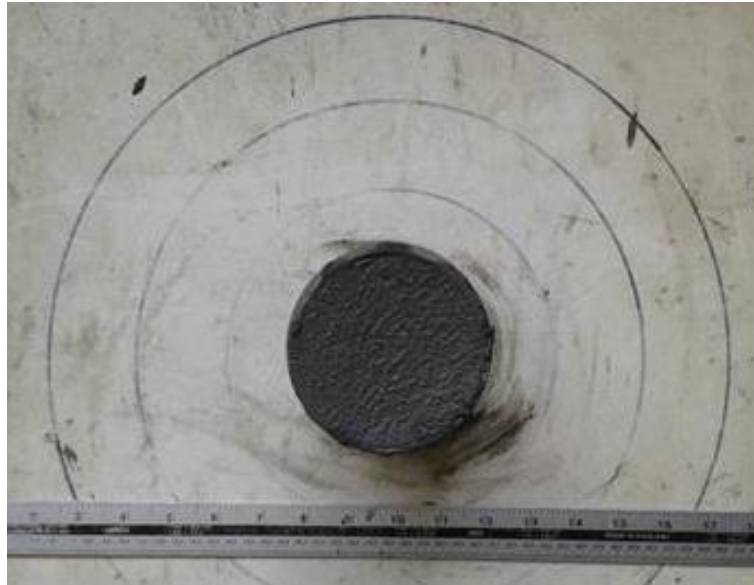


Figure 3.9 Spreading test to measure the mixture consistency

3.4.2 Properties in Hardened Condition

The composition of the RPC mixture in this study was adapted from Yazici *et al.* (2008) and was modified in terms of water-binder ratio, silica fume content, fibre type, pressure and heat curing method. Therefore, to evaluate its physical and mechanical properties this study applied four varying conditions of curing: without pressure and cured in water (code A); without pressure and cured in dry oven (code B); with pressure and cured in water (code C); with pressure and cured in dry oven (code D).

3.4.2.1 Flexural Strength

Prism samples with dimensions of 40 x 40 x 160 mm were used to determine the flexural strength and toughness. Flexural specimens were tested at a loading rate of 0.1 mm/min at mid-span with a clear distance between simple supports of 100 mm conforming to BS EN 196-1:2011 as shown in Figure 3.10. On both sides of the middle span, linear variable differential transformers (LVDT) were installed to measure the deflection of the sample during the loading process (Figure 3.11).

Plotting the load and deflection, the toughness of the sample could be analysed by calculating the area under the load–deflection curve up to 2.5 mm mid-span deflection.

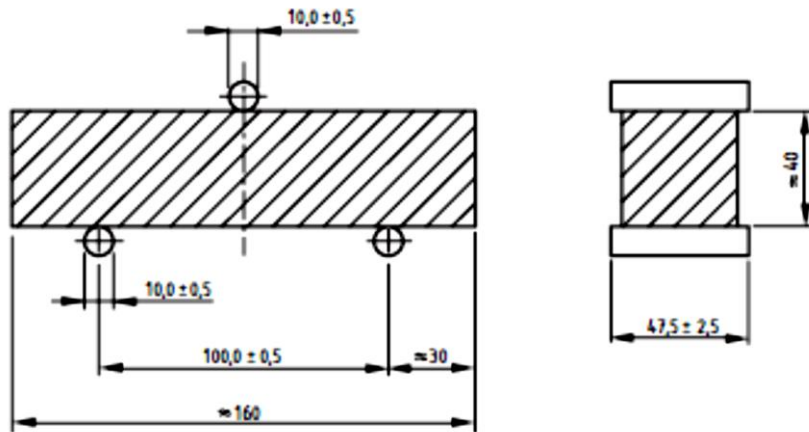


Figure 3.10 Setting up the span in flexural test (BS EN 196-1, 2011)



Figure 3.11 Setting up the LVDT on two sides of a prism

The addition of carbon fibres to an RPC mixture has a slight influence on the flexural strength, but statistically significantly influences the toughness and flexural modulus. This result agrees with those found by Johnston (2006) who mentioned that the improvement of carbon fibre is related to the increase in

toughness. Toughness is the ability of a material to absorb energy before rupture which can be accounted for from the area under the load-deflection curve in the flexure test (Yazici *et al.*, 2009). It is also possible to define the flexural modulus from this curve using Equation 3.1 (Horners, 2008):

$$E_f = \frac{L^3 m}{4bd^3} \quad (3.1)$$

Where:

E_f = Flexural Modulus of elasticity, (MPa)

L = Support span, (mm)

b = Width of test beam, (mm)

d = Depth of tested beam, (mm)

m = The gradient of the initial straight-line portion of the load deflection

3.4.2.2 Compressive Strength

The compressive strength test was conducted at 7-d or 28-d using one part of the two broken pieces from the flexural test conforming to BS EN 196-1:2011. The contact pressed area of the sample was 40 x 40 mm and the height was 40 mm (Figure 3.12). The samples were tested at 7-d and 28-d under compressive machine with a maximum capacity of 500 KN and load rate of 2400 N/s in accordance to BS EN 196-1:2011. This test results in the maximum load, which was then used to calculate compressive strength by dividing it by the surface of the contact area. The average of compressive strength is taken from three samples and presented in a table with standard deviation (SD) calculation by excel spreadsheet (see in Appendix A).



Figure 3.12 Setting out of sample for compressive test

3.4.2.3 Thermal Conductivity

Thermal conductivity was established to describe the capability of RPC to transport heat while it is exposed to high temperature. The thermal conductivity test used a specimen which was made by cutting the middle of an RPC prism sample with about 20 mm of thickness. The specimen was then treated in the same way with specimens for compressive strength testing (see in sub-chapter 3.5.1.1). All specimens, with or without high temperature exposure, were treated in an oven at 60 °C for 2 hours to ensure uniformity of water content on the surface of specimens.

Testing was run using a thermal conductivity analyser, produced by C-Therm, which uses the modified transient plane source technique (sensor). This technique uses a one-sided interfacial heat reflectance device which produces a constant current heat source to the surface of the sample (Figure 3.13). To improve heat flow between sensors and sample, the testing employed a thermal joint compound of Wakefield solution type 120 silicone. Thermal conductivity was measured ten times for each sample.



Figure 3.13 Setting up thermal conductivity test

3.4.3 Microstructure Test

3.4.3.1 Scanning Electron Microstructure (SEM)

SEM is a method to obtain high-resolution images of the sample's surface. This method can be combined with an energy dispersive x-ray spectrometer (EDS) to analyse qualitative and quantitative information of chemical composition.

Samples for SEM tests were made from fractured bulk specimens of RPC cubes. Three representative sub-samples were mounted fracture face down and cold mounted under vacuum in 2-part epoxy resin. Mounted samples were ground using SiC paper (400, 600, 800 and 1200 grit) on 20cm diameter wheels at a rotational speed of 250 rpm, followed by polishing using 6 μ m then 1 μ m diamond pastes. Polished samples were washed using acetone and dried under a hot air blower, followed by sputter coating with ~15nm thick carbon using an Edwards 306 vacuum Coater.

A Philips XL30 field emission gun environmental scanning electron microscope (FEG-ESEM) was used to take the images (Figure 3.14). The mounted and coated samples were placed in a vacuum chamber (Figure 3.15).

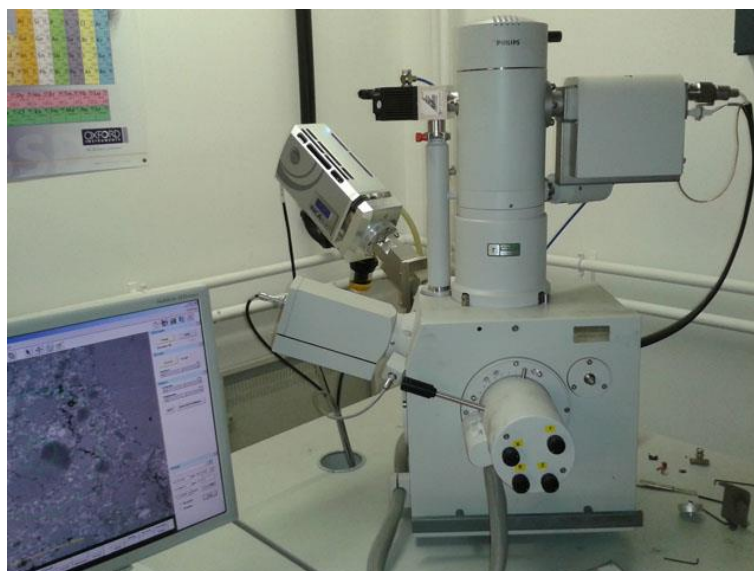


Figure 3.14 SEM equipment fixed with EDS

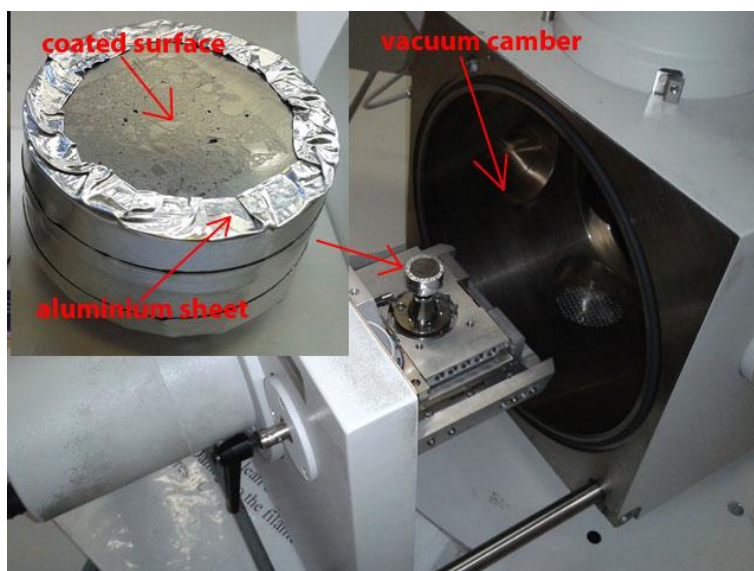


Figure 3.15 Placing the mounted and coated sample in vacuum chamber

Micrographs were recorded using an Everhart-Thornley type Secondary Electron (SE) detector and a Back Scattered Electron (BSE) detector supplied by K. E.

Developments. The FEG-ESEM operating conditions are 20 kV accelerating voltage, 4.0 spot size, and 10 mm working distance. Representative micrographs were recorded from randomly selected aggregate particles and analysed using ImageJ 1.47v (National Institutes of Health, USA). Images were smoothed using a 2px median filter, before bracketing the upper/ lower limits of the greyscale histogram by manually adjusting contrast/ brightness. The porosity could then be segmented manually using the default threshold algorithm.

On each SEM sample, three cross-sectioned aggregates were randomly selected and grids measuring 5 μm (thick) x 50 μm (wide) were applied from the aggregate surface at distances ranging from 0 to 75 μm (15 grids in total). The number and total area of pores were assessed using the 'analyse particle' tool. Porosity was defined by dividing the total area of particles by the area of grid. The mean average data from three samples was first plotted, and the intersection between linear trend lines (at the inflection point that indicates the transition between ITZ and bulk porosity) was used to define the ITZ distance.

Elemental mapping was performed using an Energy Dispersive X-Ray Spectrometer (EDS), developed by Oxford Instruments Inc. The microstructure test using EDS can reach 133eV resolution of the Mn K_{α} peak at FWHM.

Quantitative EDS was conducted using four iterations at a 35° take-off angle, and with 60 seconds live time and 30 – 40 % dead time. During EDS analysis of the interfacial transition zone (ITZ), a series of grid areas (10 μm wide x 40 μm long) were scanned starting from the aggregate edge and moving away at 10 μm intervals up to a maximum distance of 70 μm . A set of results from EDS analysis is reported in an inset table, alongside a spectrum and an SE image showing the analysis location (see an example in appendix).

3.4.3.2 Mercury Intrusion Porosity (MIP)

Mercury intrusion porosimetry (MIP) has been widely used to study the pore structure characteristics of cement-based materials including pore diameter, pore distribution, porosity and density (Diamond, 2000). The principal of the MIP test is by using high-pressure oil to press mercury into the specimen and measure the mercury intrusion volume at different pressure points to reflect the connective pore structure. The result of this method depends on factors such as contact angle and surface tension of mercury, sample preparation, sample drying technique, and rate of pressure application (Kumar and Bhattacharjee, 2003).

MIP in this research was performed using a Micromeritics Autopore IV 9500.V1 with a maximum pressure of 60,000 psi enabling the measurement of pore diameters from 360 – 0.005 μm as shown in Figure 3.16. Irregular sub-samples (approx. 3-4 g) were produced by cleaving from the 40 mm parent cube samples and placed in a 5cc solid penetrometer. The contact angle and surface tension parameters were taken as 140 ° and 0.485 N/m², respectively.

The specimens were placed in the penetrometer and put under vacuum to be filled by mercury with conditions ranging from low pressure up to 20 $\mu\text{m}/\text{Hg}$). Mercury filling was then continued by high-pressure up to maximum 60,000. After reaching the highest pressure, the mercury was then extruded under vacuum. The mercury intrusion volume was recorded at each pressure point. The relationship between intrusion pressure and equivalent pore diameter is defined by Washburn's equation:

$$d_p = \frac{-4 * \sigma^{Hg} * \cos(\theta)}{p * k} \quad (3.2)$$

Where: d_p is the pore diameter (μm); σ^{Hg} is the surface tension of mercury (dynes/cm); θ is the contact angle between mercury and the specimen surface; p is the press pressure (psi); and k is the transfer constant ($10^{-4} \text{ cm}/\mu\text{m} \times 68947 \text{ psi/dynes cm}^{-2}$).

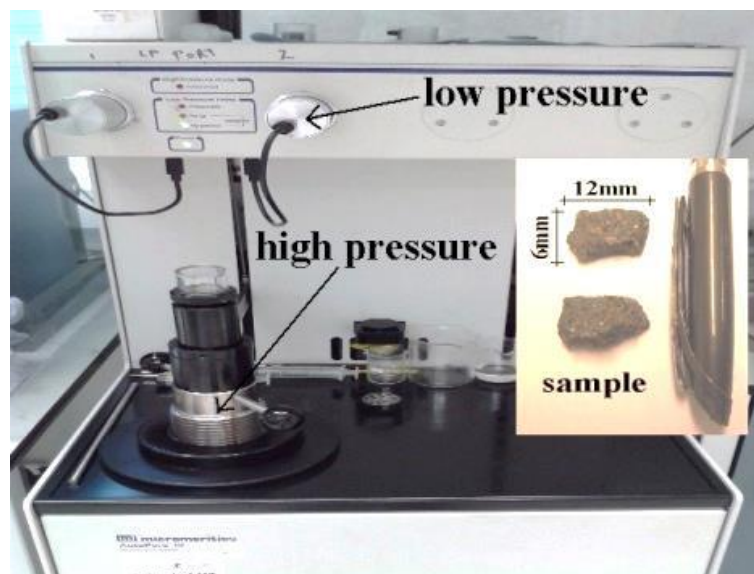


Figure 3.16 MIP equipment and sample dimension

3.4.3.3 Thermogravimetric Analysis (TGA)

TGA is a thermal analysis method to evaluate the physical and chemical properties of material by measuring the amount and rate of weight change as a function of temperature in a controlled temperature environment (TA instrument, 2012). The results of TGA can indicate the chemical composition of materials and their thermal stability at temperatures up to 1200 °C. The results are correlated with decomposition (breaking a part of chemical bonds), oxidation (loss of electrons), or dehydration reaction (loss of water with elevated temperature).

In normal reactions, hydration of the cement grains produces hydrated minerals. Instead, when heat curing is applied in RPC the composition of hydrated material will change, mainly due to the transformation of C-S-H. To analyse the hydrated composition in cement paste, many scholars usually use thermogravimetric analysis (TGA) which is a measurement technique based on the weight loss under high temperature exposure. The results of TGA are presented as a curve between the percentage of weight loss and the exposure temperature. The weight loss curve has been used here to indicate the reactivity of the cement. This means that in a range of applied temperatures, the greater the weight loss the greater amount of the associated hydration products in the paste (Cassagnabere *et al.*, 2009).

As the results from TGA vary between scholars, Alarcon-Ruiz *et al.* (2005) suggested to group the range of temperatures that indicate the main hydrated groups as follows: 30 - 105 °C due to evaporation of free (capillary) water; 110 - 170 °C due to decomposition of ettringite; 180 - 300 °C due to partial dehydroxylation of C-S-H (possibly indicating partial transformation of C-S-H gel to xonotlite); 400 - 500 °C dehydroxylation of portlandite (Ca(OH)₂); 700 - 900 °C due to calcination of CaCO₃. In addition the presence of xonotlite is indicated by further decomposition at temperatures of about 800 °C (Cheyrezy *et al.*, 1995), and so most likely results in a compound or convolved mass loss increment coinciding with that of calcite.

The chemical composition of RPC samples was analysed using a TA Instruments SDT Q500; a research grade thermogravimetric analyzer with responsive low-mass furnace, sensitive thermobalance, and efficient horizontal purge gas system (Figure 3.17a).

TGA samples were taken from the inner core of three cube specimens and then ground (using ceramic mortar) to a fine powder. Sub-samples of the prepared

powder (20–30 mg) were placed in aluminium pans (Fig.3.17b). Heating was ramped from ambient (20 °C ±2) to 1000 °C at a constant heating rate of 20 °C/min in a 100% N₂ atmosphere.

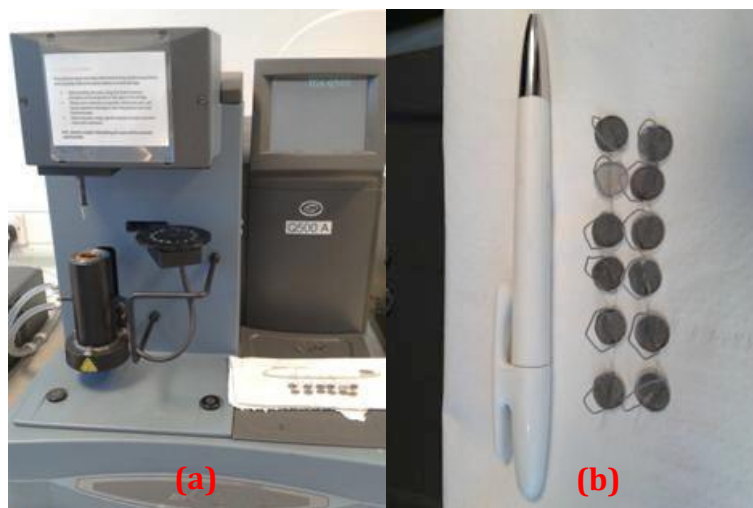


Figure 3.17 TGA test (a) Instruments SDT Q500, (b) Sample on aluminium pans

3.4.3.4 X-ray Diffraction (XRD)

XRD is an analysis technique to identify minerals within a crystalline finely ground material. The technique has been developed based on a theory that a crystalline substance acts as a three-dimensional diffraction grating for X-ray wavelengths, similar to the spacing of planes in a crystal lattice which was found by Max von Laue in 1912 (Eckert, 2012). Both constructive interference of monochromatic X-ray and a crystalline sample are fundamental factors in this method. The X-rays generated by a cathode ray tube are filtered to produce monochromatic radiation, then collected to concentrate and direct at the sample. Constructive interference is produced after the interaction between X-rays and the sample occurs (Figure 3.18). Using Bragg's Law, the wavelength of the electromagnetic radiation can be determined using equation 3.2:

$$n\lambda = 2d \sin \theta \quad (3.2)$$

Where n is an integer; λ is the wavelength of the incident X-ray beam; d is the distance between atomic layers in a crystal; θ is angle of incidence.

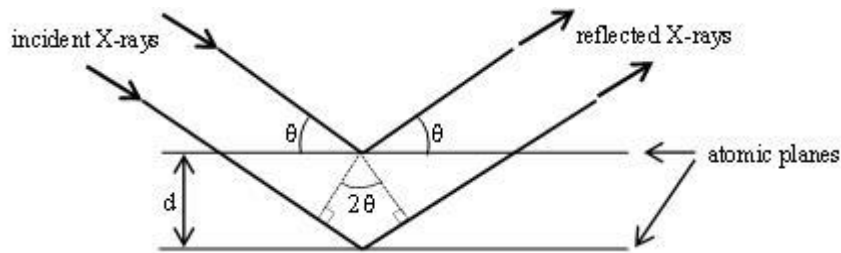


Figure 3.18 Principal Bragg's Law

These diffracted X-rays are then detected, processed, and counted. By scanning the sample through a range of 2θ angles, all possible diffraction directions of the lattice should be attained due to the random orientation of the powdered material. Conversion of the diffraction peaks to d -spacings allows identification of the mineral because each mineral has a set of unique d -spacings. Typically, this is achieved by comparing d -spacings with standard reference patterns.

This study measured bulk powder X-ray diffraction (XRD) patterns using a Bruker D8 diffractometer, operating in Bragg–Brentano focusing geometry, and used Cu K α radiation ($k = 1.5418 \text{ \AA}$) from a generator operating at 40 kV and 25 mA.

The diffractograms were recorded in a 2θ range from 10° to 60° , with a 2θ step size of 0.02 and a step time of 1 s. The samples were prepared from three cubes and mixed together before putting them in a drying oven to constant mass at 70°C , followed by manual crushing using an agate mortar & pestle. The samples were mounted by placing on a powder sample holder and levelled using a glass slide as shown in Figure 3.19.

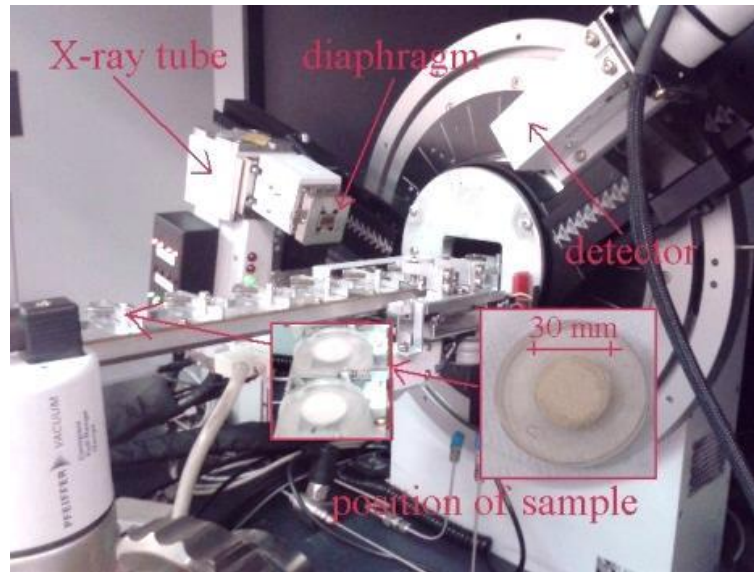


Figure 3.19 Setting up XRD test

3.5 High Temperature Exposure on RPC Specimens

This section presents the regimes of high temperature exposure which were applied to RPC specimens. The regimes were adopted from the study of Tai *et al.* (2011) with a heating rate of 2 °C/min followed by holding at constant temperature for 30 minutes at every 100 °C increment of temperature. Every single test used three different samples, except for the heating-cooling cycles.

3.5.1 Fixed Temperature

3.5.1.1 Temperature Increments

A fixed temperature was applied to test the fire endurance of RPC. After 28 days, all prism specimens were placed in the oven. The temperature of the oven was raised continually at the rate of 2 °C/min to a target temperature and held for 30 minutes. This method was proposed by Tai *et al.* (2011), as shown in Figure 3.20. The test used four target temperatures: 20 °C (non-heated), 400

°C, 500 °C, and 800 °C. These temperatures were chosen considering that the main elements change their structure at those levels such as dehydroxylation of portlandite ($\text{Ca}(\text{OH})_2$) at about 400 °C, quartz reaction at about 500 °C, and calcination of CaCO_3 after 700 °C (Alarcon-Ruiz *et al.*, 2005). After exposure, the samples were cooled down in the oven, and then kept in a curing room at 10 °C for one day, and finally tested for their residual compressive strength.

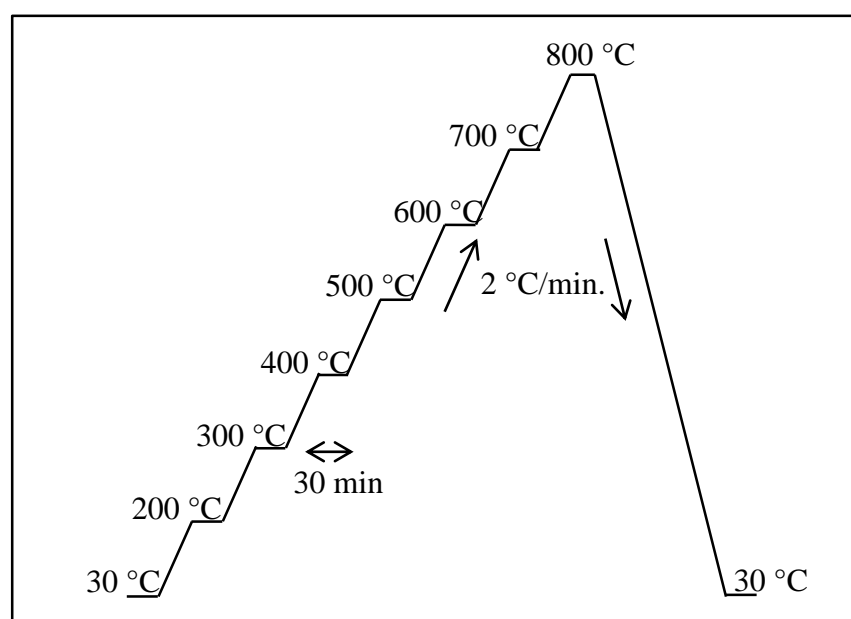


Figure 3.20 Heating scenario for temperature increments

3.5.1.2 Duration of Exposure

The treatment of samples in this part modified the method used by Liu & Huang (2009)., who put samples in a heavy-oil burning furnace at a fixed temperature of 500 °C. In this study, the samples were put in an oven following the previous set of tests, but instead the temperature was raised incrementally from 30 °C to 500 °C at a rate of 2 °C/min (Figure 3.21). The duration of hold time upon reaching 500 °C was varied between 30, 60, 90 and 120 minutes. The cooling down process was identical to the previous test.

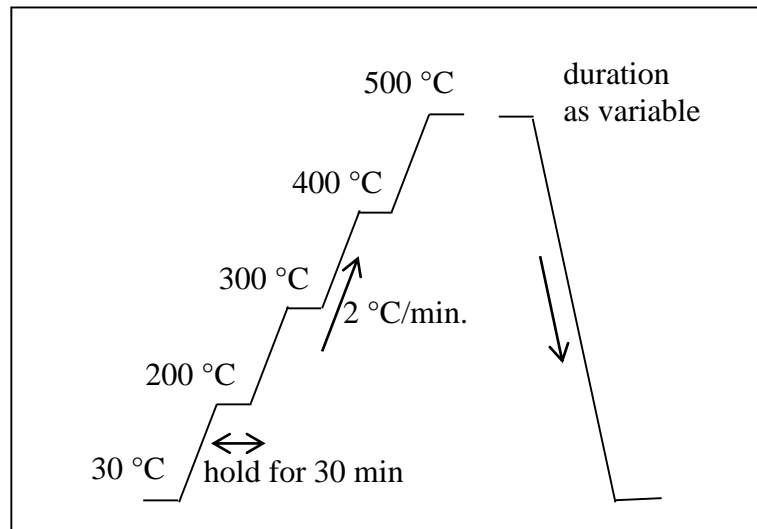


Figure 3.21 Heating scenarios for duration exposure

3.5.2 Cyclic Heating and Cooling

In reality, a concrete structure can be subjected to high temperature several times, such as in a fire. In such situations, the concrete structure could be quench cooled by water in the event of the sprinkler system being activated. Due to these considerations, two scenarios of cooling were established in this study; air cooling and water cooling.

3.5.2.1 Cyclic Heating and Air Cooling

In this part, the samples were heated to a fixed temperature of 500 °C. The temperature was held at 500 °C for 30 minutes then decreased to 30 °C at a rate of 2 °C/min. The exposure to heat was started again after 4 hours, during which time the sample had reached ambient temperature before starting the next cycle of heating (Figure 3.22). Cyclic exposure in this study was repeated using one, two, three, four and five cycles.

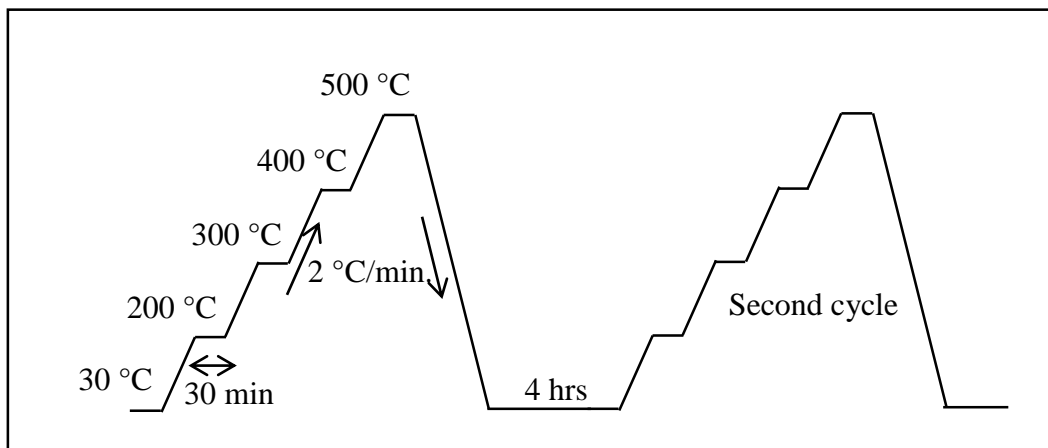


Figure 3.22 Heating scenarios for cooling in air

3.5.2.2 Cyclic Heating and Water Cooling

The heat exposure steps in this part were exactly the same as the previous (air cooled) tests, but after exposure at 500 °C for 30 minutes the samples were taken out from the oven and submerged in cold water immediately for four hours, and then removed and air dried until they equilibrated with ambient room temperature (Figure 3. 23). The heating was started again 24 hours after the first treatment. The maximum number of cyclic exposures was only two.

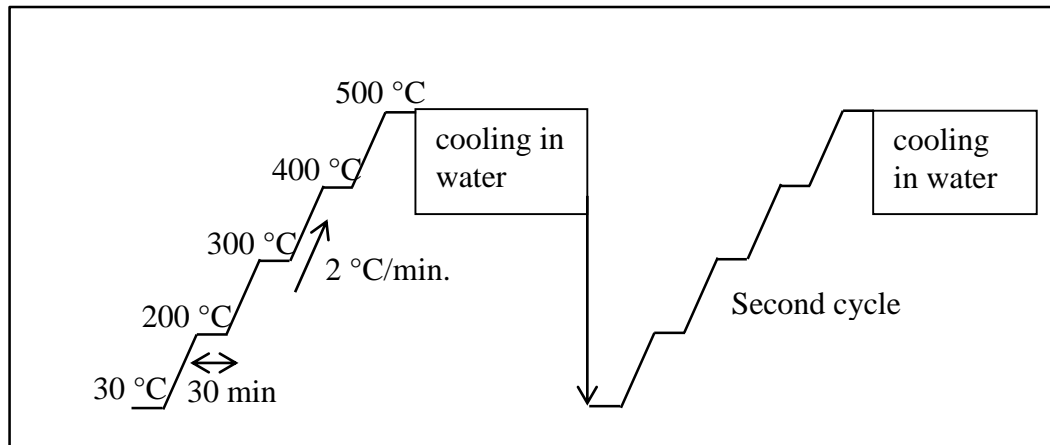


Figure 3.23 Heating scenarios for cooling in water

3.6 Summary

In brief, the experiments followed three stages: the optimisation of RPC, the transformation of microstructure properties, and the response to high temperature exposure and cooling. Firstly, in order to determine the optimum treatment for heat curing, the experiments investigated the mixture composition focussing on the impact on mechanical properties of variables such as heating rate, heating duration, and starting time of heating (see Chapter 4 for further details). Secondly, the experiments then investigated the transformation of the microstructural properties of RPC either before or after treatments including pore network evolution, the chemical elements formed, and the ITZ. The transformation was observed in relation to four types of treatments: (A) without pressure and cured in water, (B) without pressure and heat cured in a drying oven, (C) with pressure and cured in water, and (D) with pressure and heat cured in a drying oven (see Chapter 5). The third group of experiments investigated the mechanical and microstructure properties of RPC after high temperature exposure in fixed temperature and cyclic heating. Focussing on fixed temperature properties, the study then examined the residual compressive strength and microstructural properties.

Chapter 4- Optimising Conditions and Mechanical Properties of RPC

4.1 Introduction

The manufacture of RPC has traditionally been achieved by applying pressure and heating while the cement sets. This condition has two different benefits; pressuring the cement improves its density and heating it accelerates the pozzolanic reaction (Richard & Cheyrezy, 1995).

This chapter presents the results of experimental work undertaken to explore the effect on the mechanical properties of RPC that occur when pressure and heat conditions are varied during curing. In the first set of experiments the effect of three temperature variables was investigated; the rate at which heating was increased, the time during which heat was applied and the delay before applying heat to the sample. For the first experiment, samples were prepared from an RPC mixture containing no carbon fibre. After optimisation of the three temperature variables described above, an evaluation of the sample compressive strength was made. In the second experiment, the effect of varying pressure and heat during sample curing was investigated and comparatively evaluated in terms of compressive strength, density and porosity. Finally the mechanical properties of RPC with carbon fibre were investigated in a similar manner, again with varying combinations of pressure and heat conditions during curing. This section discusses the flexural strength, toughness, modulus of elasticity and compressive strength of the samples and the results of samples with and without carbon fibre are compared. The results are then summarized and the correlation between the empirical findings and predicted outcomes discussed.

4.2 Properties of Fresh Mixtures

The properties of a fresh concrete mix can generally be adjusted as required by varying the mix proportions. This is done dependent on where the fresh concrete is to be placed on site and the desired performance of concrete in its hardened state. The properties are commonly accepted to be the workability, the setting time and the degree of hydration all of which are mostly affected by the water content (Neville, 2011).

4.2.1 Setting Time

The standardised mixture composition used to test setting time has to adhere to BS EN 197-1:2005 while the composition of RPC includes additional powders (silica fume + GGBS) and superplasticizers (SP). The best of three samples for both mixtures is shown in Table 4.1.

A standard mixture conforming to BS EN 197-1:2011 has a minimal initial setting time of 60 minutes for CEM1 52.5. However, RPC mixtures have uncommon properties, needing 285 minutes for the initial setting period and 570 minutes for the final setting period. This is 3.8 times greater than standard mixtures for initial setting and 3.6 times greater for final setting. It is believed that this setting time is mainly affected by the water content (Neville, 2011). Although an RPC mixture has a lower water-binder ratio (0.2) than the standard mixture (0.3), the RPC mixture contains a large amount of free water because of the presence of water within super plasticizer (SP). If the SP material comprises 80 % water, then the water-cement ratio in the RPC mixture becomes 0.48, or 60 % higher than in the standard mixture. In addition, the use of SP greater than 5 % of binder material (or 10 % of total cement alone) may not conform to the respective standards for a test mixture because the high dosage of

superplasticizer affects the solubility and the rate of solution of calcium sulphate ions from the cement (Neville, 2011).

Table 4.1: Composition of mixtures and the average of setting time taken from three samples

Mixture	Composition ratio					Setting time (mins.)	
	Cement	Water	Sand	Other powder	SP	Initial	Final
Standard	1	0.3	3	-	-	75	160
RPC	1	0.4	2	1	0.1	285	570

4.2.2 Workability

The test for consistency of a fresh RPC mixture was performed immediately after mixing according to ASTM C230 as done by Nambiar & Ramamurthy (2008); measuring the spread diameter and comparing it to an initial diameter of 75 mm. Figure 4.1 shows that a RPC mixture containing carbon fibre appears as plastic flowing and spreadable. The consistency measurements of three fresh RPC mixtures resulted in diameters of spreading of between 14 and 17 cm which is around 150% higher than the initial diameter and more workable than the mixture in Yazici *et al.* (2008). This higher flow value might be caused by an increase of the water/binder ratio to 0.192, instead of the 0.132 ratio used in the initial reference (Yazici *et al.*, 2008). In addition, an RPC mixture with 0.13 water/cement ratio seems sticky and viscous with zero slump (Shaheen & Shrive, 2006). Using a high water/binder ratio of 0.28 can result in an increase of the flow value to 200%, but the compressive strength is low at about 75 MPa (Liu and Huang, 2009). This confirms that the consistency of an RPC mixture is significantly influenced by water content.

It appears that decreasing the silica fume content from 35 % to 25 % is another factor in consistency. The effect comes from reducing the number of grains of finer material which will result in a lower surface area, thereby increasing the

cement coating and reducing the friction between grains. However in a study by Yazici *et al.* (2008), they found that when the silica fume content was reduced there was no influence on the flow value of the RPC mixture.

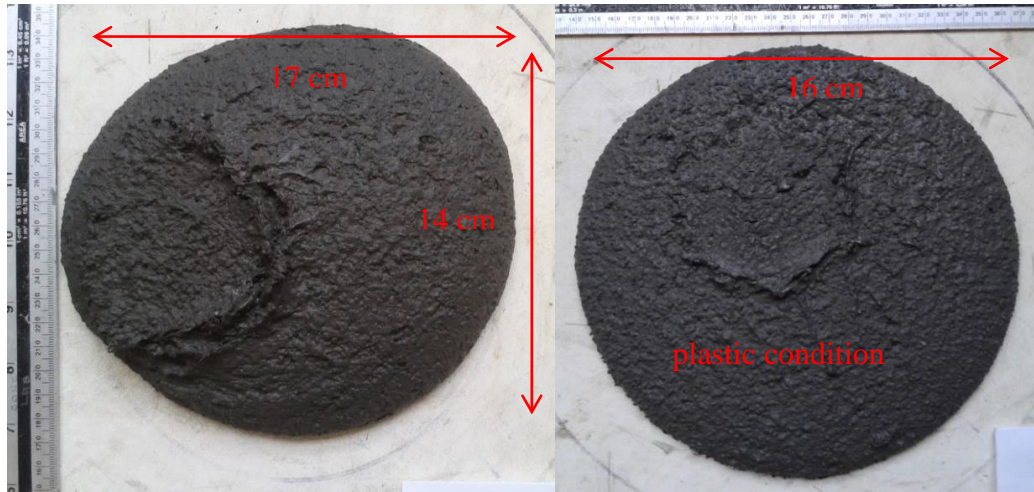


Figure 4.1 Fresh mixture and consistency measurement

4.3 Optimisation of Cement Cure

The addition of heat during the curing period affects the strength of RPC and is mostly dependent upon three factors; the method of application, the temperature and duration of cure. Applying high temperature to concrete has two consequences which are, accelerating the chemical reaction of hydration and inducing tensile stress in the cement paste (Neville, 2010). This tensile stress occurs due to the expansion of entrapped air inside pores which causes them to become pressurised (Anderberg, 1997). To optimize the heat curing process, three factors are evaluated in this study: the rate of heat application, the duration of heat application and the time delay before heating is applied.

4.3.1 Heating Rate

The heating rate has a correlation with the speed of evaporation, this in turn influences the extent of air voids and hydration reaction in the concrete

(Sadrekarimi, 2004). A low heating rate may decrease the dehydration rate by allowing sufficient time for thermal diffusion to occur, which influences the final compressive strength of the concrete. Therefore three different rates, namely 10, 50 and 100 °C/hr were evaluated in this study. Samples were tested in compression at 7-d and 28-d using two parts of a broken prism. The result is shown in Figure 4.2.

The compressive strength, at 7-d and a heating rate of 10 °C/hr, is 79 MPa for a non-pressured (NP) sample and 100 MPa with pressure (WP). This is stronger than the qualification of high strength concrete performance (HSCP) according to Neville (2011). At 28-d, the compressive strength continuously increases up to 89 MPa for NP and 111 MPa for WP. When the heating rate is increased to 50 °C/hr, the compressive strength at 7-d increases by 41 % (NP) and by 48 % (WP) compared to the numbers achieved for the 10 °C/hr samples.

At 28-d, however, compressive strength remains relatively stable for NP and drops about 14 % for WP compared to the same samples is at 7-d. It is supposed that the hydration and pozzolanic reactions have been accelerated with the application of heat but that micro cracks are also produced. Increasing the heat application level to 100 °C/hr has less effect on compressive strength compared to using 10 °C/hr. Compressive strength changes at this heat rate, either at 7-d or 28-d for both NP and WP, are within the calculated range of error for the measured results and can be ignored.

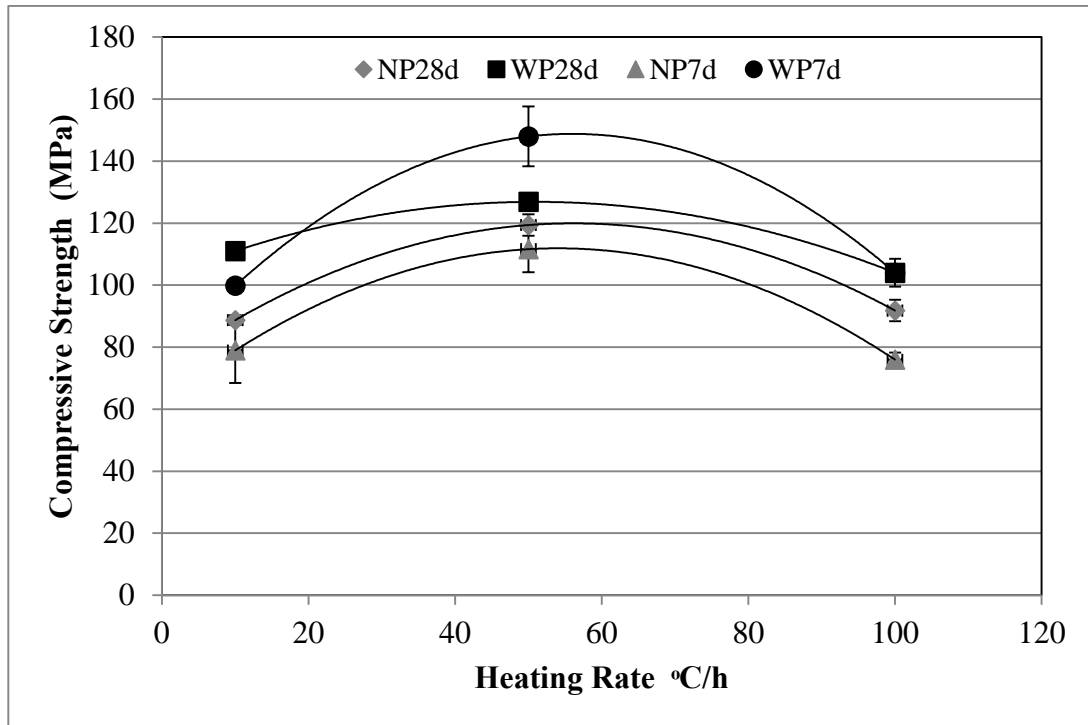


Figure 4.2 Compressive strength-heating rate curves for a heating duration of 48 hours after 2 days of casting.

The lack of change in compressive strength with high temperature could mean that the high rate heating induces immediate evaporation of water from the C-S-H gel and causes a rapid increase in the pressure of pores which in turn increases the tensile stress in the cement paste. If this tensile stress is higher than the tensile capacity of RPC at 2-d (the point at which pressure is applied) microcracks are induced around the pores. Microcracks, which have been formed during the setting period due to natural shrinkage and grain movement after pressure application, could increase in number and width after heat curing. Consequently, the reason for achieving lower compressive strength in samples with heating rates of 10 and 100 °C/hr could be less effective hydration and pozzolanic reactions and the development of microcracks respectively (Richard & Cheyrezy, 1995).

Applying pressure followed by heat during the curing period significantly affects the compressive strength by up to 30 % at 7-d and 15 % at 28-d compared to sample cured without the application of pressure. This percentage is in agreement with the results of Yazici *et al.* (2008) and Sadrekarimi (2004). They observed incremental improvements in compressive strength of up to 30 % and 21 % after pressure condition, respectively. The increase of strength could be explained by the reduction of the volume of entrapped air voids, removing excess pore water, and decreasing the bulk porosity (Richard & Cheyrezy, 1995).

4.3.2 Heating Duration

For this experiment, samples were heated to a maximum temperature of 240 °C with a ramp rate of 50 °C/hr in a drying oven. The maximum temperature was applied for durations of 12, 24 and 48 h. The measured compressive strengths in the samples at 7-d and 28-d are presented in Figure 4.3.

As can be seen in Figure 4.3, the curve shows that there is no optimum compressive strength from the three variations of heat duration tested. However, the compressive strength tends to increase with an increase of duration for all samples. At 7-d, the compressive strength increases progressively and not linearly with heating duration. It is found that the compressive strength of samples with heating duration of 12, 24 and 48 h are 79.02, 76.34, 111.60 MPa for NP and 83.20, 84.62, 147.94 MPa for WP, respectively. The difference is less significant at 12 h compared to 24 h and becomes very significant to 48 h as there is increase of around 45 % (NP) and 75 % (WP). For the 28 day samples the trend is more gradual with the difference in compressive strength of both types of sample at around 20 %.

This result shows that the duration of heating is an important factor which affects the compressive strength of RPC and the properties of the microstructure (Cwirzen, 2007). The effect shows correlation with the acceleration of the rate of cement hydration and pozzolanic reactions for both silica fume and quartz sand. In addition, the duration of heat condition results in an increase in the strength of the RPC due to the amount of C-S-H produced and the change in crystal formation from tobermorite to xonotlite (Tam *et al.*, 2012).

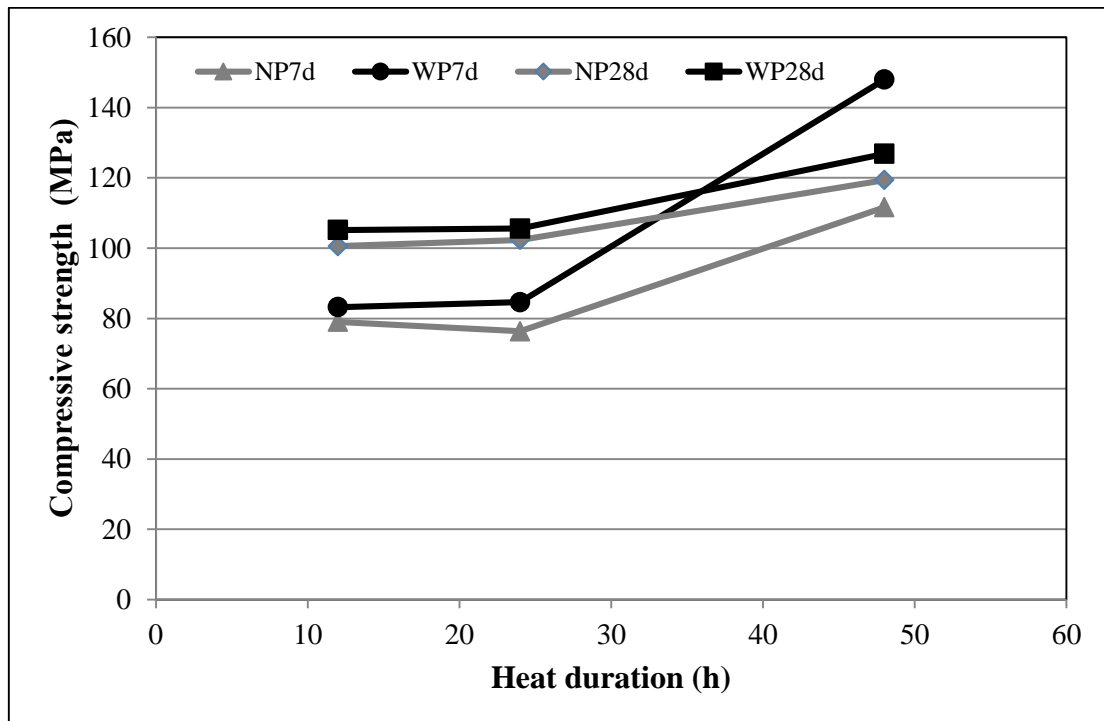


Figure 4.3 Compressive strength-heat duration curves for a heat rate of 50 °C/hr after 2 days of casting.

4.3.3 Heating Start Time

For this experiment, three samples were heated under identical temperature conditions of 240 °C at a ramp rate of 50 °C/hr in a drying oven. The time of sample placement in the oven after casting was varied between samples with

delays of 1, 2, and 3 days. The comparison of compressive strengths for the three different delay times at 7-d and 28-d is presented in Figure 4.4.

Figure 4.4 shows that the optimum compressive strength is found when the heat condition is applied after a delay of 2 days from casting, both at 7-d and 28-d, for both NP and WP samples. Although the rate of strength development in concrete under normal curing conditions is influenced by the rate of hydration after one or two days, it will still increase gradually with time (Domone, 1996). The results from applying heat curing in RPC samples at 3 days show disagreement with this theory, with a contradictory result of a 45 % reduction in compressive strength compared to the one with applied heat curing after 2 days. In any condition, the compressive strength of WP samples is always higher than NP samples for all conditions because pressure condition changes the physical microstructure of the mixture before final setting is achieved by a densification mechanism (Richard & Cheyrezy, 1995).

The reason for optimum compressive strength being achieved by heating at 2 days may be explained by hydration theory (Domone, 1996). On the first day of hardening, tobermorite [C-S-H] gel is formed in much higher quantities than ettringite and portlandite [$\text{Ca}(\text{OH})_2$] and starts to form C_4AF hydrate. During the second day, the volume of hydrated phases increases and the volume of ettringite decreases as it converts to monosulphate, and on the third day the density of hydrate phases begins to increase significantly. Moreover the majority of ettringite has converted to monosulphate prior to the onset of the hydrate phase densification at 2 days. Given that the above is a valid description this suggests that the highest compressive strength, while heat curing is applied at 2 days, could be due to acceleration of hydrate phase densification whilst the risk of microcracks initiation/ enlargement resulting from thermal expansion of partially-hardened hydrate phases is avoided.

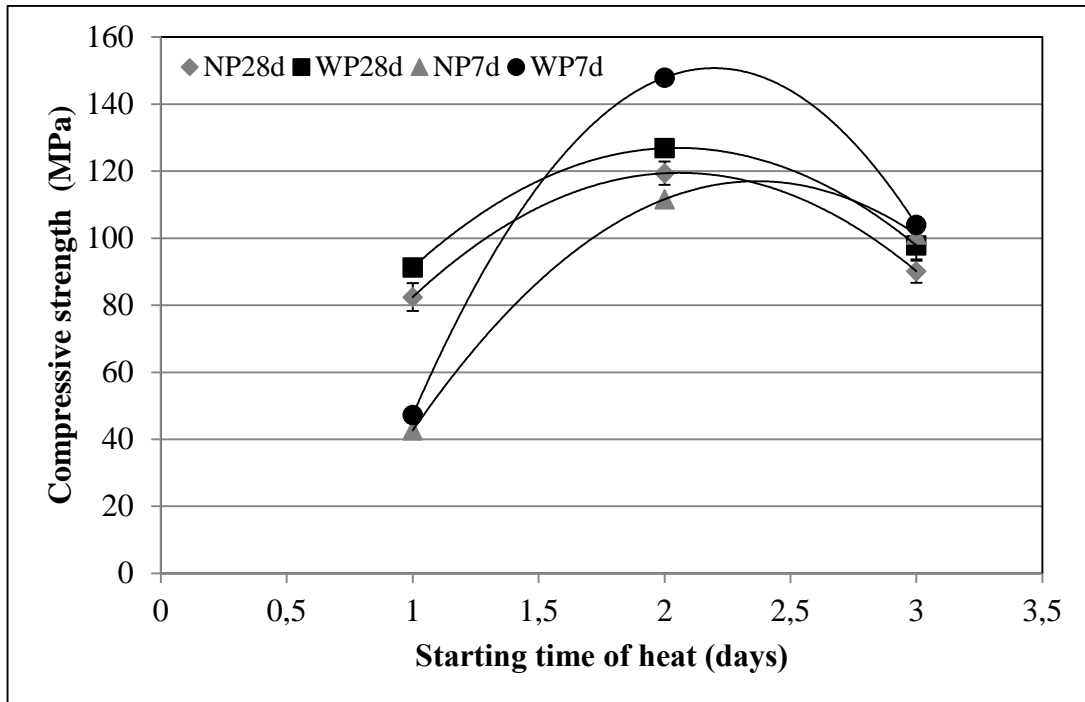


Figure 4.4 Compressive strength-heated starting time curve for heating rate of 50 °C/hr and duration of 48 h

4.3.4 Significance Analysis

The result of the compressive strength tests in the experiments above show variation. Therefore a student's t-test was applied to examine whether there is significant difference between two values by comparing the means of samples with a t-value of 95 % confidence. The results of the t-test for samples of both NP and WP are presented in Table 4.2. The t-value is accounted from two variables in the same treatment, for instance in a heating rate of 10 and 50 °C/h or 50 and 100 °C/h with t-value 10.68 and 7.53, respectively. Based on the t-table at 4 degrees of freedom, it is found that a t-value of 2.78 gives a 95 % confidence level and 4.60 a 99 % confidence. The results of this analysis demonstrate that a significant difference of results is found between NP and WP samples for the same experimental conditions. The significance of the difference at a 95 % level of confidence is present when the results of the optimum curing

variables (a heating rate at 50 °C/h, a heating duration at 48 h and a heating start time at 2 days) are compared to others. The t-value exceeds 4.60 with the implication that the variance of these results is very highly significant.

Table 4.2: Analysis Student's t-test of compressive strength for all factors

Factor	Var.	Strength (MPa)			Average	t-value	Significant
		Sample1	Sample2	Sample3			
Non pressured (NP)							
Heating rate (°C/hr)	10	88.63	86.69	90.88	88.73	-	-
	50	123.13	114.38	120.63	119.38	10.68	Yes
	100	91.13	87.69	96.56	91.79	7.53	Yes
Heating duration (hours)	12	100.63	99.56	101.44	100.54	-	-
	24	104.61	98.88	103.55	102.35	5.42	Yes
	48	123.13	114.38	120.63	119.38	7.09	Yes
Heating start (day)	1	76.44	83.94	86.88	82.42	-	-
	2	123.13	114.38	120.63	119.38	9.12	Yes
	3	86.50	88.81	95.19	90.17	7.94	Yes
With pressured (WP)							
Heating rate (°C/hr)	10	112.36	108.96	111.67	111.00	-	-
	50	127.78	129.17	123.61	126.85	8.07	Yes
	100	101.18	112.71	107.92	107.27	5.24	Yes
Heating duration (hours)	12	106.58	103.36	105.53	105.15	-	-
	24	110.49	102.83	103.36	105.56	7.14	Yes
	48	127.78	129.17	123.61	126.85	11.30	Yes
Heating start time (day)	1	85.97	91.18	91.32	89.49	-	-
	2	127.78	129.17	123.61	126.85	15.40	Yes
	3	103.82	97.71	91.94	97.82	7.61	Yes

4.4 Effect of Condition on Physical Properties

4.4.1 Compressive Strength

The compressive strength is tested from three samples at 7-d and 28-d curing. During testing, most samples display a normal failure mode in which approximately similar cracks appear on the four exposed faces, with little

damage to the face in contact with platens, and a double pyramid shape is formed as shown in Figure 4.5.



Figure 4.5 Normal failure mode of RPC in compression forming a double pyramid shape

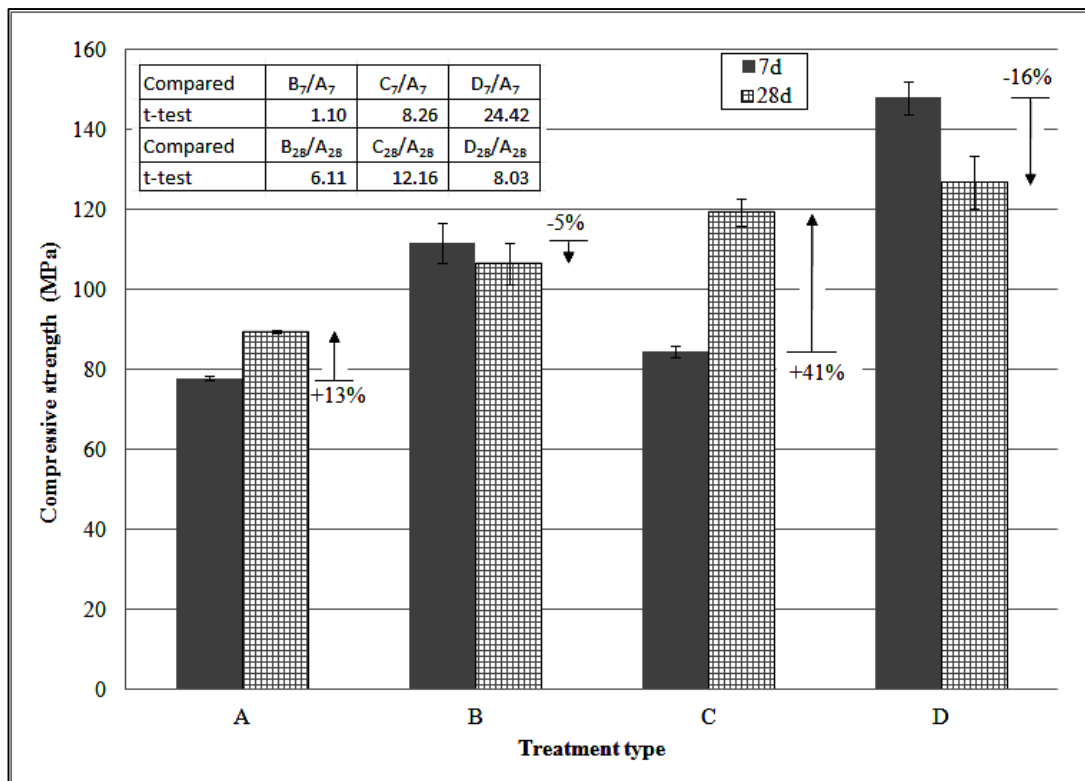


Figure 4.6 Compressive strengths for conditions A - D at 7-d and 28-d (Helmi *et al.*, 2013).

The average of the measured compressive strengths of each experimental condition (A-D) is presented in Figure 4.6. The untreated mixture (A) produces a compressive strength of 77.75 MPa at 7-d and this increases by 13 % to 89.58 MPa at 28-d. Following static pressure (C) condition during setting, the 28-d compressive strength increased to 119.38 MPa, which is a 41 % increase over its 7-d strength. Since the pressure condition during setting is likely to reduce the pore volume and pore diameter of entrapped air voids, it can be assumed at this stage that the compressive strength of C is slightly higher than A at 7-d because of some reduction in the diameter of macro defects (pores).

Correspondingly, this would theoretically allow a larger proportion of the total pore volume to be filled by C-S-H and associated Portlandite during hydration, and so could account for the large increase in 28-d strength for C compared to A (Yazici *et al.*, 2008).

The application of heat during curing increases the mean compressive strength by 32 % without pressure (B) and by 41 % with pressure (D) at 7-d. However, at 28-d the compressive strength of both decreases by 5 % for B and 16 % for D. Heated curing has a very significant effect on 7-d compressive strength (B and D), which is most likely related to acceleration of the pozzolanic reaction and hydrate transformation (Cwirjen, 2007). In addition, RPC containing silica fume with low water-cement ratio increases the aggregate-mortar bond, being more stable at high temperature (Kovler & Roussel, 2011). Heat treated samples (with or without preceding pressure condition) reduce compressive strength at 28-d compared to the 7-d strength. This is perhaps due to the formation of microcracks that are known to initiate by thermal expansion during accelerated heat curing (Tam & Tam, 2012), particularly since RPC contains a high proportion of fine-grained materials (cement, SF, GGBS).

This hypothesis is based on the assumption that post-conditioning stress relaxation has resulted in a slow progressive increase in the volume of any microcracks. The crystallisation process of hydration continuously increases after 7-d and may cause further propagation of these microcracks (Patel *et al.*, 1995). Although the bulk porosity decreases following static pressure conditioning, the volume of micro cracks apparently increases and this is worsened by heat curing. In addition heat curing induces a rapid hydration process by which is produced a non-uniform distribution of hydrates in cement pastes, and a more porous structure that remains unfilled at 28-d (Neville, 2011).

However, the compressive strength of both heat treated samples at 28-days is higher than untreated (A) by 19 % (B) and 39 % (D). Heat curing can accelerate the cement hydration and pozzolonic reaction due to the development of longer C-S-H chains (Cheyrezy *et al.*, 1995; Zanni *et al.*, 1996). In addition the C-S-H structure is crystallized much better due to high strength, with stability to shrinkage or creep and a greater resistance to chemical attack as other benefits (Dietz & Bohnemann, 2000). These assumptions will be evaluated using a microstructure analysis approach in the next chapter.

4.4.2 Density

The properties of RPC are mostly influenced by pressure and heat in the course of curing. Pressure condition has significant impacts on the compaction of the microstructure while heat curing influences the type of crystal formation during hydration (Richard & Cheyrezy, 1995; Tam & Tam, 2012). Both conditions affect density and porosity properties which generally have strong empirical correlation to the compressive strength (Neville, 2010).

In this study, density and porosity are determined gravimetrically according to BS 1881-114:1983 and based on the measurement of three prisms (40x40x160 mm) created under each of three conditions: dry air, in water, and in the drying oven. The averages of the three samples measured for the conditions described earlier (A to D) are presented in Figure 4.7 for density and Figure 4.8 for apparent porosity.

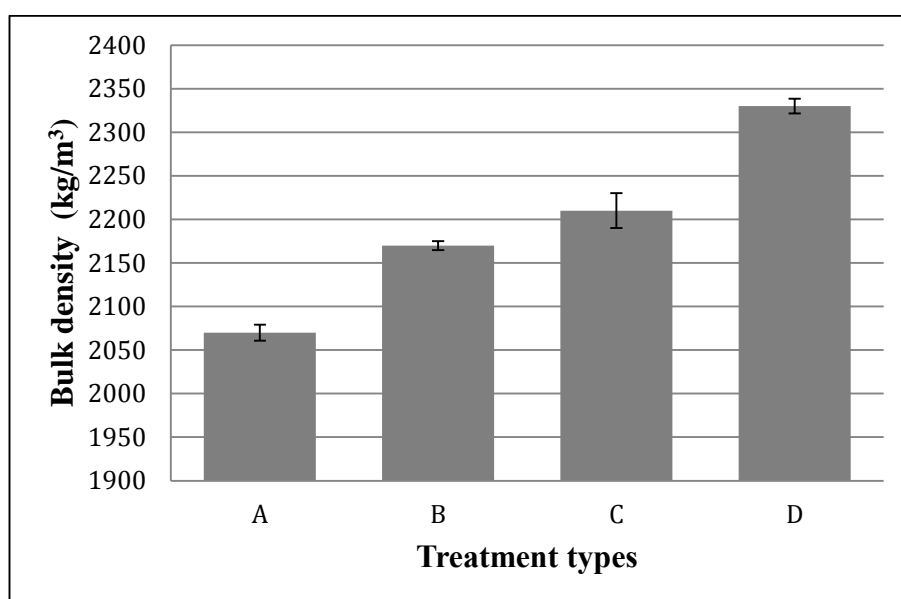


Figure 4.7 Bulk densities for all conditions at 7-d (Helmi *et al.*, 2013)

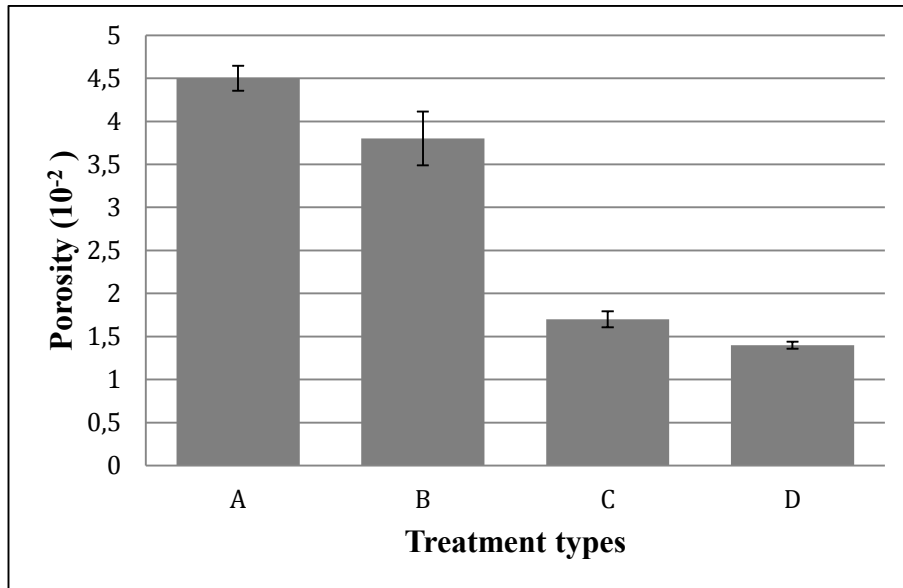


Figure 4.8 Apparent porosities for all conditions (Helmi *et al.*, 2013)

The results show that pressure condition (C) slightly increases the bulk density by 6.5 % and significantly reduces the porosity by 62.2 % through a reduction of entrapped air volume and free water removal. Previous studies have shown that spherical entrapped air-filled pores can occur in RPC despite the high percentage of superplasticizer and typically they range in diameter from 10 to 300 μm (Yazici *et al.*, 2008). The application of pressure during setting appears to reduce both the diameter and volume of these entrapped air pores, which densifies the matrix and increases bulk density as confirmed by a separate study (Yazici *et al.*, 2010). It is known that pressure applied to fresh concrete can reduce the water/binder ratio by around 4 % (Sadrekarimi, 2004). When the pressure is released after final setting, this can further reduce the bulk porosity due to expansion of the decompressed aggregates (Richard & Cheyrezy, 1995).

For heat curing conditions only (B), the density increases by 4.8 % and porosity decreases by 15.6 %. These changes in properties are similar percentages to those of conditions C and D with an increase of 5.4 % for density and a reduction of 17.6 % for bulk porosity. Richard & Cheyrezy (1995) and Hong & Glasser

(2004) all observed that heat curing can accelerate the pozzolonic reaction between amorphous silica and calcium hydroxide leading to the rapid formation of C-S-H gels. Spherical pores (caused by air entrapment) in RPC are generally air-filled or with some calcium hydroxide crystals following a standard curing, but can be filled with tobermorite (C-S-H) structures in the form of needle-like crystals when autoclave cured (Yazici *et al.*, 2010). For curing at temperatures greater than 200 °C, crystals of needle-shaped xonotlite are present together with plate-shaped tobermorite (Tam & Tam, 2012). This can lead to reductions in measured bulk porosity by pore filling with the C-S-H product and consequently alters the pore size distribution by reducing the median pore diameter (Cwirzen, 2007). The presence of xonotlite after high temperature curing will be evaluated in microstructure testing later.

4.4.3 Correlation between porosity and compressive strength

The 7-d compressive strengths of RPC for all conditions in Figure 4.6 are classified as high performance concrete (Neville, 2011) which then can be expressed as a correlation equation between bulk porosity (log scale) and compressive strength for plain concrete as follows:

$$f'_c = f'_{c,0} (1 - p)^n \quad (4.1)$$

Where: p = porosity, f'_c = compressive strength, $f'_{c,0}$ = strength of paste at zero porosity, and n = a scaling integer. This assumes that $f'_{c,0}$ equals 500 MPa for cement paste at $w/c = 0.45$ (Neville, 2011). These variables produce n -value scaling coefficients of 40.5 (A), 38.8 (B), 103.7 (C), and 86.4 (D). Despite there being a strong empirical correlation between bulk porosity and compressive strength for conventional concrete (Neville, 2011), the results for RPC show that

the correlation integer depends upon the conditions applied (Figure 4.9). When f'/ρ was plotted using $n = 40.5$ (determined for condition A by Eq.4.1), the curve intersects the data for condition B, and where $n = 103.7$ (determined for condition C) the curve is close the data for condition D.

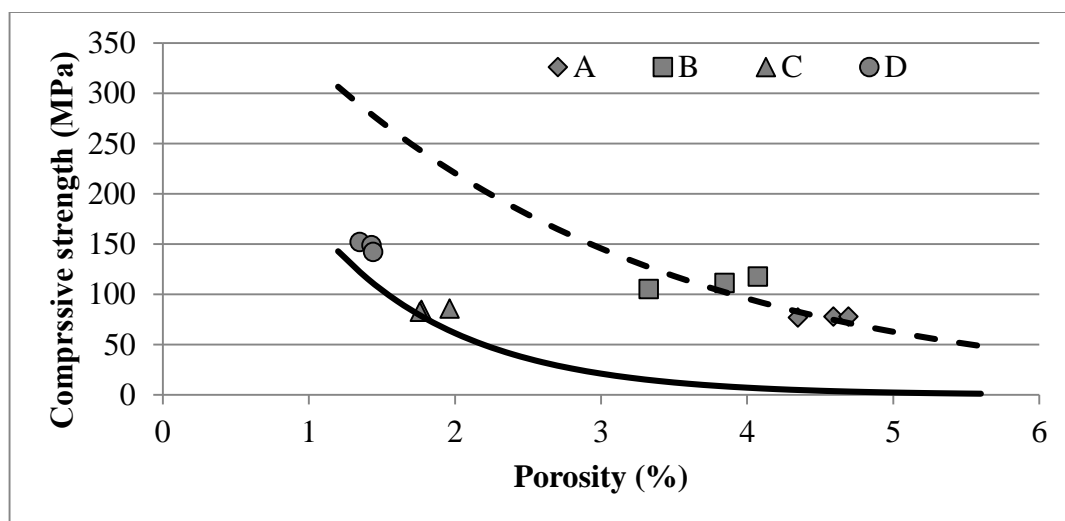


Figure 4.9 Correlation between porosity and compressive strength under each set of conditions (Helmi *et al.*, 2013)

4.4.4 Preliminary Model Proposed.

The effect of pressure on spherical entrapped air pores was evaluated by optical microscope. The samples were prepared by taking small pieces from the core of cube samples of A and C. The images were taken using a Nikon Optiphot Microscope with digital camera. The results presented in Figure 4.10 show that the matrix treated by pressure (label C) is denser and more homogeneous than the one without pressure; this indicates very low porosity. However, entrained or entrapped air pores still appear in mixture C. These spherical pores, most of which formed possibly due to the side effect of a high amount of superplasticizer, have different diameters giving a wide range between 10 and 300 μm .

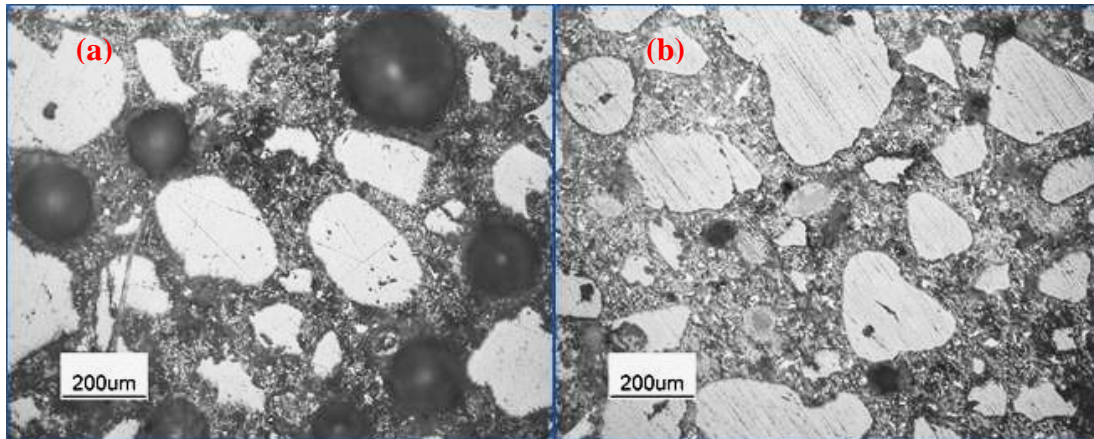


Figure 4.10 Entrapped air appearances on sample surface without heat curing: (a) for conditions A and (b) for conditions C

If a sample was heated then these pores were generally filled with crystalline phases of variable composition, possibly tobermorite or jennite (Chen & Kwan, 2012). The effect of both entrapped air and pore-filling by crystalline phases can be illustrated using the simple conceptual model in Figure 4.11. It assumes that a uniformly hydrated matrix contains randomly distributed spherical pores with diameters varying between 10 and 300 μm when cured under ambient temperature/ pressure conditions (Fig. 4.11a). When static pressure is applied to a fresh mixture, the total pore volume and the mode pore diameter both decrease (Fig. 4.11b). Heat curing accelerates the pozzolanic reaction in an already densified cement matrix leading to pore filling by crystalline hydrate (tobermorite and/ or xonotlite) formation (Fig. 4.11c). Since heat curing increases the air pressure inside pores, the hydrated matrix outside of pores becomes dense. However, this model will be developed further using microstructure testing in the next chapter.

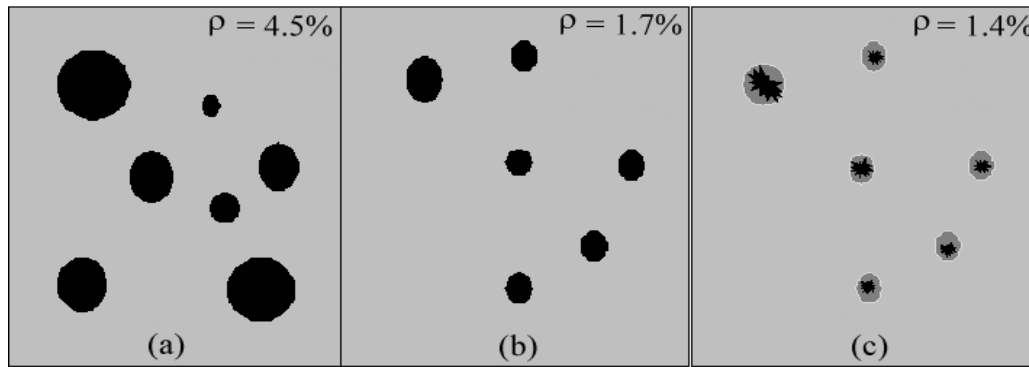


Figure 4.11 Conceptual model of curing condition effects on spherical entrapped air pores in RPC: (a) standard curing, (b) pressurized setting, (c) pressurized setting followed by heat condition during hardening (Helmi *et al.*, 2013)

4.5 Mechanical Properties of RPC with Carbon Fibre

The performance of RPC commonly containing fibres will depend on conditions during and after the setting period (Richard & Cheyrezy, 1995; Cwirzen *et al.*, 1995; Sadrekarimi, 2004; Yazici *et al.*, 2008.; Tam & Tam, 2012). The purpose of using fibre is to enhance the desirable properties of a cementitious matrix with varying degrees of performance in three areas, tensile strength, ductility and durability. This provides an increase in the stress at which the matrix starts to crack; an improved strain capacity after peak load; and modification of crack development (Johnston, 2006).

Performance of concrete containing fibres under load will be influenced by three main factors i.e. volume of fibres, physical properties of fibres and matrix, and bond of both (Hannant, 1998). The effect of fibres generally is greater in flexural strength than in compression strength (Johnston, 2006). In addition, the presence of fibres in a concrete mixture also improves flexibility, toughness, impact resistance, and freeze-thaw durability (Chou, 2000).

4.5.1 Flexure Strength

Flexure testing of RPC prisms (40x40x160 mm) in this study refers to the Yazici *et al.* (2009) method by three-points loading with 0.1 mm/min rate and 100 mm clear distance between supports. Test results in flexure of RPC with carbon fibre (labelled CF) are then compared with those without fibre or non-fibre (labelled NF) which are then evaluated under four conditions as with previous work. The flexural strength is the average of three samples as presented in Figure 4.12.

If the flexural strength of RPC samples with carbon fibre is compared with those without carbon fibre under the same conditions of curing, the results show a variation of effect by -2.37 % for A, 16.42 % for B, 28.85 % for C, and 14.32 % for D. Overlapping error bars are shown in condition A from which it can therefore be assumed that NC and NF are similar strength. While the RPC with carbon fibre is compared to the same mixture in condition A, the conditions used commonly improve the flexural strength in a range of 30 – 40 %. It is found that the addition of carbon fibre has a significant effect on flexural strength of an RPC mixture if any of the altered conditions of curing are applied to the samples.

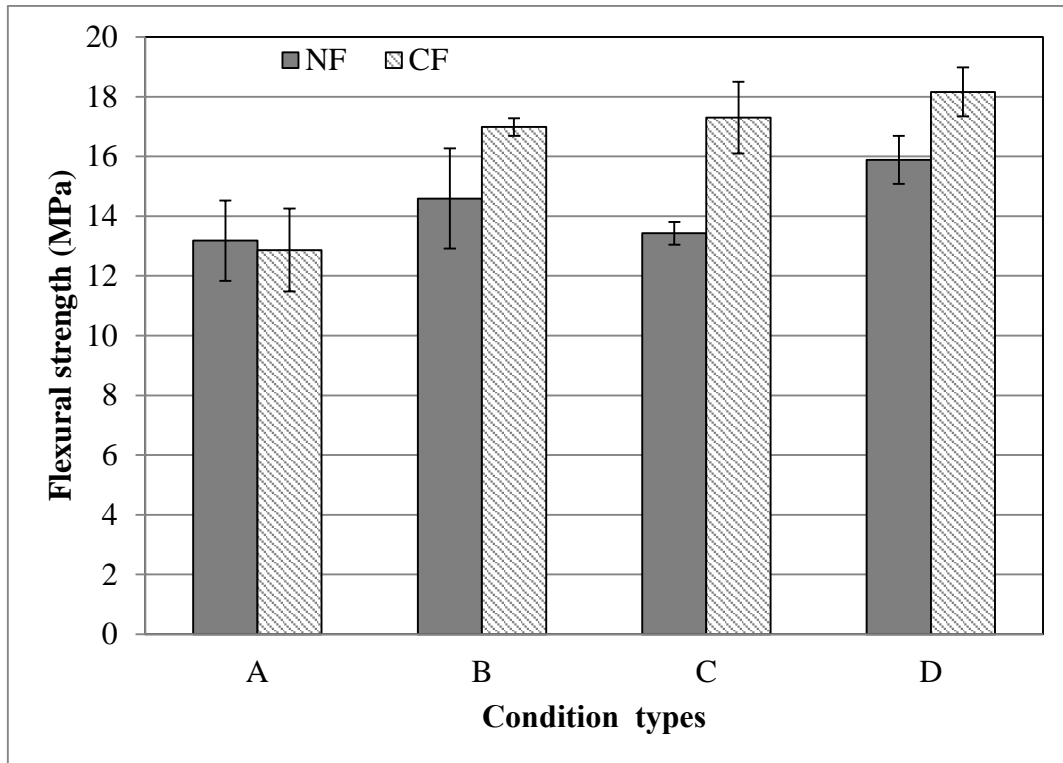


Figure 4.12 Comparison of flexural strength between RPC non-fibre (NF) and with carbon fibre (CF) for all conditions.

4.5.2 Toughness and Flexural Modulus

Flexural testing for all types of curing conditions shows that there is a brittle failure mode as samples suddenly rupture after peak loading with only a small prior deformation. Deflection after peak load consequently cannot be recorded. To evaluate the effect of carbon fibre in RPC mixtures, the results of measurements from three samples under condition D, both NF and CF, are plotted in a figure correlating the load and deflection as shown in Figure 4.13.

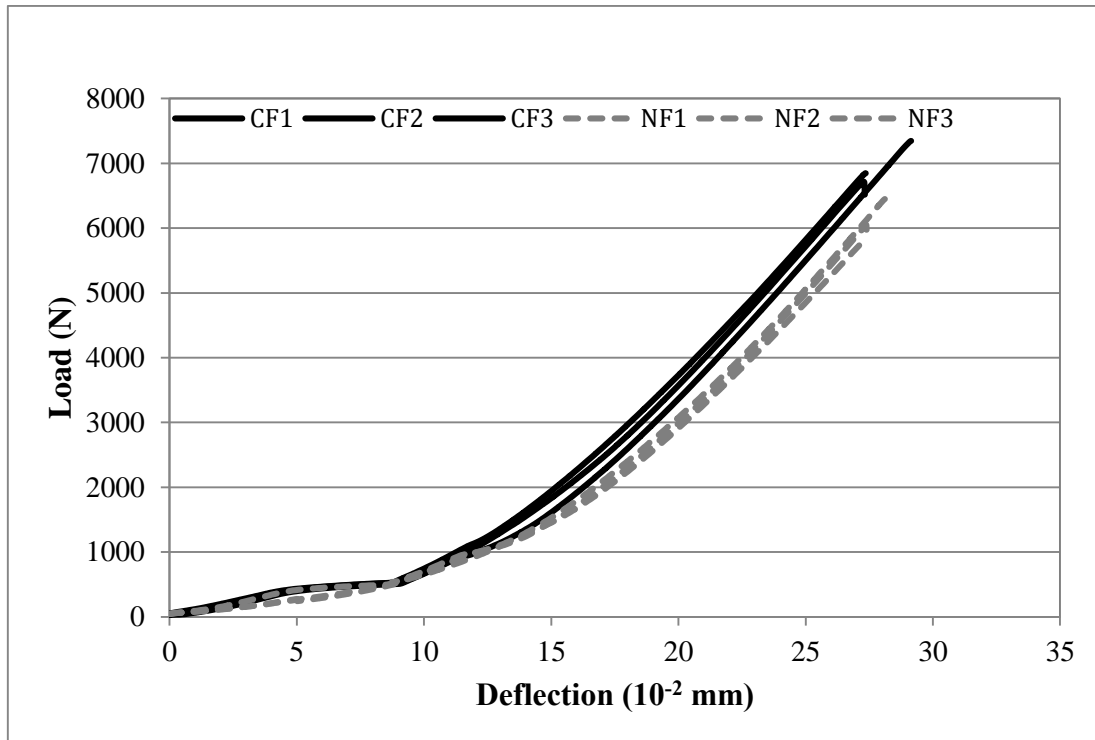


Figure 4.13 Load and deflection curves for NF and CF with condition D showing immediate rupture after peak load

The presence of fibre has no effect on the failure mode, sudden rupture after peak loading (brittle) as with the RPC without fibre. The improving strain capacity after peak load in RPC with carbon fibre does not appear in the curve which is a different behaviour to that displayed by RPC with steel fibre in Yazici *et al.*, (2009). It implies that the behaviour of carbon fibre after high temperature curing is the main cause of this rupture mode. It is already known that steel fibre has a thermal coefficient of expansion similar to that of plain concrete (Khodur & Sultan, 2003) about $13.51 \times 10^{-6}/^{\circ}\text{C}$ (Neville, 2011). This is higher than carbon fibre which is about $2.1 \times 10^{-6}/^{\circ}\text{C}$ (Pradere & Sauder, 2008). If the RPC sample is cured at a high temperature and then cooled in air, the expansion and shrinkage of carbon fibre is less than the cement paste or steel fibre. This behaviour may reduce the bonding mechanism between the paste and the carbon fibre which consequently reduces the fibre pull out strength.

On the other hand, the pull out pressure of carbon fibre at ambient temperature is also lower than steel fibre with 1.29 MPa for carbon fibre (Katz *et al.*, 1995) and 5.48 MPa for steel fibre (Chan & Chu, 2004). The use of carbon fibre in low volume fractions (0.1 %) is believed to be additional factor which causes failure soon after the maximum load (Johnston, 2006). It seems that the low bonding between carbon fibre and cement paste is caused by heat curing and is a main cause of brittle failure in RPC. This will be evaluated later through SEM images on the surface of carbon fibre in Chapter 5.

The toughness is accounted from the area under load-deflection curve and the flexural modulus uses equation 3.1. The result is presented in Table 4.3. The presence of carbon fibre in the RPC mixture significantly increases toughness by 20% and slightly increases flexural modulus by 6%. It seems that the improvement is due to the role of fibres in suppressing crack progression. As a result, additional energy is absorbed before complete separation of the sample occurs. However, the presence of carbon fibre may increase porosity which consequently changes the behaviour of RPC samples up to peak load, becoming more ductile.

Table 4.3: Toughness and flexural modulus result for NF and CF with condition D

Type	NF				CF			
No	Load (N)	Deflec. (10 ⁻² mm)	Tough's (N.mm)	E_f (MPa)	Load (N)	Deflec. (10 ⁻² mm)	Tough's (N.mm)	E_f (MPa)
1	6448	28.1	584	4547	7345	29.1	694	4774
2	6047	27.4	519	4527	6847	27.4	631	4639
3	6448	27.3	500	4330	6719	27.3	606	4742
Average			535	4468			644	4718

4.5.3 Compressive Strength

In compressive strength, the role of fibres is not to reinforce the matrix in the direction of applied stress but to improve the behaviour of the sample near the point of total failure (Johnston, 2006). The compression test results for NF and CF under all conditions of curing are presented in Figure 4.14. In condition A, the compressive strength of CF is slightly higher than NF. Although the bond between carbon fibre and cement paste is weak, the improvement is probably due to the role of carbon fibre in preventing crack progression randomly (Chung, 2000). However, as the error bars overlap, the compressive strength of both can be assumed to be similar.

Under condition B, the presence of carbon fibre in the RPC mixture slightly increased the compressive strength by 2 %. Nevertheless, this differentiation is not significant according to the error bars. The compressive strength of RPC with carbon fibre heated in a dry oven displays different results compared to the samples with steel fibres following a dry oven curing (Tam & Tam, 2010) or with steel fibres in autoclave curing (Yazici *et al.*, 2008). Though curing in a dry oven also forms xonotlite (Tam & Tam, 2010), it does not improve the compressive strength significantly when the sample contains carbon fibre. This is due to the different thermal expansion coefficients between carbon and steel fibre, because of which the carbon fibre results in higher internal thermal stresses (Szoke, 2006).

Under condition C, compressive strength increased slightly up to 6 %. The reason for this increase could be that the pressure has moved the grains of binder around the fibre to be closer and more compacted which consequently may increase the bond between cement paste and fibre. In addition pressure also may reduce the porosity of cement paste. This fact could also support the explanation

of condition B that the different expansion of cement paste and carbon fibre during heat curing could be a reason for the relatively low compressive strength.

For condition D, the measured compressive strength slightly increased up to 7 %. The influence of carbon fibre is reduced due to the wide difference in thermal coefficient of expansion between carbon fibre and the cement paste (as explained in condition B). These compressive strength results are statistically similar indicated by the overlapping error bars. However, condition D is suggested as a method to use to produce RPC samples with good properties of RPC from a mechanical or microstructural perspective. There are two advantages of applying condition D: pressure can compact the matrix which then increases the ability of the added carbon fibre to mitigate the initiation of micro defects of concrete and subsequent bridge cracking (Chen & Liu, 2014); heat curing increases pozzolanic reaction and transforms C-S-H becoming tobermorite and xonotlite (Richard, 1995; Cheyrezy *et al.*, 1995; Zanni *et al.*, 1996; Cwirzen, 2007).

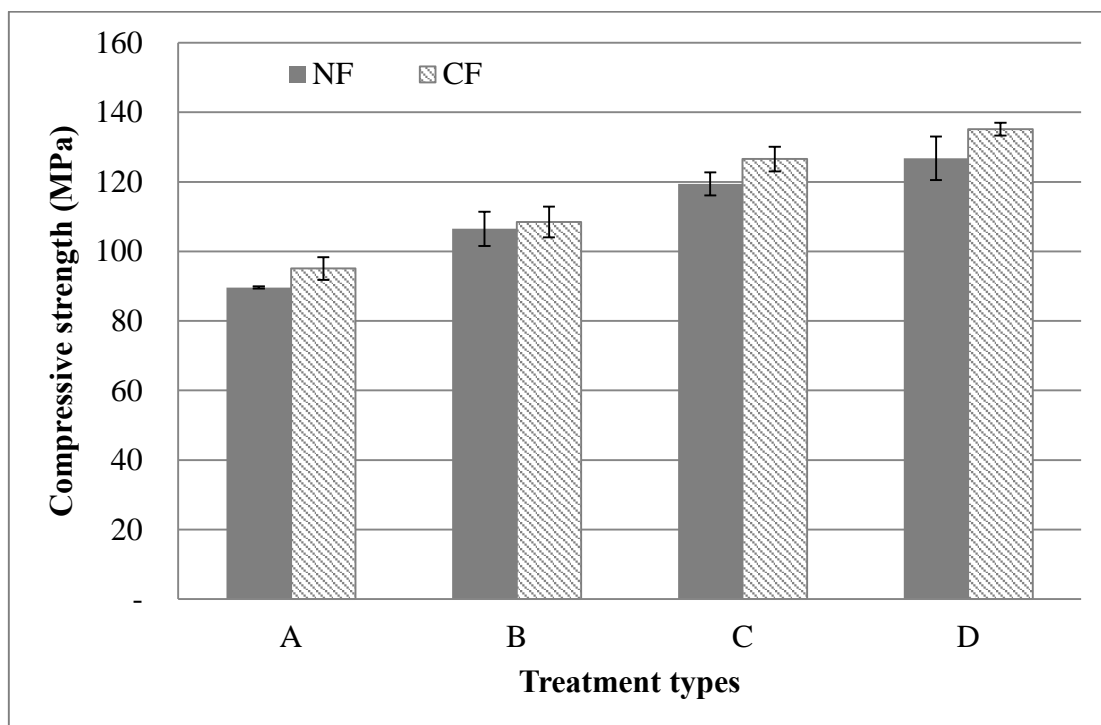


Figure 4.14 Compressive strength NF and CF for all conditions showing the overlapping of error bars between both.

4.5.4 Correlation between Compressive and Flexural Strength

Compressive strength is a common requirement in structural design while tensile strength is necessary for certain construction work such as highway and airfield slabs which look to combine compressive strength with cracking resistance.

These strengths generally have a close correlation so that when compressive strength (f'_c) increases then the tensile strength (f_t) increases as well. However, this correlation will be affected by many factors such as w/c ratio, aggregate type and additional material in the mixture (Neville, 2011).

The correlation of between both strengths may be presented in an empirical power's formula (Neville, 2011):

$$f_t = k(f'_c)^n \quad (4.3)$$

where k and n are coefficients, suggesting a range of values between $\frac{1}{2}$ and $\frac{3}{4}$ for n .

Figure 4.15 shows the correlation between the compressive and flexural strength of RPC in this study, combined with the data of Yazici *et al.* (2009). The power's equation to figure out that correlation looks compatible for both results.

However, the curve expresses the exponential equation of 0.27 for k and 0.87 for n which are not in a range as suggested by Neville (2011).

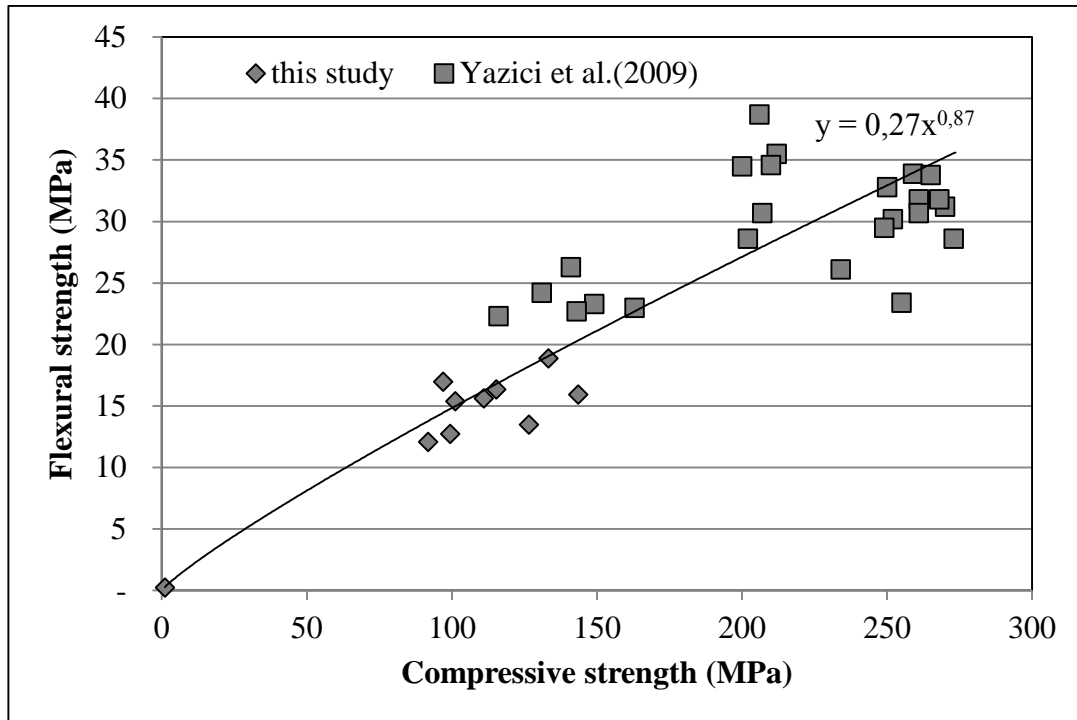


Figure 4.15 Correlation between compressive and flexural strength of RPC, data in this study merged with Yazici *et al.* (2009)

4.6 Summary

RPC composition using GGBS as cement replacement and a high amount of superplasticizer results in different fresh mixture properties compared to a standard mixture. The setting time of RPC is longer; about four times greater than that of standard cement due to an increase of free water content in the mixture. The use of superplasticizer of 10 % of cement content also influences the setting time due to changing the solubility and the rate of solution of calcium sulphate ions from cement. The consistency of fresh RPC shows a plastic flowing and spreadable mixture. The mixture can spread about 150 % greater than its initial diameter due to a higher water/binder ratio of 0.192, instead of 0.132 quoted by other scholars. These results confirm that water content significantly influences the properties of fresh RPC mixture.

Optimising heat curing has been explored in three ways, i.e. heating rate, heating duration and heating start time. A heating rate at 50 °C/hr results in the highest compressive strength about 40 % more than these at 10 or 100 °C/hr due to the proportional effect on, pozzolanic reaction and microcracks formed in paste. A heating duration of 48 hours lead to a maximum compressive strength compared to the samples at 12 and 24 hours due to the acceleration of both reactions (hydration and pozzolanic) and the increase in the of amount crystal transformation from tobermorite to xonotlite. Heat curing applied at 2 days after casting results in the maximum compressive strength due to heat-induced acceleration of hydrate phase densification whilst avoiding the risk of microcrack initiation/enlargement resulting from thermal expansion of partially-hardened hydrate phases. It is concluded that the optimum condition of heat curing is starting at 2-day after casting with a rate of 50 °C/hr for 48 hours.

In compression, RPC samples mostly produce normal failure modes forming a double pyramid shape. By comparing these to a reference (A), the pressure condition (C) increases compressive strength slightly at 7-d and significantly at 28-d; while a heat curing condition only (B) or with pressure (D) increases compressive strength significantly for both 7-d and 28-d of sample ages. The application of pressure reduces both the diameter and volume of entrapped air pores, densifies the matrix, increases bulk density, and reduces porosity; while heat curing may accelerate the pozzolanic reaction, induce pore filling, and reduce porosity.

The addition of carbon fibre in the RPC mixture results in variation of flexural strength compared to the samples without carbon fibre: -2.37 % for A, 16.42 % for B, 28.85 % for C, and 14.32 % for D. Any of the conditions used can improve the flexural strength of RPC in a range of 30 – 40 % compared to the reference (condition A). The presence of carbon fibre in the RPC mixture

increases toughness by 20% and flexural modulus by 6%; however, it still results a brittle failure as in the RPC without carbon fibres. The difference of thermal expansion coefficients between carbon fibre and cement paste might be assumed as the main factor influencing the bonding mechanism between paste and carbon fibre due to its behaviour during heat curing conditions.

Chapter 5- Microstructure of RPC

5.1 Introduction

Most scholars agree that heat curing affects the hydration reaction, microstructure and microchemistry of RPC. In general, low heat temperature curing (up to 90 °C) can accelerate the pozzolonic reaction, while high temperature curing (more than 150 °C) can also transform the species of hydrate crystals. The properties of concrete after exposure consequently depend on the chemical and physical changes in hardened cement paste (hcp), aggregate, and at the interface (Xu *et. al.*, 2001).

This chapter presents the microstructural properties which were analysed in order to achieve a fundamental understanding of the effects of high temperature (applied as a curing treatment) on the setting period of RPC mixtures.

Microstructural properties were experimentally investigated by examining the morphology of hydrates, crystalline phases, porosity, pore size distribution and interfacial transition zone (ITZ) characteristics. A model of microstructure behaviour after treatment is proposed based on the investigation.

5.2 Morphology of Cement Paste Based on SEM Test

It is well known that pressure setting applied to fresh RPC mixtures can increase their density due to the reduction of entrapped air pores, both in terms of diameter and number, and the associated removal of free water content. On the other hand, the use of high cement content and low water-cement ratio results in a mixture of anhydrous and hydrated material. In addition, applying high temperature curing affects not only the prevention of the hydration process of

cement grains but also induces microcracks in the hardened paste due to evaporation and the transformation of CSH gel (Tam *et al.*, 2010).

5.2.1 Entrapped Air Pores

In general RPC has a denser matrix phase and is more homogeneous than normal concrete. However it still contains entrapped air pores with a wide range of diameters between 10 and 300 μm , which are formed by using high amounts of superplasticizer in the RPC mixture (Yazici *et al.*, 2008). Entrapped air pores are generally spherical and much larger than any other type of pore.

In SEM images of cementitious materials, several kinds (and length scales) of pores can be observed as shown in Figure 5.1. Polished cross-section RPC specimens were prepared and imaged, and analysed using the secondary electron (SE) detector at 10 mm working distance. Figure 5.1 (a) and (b) show that RPC without pressure treatment had some entrapped air pores with a maximum diameter of about 200 μm . When pressure was applied to fresh mixtures, the number and diameter of large entrapped air pores were reduced by around one order of magnitude (Fig 5.1 (c) and (d)). In addition, the matrix of specimens appeared denser than those without pressure. It is suggested here that some of pores have been closed altogether with spill out of free water, whilst others are changed physically becoming smaller in diameter and greater in number. This finding supports most scholars' statements that applied pressure on fresh mixtures can reduce the pore volume and mean diameter, and consequently increase matrix density (Richard *et al.*, 1995; Yazici *et al.*, 2008; Helmi *et al.*, 2013).

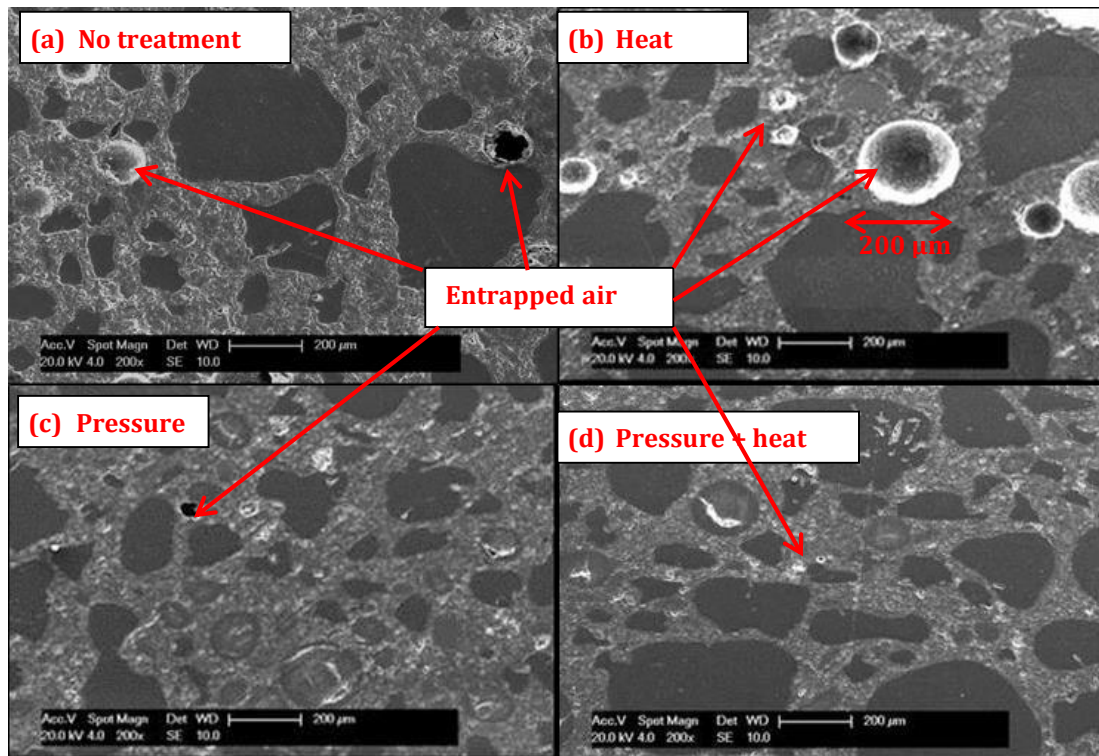


Figure 5.1 Secondary electron micrographs of polished cross-sections through RPC samples following (a) no treatment, (b) heat treatment during hardening, (c) static pressure treatment during setting, and (d) combined pressure and heat treatment. The diameter and volume of entrapped air pores have been reduced by around one order of magnitude.

5.2.2 Anhydrous and Hydrated Materials Formed after Treatments

Microstructural investigations using SEM can indicate unreacted (anhydrous) and reacted material (hydrates) in the paste based on the atomic number contrast level (Scrivener, 2004). Images captured by the backscattered electron (BSE) detector are appropriate to describe the hydrates formed because back scattered electrons originate from greater depths within the sample (Scrivener, 2004). In general, anhydrous grains have a lighter colour than the hydrates as they have a higher atomic number. In anhydrous grains, the brightest one is ferrite solute solution (Fss) followed by alite (C_3S), aluminate (C_3A) and belite (C_2S). In hydrated grains, Portlandite (CH) has a lighter grey than C-S-H, ettringite or AFm phase. In fact it is difficult to differentiate between them based on this grey level

alone. However, ettringite can be easily identified as a large mass of crystals with a needle-like morphology (Diamond, 2004).

Figure 5.2 shows images that were captured using the BSE detector, and for all cement treatments (A – B). The image is presented at low magnification (500x) in order to evaluate the effects of treatments on the hydration of cement grains in cement paste, especially on the presence of anhydrous phases. Higher magnifications (2000x) are shown later during discussion of micro cracks. In general all images show that anhydrous material is widely spread throughout the cement paste. It means that most of the cement paste contains anhydrous regions in every specimen for all treatments but at different levels of relative intensity. In addition, C-S-H as a main product of the hydration reaction in RPC, fills intergranular spaces within the paste for all treatments. This homogeneity is observed because RPC mixtures contain finer materials, which can fill the gaps between them and easily move.

The RPC sample without treatment (see Figure 5.2 (a)) appears to show the morphology of the paste to be less dense with the presence a large number of micro pores. Some gaps between anhydrous cement grains and C-S-H phase also appear to exist. It is supposed that there was a formation of pores without any product of hydration, as previously observed by Cwirzen (2007). C-S-H is indicated by the dark grey zones between each aggregate and appears poorly crystallised, *i.e.* mainly amorphous. This could be an indicator that free water in the mixture had supported the hydration reaction of the cement grains. However, this free water commonly induces an increase in the volume of micro pores after final hardening. Figure 5.2(a) also shows the presence of ettringite amongst the bulk C-S-H phase.

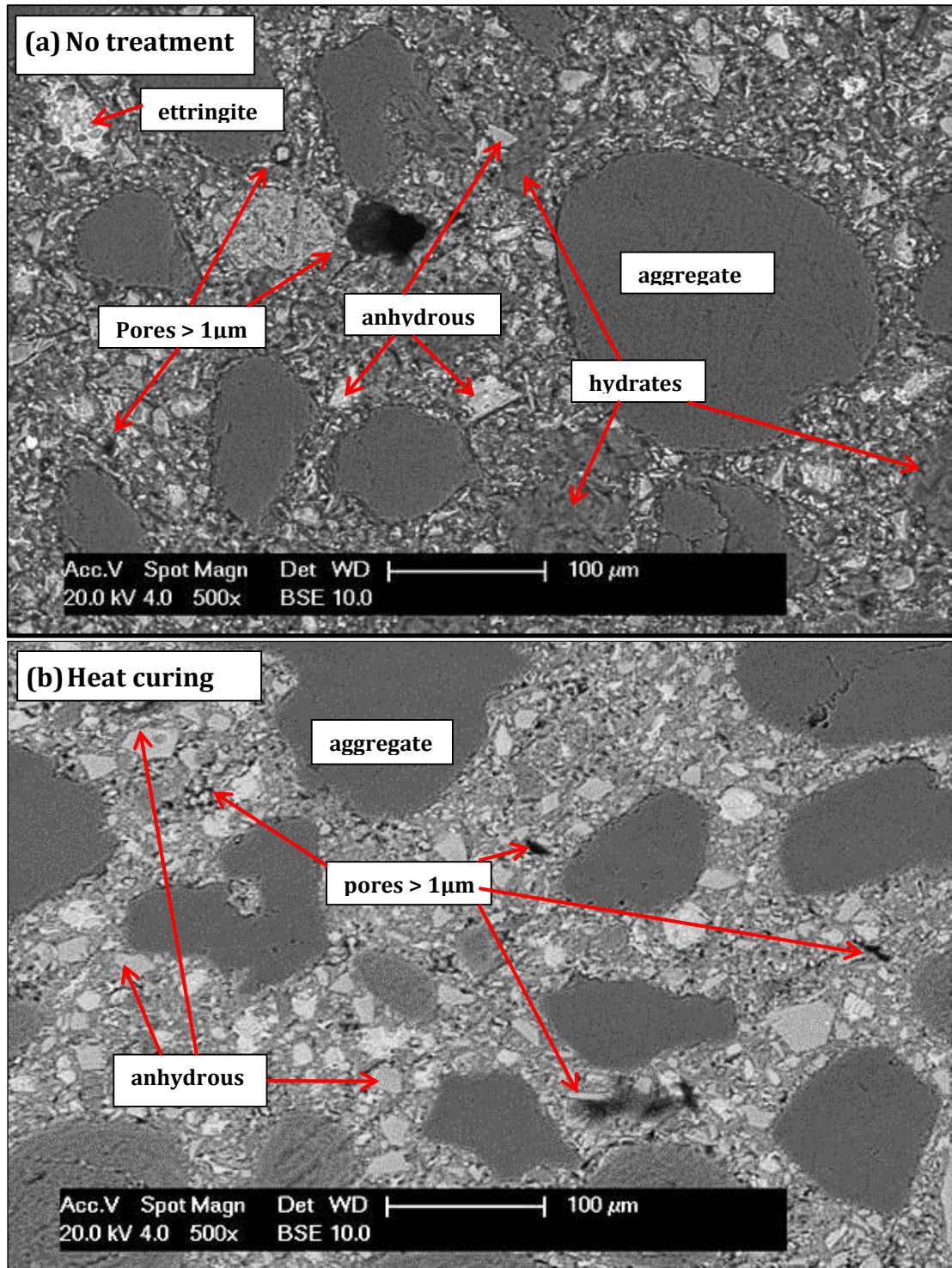


Figure 5.2 Backscattered electron micrographs of polished cross-sections through RPC samples following (a) no treatment, and (b) heat treatment during hardening. The intensity of anhydrous grains has been increased by heat curing due to quick evaporation.

Figure 5.2 (b) shows a lower density hardened paste with the apparent presence of more micro pores. The C-S-H formed after heat curing is mostly well crystallised, as observed in previous studies (Yazici *et al.*, 2013). The presence of anhydrous material appears higher, which suggests that heat curing prevented the hydration reaction of cement grains perhaps due to evaporation during hardening. The irregular shape of pores observed after this treatment suggests that heat curing creates increased pressure within existing pores that could result in elongation and the distended pore shapes that were observed.

In Figure 5.3 (a), the cement paste appears denser than that of previous samples. The anhydrous materials were found to be visually similar compared with Figure 5.2 (b). Microcracks were observed on both the surface of the aggregates and within paste. It was assumed that the pressure treatment applied to the fresh mixture (after about 5 hours after casting) induced some aggregate movement and created a small gap between aggregate and paste. Furthermore, pressure treatment has forced some of the free water to extrude from the mixture, and so some cement grains have only partially hydrated. Some regions appear to show a denser paste with evidence of micro pores < 1 μm diameter (see circles in Figure 5.3). This suggests that applied pressure in fresh RPC mixtures can induce micro crack formation around the aggregate whilst forming a denser hardened cement paste.

The combined application of both pressure and heat treatment (in Figure 5.3 (b)) resulted in a cement paste morphology (at macro scale) similar to that of pressure-only, *i.e.* dense, with well-dispersed anhydrous particles and micro pores. The observations revealed little difference in the abundance of micro pores < 1 μm diameter but with the presence of micro cracks surrounding the pore walls. It is suggested that these are due to the progression of microcracks,

initially-formed during early age curing, which are prolonged and widened by air pressure after the heat curing process began.

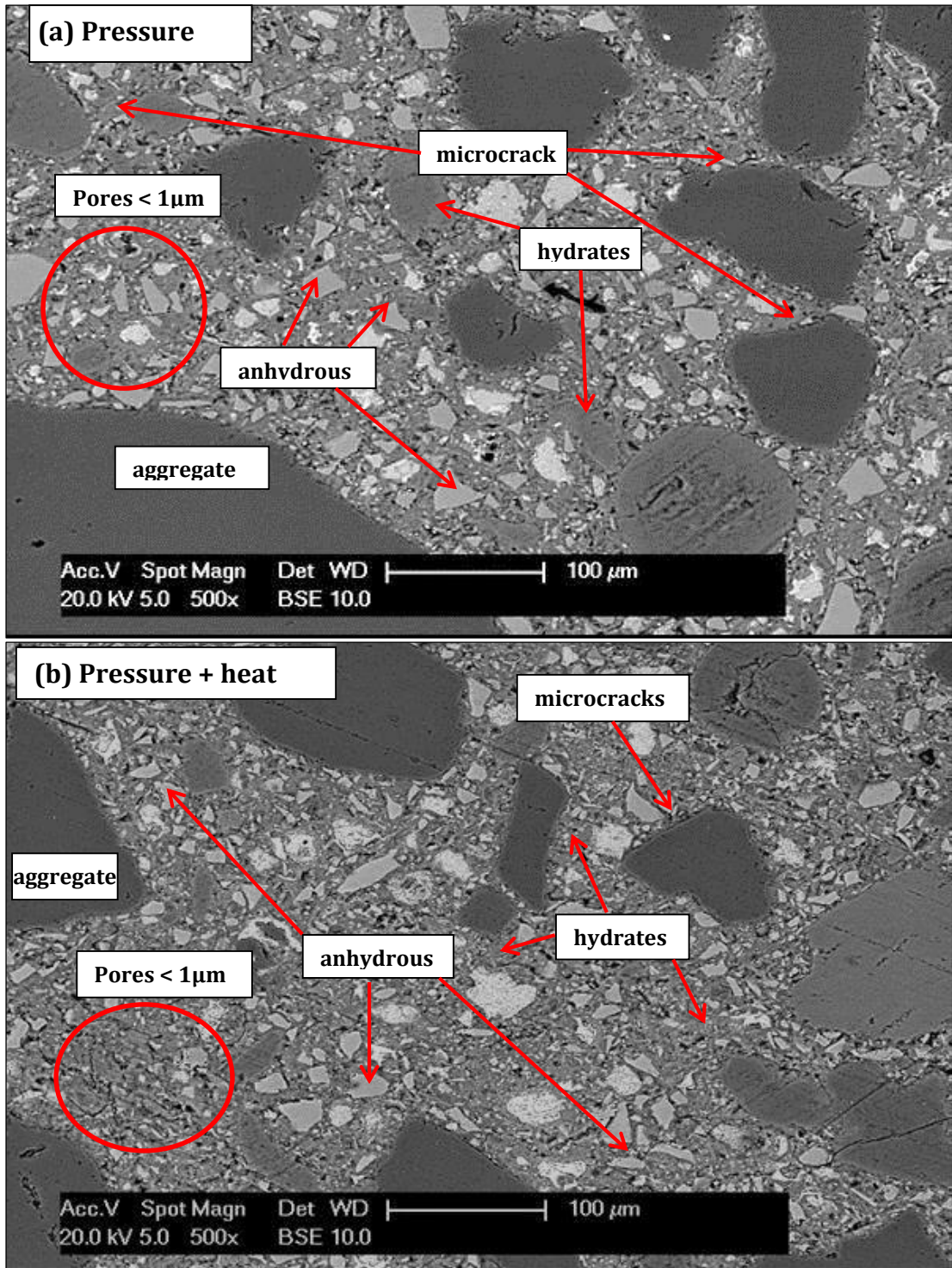
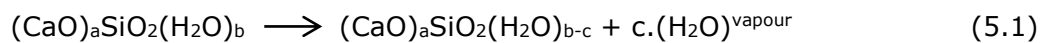


Figure 5.3 Backscattered electron micrographs of polished cross-sections through RPC samples following (a) static pressure treatment during setting, and (b) combined pressure and heat treatment. The intensity of anhydrous grains and microcracks have been increased by pressure due to lowering free water content and much more after heat curing.

This could be due to air held within the pore and which subsequently expanded during the heating process. This would result in tensile stress inside the pore and the development of micro cracks, as proposed by Hertz (2005). Heating concrete up to 240 °C can produce vapour from the free water held inside and from dihydroxylation of the C-S-H. The dehydration reaction is expressed as follows: (Zhang & Ye, 2012):



The vapour then flows to lower pressure areas such as the outer concrete surface or into pores which have impermeable walls inside. As temperature increases, the pressure in the pores increases as well. When the pressure exceeds the tensile strength of the concrete, then micro cracks appear and progress away from the pores (Anderberg, 1997).

It seems that pressure applied to fresh mixtures improved the matrix phase properties due to an increase of density and a decrease of porosity. Furthermore this pressure builds an interlocking system between the paste and the aggregate (Yazici *et al.*, 2010). Although pressure treatment results in more anhydrous material due to less free water, it can enhance the void filling effect with silica fume particles and thus enhance and densify the matrix (Tam *et al.*, 2010). After applying heat curing, the compacted matrix did not appear to change in terms of the relative amount of anhydrous grains. However, the appearance of micro cracks was found to occur more frequently perhaps due to crack progression originating at pore walls and exacerbated by the increase of air pressure inside the pores. In addition, high temperature curing increased the rate of pozzolanic reaction between the silica fume and increasing the apparent amount of C-S-H product, as observed in previous studies (Zanni *et al.*, 1995).

5.2.3 Microcracks Appearance

It is well known that micro cracks always exist in cementitious material because of the thermal transportation that occurs during the hydration reaction, and the shrinkage that follows after the setting period (Neville, 2011). The presence of micro cracks is also common in RPC and much more so when heat curing is applied to RPC specimens during the setting period (Tam & Tam, 2012).

Figure 5.4 shows examples of SEM images at higher magnification (x2000) revealing greater detail on the hydrated grains and micro cracks. Three specific grains of interest are marked in this figure. The grain marked "A" is representative of fully hydrated C-S-H, which is normally placed around the cement grains (Scrivener, 2004). The grain marked "B" is an anhydrous grain of alite which has partially reacted. The grain marked "C" is an anhydrous grain of belite, which has some banding due to different solute contents (Diamond, 2004).

Figure 5.4 (a) shows the typical cement paste morphology observed for samples without treatment, which are characterised by having less density but with some gaps between the anhydrous cement grains and the C-S-H phase. The structure of C-S-H appears to be an amorphous, poorly crystalline structure and, as previously observed by Cwirzen (2007). Microcracks (highlighted by circles in Figure 5.4) about 1 μm wide were present in some areas of the paste, perhaps due to the autogenous shrinkage process. Furthermore the heat curing at 240 °C induces additional micro cracks, as shown by Figure 5.4 (b). The progress of micro cracks could be from the further development of existing micro cracks, such that they become longer and/or wider due to air pressure expansion. Small fractures could also be happening because of the increased air pressure of entrapped air voids during heat curing. Damone (1998) suggested that the maximum thermal expansion is reached in partially dry conditions and is typically

$18 \times 10^{-6}/^{\circ}\text{C}$ for cement paste, and $11 \times 10^{-6}/^{\circ}\text{C}$ for quartz aggregate. This difference in coefficient is also believed to contribute to the micro crack formation because it results in a difference in behaviour during heat curing and the subsequent cooling process, and thermal stress occurs.

Pressure treatment might also cause microcracks between hydrates (Figure 5.5 (a)). These microcracks could be developed because of two reasons; (i) less free water after being forced by pressure, which disrupts the hydration reaction, and/or (ii) moving material grains (including aggregate and paste) during pressure implementation. The combination of pressure and heat curing as shown in Figure 5.5 (b) results in micro cracks as for treatment C but with longer and wider micro cracks. This pattern is assumed to occur when air flows through existing micro cracks and becomes trapped at the end of dead end pores. Some very fine micro cracks were observed at the outer side of pores, the propagation of which resemble that of a small explosion. It is hypothesised that this occurs when air pressure is entrapped in impermeable pores and continuously increases until it exceeds the tensile strength of the surrounding concrete (Bazant & Thonguthai, 1979; Kahlifa *et al.* 2000).

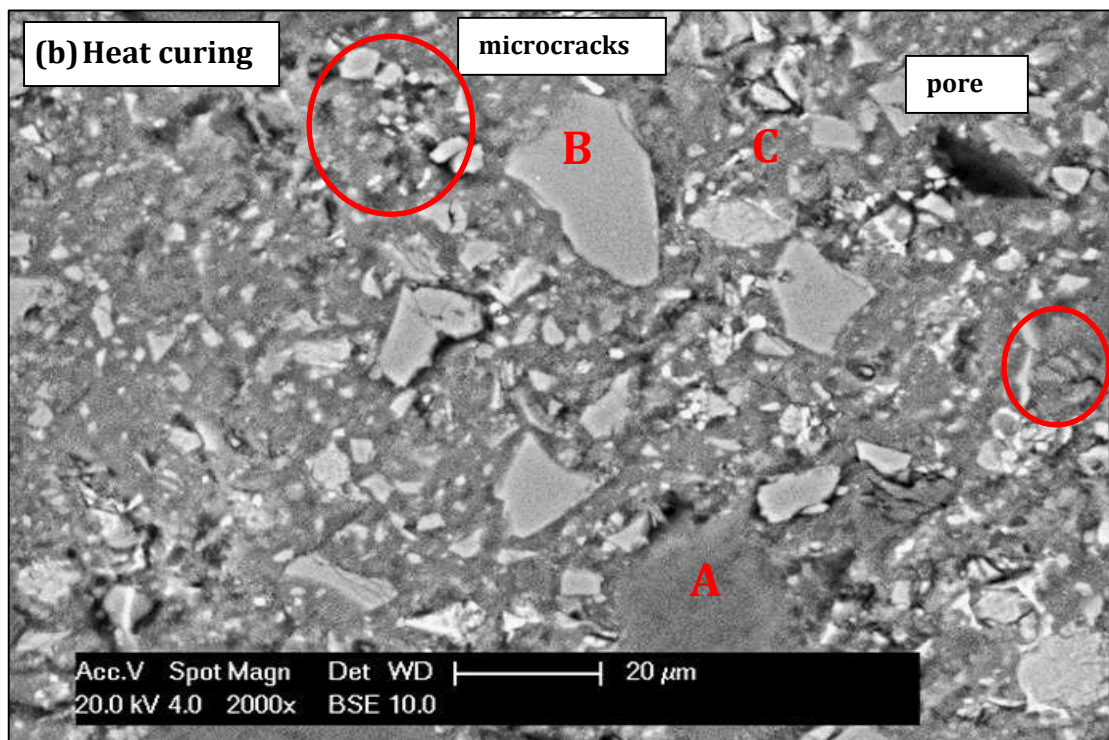
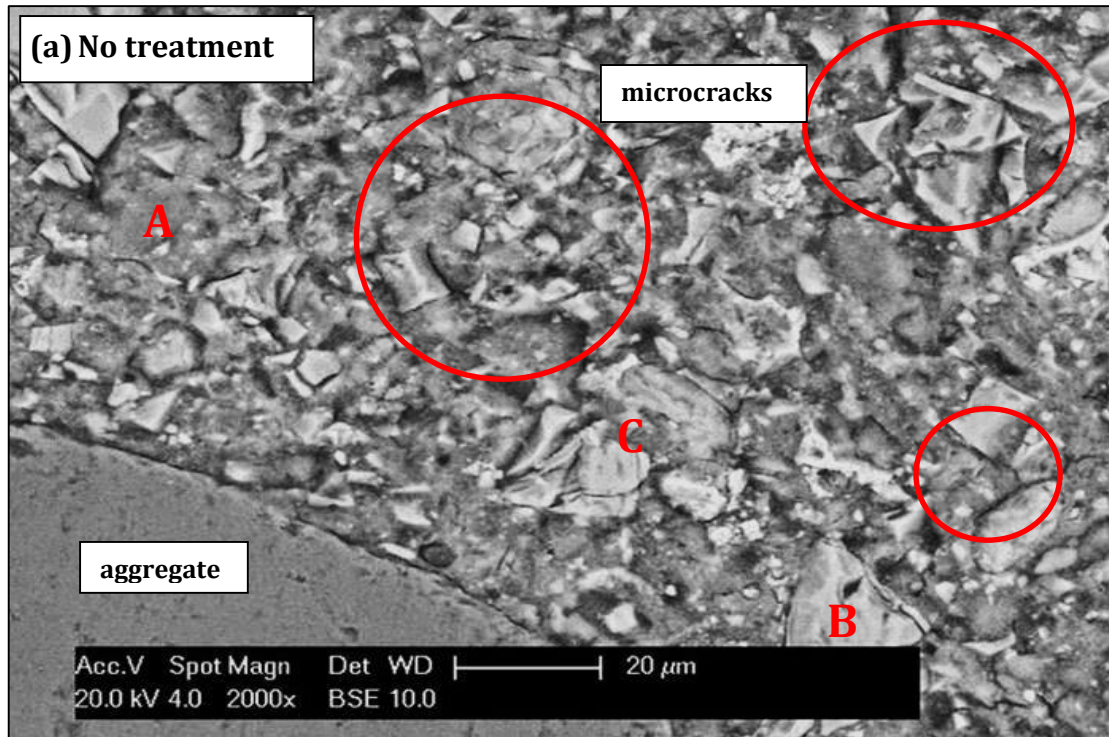


Figure 5.4 Higher magnifications by 2000x of BSE micrographs describing microcracks (red circles) and hydrated formed for (a) no treatment, (b) and heat treatment during hardening. The microcracks exist in paste have been increased by heat curing surrounding pores due to small explosions mechanism.

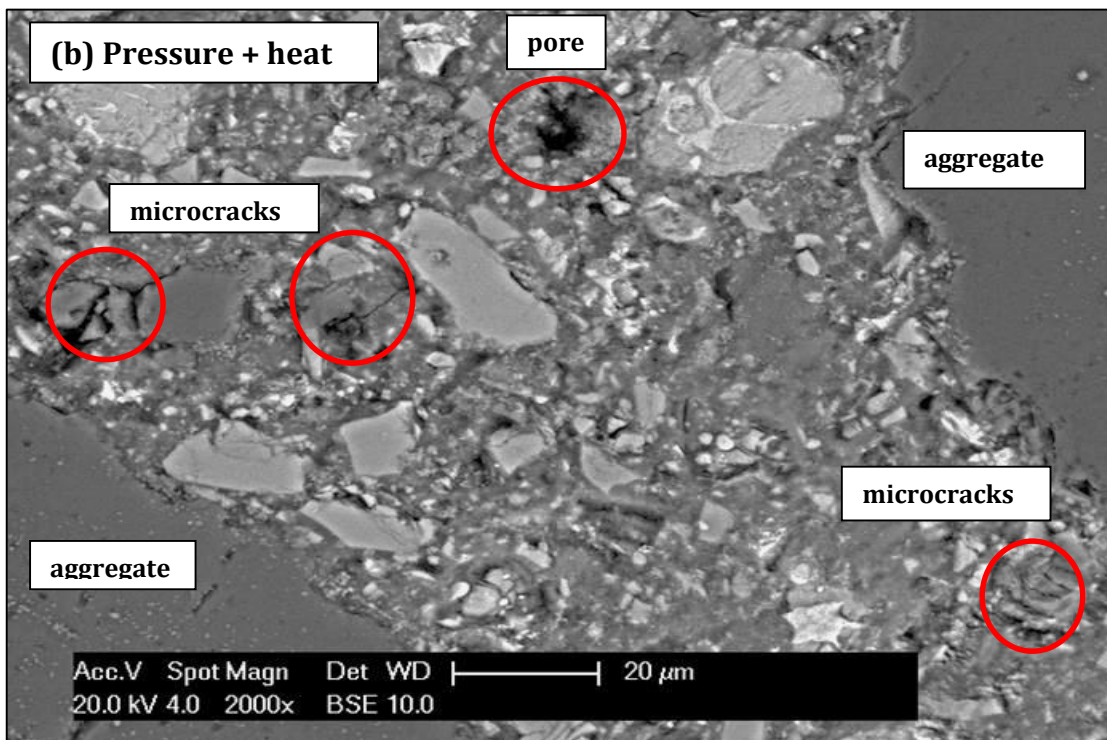
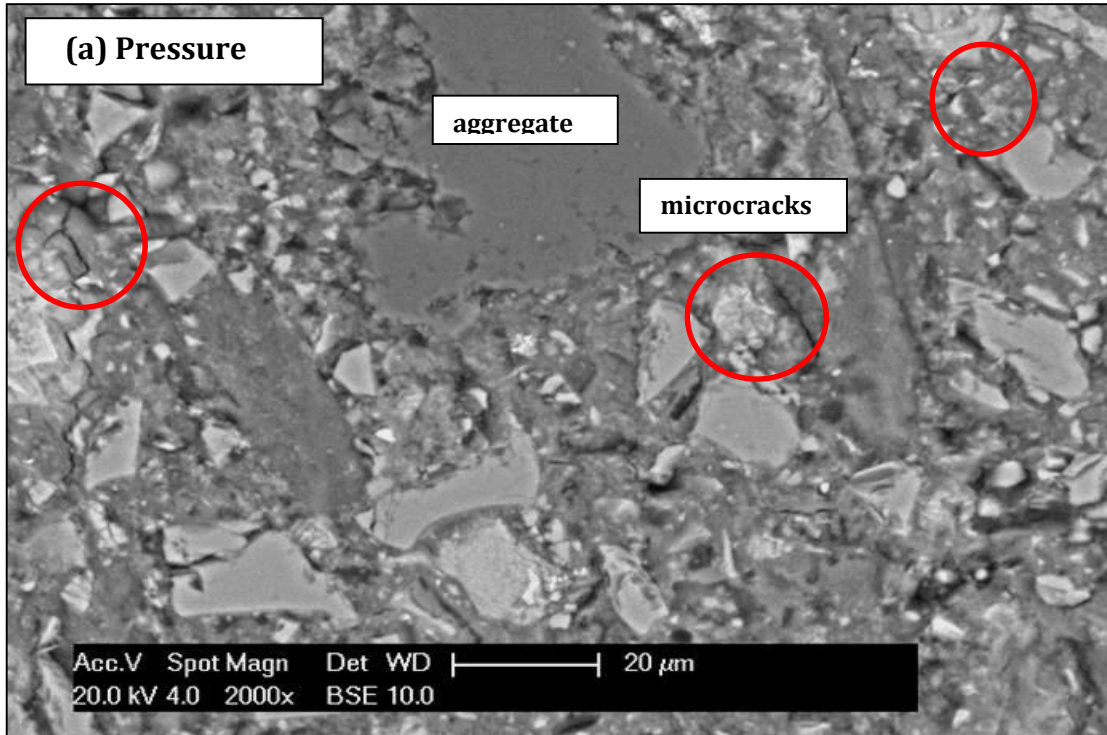


Figure 5.5 Higher magnifications of BSE micrographs describing microcracks and hydrated formed (a) static pressure treatment during setting, and (b) combined pressure and heat treatment. Small explosions also occur in treatment D.

5.2.4 Pore Filling after Heat Curing

Most scholars agree that heat curing induces a pore filling mechanism caused by the formation of pozzolan-derived C-S-H phases, the rate of formation for which is exothermically driven. At a temperature of 90 °C it can accelerate the hydration reaction, and therefore transform both the microstructure and microchemistry of RPC (Cwirzen, 2007). Tam & Tam (2012) found that tobermorite was characterised by plate-like crystals formed at a temperature of around 150 °C, whilst xonotlite was observed as needle-shaped crystals that occur at temperatures above 200 °C. At higher temperatures, between 200 and 250 °C, the chain length of C-S-H can be modified from trimer to pentamer or hexamer, with some dehydroxilation of cement gel due to both acceleration of hydration and the pozzolanic reaction (Cheyrezy *et al.*, 1995; Zanni *et al.*, 1996).

The pore filling mechanism of RPC in this study is shown in Figure 5.6. Figure 5.6 (a) presents the pore morphology with no heat curing treatment. The pore inside looks nearly clear with an irregular coarse surface, and small pores with a diameter of about 1 µm. The small platy-shaped hydrate, possibly found in RPC at ambient temperature curing, is identifiable as C-S-H (Yazici *et al.*, 2008). The structure of this C-S-H typically is like a rigid gel which is amorphous or with poorly crystalline structure (Tam *et al.*, 2010).

Figure 5.6 (b) shows some pores of specimens after heat curing, and they are filled by some platy-shaped and needle-shaped crystals. The platy-shaped crystals are identified as tobermorite ($\text{Ca}_{4+x}(\text{H}_{2-2x}\text{Si}_6\text{O}_{17}.5\text{H}_2\text{O})$ or $(\text{C}_5\text{S}_6\text{H}_5)$ which has properties such as: a hardness of 2.5 on the Mohs scale, relatively stable with a CaO/SiO₂ molar ratio of 0.83. The needle-shaped crystals are called xonotlite ($\text{Ca}_6(\text{Si}_6\text{O}_{17})(\text{OH})_2$ or $\text{C}_6\text{S}_6\text{H}_2$), with properties similar to those of tobermorite but having a CaO/SiO₂ molar ratio of 1.0 (Tam & Tam, 2012).

This observation finds agreement with those of previous scholars (Yazici *et al.*, 2008; Tam & Tam, 2012), where high temperature curing could transform C-S-H to tobermorite or xonotlite and fill the pores inside the specimen. The mechanism of the transformation is that heat treatment extracts water from the hydrates, which is then trapped inside the pores. It is firstly transformed to tobermorite, then secondly into xonotlite as a final structure (Cheyrezy *et al.*, 1995; Tam *et al.*, 2010). This transformation mainly depends on both the temperature level and the duration of heating (Tam *et al.*, 2010).

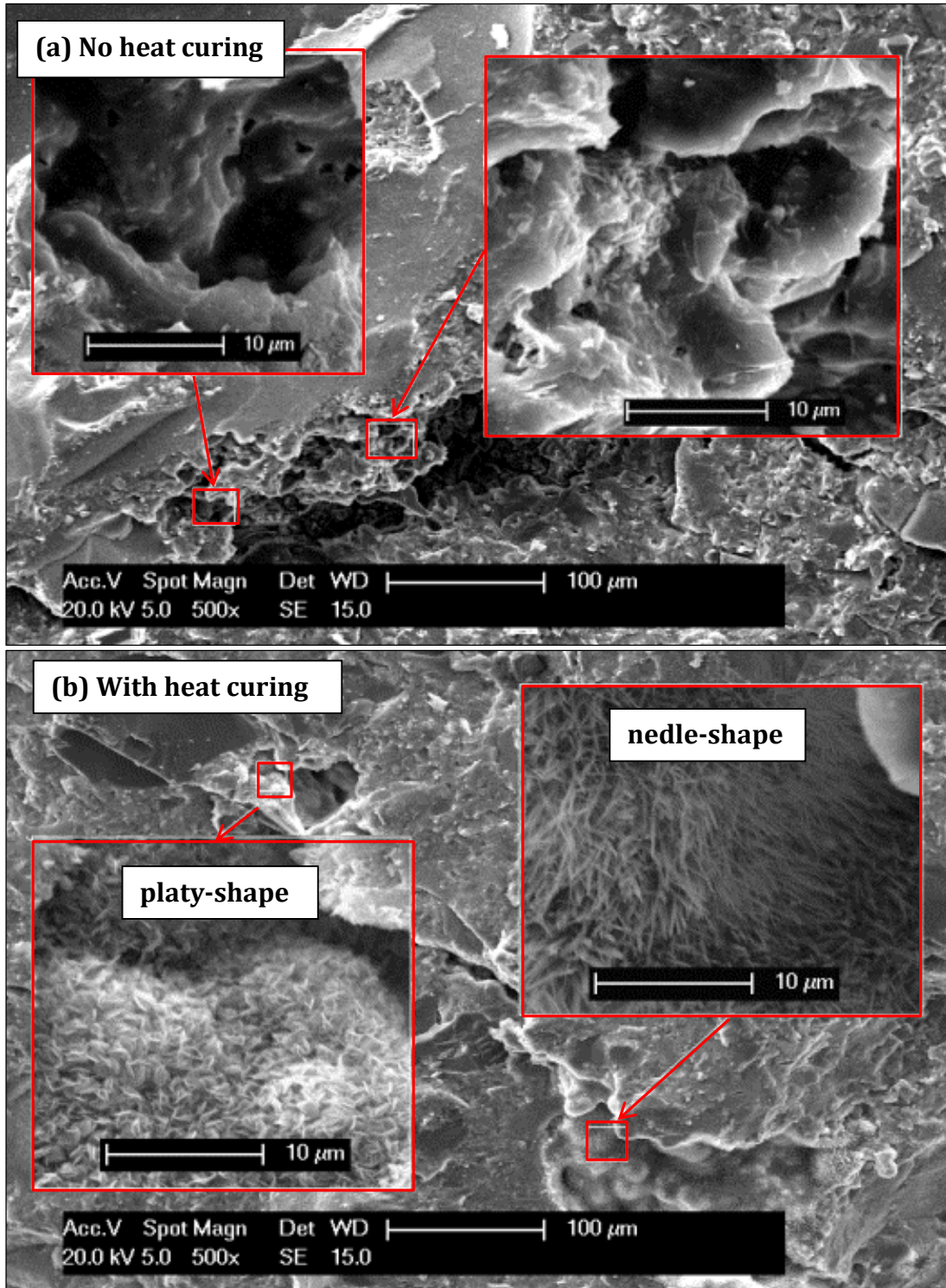


Figure 5.6 SE micrographs on surface of a fracture specimen describing pore filling mechanism (a) no treatment, (b) heat treatment. Insert A: group of ettringite crystal located in pores; insert B: groups of tobermorite (platy-shape) and xonotlite (needle-shape) filled in pores. Heat curing induces pore filling mechanism.

5.3 Chemical Composition of Hydrated Materials

All hydrates of cement contain chemically bound water in their microstructure. In concrete exposed to above 105 °C hydrate products will release most bound water and transform their hydrates into other phases. This transformation is typically not fully reversible.

5.3.1 Crystalline Phase Based on Mass Loss

Thermogravimetric curves representing for all treatments are presented in Figure 5.7. This shows some lines are overlapping at certain temperature ranges, which indicates that the amount of hydrate is similar. Among the four curves the overlapping lines can be grouped into two patterns: those without heat curing (curve A and C) and those with heat curing (curve B and D). Without heating, the curves are relatively close at the temperature range of 180 – 300 °C, which indicates a similar amount of the C-S-H phase. At higher temperature ranges the trend is slightly different between curve C and A. This suggests that the amount of Ca(OH)_2 and CaCO_3 is less than for A. In other words, pressure treatment appears to slightly reduce the amount of portlandite or 'free lime', which could be a consequence of water expulsion during setting.

The alterations are different in curves B and D, however. Here the pressure treatment has almost no effect on the amount of hydrate. Although both curves overlap at temperatures below 180 °C, they have a similar trend in the last three ranges. However, the position of both curves is higher than A and C meaning that heat curing reduces the quantity of C-S-H gel phase due to transformation reaction and Ca(OH)_2 due to an acceleration of the pozzolanic reaction. At temperatures below that required for the dehydroxylation of portlandite, heat curing most likely has accelerated the pozzolanic reaction to combine portlandite with the amorphous silica (contained within condensed micro silica) to form

additional calcium silicate hydrate (C-S-H), assuming the reaction given in Eq.

5.2 (Alarcon-Ruiz *et al.*, 2005):

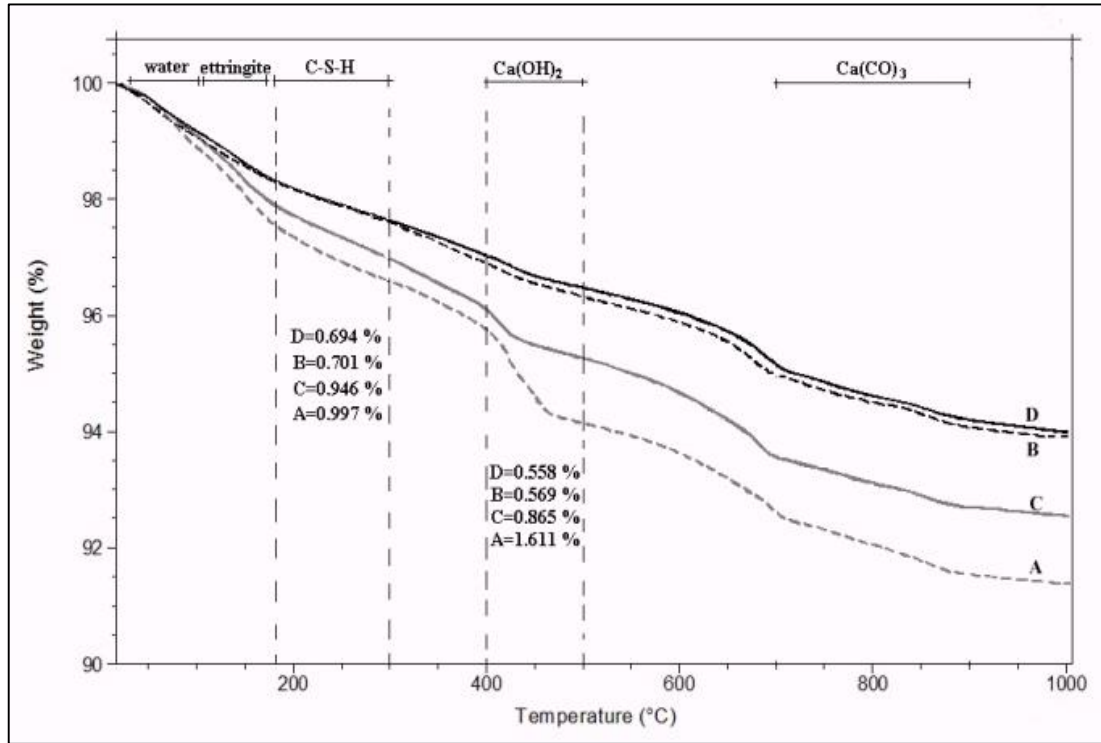
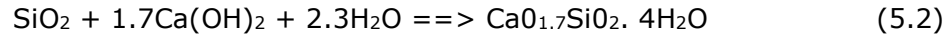


Figure 5.7 Mass loss of hydrate formed for all treatments: no-treatment (A); heat curing only (B); pressure only (C); both pressure and heat curing (D). Treatments decrease the hydrate formed which indicates the increase of anhydrous grains.

It is well known that heat curing can both transform C-S-H to xonotlite and accelerate the pozzolanic reaction producing a different form of C-S-H. The transformation of these hydrates can be estimated by calculating the weight loss as shown in Table 5.1. Pressure treatment slightly decreases the C-S-H quantity due to reduced water content and increasing the proportion of anhydrous cement grains. Heat curing treatment encourages the dehydroxylation/ transformation of C-S-H and reduces the mass loss by 0.296 wt% (B) and 0.252 wt% (D) compared to A and C, respectively. In higher temperature ranges, the quantity of

portlandite was decreased by 1.042 wt% (B) and 0.307 wt% (D), which indicates acceleration of the pozzolanic reaction. After transformation of the C-S-H to xonotlite, and the pozzolanic reaction, this will logically increase the total quantity of hydrates formed. In this investigation the values were 31.475 %, 13.212% and 31.274% for B, C and D, respectively. However these differences might partially be an indicator of the increase in the proportion of anhydrous grains.

Table 5.1 : The average of mass loss (wt%) for key temperature ranges determined by TGA analysis

Temp (°C)	A	B	C	D	Notes
30-105	1.052	0.845	0.884	0.763	Water
110-170	1.028	0.592	0.901	0.650	Ettringite
180-300	0.997	0.701	0.946	0.694	C-S-H
400-500	1.611	0.569	0.865	0.558	Ca(OH) ₂
700-900	1.077	0.913	0.859	0.945	CaCO ₃
110-1000	7.463	5.114	6.477	5.129	Hydrate loss
		31.475	13.212	31.274	% hydrate decrease

5.3.2 Crystalline Phase Based on XRD spectrum

The presence of both tobermorite and xonotlite is believed to be a major factor contributing to the compressive strength development in RPC. The presence of these hydrates can also be evaluated by X-ray Diffraction (Cheyrezy *et al.*, 1995); a technique to determine the mineral composition of crystalline solids. It has advantages due to a short time of preparation and the capability to distinguish the different anhydrous phases (Scrivener *et al.*, 2004). Furthermore, anhydrous cement such as alite and belite (both 71% of total contents), and which always remains due to very low water-cement ratio, (Cheyrezy *et al.*, 1995) can also be detected by this method.

Figure 5.8 shows the XRD diffractogram of the RPC mix constituents. It confirms that the alite and belite major intensity peaks, characteristic of unhydrated cement, were found at $2\theta = 30.4^\circ$ and 31.0° , respectively. This suggests that the low water content is not sufficient to support full hydration of the anhydrous cement grains, and that pressure applied in the setting period decreases the amount of free water available.

The Figure 5.8 also shows loss of the major portlandite peaks ($2\theta = 18.1^\circ$ and 33.8°) following heat treatment (B and D), along with reduction in alite and belite peak intensity and occurrence (with significant intensity) of the shouldered xonotlite peaks ($2\theta = 28.9^\circ$ and 31.7°) adjacent to the main calcite peak ($2\theta = 29.5^\circ$). Portlandite, as one of primary cement hydration products, is very soluble and could be consumed in the pozzolonic reaction by silica fume after heat curing (Matte & Moranville, 1999). The loss of portlandite after high temperature curing agrees with the results of Cheyrezy *et al.* (1995) and suggests that the pozzolanic ratio of RPC (after being cured at temperatures of 250°) is about 97%. This means that almost all portlandite in the sample had been consumed by the pozzolanic reaction. The presence of xonotlite in treatment B and D samples is probably due to the hydrothermal condition in the inert part of the specimen from C-S-H transformation. Ettringite peaks (at $2\theta = 11.3^\circ$ and 21.5°) were not observed in Figure 5.8. This suggests that after accelerated curing it may have fully converted to the monohydrate (AFm) phase and that the quantity of C_3A in the cement is relatively small.

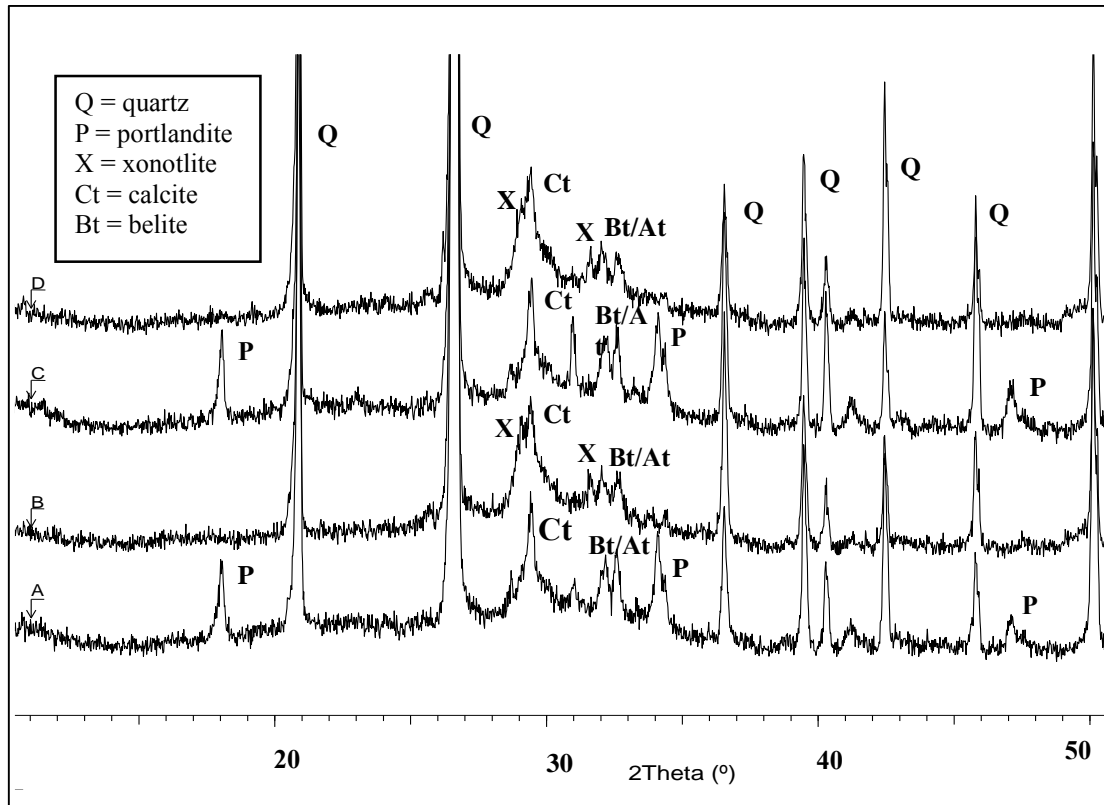


Figure 5.8 XRD diffractograms of RPC bulk powder samples following treatments A – D. Heat curing produces xonotlite and reduces portlandite which indicate the transformation of C-S-H and pozzolanic reaction.

5.4 Interfacial Transition Zone Properties

5.4.1 Hydrated Materials in the ITZ

EDS analysis was implemented in a study across the ITZ for all treatments (A – D), and as a function of distance from the aggregate boundary (incrementally from 10 - 70 μm distance). The average mass of each element recorded for each specimen is calculated and presented in Table 5.2.

Table 5.2: Atom ratio average of three measurements in ITZ

Treatment	Distance/ atom ratio	10	20	30	40	50	70
A	Ca/Si	0.835	1.039	1.900	1.078	1.200	1.330
	S/Ca	0.061	0.049	0.042	0.041	0.052	0.038
	(Al+Fe)/Ca	0.157	0.204	0.322	0.188	0.188	0.187
B	Ca/Si	1.558	1.883	1.063	1.203	1.433	1.285
	S/Ca	0.045	0.028	0.045	0.046	0.043	0.043
	(Al+Fe)/Ca	0.210	0.245	0.162	0.252	0.181	0.227
C	Ca/Si	0.987	1.262	0.942	1.033	1.369	1.110
	S/Ca	0.053	0.073	0.051	0.043	0.042	0.030
	(Al+Fe)/Ca	0.174	0.176	0.172	0.208	0.117	0.171
D	Ca/Si	1.247	1.352	1.123	1.242	1.096	1.390
	S/Ca	0.052	0.042	0.034	0.045	0.054	0.039
	(Al+Fe)/Ca	0.209	0.349	0.244	0.302	0.121	0.229

There is no significant difference in the values of Ca/Si, (Al+Fe)/Ca and S/Ca among all treatments. However, there is a fluctuation in atomic mass ratio at long distances from the aggregate. Comparing treatments B/D and A/C, respectively, the ratio of Ca/Si and Al+Fe/Ca is slightly increased, but the ratio of S/Ca is decreased at a distance of up to 20 μm . Furthermore, the atomic mass ratio fluctuates towards the bulk matrix area ($\sim 70 \mu\text{m}$). This indicates that heat curing accelerates the pozzolanic reaction near quartz aggregates, shown by an increase in the quantity of C-S-H and reduced CH. The ratio of Ca/Si increases to >1 , which can indicate the transformation process happening and perhaps containing xonotlite. The lower S/Ca might indicate that heat curing reduced the quantity of CH due to the pozzolanic reaction, whilst also inhibiting the formation of monosulphate (Cwirzen, 2007). It seems that EDS cannot directly provide evidence of xonotlite formation, whereas the SEM images are able to show an

indication that crystal morphology consistent with xonotlite is present within pores.

All atomic ratios for all treatments are grouped and plotted in two combinations: (Al+Fe)/Ca to Ca/Si ; and S/Ca to Ca/Si , as presented in Figures 5.9 and 5.10, respectively. The hydrates of CSH, AFm and CH are classified according to Trägårdh (1999) as follows:

$$\text{C-S-H} \quad 0.8 \leq \text{Ca/Si} \leq 2.5 ; (\text{Al+Fe})/\text{Ca} \leq 0.2 \quad (5.3)$$

$$\text{CH} \quad \text{Ca/Si} \geq 10, (\text{Al+Fe})/\text{Ca} \leq 0.4 ; \text{S/Ca} \leq 0.04 \quad (5.4)$$

$$\text{AFm} \quad \text{Ca/Si} \geq 4, (\text{Al+Fe})/\text{Ca} > 0.40 ; \text{S/Ca} > 0.15 \quad (5.5)$$

Both figures show that the atomic ratios spread in a large range and are mostly outside the marked area of hydrates.

The variation in atomic ratio of C-S-H and CH for all treatments (A – D), as a function of distance from the aggregate boundary (10 μm - 70 μm), was observed to be insignificant (see Figure 5.11). Within this region the occurrence of C-S-H appears to be significantly more dominant than that of CH within the paste, by considering the Ca/Si ratio in the range of 0.8 – 2.5. The reason for this phenomenon is perhaps because the ITZ forms pores in the paste (*i.e.* 'wall effect' packing) during formation around the aggregate boundaries. These pores are subsequently filled by the much smaller diameter SF grains, themselves latterly taking part in the pozzolanic reaction (Tragardh, 1999; Scrivener *et al.*, 2004).

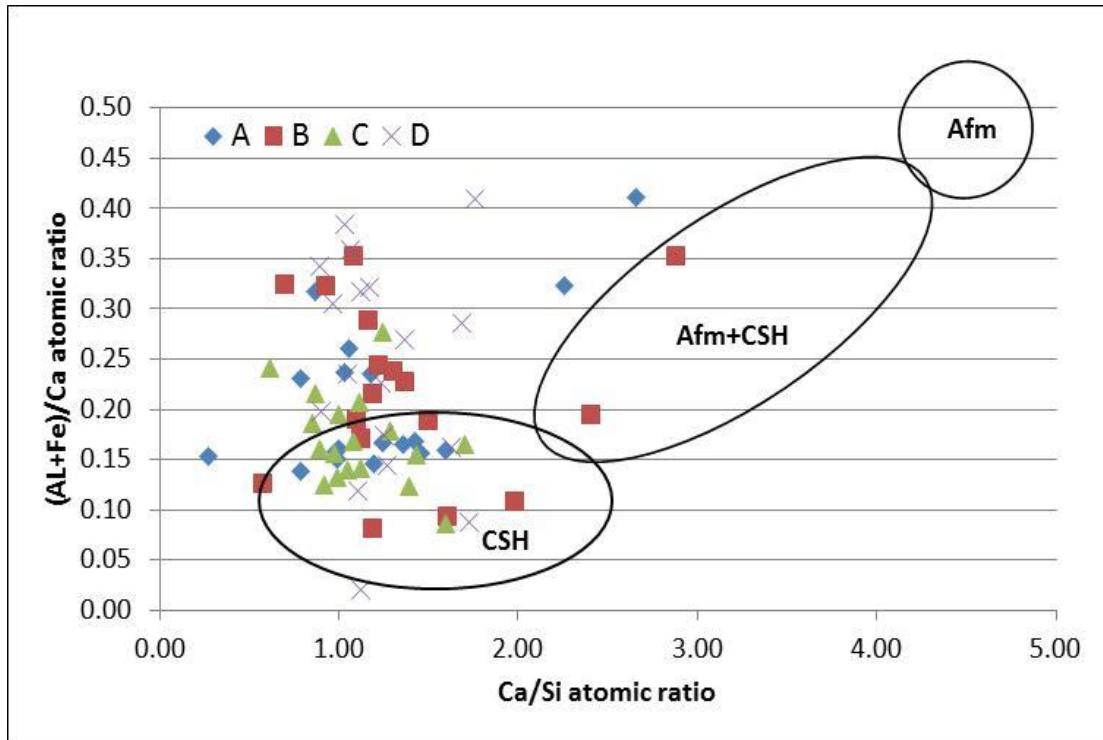


Figure 5.9 Atomic ratios between (Al+Fe)/Ca and Ca/Si for all treatments

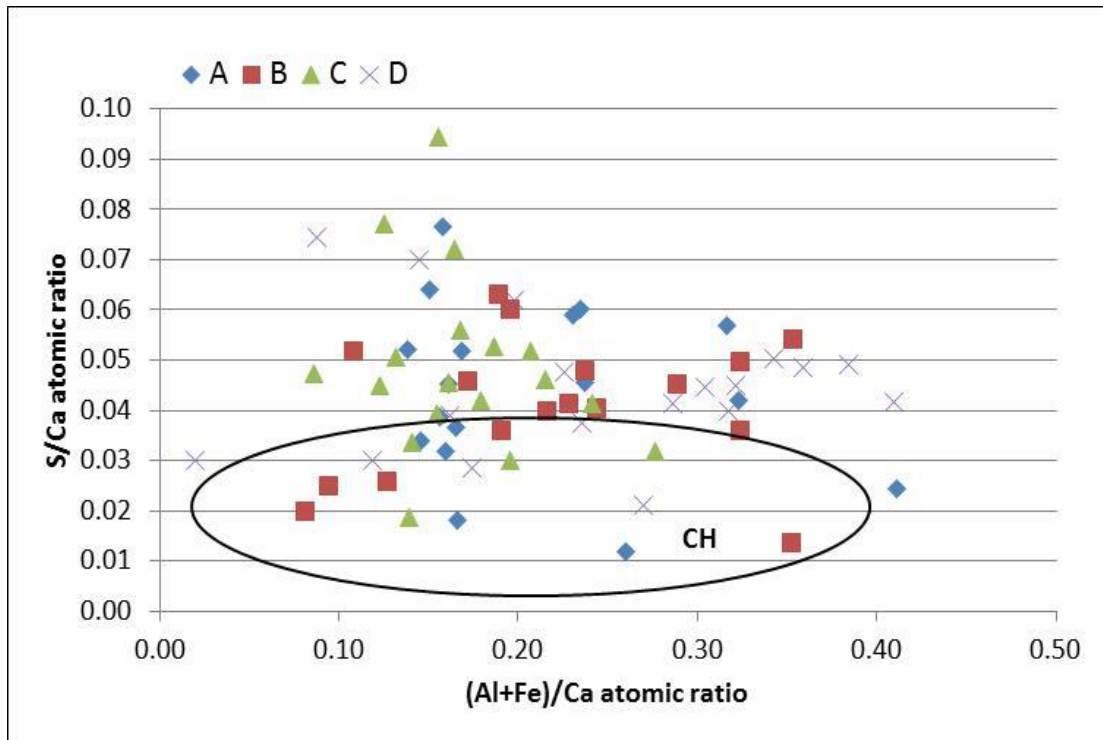


Figure 5.10 Atomic ratios between S/Ca and (Al+Fe)/Ca for all treatments

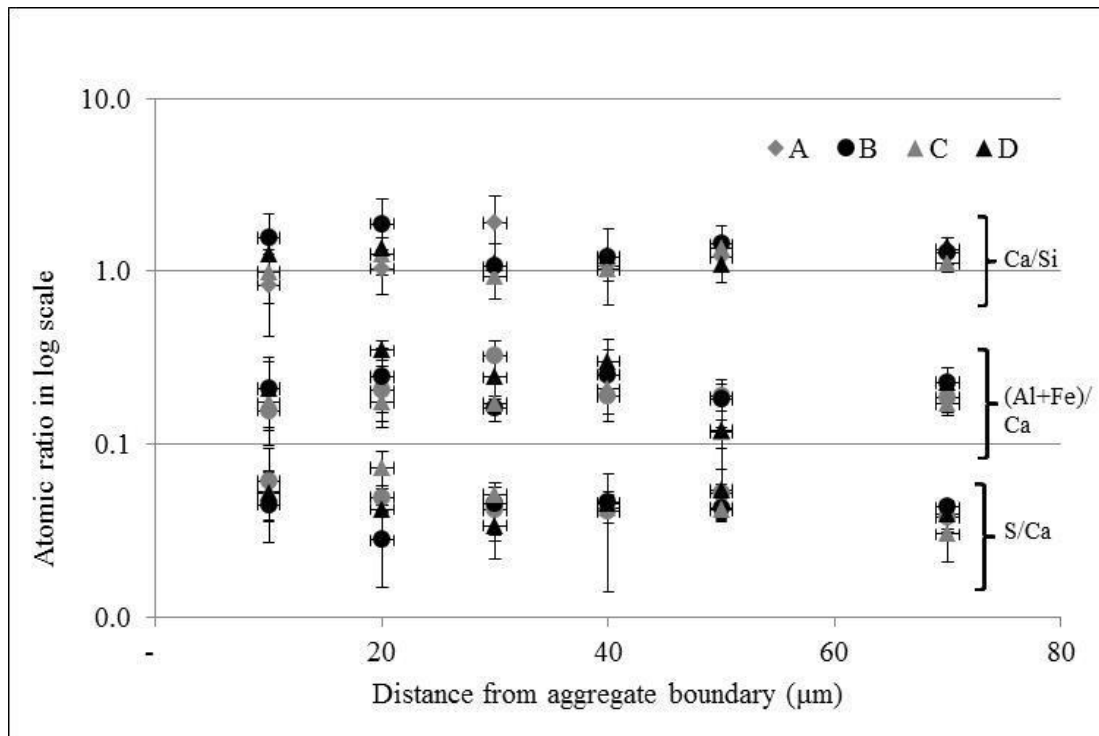


Figure 5.11 Spatial distribution of atomic ratio across the ITZ as a function of distance from an aggregate grain boundary determined using quantitative EDS.

5.4.2 ITZ Thickness

Local porosity surrounding the aggregate surface was analysed in this study using grid areas of $5 \times 50 \mu\text{m}$ on SEM images at a magnification of 1000x (see Figure 5.12). The mean average of porosity was taken from three specimens, as shown in Figure 5.13. ITZ thickness is defined here as the distance from the aggregate edge where the porosity curves intersect with the observed porosity of the bulk paste (see Figure 5.14). The results are summarized in Table 5.4.

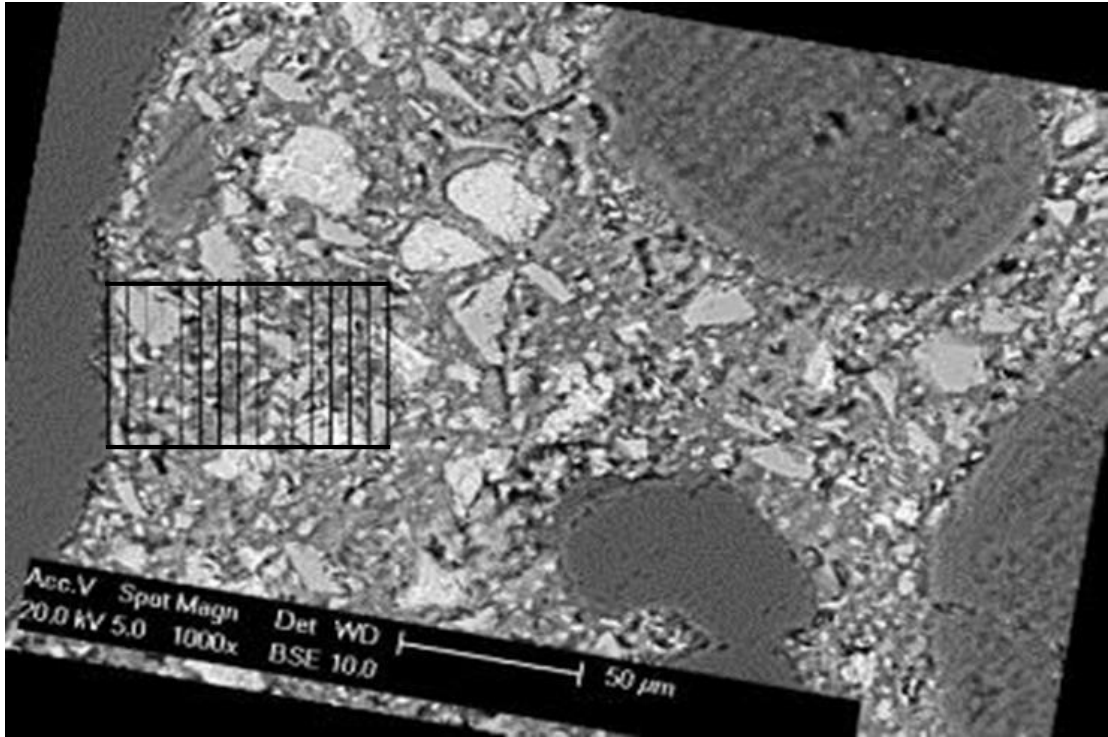


Figure 5.12 Example plot of 15 grids area @5x50 μm in treatment D.

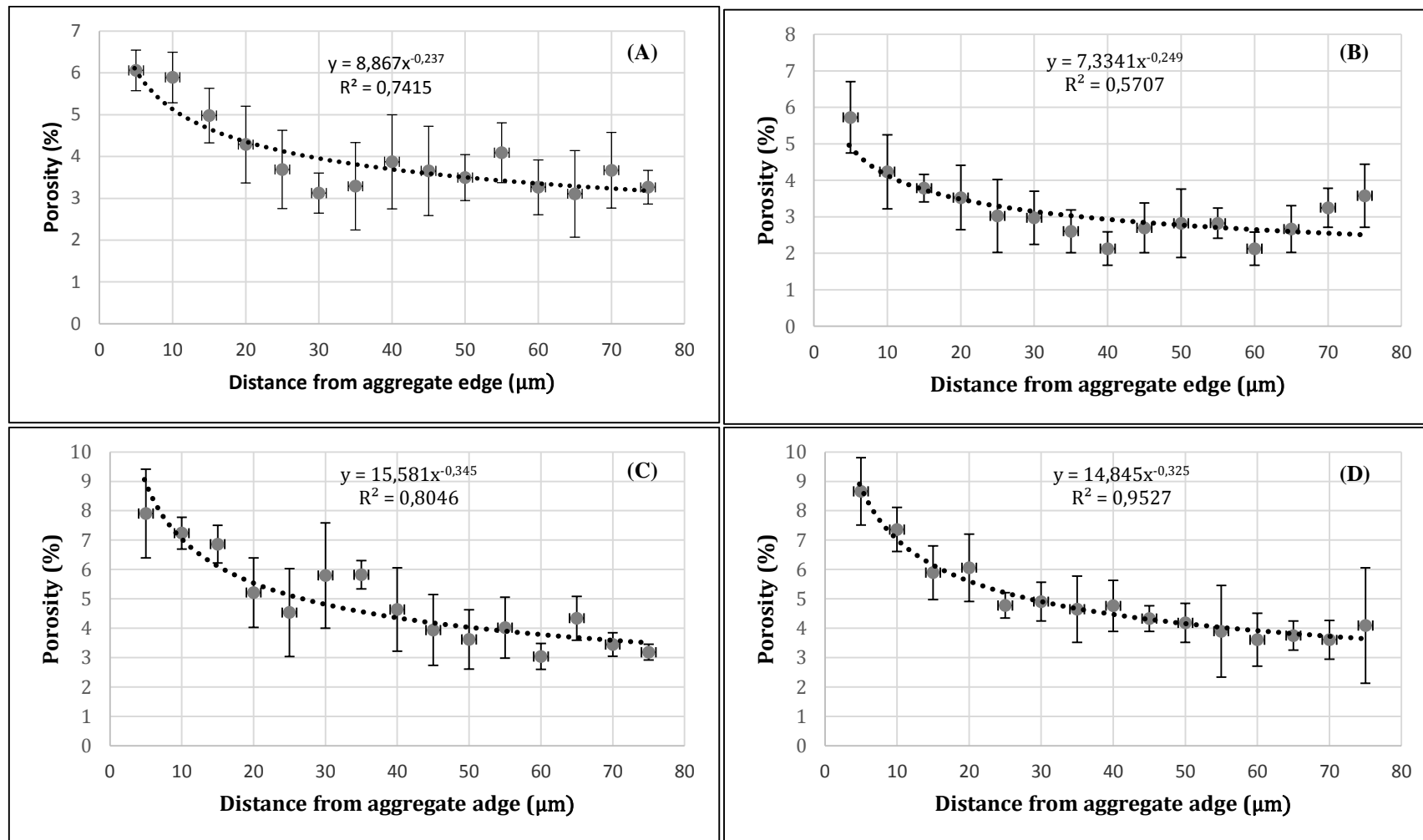


Figure 5.13 Bulk porosity as a function of distance from an aggregate grain boundary determined using segmentation image analysis of BSE micrographs.

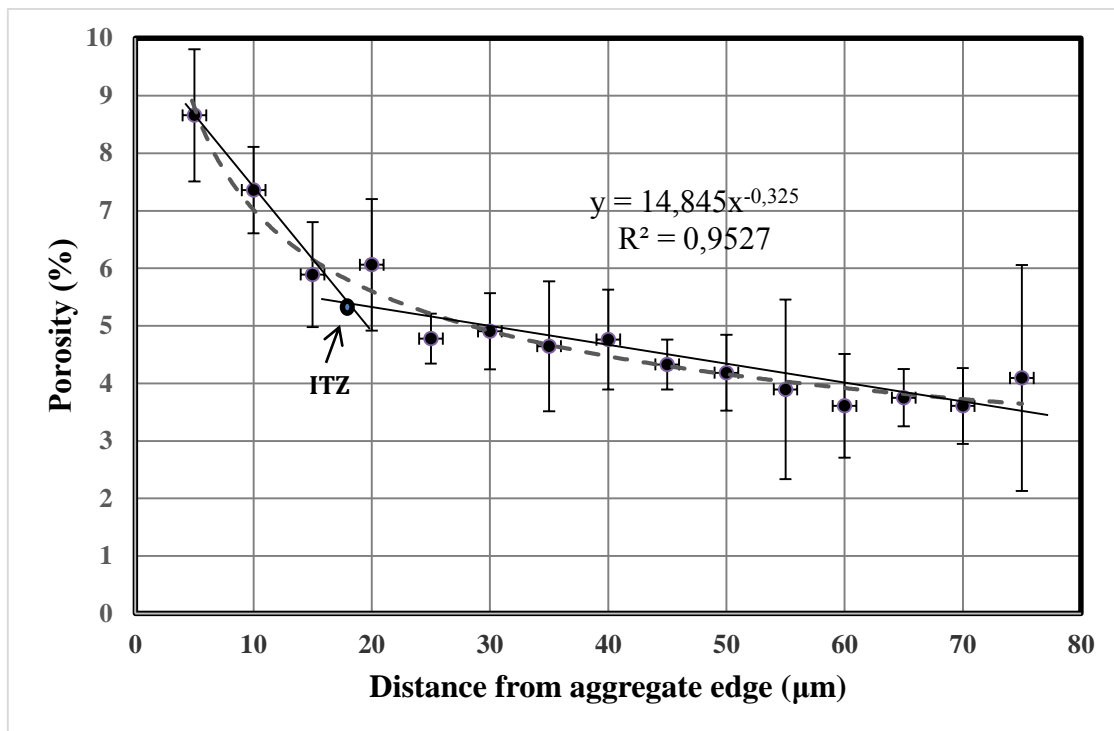


Figure 5.14 Example plot of mean porosity as a function of distance (treatment D) with interpolated ITZ distance.

Table 5.3: Thickness and porosity in ITZ

Treatments	A	B	C	D
Thickness (μm)	17.3	17.9	16.9	17.1
Porosity (%)	4.3	3.4	5.4	5.3

All curves have similar slope trend lines resulting in an intercept (ITZ thickness) of 17 - 18 μm. However, all treatments have different local porosity values. The ITZ thickness was reduced from 17.3 μm (A) to 16.9 μm (C) by pressure treatment, and increased after heat curing to 17.9 μm (B). However, these changes are statistically insignificant due to the standard deviation of porosity measurements. The local porosity values near to the aggregate boundary are slightly higher and decrease with distance towards the bulk paste. It seems that the treatment that accelerated the hydration in RPC has no significant effect on ITZ thickness,

elemental composition or local porosity. This is a significant finding because it shows that pressure treatment, when applied during setting, does not adversely affect the degree of porosity within the ITZ phase; rather it appears to affect the mortar phase by the same degree.

Gao *et al.* (2014) suggested an equation to describe the porosity profile starting at the aggregate surface until ITZ thickness with a power law function as follows:

$$\varphi(x) = \varphi_{if} - (\varphi_{if} - \varphi_{bulk}) \left(\frac{x}{d}\right)^\beta ; x \leq d \quad (5.6)$$

where $\varphi(x)$ is the porosity value at distance x from to the aggregate surface; φ_{if} is the porosity value at the closest aggregate surface; φ_{bulk} is the porosity value of bulk paste; d is the ITZ thickness; β is the gradient of porosity profile within the ITZ.

In this study, values of φ_{if} and φ_{bulk} were defined from the mean average of three specimens at a distance of 5 μm and 75 μm , respectively; β was defined from linear regression of the first three data points. These variables resulted in an equation for all treatments as listed in Table 5.4. The pressure treatment had no effect on the β value, whilst heat curing significantly increased it. By combining with pressure (treatment D) the β value can be increased by up to two times compared to treatment A. It should be noted that heat curing induced the greatest increase in total porosity. It appears that the quartz aggregate properties significantly affect the degree of porosity formed, due to the difference in thermal expansion coefficient between quartz aggregate and cement paste (Neville, 2010).

Table 5.4: Equation of porosity up to ITZ thickness according to equation (5.6)

Treatments	φ_{if} (%)	φ_{bulk} (%)	β	d (μm)	$\varphi(x) =$
A	6.06	3.26	0.108	17.3	$6.06 - 2.8 \left(\frac{x}{17.3} \right)^{0.108}$
B	5.73	3.58	0.194	17.9	$5.73 - 2.15 \left(\frac{x}{17.9} \right)^{0.194}$
C	7.9	3.18	0.104	16.9	$7.90 - 4.72 \left(\frac{x}{16.9} \right)^{0.104}$
D	8.66	4.09	0.277	17.1	$8.66 - 4.57 \left(\frac{x}{17.1} \right)^{0.204}$

5.5 Pore Size Distribution and Porosity

5.5.1 Pore Distribution

The effect of treatments on pore network geometry for all treatments was investigated using MIP. The result forms a correlation curve between pore size distribution and cumulative mercury intrusion, as presented in Figure 5.15.

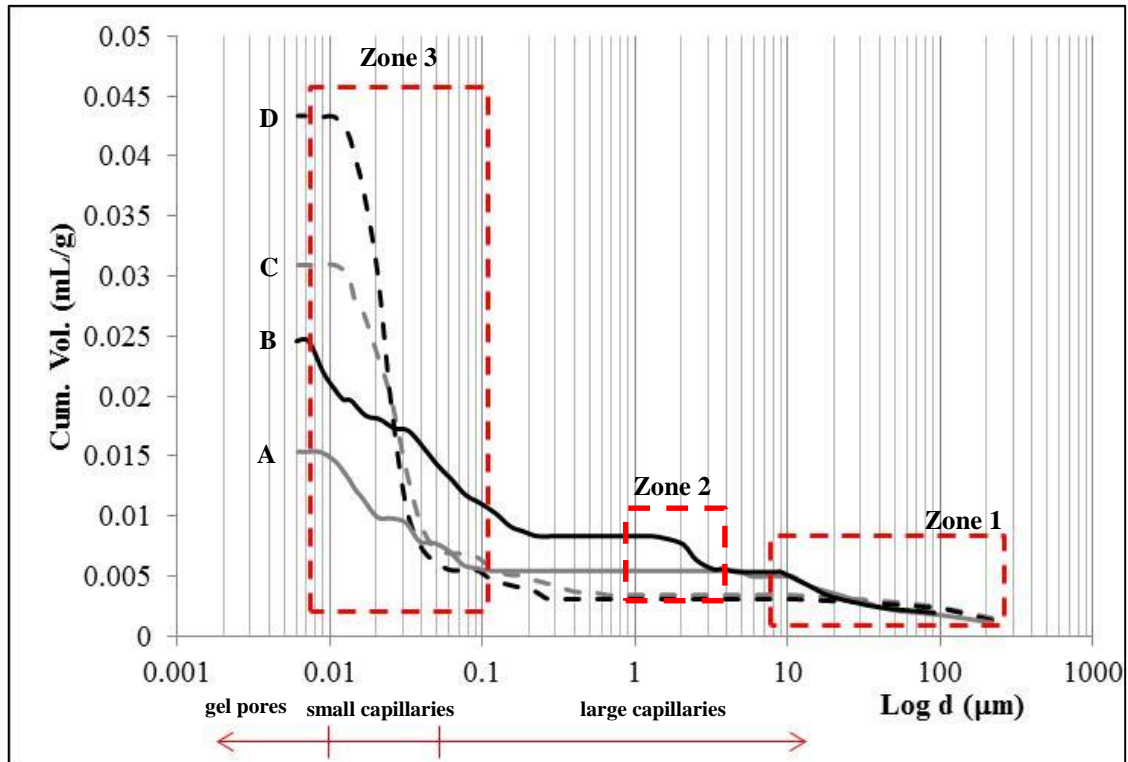


Figure 5.15 MIP cumulative intrusion-pore diameter plot. Cement pore size range classification is interpolated from Domone (1996) for a w/c of 0.22.

Hydrated cement in RPC contains pores with varying diameter ranging from 200 μm to 5 nm. Cement gel containing silica fume may result in hydrates with pore diameters less than 0.003 μm , however this represents the detection limit for MIP (Matte & Moranville, 1999). The cumulative intrusion curves are divided into three distinct zones, which emphasizes significant changes of intrusion behaviour and pore classification, based on the definitions provided by Domone (1996). In addition, pore size distribution was also accounted and grouped in particular ranges as presented in Table 5.5.

Table 5.5: Volume fraction distribution (%) of pore diameters

Range pore diameter (μm)	Treatment			
	A	B	C	D
>10	22.87	21.73	11.06	7.12
10 - 1	12.63	12.15	0.00	0.00
1 - 0.1	0.00	11.31	10.26	3.80
0.1 - 0.05	15.10	12.93	2.41	3.46
<0.05	49.41	41.88	76.28	85.62
Total	100.00	100.00	100.00	100.00

Zone 1 shows that the pore size distribution of A and B closely overlap having values 22.87 and 21.73 %, respectively. This suggests that the effect of heat treatment on macro pore volume (*e.g.* by pre-filling from hydration) is small. The curves of C and D show also overlapping by 11.06 and 7.12 % and across both A and B curves but have less pore volume. This measurement indicates that pressure treatment reduces the volume of entrapped air voids above 10 μm diameter, whilst additional heat treatment changes the macro pore volume by filling them with hydration products (see in Figure 5.6). These explanations are supported by the earlier SEM observations and direct measurements of representative entrapped air voids (identified by their rounded bubble-shaped morphology) as shown in Figure 5.1.

Zone 2 shows a change of pore distribution where it presents a significant increase in pore volume at approximately 2 - 3 μm diameter for treatment B. This suggests that the compressed air voids exist and heat curing can expand the compressed gas inside pores, which could result in extended cracking. This phenomenon does not appear in curve D and suggests that pressure makes the pore diameter smaller whilst increasing gel pore volume.

Zone 3 shows the highest volume of intrusion, which represents the vast majority of pore volume and includes only sub-micron porosity in the anticipated range for cement gel at this water/binder ratio ($w/c = 0.22$; approx. 5 - 50 nm (Domone, 1996)). Heat treatment only (B) decreases pore volume in the gel pore ranges by around 16 % compared to A (no treatment); pressure treatment only (C) increases capillary pore volume by approximately 50 %; and a combination of both (D) appears to increase capillary pore volume substantially in the range of 10 - 50 nm by around 70 %. It is tentatively suggested that the formation of xonotlite, which results in the release of water molecules from tobermorite, could account for this increase.

5.5.2 Physical Pore Properties

Pore size distribution analysis has shown that pressure and heat curing can change the porosity significantly, especially in small capillaries within the cement gel. In addition, SEM images and XRD analysis have also shown the presence of both tobermorite and xonotlite as pore filling mechanisms. This suggests that these treatments encourage the evolution of pore properties, both physically and chemically.

Table 5.6 shows the result summary of physical properties measured by MIP for all treatments. The total pore volume was increased by up to three times after treatment D. Heat curing only increased the median pore diameter (in volume) and threshold pore diameter. When heat curing was combined with pressure, the median pore diameter decreased from 50.1 nm to 24.0 nm. The combined treatments in general decreased the bulk density correlating with the increase of total porosity from 3.392 % (A) to 9.150% (D). The increase of porosity after

treatment D was mainly attributed to alteration of gel pores; those with diameter less than 50 nm. It was hypothesised that pressure treatment reduced the amount of large capillaries due to the compacted grain structure, whilst heat curing increased the volume of small capillaries due to entrapped pore gas expansion and associated fracturing. The application of both treatments (D) produced the most beneficial alterations to pore properties by increasing the apparent (skeletal) density.

Table 5.6: Summary of experimental data from MIP

Parameters	Treatment				Unit
	A	B	C	D	
Total intrusion volume	0.015	0.026	0.031	0.043	mL/g
Total pore area	1.989	4.460	4.211	7.004	m ² /g
Median pore diameter (volume)	50.1	61.8	29.5	24.0	nm
Median pore diameter (area)	14.2	8.6	21.7	21.0	nm
Average pore diameter (4V/A)	30.9	23.5	29.4	24.8	nm
Bulk density at 0.51 psia	2.211	2.183	2.149	2.111	g/mL
Apparent (skeletal) density	2.288	2.315	2.302	2.323	g/mL
Porosity	3.392	5.728	6.645	9.150	%
Threshold pore diameter	92	226	48	60	nm
Total intrusion up to threshold	0.006	0.008	0.007	0.006	mL/g

5.5.3 Porosity in ITZ

It has been stated in previous discussion (see Table 5.6) that the largest proportion of pore volume was contained within the gel pores. Cho (2012), who had studied interfacial properties to classify the pore structure between capillary and ITZ pores, suggested an equation to express the ITZ pore fraction as follows:

$$P_{ITZ} = P_{total} - P_a (1 - V_a) \quad (5.7)$$

Where P_{total} and P_a are the total mercury intrusion (mL/g) for mortar and cement paste, respectively; V_a is aggregate proportion in volume; P_{ITZ} is mercury intrusion in ITZ (mL/g).

If the variable P_a is defined from the interpolation of the plot by Domone (1996) for a w/c ratio of 0.22, this results in a value of 0.03 (ml/g); V_a equals to 0.6 based on a calculation of the mixture composition by volume. P_{ITZ} was then calculated and the results presented in Table 5.8. This shows the development of the P_{ITZ} value meaning that the volume of pores increases in conjunction with the treatments applied. As P_{ITZ} indicates the pore volume near the local surface of aggregates, this result supports the previous hypothesis that ITZ porosity development is affected by heat curing due to the difference in thermal expansion coefficient between the aggregate and the cement paste, as well as aggregate movement following pressure treatment.

Table 5.7: Calculation of P_{ITZ}

Parameters	Treatment				Unit
	A	B	C	D	
Total intrusion volume	0.015	0.026	0.031	0.043	mL/g
P_{ITZ}	0.003	0.014	0.019	0.031	mL/g
P_{ITZ}/P_{total}	20.000	53.846	61.290	72.093	%

5.5.4 Effect of Hydrate Transformation on Porosity

The TGA results for wt% changes can also be used to calculate the density, related to the specific gravity of the hydrate products. If the transformations of

hydrates caused by heat curing treatment are simplified into two categories; (i) for C-S-H to transform into xonotlite, and (ii) for portlandite to transform into C-S-H, this gives an increase in bulk density of 1.99 % for B and 2.22 % for D, as shown in Table 5.9. If we consider again the transformation in gel pore volume (diameter <50 nm), then mercury intrusion can be used to account for the proportion of pore space associated with hydrate transformation or from micro cracks. Table 5.8 supports the hypothesis that the change in the volume of gel pores is partly due to the formation xonotlite and a densification of the gel pore walls.

Table 5.8: Summary of TGA inferred mineral transformations with corresponding density increase (per 1 g specimen)

Items	G	Mass loss (10^{-3} g)			
		A	B	C	D
C-S-H (jennite)	2.325*	9.97	7.01	9.46	6.94
Xonotlite	2.700*	0	2.96	0	2.52
Portlandite	2.251**	16.11	5.69	8.65	5.58
C-S-H (jennite)	2.325*	0	10.42	0	3.07
Accumulative density (10^{-3} g/ml)		60.87	62.04	42.29	43.23
Density after heat curing (%)			1.92		2.22
Accumulative pore (10^{-3} ml)		11.45	11.12	7.91	7.72
$\Delta V_{p,gel}$ after treatment (10^{-3} ml)			-0.33	-3.54	-3.73
Total intrusion for <5 nm (10^{-3} ml)		7.581	10.296	23.589	37.117
$\Delta V_{p,gel}$ after treatment (10^{-3} ml)			2.716	16.008	29.536
Total pore from microcracks (10^{-3} ml)			2.386	12.468	25.806
Percentage of pore from microcracks			87.85	77.89	87.37

* Richardson (2008)

** Balonis & Glasser (2009)

5.6 Conceptual Model Proposed for RPC Micro Structure

The treatments of static pressure during setting followed by heat curing in an RPC mixture have resulted in a multiscale transformation with respect to micro structural composition and pore geometry for four treatments: (A) without pressure and cured in water, (B) without pressure and heat cured in a drying oven, (C) with pressure and cured in water, and (D) with pressure and heat cured in a drying oven. The effect of treatments is significant at the macro scale in terms of physical-mechanical properties, but that does not involve any apparent alteration of the ITZ phase. The important points of these observations have enabled a summary of these transformations in the form of a conceptual model shown in Figure 5.16.

At the macro scale, the uniformly hydrated mortar phase contains randomly distributed spherical pores with diameters varying between 10 - 200 μm when cured under ambient temperature/ pressure conditions (A). When static pressure treatment is applied to a fresh mixture the modal pore diameter decreases by an order of magnitude with a corresponding reduction in total pore volume (bulk porosity) of 27 %. However, static pressure setting had no significant effect on apparent ITZ width (determined from localised porosity), which suggests that only porosity within the mortar phase was altered, *i.e.* not the ITZ or aggregate phases.

At micro scale, pressure treatment reduced the quantity of free water and increased the capillary pore volume in the range $\leq 0.05 \mu\text{m}$ diameter. The precise cause for this could be hypothesised that pressure-induced movement of cement grains within the paste during setting could result in a small amount of dilation creating additional pore space that is later partially filled by the cement gel as hydration proceeds. After static pressure setting treatment (C), the 28-d

compressive strength increased by 33 % compared to the untreated one (A). This appears to result from the significant reduction in entrapped air voids (macro defects) within the mortar phase. The relative increase in 28-d (late age) strength compared to 7-d (early-age) is 13 % for the untreated RPC, compared to 41 % for the pressure treated. Since the capillary pore ($\leq 0.05 \mu\text{m}$ dia.) volume increases following pressure treatment, this might be caused by dilation within the paste during setting, and the space created could allow additional C-S-H growth during hydration (and later pozzolanic reaction). Although TGA analysis of the samples in this study supports this theory, further research is required to better quantify the effects of capillary pore confinement on the C-S-H crystal growth mechanism.

Heat treatment (B) results in the formation of additional porosity in the range 1 – 3 μm , which was removed when heat treatment was preceded by pressure setting (D). As air voids of this size were not directly observed using SEM it was deduced that these voids could be microcracks. The logic is that heat treatment alone (B) would accelerate the propagation of microcracks (formed during shrinkage) due to thermal expansion of the solid phases as well as volumetric expansion of the air (and increased pressure) within entrapped voids. Preceding heat treatment with pressure setting, however, should theoretically arrest crack propagation and substantially reduce the volume of void macro defects. However, the reduction in 28-day compressive strength of 5 % (compared to 7-d strength) following heat curing (B) suggests that the proportion of competent material has reduced due to further micro crack propagation, because neither the ITZ nor the composition significantly altered during this time. The fact that heat curing preceded by pressure treatment (D) resulted in an even larger decrease in 28-d strength of 16 % (compared to 7-d) suggests that this micro crack propagation is likely to have resulted from pressurisation of entrapped air voids, *i.e.* from compression followed by thermal expansion.

In D treatment, heat curing reduced the quantity of portlandite by up to 0.307 wt%, which corresponded to an increase in C-S-H of 2.226 wt%. This most likely resulted from acceleration of the well-known (exothermic) pozzolanic reaction that transforms portlandite to calcium silicate hydrate. The elevated temperature used for curing is sufficiently high to result in further transformation of calcium silicate hydrate phases to xonotlite. Inside the gel pore network, heat curing induces further crystalline hydrate formation (*i.e.* hydration reaction) and transformation of existing crystalline hydrates; namely portlandite → calcium silicate hydrate and calcium silicate hydrate → xonotlite.

Since each transformation results in the dissociation of water and a significant increase in specific gravity (and hence skeletal density) the gel pore volume is substantially increased in the range $< 0.05 \mu\text{m}$. Heat curing also had no significant effect on composition as a function of depth within the ITZ region (*e.g.* the Ca/Si atomic ratio) or when compared to the mortar phase. Heat treatment alone (B) resulted in a greater increase in 7-d strength compared to pressure treatment alone (C), apparently as a result of an accelerated pozzolanic reaction. The higher strength following heat treatment (B) relative to untreated (A) is therefore a result of greater C-S-H volume through an accelerated pozzolanic reaction, and increased skeletal density in the cement gel resulting from transformation of tobermorite to xonotlite at elevated temperatures. When heat curing is preceded by pressure treatment during setting (D) the capillary pore volume is first increased, and then both the hydration and pozzolanic reactions are accelerated by heat treatment during the hardening phase with subsequent increases in gel skeletal density. Therefore, this combination of treatment results in a microstructure that exhibits the highest early-age and late-age compressive strength for an RPC mix.

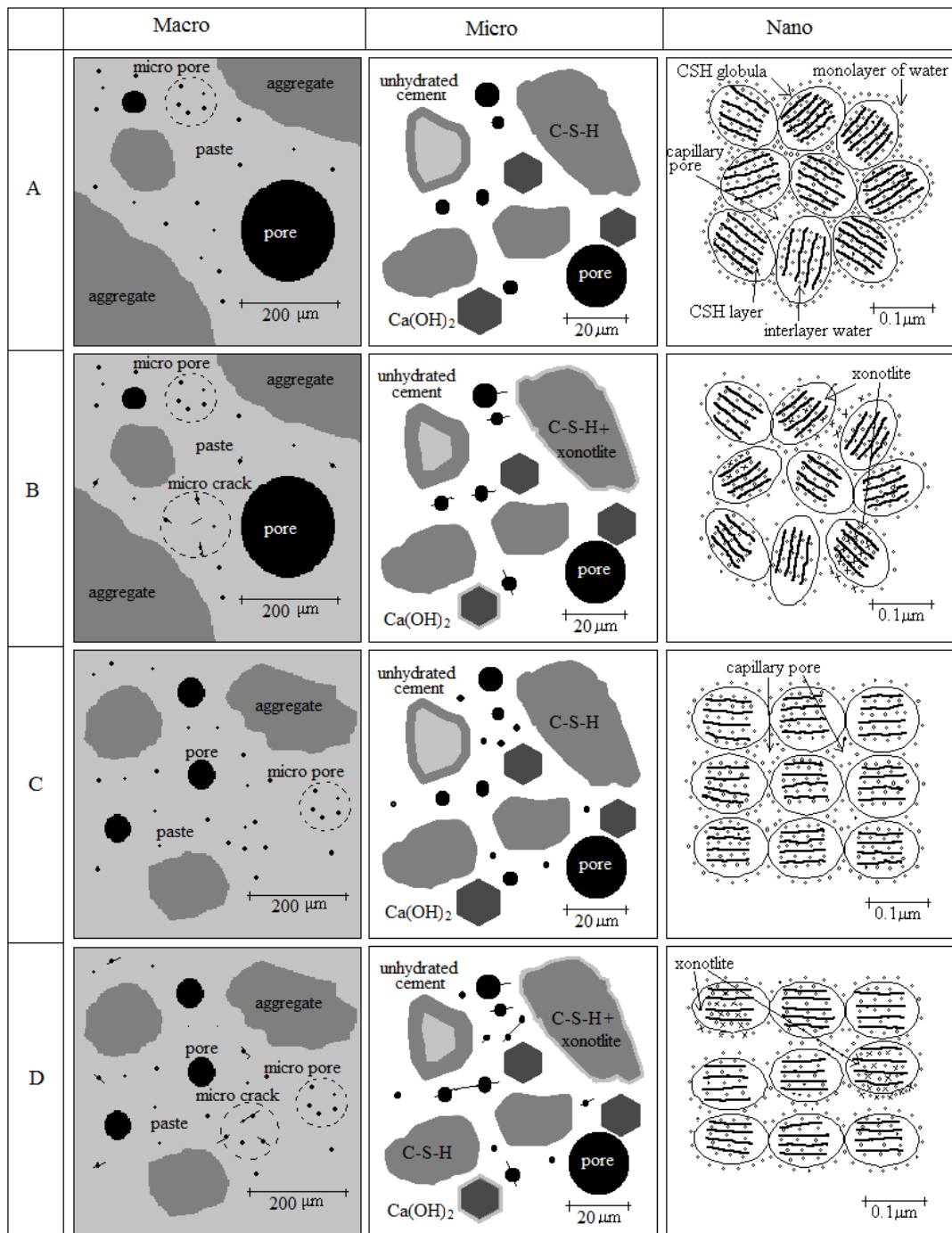


Figure 5.16 Conceptual model of RPC microstructural alterations resulting from all treatments (A-D).

5.7 Interfacial Binding with Carbon Fibres

In the previous discussion, it has been mentioned that pressure affects the density of the paste around aggregates (and hence also fibres), and that heat curing can fill micro pores. To evaluate the effects of both treatments, the microstructure of the interfacial zone surrounding carbon fibres was qualitatively compared for treatments A and D, as shown in Figure 5.17. Figure 5.17a shows the carbon fibre at the fracture surface of the specimen without any treatment (A). The surface of the fibre appears very smooth without any scratches or de-bonded paste, indicating poor adhesion between the cement paste and the carbon fibre. Figure 5.17b shows the surface of the paste after the carbon fibre has been pulled out (during prism rupture). There are many micro pores with a diameter of around 0.1 μm on this surface. Applying pressure and heat curing still has no apparent effects on the surface of carbon fibre (see Fig. 5.17c). However, both treatments cause the cement paste to become noticeably denser with longitudinal crack propagation (see Fig. 5.17d).

These observations support previous discussion about RPC behaviour in flexural tests (Chapter 4), which shows brittle rupture and loss of strength after peak load. It appears that treatments applied to RPC specimens have little effect in enhancing the adhesion between carbon fibres and cement paste. In addition, the undamaged surface of the carbon fibre suggests a pure friction bond mechanism with a constant rate of fibre pull-out (Katz *et al.*, 1995). It was found that the adhesion between carbon fibre and cement paste is the main limiting factor in brittle rupture, whilst the pressure and heat treatments can only develop the paste properties as opposed to the composite. This disadvantage can perhaps be improved by treatments focussed on preparation or functionalisation of the carbon

fibre surface such as by heating, ozonization, or NaOH solution etching (Chung, 2000).

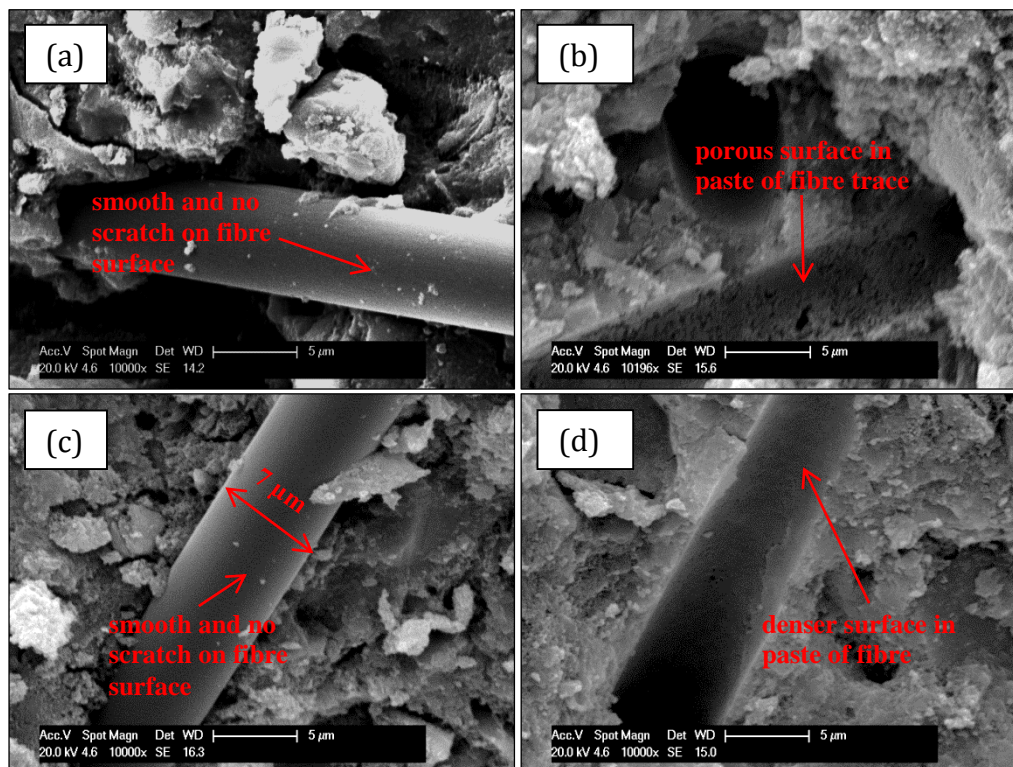


Figure 5.17 Interfacial carbon fibre for treatment A and D: (a) and (b) are surface of carbon fibre and cement paste in treatment A; (c) and (d) are surface of carbon fibre and cement paste in treatment D.

5.8 Summary

Static pressure treatment applied to fresh mixtures of RPC (before and during setting) resulted in denser cement paste due to loss of some entrapped air together with spill out of free water. Pores were physically transformed by reduction in mean diameter and volume, especially in the capillary pores. Hardened RPC paste always appears to consist of some hydrated and anhydrous materials, which is most likely due to the very low water-binder ratio. Pressure and /or heat curing treatments increased the proportion of anhydrous grains. It is

suggested that this occurs as a consequence of less free water after pressure and the rapid evaporation of water from C-S-H gel after heat curing.

In RPC without any treatment, the initial microcracks appear due to the shrinkage process of cement paste during hardening. A relatively large volume of macro pores formed due to entrapment of air and was later occupied by free water. Pressure treatment develops the micro cracks further, apparently due to the disruption of the hydration reaction (from less free water) and the movement of grains within the mortar (matrix). Heat treatment encourages the micro crack elongation and also widening, which correlates with the suggested increase in entrapped air void pressure.

The pore filling mechanism in RPC specimens only happens after heat curing treatment. Pores in samples without heat curing appear empty with irregular coarse surfaces. Pores in samples with heat curing appears to be filled by tobermorite in the form of platy-shaped crystals, and xonotlite in the form of needle-shaped crystals. This suggests that heat treatment extracted water from these hydrates, which were firstly transformed to tobermorite then xonotlite as a final structure. Treatments influenced the amount of hydrate products produced. Pressure treatment reduces the amount of hydrates and increases the amount of anhydrous material, due to water expulsion during setting. Heat curing reduces the volume of C-S-H gel phase due to transformation from C-S-H to tobermorite and/or xonotlite and reduces the amount of $\text{Ca}(\text{OH})_2$ due acceleration of the pozzolanic reaction.

XRD confirmed the presence of alite and belite, *i.e.* anhydrous cement grains. Though the loss of portlandite may indicate that it was consumed by the pozzolonic reaction, mass balance calculations suggest that heat curing is only able to account for around 70% of this. The treatment influencing the hydration in

RPC had no significant effect on ITZ thickness, elemental composition or local porosity. Pressure and heat curing treatments did not appear to adversely affect the degree of porosity within the ITZ, rather they appeared to affect only the mortar phase.

Pressure appeared to significantly reduce the macro pore volume by compressing (and expelling) entrapped air voids above 10 μm diameter, while heat curing filled voids with hydration products. Pressure treatment only substantially increased capillary pore volume in the range of 10 – 50 nm by approximately 50 % due to the compacted grains structure. The treatments significantly affect the macro scale physic-mechanical properties of RPC but did not involve any apparent alteration of the ITZ phase.

Chapter 6- Durability of Hardened RPC Under High Temperature Exposure

6.1 Introduction

The durability of concrete describes the ability of concrete to remain serviceable during its lifetime (Domone, 1996). Degradation of ability commonly appears in concrete during its service and consists of two groups that are chemical (*e.g.* sulphates and acid) and physical (*e.g.* frost and fire). This degradation generally is measured by property changes in the concrete, either mechanically and/or microstructurally, and also mass loss.

This chapter presents the durability properties of RPC after exposure to high temperature in two scenarios; (i) increment in temperature and (ii) cyclic fixed temperature aging. Specimens were made from RPC mixture containing 0.1 % V_f of carbon fibre, which was treated by static pressure during setting and heat curing during hardening (treatment D), as detailed in Chapters 4 and 5. The properties were evaluated using several methods:

- mechanical properties were tested in terms of compressive strength
- physical properties were observed in terms of colour changes and thermal conductivity measurement
- microstructural properties were observed using SEM images with image analysis, followed by gravimetric mass loss, and pore size distribution using MIP. Crack progression was observed on sample surfaces using SEM images.

6.2 Properties of RPC in Fixed Temperature Exposure

6.2.1 Appearance and Colour Change

The observations on sample surfaces after high temperature exposure can be used to indicate the damage of concrete through colour change, cracking and spalling (Arioz, 2007). Figure 6.1 shows the appearance on the no-scale surface and cross section of RPC samples for four exposure conditions, 20 °C (ambient), 400 °C, 500 °C and 800 °C. The specimen surface images were captured using a digital camera immediately after exposure and cooling back to ambient temperature, whilst the cross section images were captured from broken specimens following a compression test.

At ambient conditions (20 °C), the colour of the specimen surface was grey. These values indicate the density each colour and to be used as comparison for exposure samples. It appears that some voids on the surface occurred due to entrapped air on the mould during casting. Very fine irregular patterns (crazing) also appeared which was perhaps due to the movement of constituents during the pressure treatment process. In cross section, part of the specimen appeared to have a lighter grey colour towards the surface and to a depth of approximately 1-2 mm. It is suggested that this was a consequence of the heat curing treatment (at 240 °C), which is known to create a sequence of changes including the evaporation of capillary and structural water, as well as transformation of ettringite and C-S-H. Structural water is defined as the amount of water needed by cement grains to react forming CSH, CH, Afm, Aft phases (Haha *et al.*, 2009). This can form a more porous and weaker structure in hardened cement paste (Hager, 2013). The quartz aggregate colour appeared to be unaltered from the original colour; yellowish brown, most likely because quartz material chemically transforms at temperatures of about 500 °C (Tai *et al.*, 2011).

At 400 °C, the surface of the RPC specimens turned to a lighter grey colour both on the surface and inside, most likely due to furtherance of the same chemical alterations described above for high temperature curing. It appears that some smooth cracks on the surface occurred due to the contrast in thermal expansion coefficients between quartz aggregate and cement paste (Tai *et al.*, 2011). In cross section, the thickness of the lighter coloured outer specimen slightly increased by 3-4 mm. The damage gradient in cross section of the sample was also different. It is hypothesised that this was due to the increase in temperature gradient between the surface and the inside of the concrete (Kahlifa *et al.*, 2000).

When the temperature was elevated to 500 °C, the specimen surface became a darkish grey. The cracks anastomosed on the surface and increased in both width and length, compared to the ones at 400 °C. Heating induced colour alteration in the outer part of the cross section to a depth of around 4 - 5 mm. The quartz aggregates turned to a darkish brown due to partial transformation of the quartz. At this temperature micro cracks appeared on the surface of the aggregate because of the difference in thermal expansion coefficient between quartz and paste inducing paste spalling on the specimen surface.

At 800 °C, the colour of the surface turned to brownish grey. The cracks on the surface increased in terms of width, length and number. The surface appeared friable and brittle with some large pores due to spalling of thin paste which covered quartz local to the surface. This probably correlated to the formation of an impermeable wall for gases, which then induced small 'explosions' inside the pores due to pressurisation of the voids from thermal expansion of the gas (Anderberg, 1997). The micro cracks which formed at 500 °C in the ITZ, near the surface of the specimen, caused the cement paste to detach easily after exposure

to 800 °C. In cross section, heating turned the matrix colour to a light grey in a region approximately 12-15 mm thick.

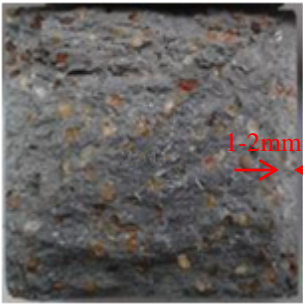
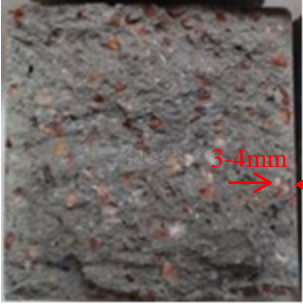
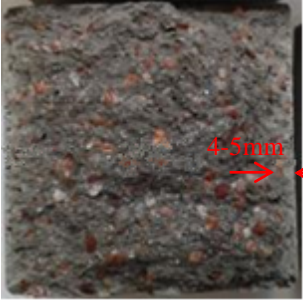
T	Surface	Cross section
20°C		
400°C		
500°C		
800°C		

Figure 6.1 The appearance and colour on the surface and cross section of RPC specimens for four temperature conditions: ambient, 400 °C, 500 °C and 800 °C. The colours changes are mostly affected by chemical reactions or transformation of hydrates.

6.2.2 Thermal Properties

The mass loss and thermophysical properties, including thermal conductivity and specific heat capacity, were investigated for samples treated under four conditions, *i.e.*, $T = 20\text{ }^{\circ}\text{C}$, $400\text{ }^{\circ}\text{C}$, $500\text{ }^{\circ}\text{C}$, and $800\text{ }^{\circ}\text{C}$. The specimen testing can measure the thermal conductivity (λ) and effusivity (β). The bulk density (ρ_d) was measured at ambient temperature using the gravimetric technique after exposure and cooling at ambient temperature. The specific heat capacity (C_p) and thermal diffusivity (α) were both calculated using Equations 6.1 and 6.2, respectively. The results of testing are presented in Table 6.1 and Appendix A.

$$\beta = \sqrt{\lambda\rho_d C_p} \quad (6.1)$$

$$\alpha = \frac{\lambda}{\rho_d C_p} \quad (6.2)$$

Table 6.1: The average result of bulk density, thermal conductivity, thermal effusivity and specific heat capacity after high temperature exposure

Temp. $^{\circ}\text{C}$	Bulk density g/cm^3	Thermal conductivity $\text{W}/\text{m}\cdot\text{K}$	Thermal effusivity $\text{W}\cdot\text{s}^{1/2}/\text{cm}^3\cdot\text{K}$	Thermal diffusivity $10^{-7}\text{m}^2/\text{s}$	Specific heat $\text{J}/\text{kg}\cdot\text{K}$
20	2193	1.522	1709	7.931	875
400	2024	1.443	1665	7.511	949
500	2018	1.416	1649	7.374	952
800	1993	0.781	1275	3.752	1044

6.2.2.1 Bulk Density

Bulk density was measured gravimetrically after exposure to indicate the mass loss. The results of the calculations are shown in Table 6.1. It shows that mass loss of the RPC increased in line with the temperature increment by 7.68, 7.96

and 9.09 % for temperature of 400, 500 and 800 °C, respectively. The mass loss at 400 °C and 500 °C was similar (and mostly correlated to) the dehydration reaction of hydrates such as portlandite, and the dehydroxilation of C-S-H (Liu & Huang, 2009). In addition, micro cracks that spread across the surface and matrix appeared to cause volumetric expansion and consequent decrease in density. The loss mass at 800 °C, which corresponded to the calcination of calcium carbonate, slightly increased in comparison to the samples treated at 500 °C.

6.2.2.2 Thermal Conductivity

The thermal conductivity (λ) is the coefficient of resistance to heat flow driven by a temperature gradient between two points in a material. At ambient temperature (see Table 6.1), the thermal conductivity of RPC from the three specimens was between 1.43 and 1.59 W/m.K (see in appendix). These values were lower than for common concrete, which have a thermal conductivity range of 2.15 - 2.51 W/m.K (Neville, 2011). Although carbon fibre is known to be thermally conductive, its presence in RPC appears to decrease the bulk thermal conductivity. It is hypothesised that this was due to the increase of air void content in the specimen rather than to effects from fibres themselves (Khalik & Kodur, 2011).

After exposure, the thermal conductivity initially decreased by 5 % after 400 °C and 7 % after 500 °C. This is most likely due to moisture loss from evaporation of free water in the matrix (Khalik & Kodur, 2011) leading to a reduction in density (Shin *et al.*, 2002) and increased porosity and fracturing. Regarding the error bars shown in Figure 6.2, the effect of exposure at 500 °C was not significant and can be assumed to be similar to that at 400 °C. At 800 °C, the thermal conductivity

significantly decreased by 49 %. This was most likely because of the lack of competent material after extensive air void formation and crack propagation.

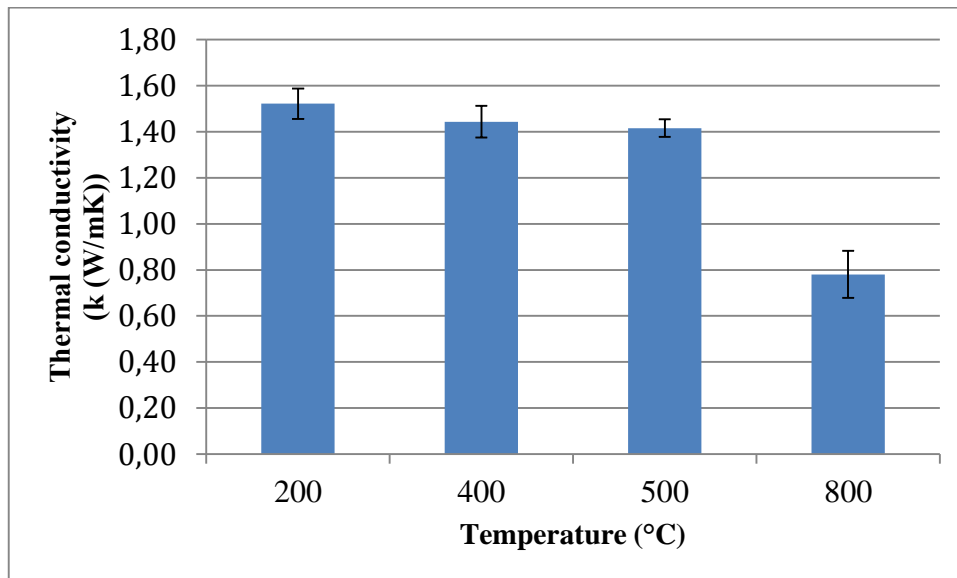


Figure 6.2 Thermal conductivity of RPC after high temperature exposure

6.2.2.3 Thermal Effusivity and Diffusivity

The thermal effusivity (β) is a coefficient indicating the magnitude of heat transfer on contact with a material, whilst the thermal diffusivity (α) indicates the rate of heat diffusion through a material (Najim, 2012). The thermal diffusivity of RPC was $7.931 \times 10^{-7} \text{ m}^2\text{s}^{-1}$ which is lower than the average value for common concrete ($1.667 \times 10^{-6} \text{ m}^2\text{s}^{-1}$) (Neville, 2011). Table 6.1 shows that both the effusivity and diffusivity properties of RPC decrease in line with the increase of exposure temperature. The heating of specimens at 400 °C and 500 °C did not appear to have a significant effect on the thermal properties. However, specimens heated at 800 °C saw decreases in both properties by 25 % and 53 % for effusivity and diffusivity, respectively. This decrement was hypothesised to be due to the correlation between density/ porosity and thermal conductivity.

6.2.2.4 Specific Heat

The specific heat capacity (C_p) is the amount of heat needed to change the temperature of 1g of material by 1°C. In concrete this property is mainly influenced by bulk porosity and constituent properties, as well as water content and specimen temperature (Neville, 2011). The specific heat capacity of RPC was determined by calculation based on equation 6.1. The results of calculation are opposite to those for effusivity in that specific heat capacity increased in line with the increase of temperature exposure. It was hypothesized that the increase of temperature correlated to the decrease in density and thermal conductivity.

6.2.3 Mechanical Properties

6.2.3.1 Residual Compressive Strength

The residual compressive strength can describe the durability properties of RPC for application as a building material after exposure to fire (Liu & Huang, 2009). The results of compression testing at ambient temperature were used as reference to compare with those after exposure at high temperature, as shown in Figure 6.3. The error bars represent the standard deviation from three samples at each temperature level.

The compressive strength of RPC with carbon fibre at ambient temperature initially was 138.68 ± 5.72 MPa. Specimens were cured after 2 days of setting in a drying oven at 240 °C for 48 h. This resulted in some micro crack formation in specimens, perhaps due to internal movement of mix constituents during pressure treatment and also differential thermal expansion between the aggregates and paste. This means that heat curing and pressure implemented at the same time

during the setting period (early age), by autoclave for instance, may result in higher compressive strength.

High temperature exposure decreased the compressive strength of RPC after different levels of degradation. At 400 °C, compressive strength slightly decreases by 6.71 % due to the dehydroxilation of the hydrates, *i.e.* ettringite, C-S-H and CH. At 500 °C, the degradation of compressive strength increased by 8.91 %. Although this averaged slightly higher than that at 400 °C, the difference was not significant due to the overlapping error bars. At 800 °C the compressive strength of RPC dropped sharply by 74.33 % due to calcination which breaks down the C-S-H.

In general, the strength of RPC degrades at high temperatures (as does common concrete), which follows three stages of degradation: (i) evaporation of water within the concrete starting at 105 °C which induces a pressure in pores leading to cracking and spalling; (ii) differential expansion between the cement paste and aggregate starting above 500 °C which results in thermal stresses and cracking in the ITZ; and (iii) breakdown of hydrates (calcination) starting from 700 °C which breaks the atomic bond (Domone, 1996). The reduction in compressive strength of RPC after exposure has been correlated to two behaviours; shrinkage and thermal expansion behaviours (Tanyildiz, 2008). The shrinkage is caused by evaporation of water, dehydration and decomposition of hydrates; while the thermal expansion causes cracks due to the heterogeneity of thermal conductivity in the mixture components. Cracks may also occur in the paste due to transformation of C-S-H to become tobermorite and/or xonotlite.

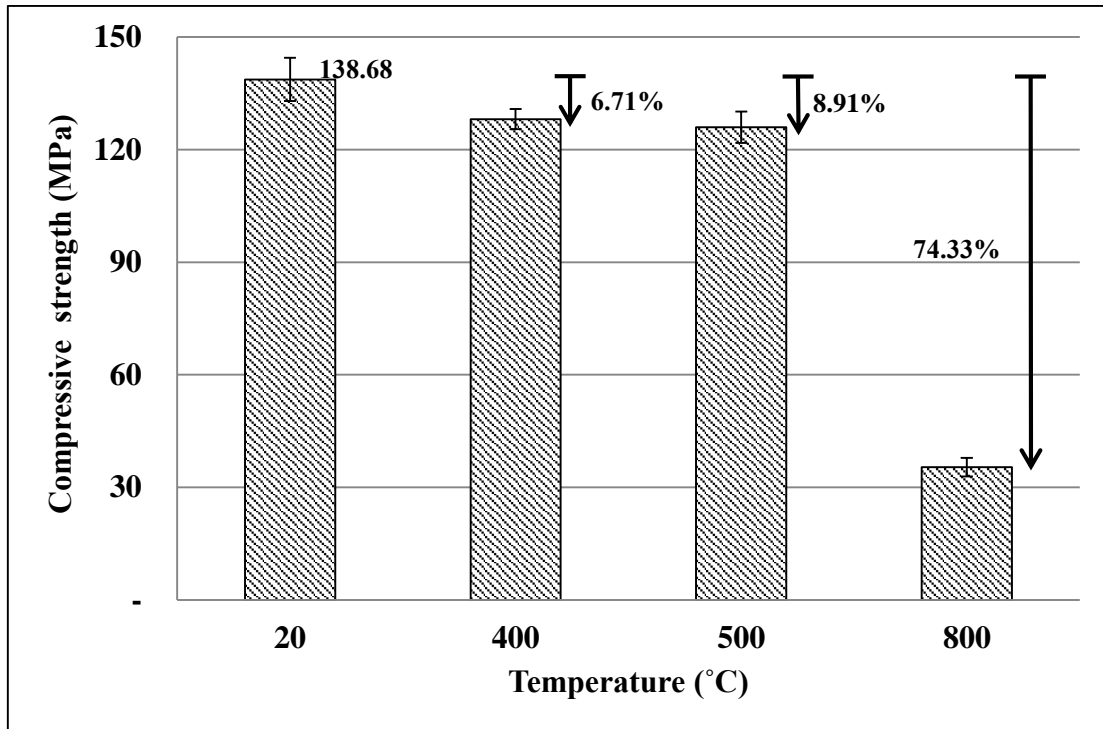
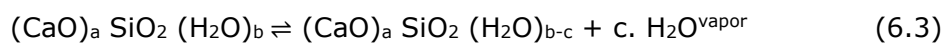


Figure 6.3 Residual compressive strength of RPC after high temperature exposure.

The dehydration, together with evaporation of capillary water, has an important role in developing the high pore pressure and explosive spalling of concrete, which is dominated by the hydration phase of C-S-H and CH with the following reactions (Zhang & Ye, 2012):



The compressive strength degradation of RPC with carbon fibre used in this study is less than the RPC with steel fibre, *i.e.* by 21.7 % at 500 °C (Liu & Huang, 2009), by 18 % at 500 °C and by 82 % at 800 °C (Tai *et. al.*, 2011). Tanyildiz (2008) who studied the properties of lightweight concrete using carbon fibres under high temperature exposure found that the residual compressive strength at

800 °C was 35 %. The advantages of carbon fibres in RPC mixtures are due to the very small diameter of carbon fibres (7 µm) and good fibre dispersion to strengthen all parts of the paste uniformly (Yao *et al.*, 2003). In addition, when RPC specimens are heated, carbon fibres provide bridging of micro cracks in the paste without yield up to 800 °C (Tanyildiz, 2008).

6.2.3.2 Initial and Residual Compressive Strength Correlation

The degradation of compressive strength in this study seems to follow similar trends to those of other scholars who have studied the effect of high temperature on fibre concrete and RPC (Chen & Liu, 2004; Tai *et al.*, 2011; Poon *et al.*, 2004a). If their results are compared with this study, it can form a correlation curve between compressive strength before and after exposure as shown in Figure 6.4. By regression, the correlation between two strengths can be expressed in an equation as follows:

$$\frac{f'_{cT}}{f'_c} = 2 \times 10^{-6} T^2 + 9 \times 10^{-4} T + 0.9745 \quad (6.6)$$

where f'_c and f'_{cT} represent the compressive strengths of RPC before and after high temperature exposure. This equation indicates the trends of increasing compressive strength after exposure in the range 100 °C to 300 °C. This equation is close to the behaviour previously reported for RPC that heat curing increases the compressive strength by around 15 % at temperatures between 200 - 300 °C, due to significant acceleration of the pozzolonic reaction and transformation of tobermorite to xonotilite (Tai *et al.*, 2011).

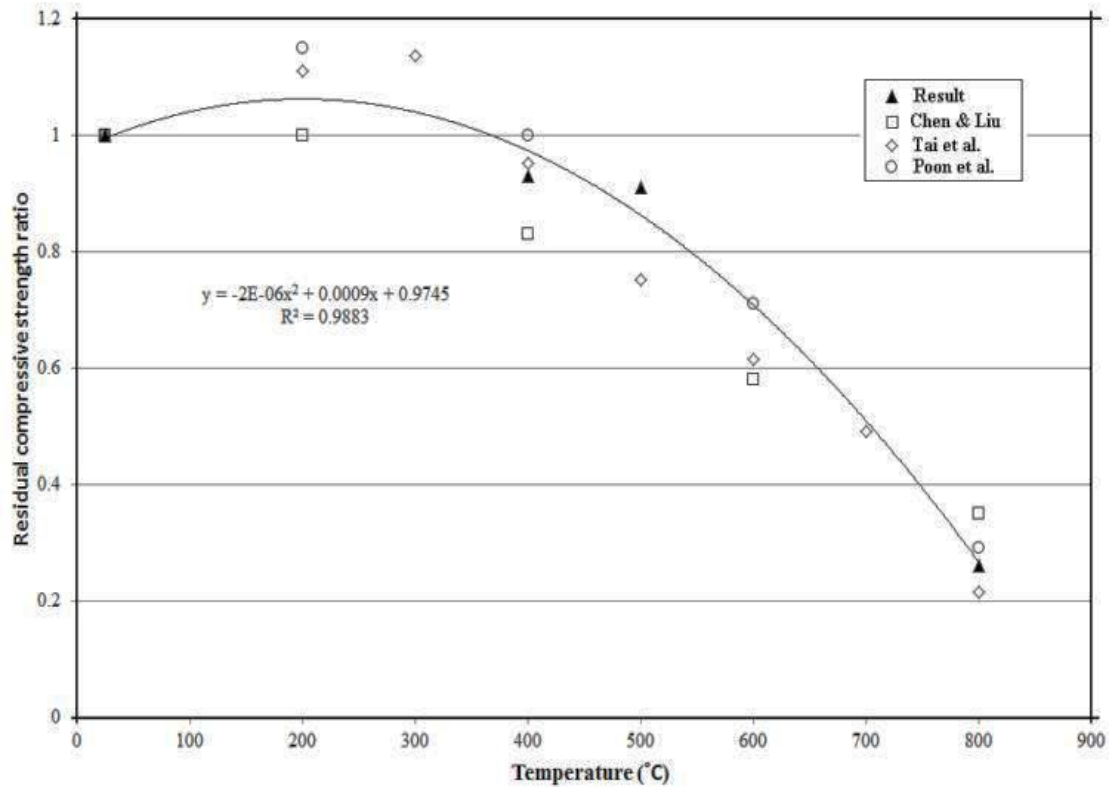


Figure 6.4 Ratio of residual compressive strength after exposure compared to the results of other scholars.

6.2.4 Microstructural Properties

The decreasing factors of compressive strength after high temperature exposure can be analysed further by correlating with the microstructure properties such as: chemical alteration, coarsening of pores, and crack progression.

6.2.4.1 Composition of Hydrates

Elevated temperature generally induces chemical reactions of certain hydrates in concrete. The results of thermogravimetric analysis carried out on post-exposure RPC samples are shown in Figure 6.5. The reference curve (20 °C) shows that the weight loss, in the temperature range 30 - 105 °C, of 1.250 % corresponds to the evaporable water which is not considered as part of the decomposition of cement

hydrates. After that point, the curve shows three regions with rapid weight losses. The first is weight loss, in a temperature range between 110 and 300 °C, of 1.313 % is due to the dehydration reactions of several hydrates, *i.e.*, decomposition of ettringite, loss of water from aluminate hydrates, and decomposition of the C-S-H. The second mass loss was observed at temperatures between 450 – 500 °C (0.454 %) and corresponds to the dehydroxylation of portlandite. The last mass loss range appears at temperatures above 600 °C, which corresponds to the calcination of calcium carbonate by 0.824 %.

After high temperature exposure, the mass loss points were also located in the same three regions identified above. The first mass loss is by 0.416 % for temperature of 400 °C, by 0.196 % for 500 °C, and by 0.001 % for 800 °C. The last value is least, which indicates that exposure of the RPC at temperatures of 800°C caused the total evaporation of water in ettringite and C-S-H. The second region shows the amount of portlandite decrease due to dehydroxylation reaction after exposure from 0.45 % (as reference) to a further 0.397 %, 0.115 %, and 0.011 % for 400 °C, 500 °C, and 800 °C, respectively. The weight loss at temperature 400 °C and 500 °C is relatively similar to the reference, but it drops sharply to 70 % after 800 °C. It supposes that most hydrates have been calcined after exposure at 800 °C.

The total mass loss by 25 % and 38 % compared to the reference caused a decrease in strength of 6.71 % and 8.91 % for temperature 400 °C and 500 °C, respectively. Total mass loss reached 84 % after exposure to 800 °C, and the compressive strength decreased by 74.33 %. It is known that cement paste has the most important role in the durability of concrete during high temperature exposure (Arioz, 2007). The degradation of compressive strength, which is influenced by the mass loss of RPC in this study, shows a good agreement with

Arioz's statement. It can be noted that the decomposition of ettringite, C-S-H and portlandite at temperatures up to 500 °C slightly influences the compressive strength, while at 800 °C it decreases sharply due to coarsening of pores in the paste and degradation of the cement chemical bonding (Liu & Huang, 2009). It can be found that high temperature exposure changes cement hydrate formation, which consequently influences the compressive strength of RPC.

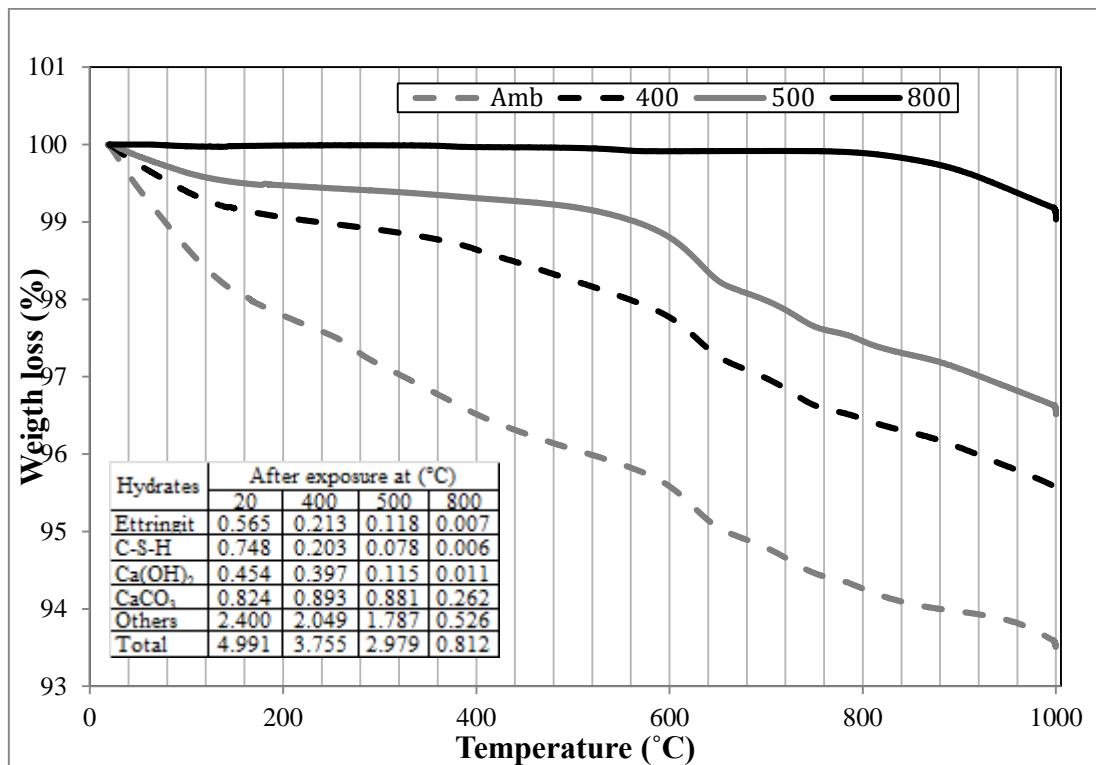


Figure 6.5 Mass loss-temperature plots showing the main hydrate content after high temperature exposure

6.2.4.2 Pore Size Evolution

The elevated temperature appeared to induce coarsening of the pore size, which influences other concrete properties such as strength, durability, and permeability (Xu *et al.*, 2001). The pore structure is critical in influencing the strength of cement paste and the performance of concrete as a whole (Neville, 2011). Pore

coarsening of concrete after high temperature exposure is commonly analysed by MIP to find the pore size distribution and total porosity (Chan *et al.*, 2000).

Table 6.2 shows the pore coarsening of RPC after exposure, which indicates the changes of porosity and average pore diameter. If compared to the reference sample, the median pore diameter increased slightly at 400 °C, almost 3 times at 500 °C, and by about 18 times at 800 °C. This indicates that high temperature exposure enlarges the pores size most likely by promoting the progression of micro cracks. The increase of total porosity may correlate not only to crack progression, but also to decomposition of hydration products such as: ettringite at temperatures of around 110 °C, C-S-H at 180 °C, Ca(OH)₂ at 450 °C, *etc.* The release of water molecules from those hydrates logically will leave some pores in the paste as well. It can be underlined that pore coarsening of RPC has a clear correlation with the physical pore properties and chemical alterations of the hydrates.

Table 6.2: Pore properties after high temperature exposure

Properties	Unit	Temperature (°C)			
		20	400	500	800
Total intrusion volume	mL/g	0.024	0.025	0.030	0.100
Median pore diameter (volume)	µm	0.012	0.018	0.031	2.054
Average pore diameter (4V/A)	µm	0.010	0.011	0.014	0.101
Bulk density at 0.51 psia	g/mL	2.221	2.205	2.130	2.017
Apparent (skeletal) density	g/mL	2.352	2.331	2.280	2.258
Porosity	%	5.377	5.571	6.586	20.208

The distribution of pore sizes after exposure is shown in Figure 6.6. It seems that high temperature has changed the distribution of the pore sizes measured. At a temperature of 400 °C, the curve has similar trends with the reference. The total

porosity slightly increases due to enlarging of capillary pores which is indicated by a decrease of pore percentage in diameter $<0.05 \mu\text{m}$. It is suggested that this correlated to the partial decomposition of ettringite and C-S-H. At a temperature of $500 \text{ }^\circ\text{C}$, the enlargement of capillary pores continuously developed as portlandite also decomposed. The increase of pores with diameter $>0.1 \mu\text{m}$ appeared to correlate with crack progression in the paste and/or in ITZ. Although quartz can partially decompose at temperatures of $580 \text{ }^\circ\text{C}$ (Morsy *et al.*, 2010), both paste and quartz aggregate expand significantly by $500 \text{ }^\circ\text{C}$ but at different rates to one another. This difference can logically induce micro cracks on the surface of the aggregate, especially following cooling. After exposure at $800 \text{ }^\circ\text{C}$, the changes to pore diameter for both ranges <0.1 and $>10 \mu\text{m}$ were more significant and quantified as 28.332 % and 43.226 %, respectively. This showed that the hydration products above continue to lose water of crystallisation plus the calcination of CaCO_3 (starting at $700 \text{ }^\circ\text{C}$) may have slightly increased porosity as well. This result agrees with other scholars; that the high temperature induced coarsening of the pore structure and is acknowledged as an important factor in causing the decrease of strength of RPC (Chan *et al.*, 2000; Xu *et al.*, 2001).

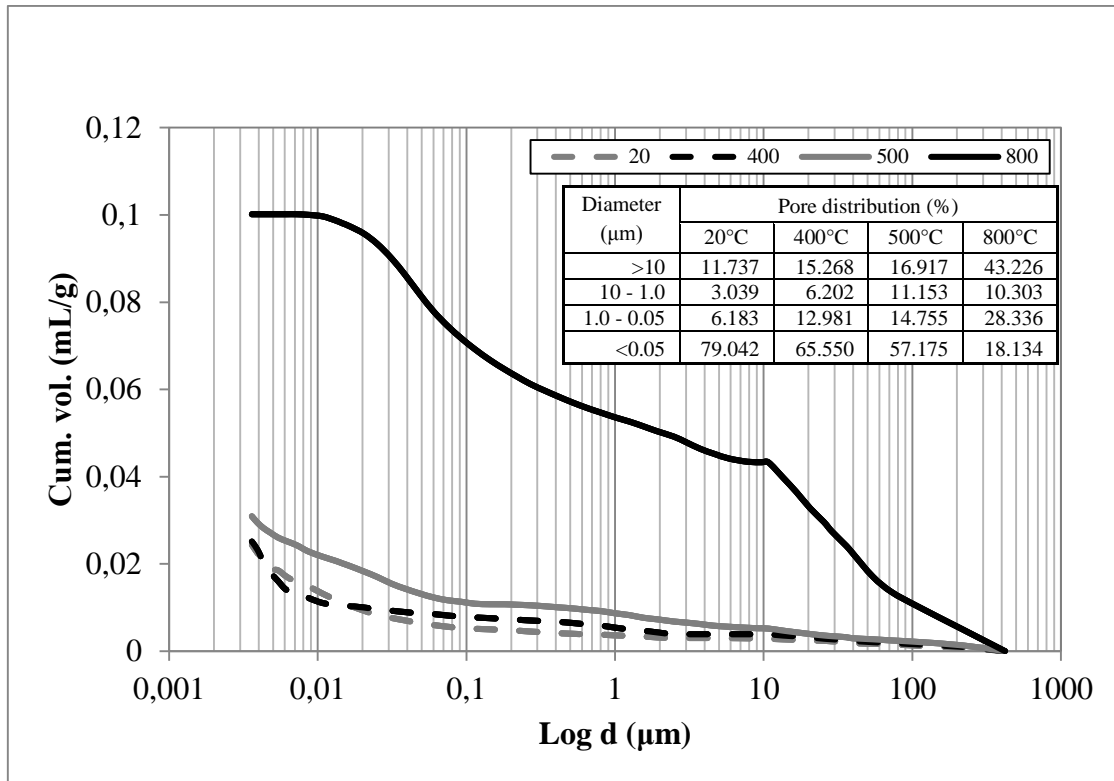


Figure 6.6 Distribution and proportion of pores in different temperature of exposure.

6.2.5 Micro Crack Progression

Most scholars agree that micro crack development at elevated temperature significantly influences the degradation of strength (Tai *et al.*, 2011; Liu & Huang, 2009; Chan *et al.*, 2000; Chen & Liu, 2004; Peng *et al.*, 2006). The micro crack progression of RPC after exposure in this study was observed by BSE imaging as shown in Figures 6.7 and 6.8.

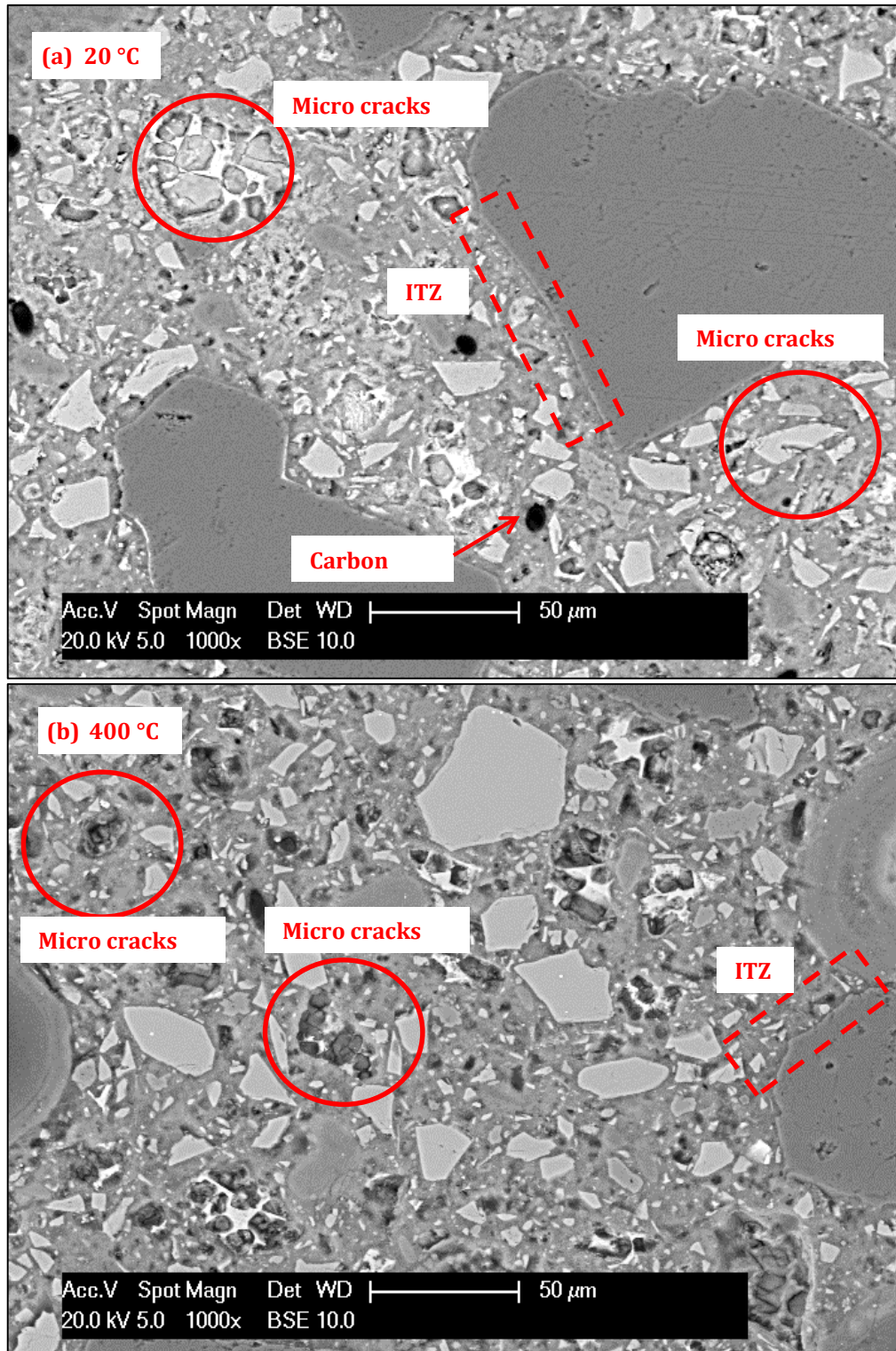


Figure 6.7 Micro crack appearance on the fracture surface of specimen core (a) at 20 °C showing dense matrix with initial micro crack (b) 400 °C showing micro crack progression on paste due to small explosion and ITZ.

Figure 6.7a shows a very dense microstructure, with some exposed carbon fibres, after exposure at ambient temperature (control sample). The entrapped air pores are also found in the matrix phase with diameters in the range 0.5 – 2.0 μm , which are believed to be due to the high amount of superplasticizer (Yazici *et al.*, 2010). The micro cracks appear to primarily occur adjacent to ettringite and surrounding unhydrated grains. There exists a dense representative area of paste adjacent to the surface of the aggregate (ITZ) which looks essentially non-porous and is in a layer up to 18 μm thick.

After specimens were heated at 400 $^{\circ}\text{C}$, the micro cracks occurred not only in the same locations as above, but also at the periphery of pores between the bulk hydrates (see Figure 6.7b). The new micro cracks are consistent with the rapid anastomosing crack propagation of a local explosion and are perhaps caused by significant air pressure increase within these pores. Exposure at this temperature also induces the appearance of some very fine cracks at the surface of aggregates, which could have been caused by a small degree of expansion of aggregate as quartz starts at temperature about 500 $^{\circ}\text{C}$.

When the exposure was increased to 500 $^{\circ}\text{C}$, micro crack progress grew intensively by enlarging the existing pore defects mentioned after 400 $^{\circ}\text{C}$ exposure. It seems that the micro cracks started to become pronounced in the bulk paste, possibly attributable to the decomposition of portlandite that had occurred. This progression consequently increased the total volume and diameter of pores, as indicated in the subset table within Figure 6.6. In addition, micro cracks in the ITZ became wider and appeared to be due to the expansion of the aggregate, as shown in Figure 6.8a. The development of micro cracks in the ITZ is consistent with the observations of Arioz (2007), who stated that the expansion of

aggregates has an important role in the compressive strength development after high temperature exposure.

Lastly, when exposed to temperatures of 800 °C disintegration of the RPC microstructure due to calcination became very apparent. The existing micro cracks progressed rapidly and the hardened paste evidently lost coherence as chemical bonding within the C-S-H phases was broken down through dihydroxylation. Decomposition of the quartz aggregates was also evident, and this is known to occur at temperatures above 580 °C as shown in Figure 6.8b. The cracks became pronounced within the cement paste and also in quartz aggregate reaching a maximum recorded width of 20 µm. Cracks occurred in all specimens and indicated almost total loss of the hardened paste coherence. The residual compressive strength after 800 °C was sufficiently high to indicate that partial sintering may have occurred, *i.e.* fusion of cement and aggregate at the asperities (Chan *et al.*, 2000). No evidence of this was recorded during SEM examinations and so the effect was either rare and localised or not apparent.

At an exposure temperature of 400 °C, micro crack development appeared to start from around the portlandite crystals and progressed to areas near the unhydrated cement grains. This is consistent with similar observations in previous studies on non-RPC samples (Piasta, 1984). The cracks progressed significantly, as three main hydrates (ettringite, C-S-H, and portlandite) have dehydroxylated at this level of temperature. At 500 °C, the enlargement in micro cracks continued and became both wider and longer. Micro cracks also occurred on the surface of aggregates due to the different thermal coefficients of aggregate and paste. During exposure, very high vapour pressure may be build up again in some pores, as discussed previously. When the location of pores with high vapour pressure is close to the surface of specimens, it may induce spalling as shown in Figure 6.1.

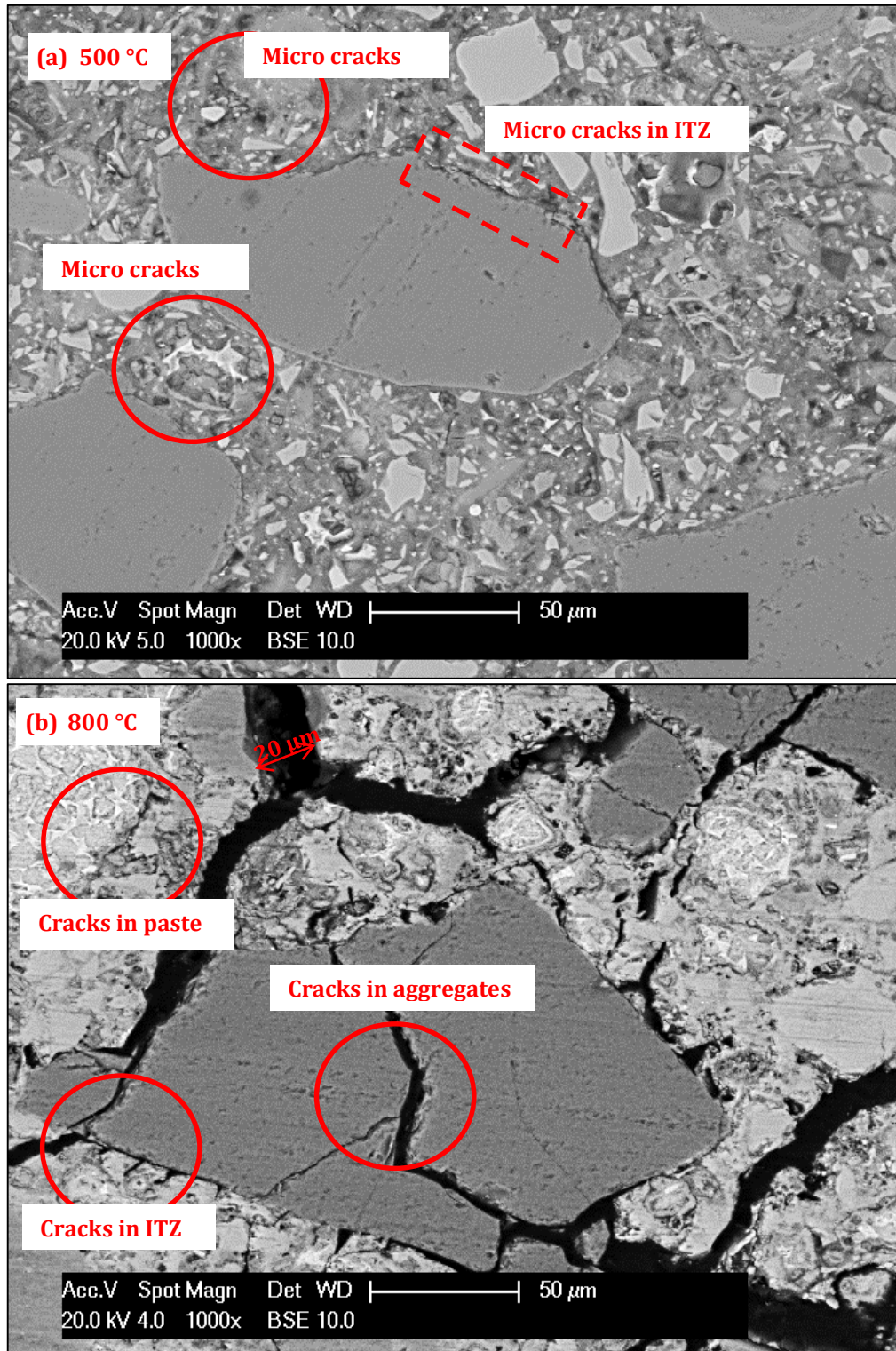


Figure 6.8 Micro crack appearance on fracture surface of specimen core (a) at 500 °C showing more micro crack in paste and wider cracks in ITZ (b) 800 °C showing micro crack in a whole of paste, ITZ and even in the quartz aggregate.

6.3 Properties of RPC After Exposure at 500 °C with Variable Heating Duration

6.3.1 Residual Compressive Strength

In this section, the specimens were heated in a computer-controlled oven at a temperature of 500 °C for different durations, *i.e.*, 30, 60, 90, and 120 minutes. Residual compressive strength of the RPC was calculated as the percentage of retained strength in the heated specimens with respect to the strength of untreated samples, as shown in Figure 6.9. The result was compared to the compressive strength of RPC without fibres, as studied by Liu & Huang (2009).

The residual compressive strength of RPC in both studies gradually decreases in line with the heating duration. In this study, the compressive strength slightly decreased by around 9 % after 30 minutes of heating, and decreased by 10, 13, and 15 % for durations of 60, 90, and 120 minutes, respectively. This trend of degradation was different from that observed by Liu & Huang (2009), who found that the residual strength of RPC decreased more significantly (starting from 30 minutes of heating) by 22 % of the initial strength. The degradation became greater in line with the longer duration, and even reduced 44 % after a duration of 120 minutes. This difference in residual strength is perhaps caused by the use of carbon fibre reinforcement in the RPC mixture for this study. Carbon fibres can provide post-crack bridging during and after exposure, which can slow crack progression and leave more competent material available within the sample. In other words, the carbon fibres appear to play an important role in improving the durability of plain RPC resulting in about a 30 % improvement (compared to conventional mixes) after high temperature exposure of up to 120 minutes.

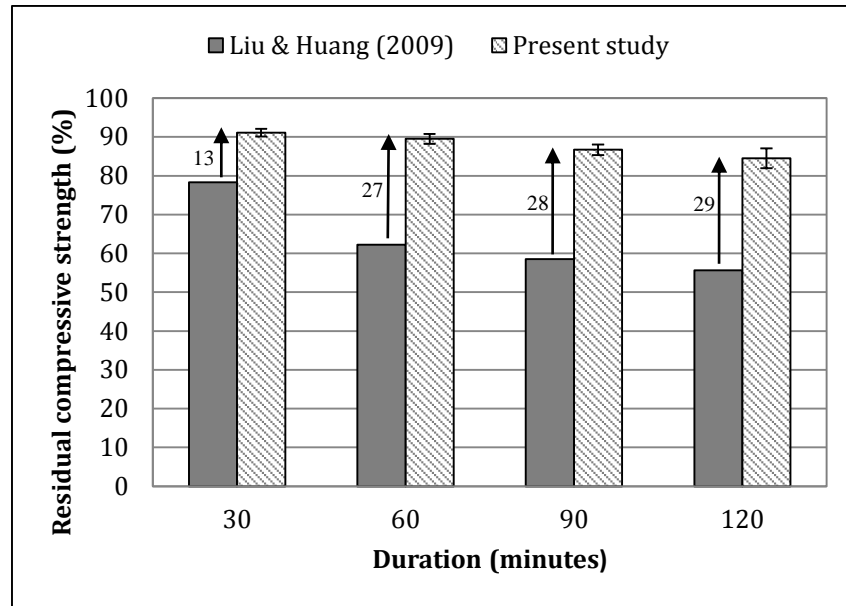


Figure 6.9 Residual compressive strength after different durations of exposure at 500 °C and comparison the results of Liu & Huang (2009) with the present study.

6.3.2 Pore Size Distribution

The decrease in compressive strength after high temperature exposure has a strong correlation with the alteration of the pore network properties, as discussed previously. The pore coarsening of RPC became more significant in line with the duration of exposure, as described in Figure 6.10. When the specimens were heated for a duration of 60 minutes or more, the volume of pores with diameter $>10 \mu\text{m}$ increased and the volume of pores with diameter between 1.0 and 10.0 μm decreased. Smaller pores seemingly developed to become larger in diameter. The exact values of pore diameter are most likely unreliable because of the degree of pore volume attributed to micro cracks, *i.e.* slit shaped pores (Washburn equation assumed circular pore cross section). On the other hand, pores with a diameter $<1.0 \mu\text{m}$ were relatively stable and appeared not to be influenced by the heating duration. After exposure for 60 and 90 minutes, the total porosity of RPC significantly increased by about 40 - 50 % although the

average pore diameter was largely unaltered (Table 6.3). Pore network coarsening became more significant after 120 minutes exposure with an increase about 70 % in both porosity and average pore diameter.

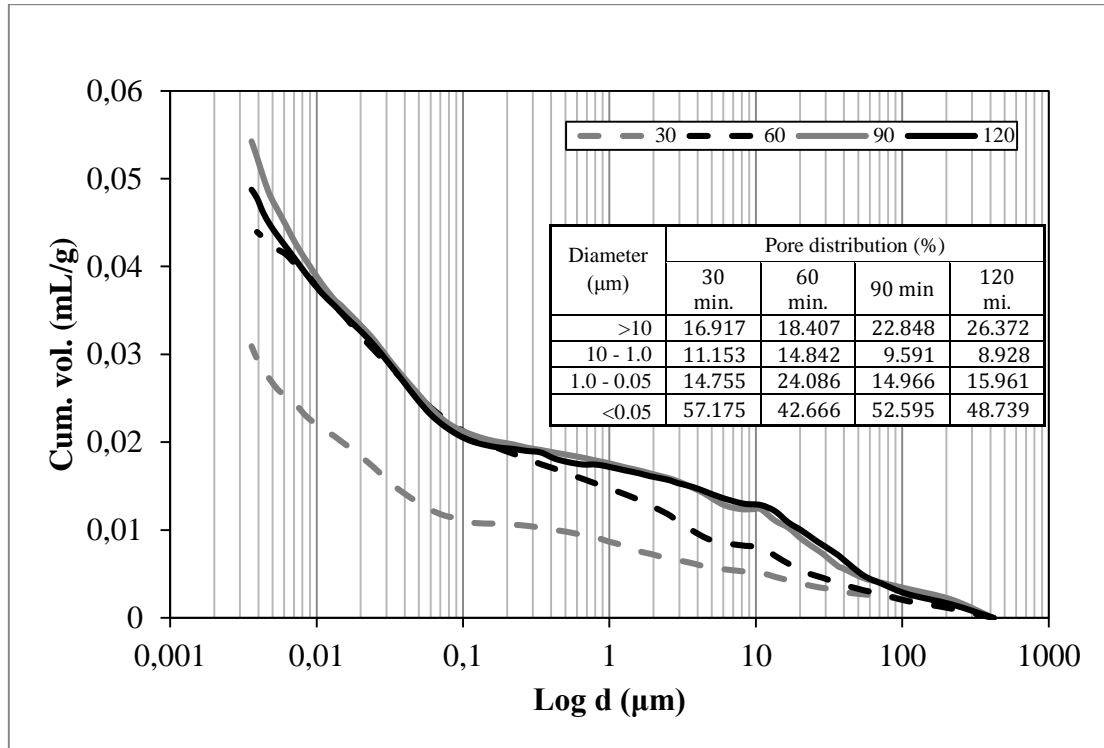


Figure 6.10 MIP cumulative intrusion vs. pore diameter after different duration of exposure at 500 °C for treatment D samples

Table 6.3: Physical properties of pores after different duration of exposure at 500 °C

Properties	Unit	Duration			
		30	60	90	120
Total Intrusion Volume	mL/g	0.030	0.044	0.049	0.054
Median Pore Diameter (Volume)	μm	0.031	0.041	0.052	0.083
Average Pore Diameter (4V/A)	μm	0.014	0.015	0.018	0.024
Bulk Density at 0.51 psia	g/mL	2.130	2.017	2.011	2.045
Apparent (skeletal) Density	g/mL	2.280	2.265	2.230	2.249
Porosity	%	6.586	9.077	9.803	10.943

6.3.3 Alteration of Cement Paste Composition

The effect of exposure duration at 500 °C on the TGA mass loss of RPC specimens is illustrated in Figure 6.11. The mass loss curves for all durations are close together up to a temperature of 650 °C. This suggests that the duration of exposure had less of an effect on the amount of hydrated components, *i.e.* ettringite, C-S-H and Ca(OH)₂. Above 650 °C, the position of the curve for the 30 minute exposure sample is noticeably different and higher than the others. This indicates that for less than 30 minutes of exposure significant quantities of hydrated components are left intact. RPC specimens heated at 500 °C for 60 minutes or more may experience mass loss from dehydroxilation of CH and C-S-H phases.

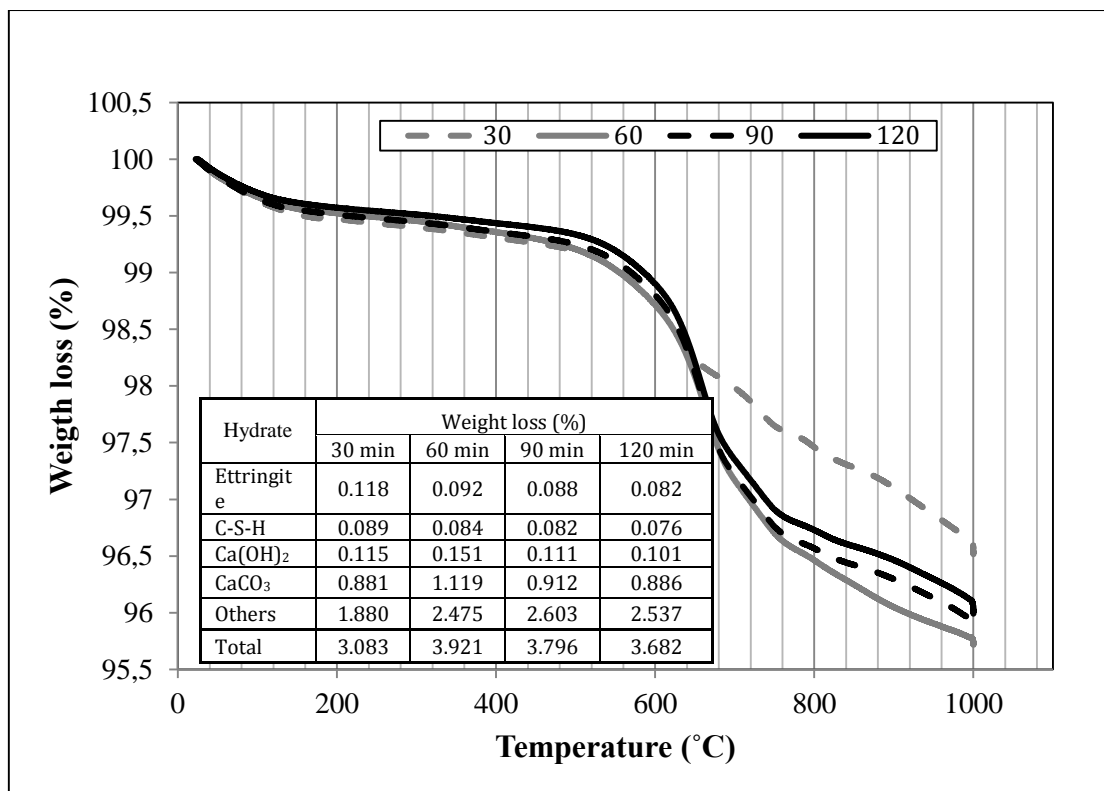


Figure 6.11 TGA mass loss for treatment D samples after exposure for different durations.

6.4 Properties of RPC After Cyclic Exposure at 500 °C

Many references have reported the properties of concrete after exposure at elevated temperature, but most only consider single exposure. To date, there have been no reported findings related to fatigue loading by cyclic high temperature exposure for RPC samples.

6.4.1 Compressive Strength

Compressive strength is one of the important indicators to describe the durability of RPC under cyclic high temperature exposure. The residual compressive strength of RPC under several cycles of exposure at 500 °C is shown in Figure 6.12. In general, the compressive strength decreased in line with the number of cycles. For single cycle exposure (1 cycle), the residual strength was about 91 %. After 3 cycles the residual strength was reduced to between 82-84 %, and further down to 78-69 % after 5 cycles. Section 6.2.4 has already explained that RPC heated at 500 °C loses compressive strength due to decomposition of several important hydrates within the paste and also coarsening of the pore network. It is therefore hypothesised that the growth of micro cracks (in size and number) is the main factor influencing the decrease of strength after cyclic aging. Specimens were exposed at the same temperature and for the same duration, and so the results from the previous sections suggest that progressive composition changes are unlikely. This would mean that the composition of hydrates would experience little change regardless of the number of cycles of exposure. This hypothesis has been tested in the following section.

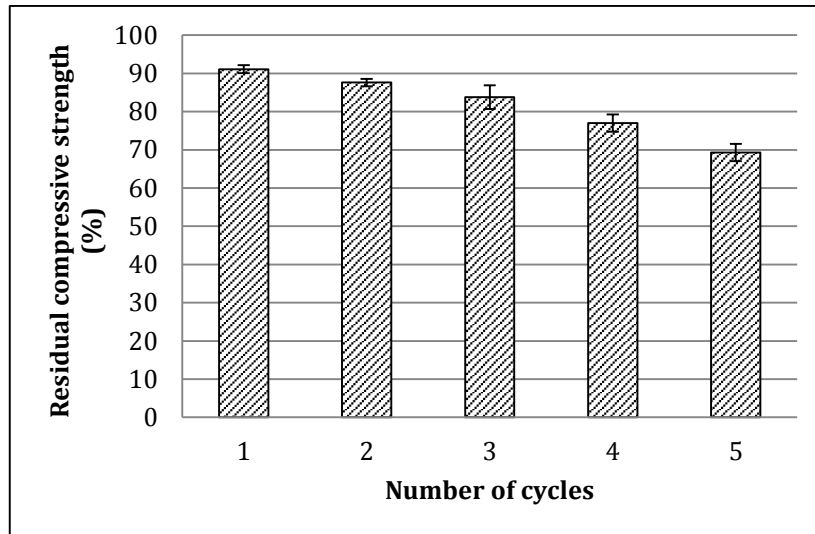


Figure 6.12 Residual compressive strength after cyclic exposure at 500 °C

6.4.2 Pore Network Evolution

Concrete structures under cyclic thermal loading experience enhanced crack propagation, which continuously forms and interconnects (Lee & Fenves, 1998). Since RPC initially contains existing micro cracks, the crack propagation under high temperature cycles can be analysed in terms of pore network evolution as well. It should be noted that MIP in these applications can only indicate the volume of intruded mercury within an order of magnitude length scale and that pore diameter values are inaccurate due to the slit shape of the micro fractures. Figure 6.13 shows the pore distribution for several heated cycles at a temperature of 500 °C.

Figure 6.13 shows that crack propagation appears to be correlated to the widening of pores. Comparing to single exposure, the volume of capillary pores after three cycles ($<0.05 \mu\text{m}$) decreases and they are replaced by larger pores, as indicated by the increase of pores in diameter range of $1.0 - 0.05 \mu\text{m}$. This alteration was followed by an increase in total pore volume from 6.5 % to about

9.0 %, as shown in Table 6.4. After 5 cycles, pores in the diameter range 1.0 - 0.05 μm experienced further significant volume increase, along with reduction in the volume of pores $<0.05 \mu\text{m}$. The total increase in pore volume was 11 % after 5 cycles and mostly due to a higher proportion of pores with diameter $>10 \mu\text{m}$. This result shows that pore coarsening after cyclic exposure had a linear correlation with pore diameter, skeletal density, and bulk porosity.

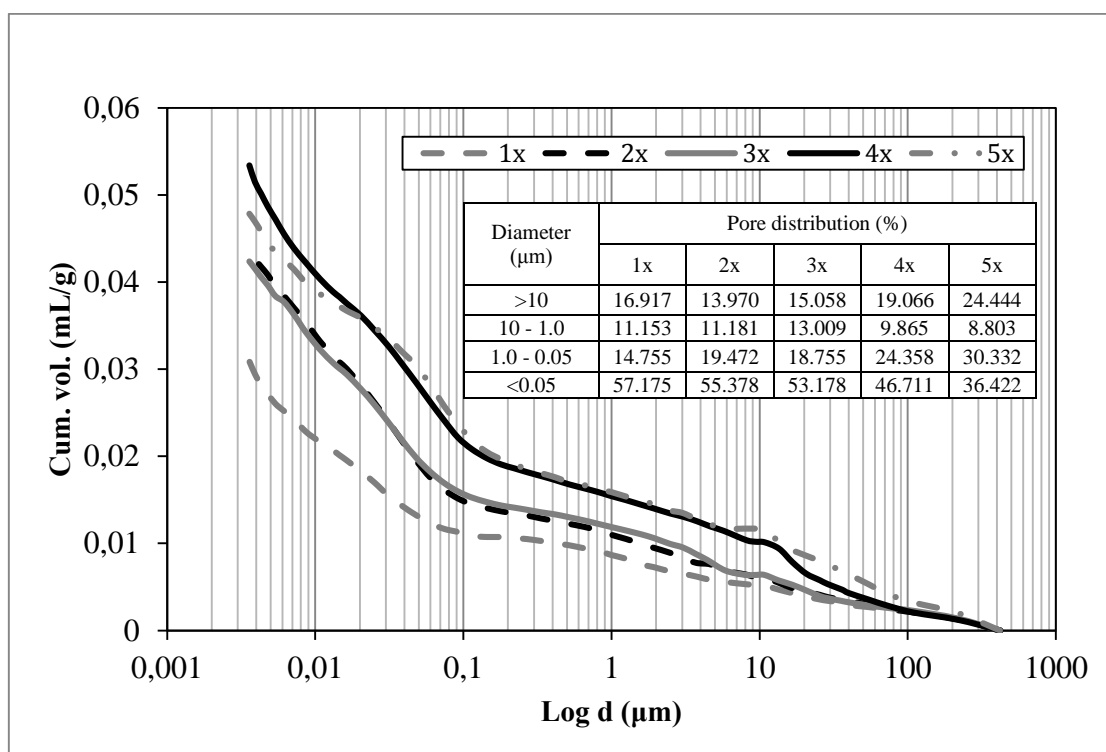


Figure 6.13 MIP pore size distribution after cyclic exposure at 500 °C

Table 6.4: Physical properties of pore network after cyclic exposure at 500 °C

Properties	Unit	Heating-cooling number				
		1x	2x	3x	4x	5x
Total intrusion volume	mL/g	0.031	0.044	0.043	0.048	0.053
Median pore diameter (volume)	μm	0.031	0.038	0.041	0.057	0.090
Average pore diameter (4V/A)	μm	0.014	0.017	0.018	0.022	0.018
Bulk density at 0.51 psia	g/mL	2.130	2.055	2.075	2.069	2.051
Apparent (skeletal) density	g/mL	2.280	2.258	2.275	2.052	2.033
Porosity	%	6.586	8.990	8.793	8.942	10.952

6.4.3 Compositional Changes by TGA after Cyclic Exposure

The mass loss of RPC after cyclic exposure at 500 °C is presented in Figure 6.14. All the curves had similar trends indicating that there was no significant change in hardened paste composition regardless of the number of cycles. This supports the earlier hypothesis that the decrease in the amount of competent material is associated with micro crack propagation. Although specimens were heated up to 5 cycles, the portlandite still existed in all specimens (but with slightly lower content), most likely due to the recrystallization of portlandite during cooling in the oven after exposure (Alarcon-Ruiz *et al.*, 2005).

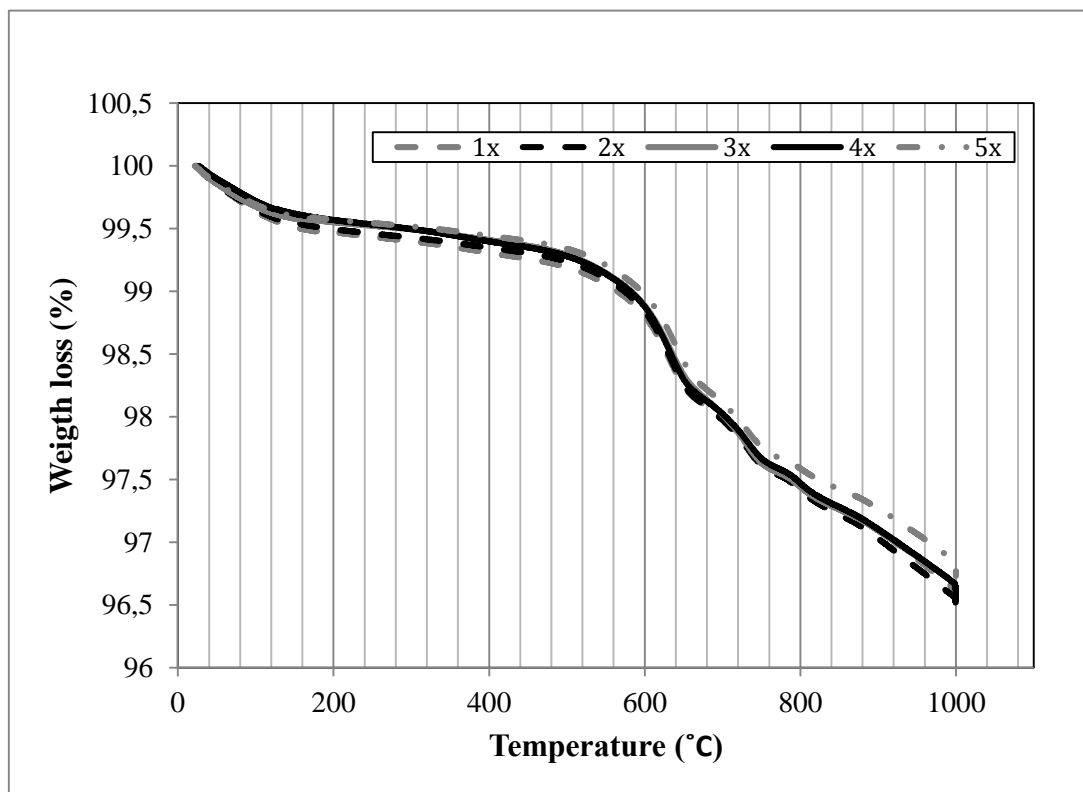


Figure 6.14 TGA mass loss for RPC after cyclic exposure at 500 °C

6.5 Properties of RPC Following Water Quenching After Heating at 500 °C

6.5.1 Compressive Strength

The dense microstructure of concrete is important to get a good durability, but it also has the disadvantage of its susceptibility to spalling after rapid temperature changes (Luo *et al.*, 2000; Chan *et al.*, 2000). Spalling rupture happens due to two factors; steep thermal gradients or high vapour pressure. The results of this investigation are relevant to RPC structures in a fire where water extinguishers can quench cool concrete that has been heated to high temperatures and cause extensive damage by thermal shock (Luo *et al.*, 2000). This study has so far found that spalling did not occur after RPC specimens were cyclically heated and cooled. This indicates that RPC generally has a good resistance to spalling, induced by thermal gradients or high vapour pressure. It should be noted that there is further potential to enhance the durability of RPC to thermal shock through the contribution of carbon fibre to prevent the micro crack progression.

Figure 6.15 shows the residual compressive strength of RPC after exposure and cooling under different conditions. RPC specimens that were heated once at 500 °C and cooled gradually inside the oven decrease the compressive strength about 9 %. When specimens were exposed to the same temperature and then cooled immediately in water, the compressive strength decreased by 25 % after a single cycle and by 34 % after two cycles. This result disagrees with some other studies (Luo *et al.*, 2000; Chan *et al.*, 2000) who found that the residual compressive strength of HPC with steel fibre at 800 °C cooled in water was slightly higher than for that cooled gradually in a furnace. They argued that the microstructure following water cooling was denser than for furnace cooling due to re-hydration of the cement component after decomposition in high temperature exposure.

This phenomenon seems not to apply to RPC and could be due to their denser, more brittle matrix (mortar) phase. It appears that heated RPC specimens with immediate cooling in water (quenching) saw significant reductions in compressive strength compared to those ramp rate cooled in a furnace. Based on previous observations for RPC materials, this is probably related to the rapid development of existing micro cracks, which logically would propagate faster with thermal shock, *i.e.* rapid cooling. This result also indicates the potential difference in the improvement of RPC durability using carbon fibre compared to HPC using steel fibre in term of strength.

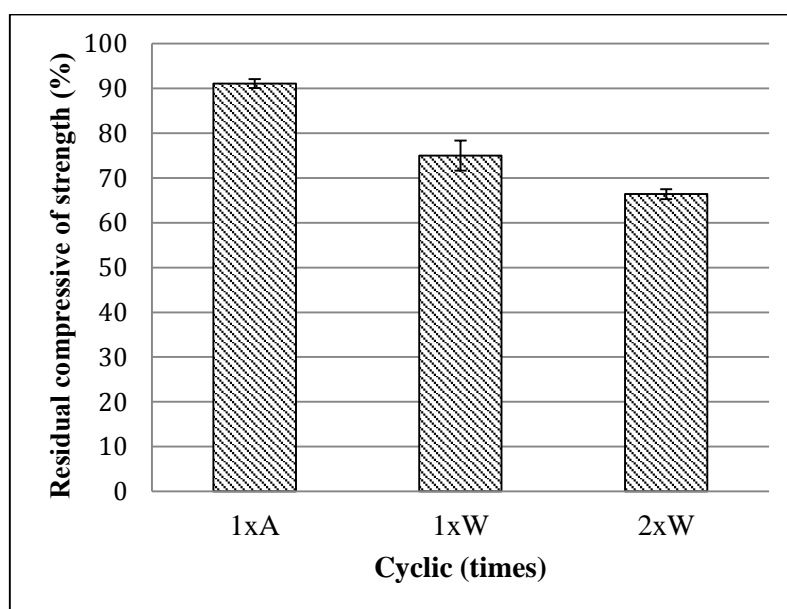


Figure 6.15 Residual compressive strength after controlled and water (quench) cooling, following initial exposure at 500 °C.

6.5.2 Pore Size Distribution

High temperature exposure generally causes the coarsening of pores which mainly affects compressive strength. Luo *et al.* (2000) found that water cooling of heated HPC at 800 °C might result in lower porosity and a denser micro structure than the those with furnace cooling. When heated specimens are cooled in water

immediately, it logically might result in further pore network coarsening due to high thermal gradient. The results of pore size distribution are shown in Figure 6.16, and the pore network physical properties in Table 6.5.

Pore size distribution for single-cycle water cooling was similar to that for oven cooled samples in the diameter range of $>0.1 \mu\text{m}$, but much greater for larger pore sizes, *i.e.* micro cracks. It appears that the increase of total pore volume from 6.586 % (by oven) to 8.481 % (by water), as presented in Table 6.5, is mainly in the capillary pore range. After two water cooling cycles, the total porosity increased dramatically by 9.447 %, or 45 % higher than the reference sample. This suggests that repeated cycles can extend both the amount and the size of micro cracks resulting in lower bulk density and less competent material.

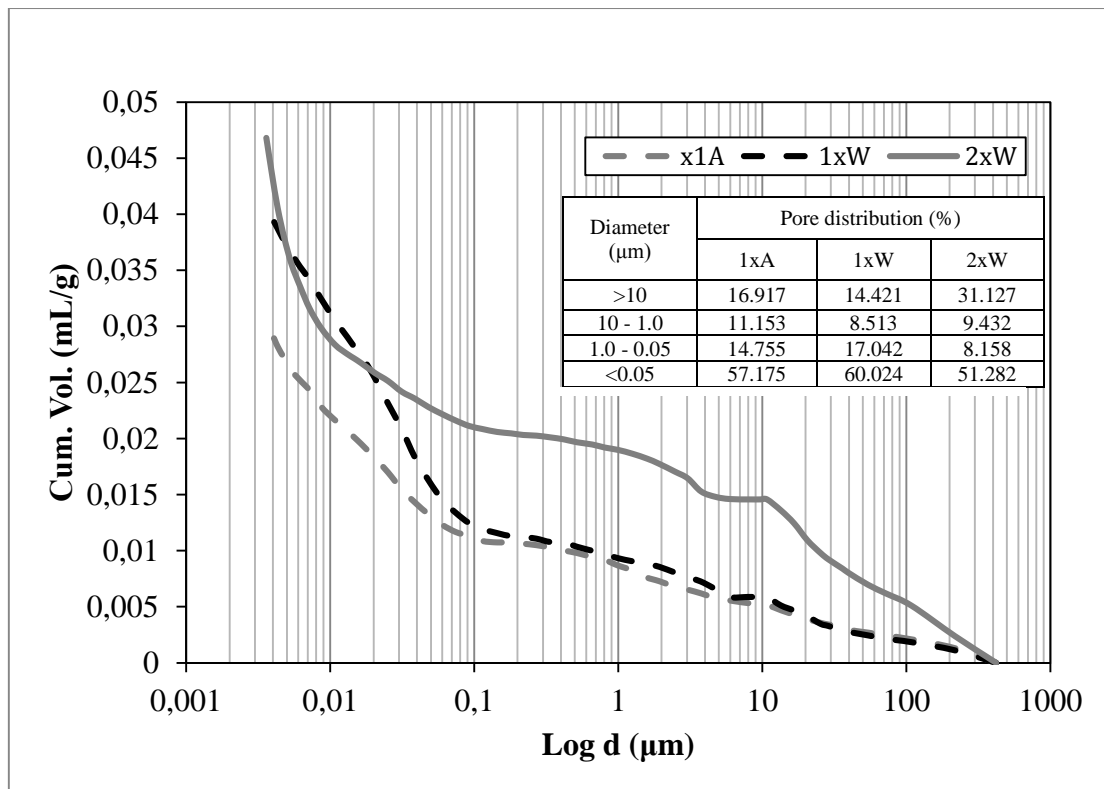


Figure 6.16 MIP pore size distribution after air and water (quench) cooling following exposure at 500 °C

Table 6.5: Physical properties of pore network after air and water (quench) cooling following exposure at 500 °C

Properties	Unit	20 °C (Ref)	Cooling		
			1xA	1xW	2xW
Total Intrusion Volume	mL/g	0.024	0.031	0.041	0.047
Median Pore Diameter (Volume)	µm	0.012	0.031	0.033	0.040
Average Pore Diameter (4V/A)	µm	0.010	0.014	0.016	0.012
Bulk Density at 0.51 psia	g/mL	2.221	2.130	2.083	2.018
Apparent (skeletal) Density	g/mL	2.352	2.280	2.276	2.228
Porosity	%	5.377	6.586	8.481	9.447

6.6 Summary

The visual observation of RPC specimens under high temperature exposure shows that anastomosing surface cracks became visible at temperatures of 500 °C and very pronounced at 800 °C. The thermo-physical properties of RPC (*i.e.* thermal conductivity, diffusivity, and effusivity) decreased in line with the increase of temperature exposure, which is more influenced by crack progression than by carbon fibre content. However, the presence of carbon fibres can improve the residual compressive strength of RPC, under high temperature exposure.

In fixed high temperature exposure, the compressive strength of RPC decreased by about 6, 9 and 74 % at temperatures of 400, 500, and 800 °C, respectively. This is strongly influenced by the shrinkage and thermal expansion behaviours of the aggregates and matrix. At 400 °C, the total hydrates were reduced by 25 % through dehydroxylation; coarsening of the capillary pores; and micro cracks between unhydrated grains, paste and aggregate. At 500 °C, the total mass loss of hydrates increases by 38 % with further extensions to micro cracks as for the 400 °C treatment samples. At 800 °C, the total mass loss sharply increased by 84

%; cement bonding degraded in the C-S-H; micro crack became pronounced throughout the entire specimen including within the quartz aggregates.

Duration of exposure at 500 °C influenced the compressive strength due to pore coarsening effects for samples exposed for 60 minutes or more. While the hydrate content was not affected by the length of exposure, the number of exposure cycles had a significant effect on the degree of pore coarsening. The rapid cooling of heated RPC in water resulted in extensive pore coarsening and rapid crack progression compared to ramp rate cooling in an oven.

Chapter 7- Conclusions and Recommendations

7.1 Conclusions

Considerable research has been done to define the properties of RPC but it has until now been less focused on high temperature experimentation. In response to this, this research aims to define the characteristics of the thermo-physical properties of RPC and to quantify the microstructure changes caused by high temperature curing during the setting period and cyclic high temperature exposure after 28 days. Mechanical properties were tested, flexural and compressive strength, from a mean of three samples. Microstructure properties were observed through the use of several instruments, i.e. microscopic optic, SEM, EDS, XRD, MIP and TGA. Thermo-physical properties were measured by thermal conductivity analyser equipment. SEM images were analysed using Image 1.47v to measure the local porosity in the ITZ.

7.1.1 (Obj.1) Optimising Heat Curing Treatment

An RPC using a high amount of GGBS and superplasticizer has different properties than from a mortar mixture with respect to fresh conditions. The consistency of fresh RPC shows a plastic flowing and spreadable mixture. Heat curing is optimal at a rate of 50 °C/hr due to the proportional effect on two processes, the pozzolanic reaction and microcracks formed in the cement paste. The optimal heat duration is 48 hours due to the acceleration of both reactions (hydration and pozzolanic) and the increase in the amount of crystal transformation from tobermorite to xonotlite. The optimal delay in heat starting time is 2-days due to heat-induced acceleration of hydrate phase densification whilst avoiding the risk of

microcrack initiation/enlargement, resulting from thermal expansion of partially-hardened hydrate phases. Most RPC specimens produced a normal failure mode forming a double pyramid shape in compression tests and brittle failure in flexural tests. Additional carbon fibre had no influence on compressive strength but gave a significant increase in flexural strength of 14 % due to the development of toughness. The brittle failure of RPC is as a result of low bonding between carbon fibre and paste.

7.1.2 (Obj. 2) Analysing Microstructure Properties to Develop a Basic Model of RPC Affected by Treatments

SEM images show that heat curing induces pore filling by tobermorite in the form of platy-shaped crystals and xonotlite in the form of needle-shaped crystals. The TGA test results from the hydration process are influenced by two factors; the pressure reduces the amount of hydrate and increases the anhydrous materials due the reduction in water, and the heat curing reduces the amount of C-S-H gel phase due to transformation reaction from C-S-H to tobermorite and/or xonotlite and reduces also the amount of $\text{Ca}(\text{OH})_2$ due to pozzolanic reaction. XRD spectra showed the presence of anhydrous cement (alite and belite), xonotlite and loss of portlandite after heat curing confirmed the pozzolanic reaction. EDS analysis results show that atom ratios of Ca/Si , $(\text{Al}+\text{Fe})/\text{Ca}$ and S/Ca fluctuate with significant distance from the aggregate; a Ca/Si ratio >1 indicates the transformation process of C-S-H to xonotlite. Porosity analysis of the ITZ reveal a thickness with a range of 17 - 18 μm and a local porosity of 3.4 - 5.4 % for all treatments.

The MIP test shows that the pore distribution is significantly affected by both pressure and heat, with a majority of the pore volume in the range 5 - 50 nm. The pressure effect on the entrapped air is the formation of voids with diameter

above 10 μm and capillary pores in the range of 10 – 50 nm; both pressure and heat curing increase the capillary pore volume by 70 % due to the air pressure mechanism and hydrate transformation. Both pressure and heat combined to produce the most beneficial pore properties as expected, such as the increase of apparent (skeletal) density, reduced pore diameter and a decreased amount of large capillaries. These are all important factors influencing the compressive strength of RPC.

RPC samples without pressure or heat curing initially contain entrapped air pores and microcracks due to the spaces formed by free water and the shrinkage process of cement paste hardening. Static pressure treatment induces a denser cement paste due to the reduction of some pores together with the spill out of free water and transformation of pores to become smaller physically (capillary pores). The application of pressure also leads to the development of microcracks due to disruption of the hydration reaction and the movement of material grains. Heat curing induces the microcracks to become longer and wider as the air pressure inside them increases.

7.1.3 (Obj. 3) Quantifying the Properties of RPC after Fixed-term Exposure to Heat

After high temperature exposure, the thermo-physical properties of RPC (i.e. thermal conductivity, diffusivity, and effusivity) decrease due to crack progression. The cracks visually occur and are clearly seen on the surface at a temperature of 500 °C and become very pronounced at 800 °C. The addition of carbon fibres significantly improves the durability of RPC in compression, higher even more so than for RPC with steel fibres.

After elevated temperature exposure, the compressive strength of RPC decreases due to shrinkage and thermal expansion. At 400 °C the compressive strength is reduced by 6 % and total hydrates by 25 %; coarsening appears in most of the pore capillaries; microcracks occur in between unhydrated grains, paste and aggregate. At 500 °C, compressive strength reduces by 9 %; the total weight loss of hydrates increases by 38 %; microcracks occur at 500 °C with additional widening of microcracks between the paste and the aggregate. At 800 °C, heating reduces the compressive strength sharply by 74 %; total weight loss increases sharply by 84 %; cement bonding is totally lost; pronounced microcracks form in the sample including within quartz aggregate. The presence of CaCO₃ is believed as the main factor of RPC's strength after exposure at 800 °C. Pore coarsening increased the porosity of RPC due to the hydration process of cement paste and formation (progression) of microcracks.

7.1.4 (Obj. 4) Quantifying the Properties of RPC after Cyclical Heat Exposure with Different Cooling Regimes

Exposure at 500 °C significantly influences the compressive strength for durations of 60 minutes or more due to pore coarsening; however, the hydrates content is not affected by exposure duration. Cyclic heat exposure also has a significant effect on the compressive strength due to pore coarsening, but the hydrates content is still not influenced. Rapid cooling of a heated RPC in water results in much worse pore coarsening and more rapid crack progression than slower cooling in an oven.

7.1.5 (Obj. 5) Characterising the Correlation between Mechanical Properties and Crack Progression

Static pressure applied during the setting of an RPC mixture followed by heat curing after two days produced a multiscale transformation with respect to micro structural composition and pore geometry. The conditions of curing significantly affect the macro scale physical-mechanical properties of RPC but that does not involve any apparent alteration of the ITZ phase. RPC heated at high temperatures decreases in compressive strength due to pore coarsening, decomposition of hydrates, and acceleration of cracks. By heating RPC at a fixed temperature of 500 °C, the pore coarsening is significantly influenced by the duration of heating, number of exposure cycles, and cooling condition after heating.

7.2 Recommendations for Future Research

This study has verified the properties of RPC mixture with reduced cement content (due to replacement by GGBS) and with carbon fibre. RPC samples were heated to high temperature during the curing period and after hardening. The effect of pressure treatment has also been investigated and the results used to build a basic model describing the microstructure evolution after treatment. The durability of RPC at elevated temperatures has been evaluated for its mechanical and microstructure properties under both single and cyclic heat exposure.

This study has shown results which indicate that the replacement of some cement content with GGBS and the use of carbon fibre makes it possible to create an RPC with compressive strength of about 140 MPa. The properties of both GGBS and

carbon fibre after heat curing have not been explored yet. Therefore, the following topics are proposed for further research:

- (1) A study on the effect of GGBS as cement replacement on the hydration reaction or pozzolanic reaction in RPC mixtures during high temperature curing.
- (2) A study on the effect of carbon fibre at higher volume fractions on mechanical and microstructure properties after high temperature exposure during the curing period or after hardening, such as pull out, compressive-flexural, and permeability tests.
- (3) A study on the durability of RPC containing PFA or metakaolin with different fibre types against abrasion, chemical reaction, or freeze and thaw.

References

- Abell, A. B., Willis, K. L., and Lange, D. A. 1999. Mercury Intrusion Porosimetry and Image Analysis of Cement-Based Materials. *Journal of Colloid and Interface Science* 211, 39–44.
- Alarcon-Ruiz, L., Platret, G., Massieu, E. and Ehrlicher, A., 2005. The use of thermal analysis in assessing the effect of temperature on a cement paste. *Cement and Concrete research*, 35(3), pp.609-613.
- Allen, A.J., Thomas, J.J. and Jennings, H.M., 2007. Composition and density of nanoscale calcium–silicate–hydrate in cement. *Nature materials*,6(4), pp.311-316.
- Anderberg, Y., 1997, February. Spalling phenomena of HPC and OC. In *NIST Workshop on Fire Performance of High Strength Concrete in Gaithersburg* (pp. 69-73).
- Arioz, O., 2007. Effects of elevated temperatures on properties of concrete. *Fire Safety Journal*, 42(8), pp.516-522.
- Balonis, M. and Glasser, F.P., 2009. The density of cement phases. *Cement and Concrete Research*, 39(9), pp.733-739.
- Bank, L.C., 2006. *Composites for construction: structural design with FRP materials*. John Wiley & Sons.
- Bažant, Z.P. and Thonguthai, W., 1979. Pore pressure in heated concrete walls: theoretical prediction. *Magazine of Concrete Research*, 31(107), pp.67-76.
- Bentz, D.P., Garboczi, E.J. and Stutzman, P.E., 1993. Computer modeling of the interfacial transition zone in concrete. *Interfaces in cementitious composites*, pp.259-268.
- Blais, P.Y. and Couture, M., 1999. Precast, prestressed pedestrian bridge-world's first reactive powder concrete structure. *Pci journal*, 44, pp.60-71.
- Blundell, S. and Blundell, K.M., 2010. *Concepts in thermal physics*. Oxford University Press.
- Bonneau, O., Vernet, C., Moranville, M. and Aitcin, P.C., 2000. Characterization of the granular packing and percolation threshold of reactive powder concrete. *Cement and Concrete Research*, 30(12), pp.1861-1867.
- Cassagnabère, F., Escadeillas, G. and Mouret, M., 2009. Study of the reactivity of cement/metakaolin binders at early age for specific use in steam cured precast concrete. *Construction and Building Materials*, 23(2), pp.775-784.
- Chan, Y.N., Luo, X. and Sun, W., 2000. Compressive strength and pore structure of high-performance concrete after exposure to high temperature up to

- 800 C. *Cement and Concrete Research*, 30(2), pp.247-251.
- Chan, Y.W. and Chu, S.H., 2004. Effect of silica fume on steel fiber bond characteristics in reactive powder concrete. *Cement and Concrete Research*, 34(7), pp.1167-1172.
- Chen, B. and Liu, J., 2004. Residual strength of hybrid-fiber-reinforced high-strength concrete after exposure to high temperatures. *Cement and Concrete Research*, 34(6), pp.1065-1069.
- Chen, J.J. and Kwan, A.K.H., 2012. Superfine cement for improving packing density, rheology and strength of cement paste. *Cement and Concrete Composites*, 34(1), pp.1-10.
- Cheyrezy, M., Maret, V. and Frouin, L., 1995. Microstructural analysis of RPC (reactive powder concrete). *Cement and Concrete Research*, 25(7), pp.1491-1500.
- Chindaprasirt, P., Chareerat, T. and Sirivivatnanon, V., 2007. Workability and strength of coarse high calcium fly ash geopolymer. *Cement and Concrete Composites*, 29(3), pp.224-229.
- Cho, S.W., 2012. Using mercury intrusion porosimetry to study the interfacial properties of cement-based materials. *J. Marine Sci. Technol*, 20(3), pp.269-273.
- Chung, D.D.L., 2000. Cement reinforced with short carbon fibers: a multifunctional material. *Composites Part B: Engineering*, 31(6), pp.511-526.
- Cwirzen, A., 2007. The effect of the heat-treatment regime on the properties of reactive powder concrete. *Advances in Cement Research*, 19(1), pp.25-33.
- Cwirzen, A., Penttala, V. and Vornanen, C., 2008. Reactive powder based concretes: Mechanical properties, durability and hybrid use with OPC. *Cement and Concrete Research*, 38(10), pp.1217-1226.
- De Larrard, F. and Sedran, T., 2002. Mixture-proportioning of high-performance concrete. *Cement and concrete research*, 32(11), pp.1699-1704.
- Diamond, S., 2004. The microstructure of cement paste and concrete--a visual primer. *Cement and Concrete Composites*, 26(8), pp.919-933.
- Dietz, T. and Bohnemann, K., 2000. Calcium silicate hydrate in fiber cement sheets and autoclaved aerated concrete. *Inorganic bonded wood and fiber composite materials*, pp.34-57.
- Dolado, J.S. and Van Breugel, K., 2011. Recent advances in modeling for cementitious materials. *Cement and concrete research*, 41(7), pp.711-726.
- Domone, P. and Illston, J. eds., 2010. *Construction materials: their nature and behaviour*. CRC Press.

- Domone, P.L.. *Concrete*, in: J.M. Illston (Ed.), *Construction Materials-Their Nature and Behaviour*, second ed., E & FN Spon, London, 1996, pp. 89-195.
- Dos Santos, W.N., 2003. Effect of moisture and porosity on the thermal properties of a conventional refractory concrete. *Journal of the European Ceramic Society*, 23(5), pp.745-755.
- Eckert, M., 2012. Max von Laue and the discovery of x-ray diffraction in 1912. *Annalen der Physik*, Lpz. 524 A83-5
- EN, BS. 12620: 2002+ A1: 2008, *Aggregates for concrete*.
- EN, BS. 197-1, 2011. *Cement-Part 1: Composition, specifications and conformity criteria for common cements*.
- EN, BS. 934-2, 2009. *Admixtures for Concrete, Mortar and Grout-Part 2: Concrete Admixtures-Definitions, Requirements, Conformity, Marking and Labelling*.
- EN, TS. 12390-3, 2002. *Testing hardened concrete-part 3: compressive strength of test specimens*.
- Gani, M.S.J., 1997. *Cement and Concrete*. London, UK: Chapman & Hall.
- Gao, Y., De Schutter, G., Ye, G., Tan, Z. and Wu, K., 2014. The ITZ microstructure, thickness and porosity in blended cementitious composite: Effects of curing age, water to binder ratio and aggregate content. *Composites Part B: Engineering*, 60, pp.1-13.
- Hager, I., 2013. Behaviour of cement concrete at high temperature. *Bulletin of the Polish Academy of Sciences: Technical Sciences*, 61(1), pp.145-154.
- Haha, M.B., Le Bescop, P., Bary, B., Gallucci, E. and Scrivener, K., 2008. Quantitative microstructural characterisation of cement paste submitted to different moderate temperature and loading conditions. In *Creep, Shrinkage and Durability Mechanics of Concrete and Concrete Structures, Two Volume Set: Proceedings of the CONCREEP 8 conference held in Ise-Shima, Japan*, (p. 25). CRC Press.
- Hall, M.R., Dehdezi, P.K., Dawson, A.R., Grenfell, J. and Isola, R., 2011. Influence of the thermophysical properties of pavement materials on the evolution of temperature depth profiles in different climatic regions. *Journal of Materials in Civil Engineering*.
- Hall, M.R., Najim, K.B. and Hopfe, C.J., 2012. Transient thermal behaviour of crumb rubber-modified concrete and implications for thermal response and energy efficiency in buildings. *Applied thermal engineering*, 33, pp.77-85.
- Hannant, D. Fibre-reinforced cements and concretes, in: J.M. Illston (Ed.), *Construction Materials-Their Nature and Behaviour*, second ed., E & FN Spon, London, 1998, pp. 359-403
- Hanson, 2009. Production and use of GGBS technical data sheet. www.hanson.com/uk.

- Hassan, K.E., Cabrera, J.G. and Maliehe, R.S., 2000. The effect of mineral admixtures on the properties of high-performance concrete. *Cement and Concrete Composites*, 22(4), pp.267-271.
- Helmi M., Hall M.R., and Rigby S.P., 2013. Treatment effects on the compressive strength of reactive powder concrete (RPC) at 7 days, In Proceeding of 33rd Cement and Concrete Science Conference. University of Portsmouth UK. 2013; 288-33.
- Hertz, K.D., 2005. Concrete strength for fire safety design. *Magazine of Concrete Research*, 57(8), pp.445-453.
- Hong, S.Y. and Glasser, F.P., 2004. Phase relations in the CaO-SiO₂-H₂O system to 200 C at saturated steam pressure. *Cement and Concrete Research*, 34(9), pp.1529-1534.
- Horners, S., 2008. Activity 20 - Bendy Wafer. Advanced Physics for Edexcel AS Physics. *Essex, United Kingdom: Pearson Education*.
- Illston, J. M. 1996. Construction Materials - Their Nature and Behaviour, E & FN Spon.
- Ji, T., Chen, C.Y. and Zhuang, Y.Z., 2012. Evaluation method for cracking resistant behavior of reactive powder concrete. *Construction and Building Materials*, 28(1), pp.45-49.
- Jin, F., Abdollahzadeh, A. and Al-Tabbaa, A., 2013. Effect of different MgOs on the hydration of MgO-activated granulated ground blastfurnace slag paste. In *Proc. Int. Conf. Sustain. Constr. Mater. Technol., Kyoto, Japan* (Vol. 2, No. 3, p. 4).
- Johnston, C.D. 2006. Fiber-Reinforced Cements and Concretes (Advances in Concrete Technology;V:3). Taylor&Francis-NY. 364p
- Kalifa, P., Menneteau, F.D. and Quenard, D., 2000. Spalling and pore pressure in HPC at high temperatures. *Cement and concrete research*, 30(12), pp.1915-1927.
- Katz, A., Li, V.C. and Kazmer, A., 1995. Bond properties of carbon fibers in cementitious matrix. *Journal of materials in civil engineering*, 7(2), pp.125-128.
- Khaliq, W. and Kodur, V., 2011. Thermal and mechanical properties of fiber reinforced high performance self-consolidating concrete at elevated temperatures. *Cement and Concrete Research*, 41(11), pp.1112-1122.
- Kodur, V. and Khaliq, W., 2010. Effect of temperature on thermal properties of different types of high-strength concrete. *Journal of materials in civil engineering*, 23(6), pp.793-801.
- Kodur, V.K.R. and Sultan, M.A., 2003. Effect of temperature on thermal properties of high-strength concrete. *Journal of materials in civil engineering*, 15(2), pp.101-107.

- Kumar, R. and Bhattacharjee, B., 2003. Porosity, pore size distribution and in situ strength of concrete. *Cement and concrete research*, 33(1), pp.155-164.
- Liu, B., Xie, Y., Zhou, S. and Yuan, Q., 2000. Influence of ultrafine fly ash composite on the fluidity and compressive strength of concrete. *Cement and concrete research*, 30(9), pp.1489-1493.
- Liu, C.T. and Huang, J.S., 2009. Fire performance of highly flowable reactive powder concrete. *Construction and Building Materials*, 23(5), pp.2072-2079.
- Liu, H.B., Tian, K.P., Liu, J.H. and Ju, Y., 2012, January. Experiment on Thermophysical Properties of Reactive Powder Concrete. In *Advanced Materials Research* (Vol. 374, pp. 1519-1522).
- Long, G., Wang, X. and Xie, Y., 2002. Very-high-performance concrete with ultrafine powders. *Cement and Concrete Research*, 32(4), pp.601-605.
- Luo, X., Sun, W. and Chan, S.Y.N., 2000. Effect of heating and cooling regimes on residual strength and microstructure of normal strength and high-performance concrete. *Cement and Concrete Research*, 30(3), pp.379-383.
- Ma, W. and Brown, P.W., 1997. Hydrothermal reactions of fly ash with Ca (OH) 2 and CaSO 4· 2H 2 O. *Cement and Concrete Research*, 27(8), pp.1237-1248.
- Matte, V. and Moranville, M., 1999. Durability of reactive powder composites: influence of silica fume on the leaching properties of very low water/binder pastes. *Cement and Concrete Composites*, 21(1), pp.1-9.
- Mehta P. K. and Monteiro P. J. M. *Concrete: Microstructure, Properties and Materials*, 3rd edn. McGraw-Hill, New York, 2006.
- Mohammed, M.K., Dawson, A.R. and Thom, N.H., 2014. Macro/micro-pore structure characteristics and the chloride penetration of self-compacting concrete incorporating different types of filler and mineral admixture. *Construction and Building Materials*, 72, pp.83-93.
- Morin, V., Tenoudji, F.C., Feylessoufi, A. and Richard, P., 2001. Superplasticizer effects on setting and structuration mechanisms of ultrahigh-performance concrete. *Cement and concrete research*, 31(1), pp.63-71.
- Morsy, M.S., Alsayed, S.H. and Aqel, M., 2010. Effect of elevated temperature on mechanical properties and microstructure of silica flour concrete. *International journal of civil & environmental engineering*, 10(1), pp.1-6.
- Najim, K.B., 2012. *Determination and enhancement of mechanical and thermo-physical behaviour of crumb rubber-modified structural concrete* (Doctoral dissertation, University of Nottingham).
- Nambiar, E.K. and Ramamurthy, K., 2008. Models for strength prediction of foam concrete. *Materials and structures*, 41(2), pp.247-254.

- Neville, A.M., 2011. *Properties of concrete*. Atlantic Publications, Inc.
- Panarese, W.C., Kosmatka, S.H. and Randall, F.A., 1991. *Concrete masonry handbook for architects, engineers, builders*. Portland Cement Assn.
- Patel, H.H., Bland, C.H. and Poole, A.B., 1995. The microstructure of concrete cured at elevated temperatures. *Cement and Concrete Research*, 25(3), pp.485-490.
- Peng, G.F., Yang, W.W., Zhao, J., Liu, Y.F., Bian, S.H. and Zhao, L.H., 2006. Explosive spalling and residual mechanical properties of fiber-toughened high-performance concrete subjected to high temperatures. *Cement and Concrete Research*, 36(4), pp.723-727.
- Peng, Y.Z., Chen, K. and Hu, S.G., 2011, April. Study on Interfacial Properties of Ultra-High Performance Concrete Containing Steel Slag Powder and Fly Ash. In *Advanced Materials Research* (Vol. 194, pp. 956-960).
- Pinto, R.C. and Hover, K.C., 1999. Application of maturity approach to setting times. *ACI Materials Journal*, 96(6).
- Poon, C. S., Shui, Z. H. and Lam, L. 2004a. Compressive behavior of fiber reinforced high-performance concrete subjected to elevated temperatures. *Cement and Concrete Research*, 34, 2215-2222.
- Poon, C. S., Shui, Z. H. and Lam, L. 2004b. Effect of microstructure of ITZ on compressive strength of concrete prepared with recycled aggregates. *Construction and Building Materials*, 18, 461-468.
- Poon, C.S., Azhar, S., Anson, M. and Wong, Y.L., 2001. Comparison of the strength and durability performance of normal-and high-strength pozzolanic concretes at elevated temperatures. *Cement and Concrete Research*, 31(9), pp.1291-1300.
- Rebentrost, M. and Cavill, B., 2006. Reactive powder concrete bridges. In *AUSTROADS BRIDGE CONFERENCE, 6TH, 2006, PERTH, WESTERN AUSTRALIA*.
- Reinhardt, H.W. and Grosse, C.U., 2004. Continuous monitoring of setting and hardening of mortar and concrete. *Construction and building materials*, 18(3), pp.145-154.
- Richard, P. & Cheyrezy, M. 1995. Composition of reactive powder concretes. *Cement and Concrete Research*, 25, 1501-1511.
- Richardson, I.G. 2008, The calcium silicate hydrates. *Cement and Concrete Research* 38 137-158.
- Sadrekarami, A. 2004. Development of a Light Weight Reactive Powder Concrete. *Journal of Advanced Concrete Technology*, 2, 409-417.
- Salmon, D.R. and Tye, R.P., 2005. Measurements of thermal and moisture properties of moist masonry materials: issues and problem areas. *Thermal Conductivity 27/Thermal Expansion*, 15, pp.207-219.

- Scrivener, K.L., 2004. Backscattered electron imaging of cementitious microstructures: understanding and quantification. *Cement and Concrete Composites*, 26(8), pp.935-945.
- Scrivener, K.L., Crumbie, A.K. and Laugesen, P., 2004. The interfacial transition zone (ITZ) between cement paste and aggregate in concrete. *Interface Science*, 12(4), pp.411-421.
- Shin, K.Y., Kim, S.B., Kim, J.H., Chung, M. and Jung, P.S., 2002. Thermo-physical properties and transient heat transfer of concrete at elevated temperatures. *Nuclear Engineering and Design*, 212(1), pp.233-241.
- Szoke, S.S., 2006. Resistance to fire and high temperatures. *PCA RD*, (2974), pp.274-287.
- Tai, Y.S., Pan, H.H. and Kung, Y.N., 2011. Mechanical properties of steel fiber reinforced reactive powder concrete following exposure to high temperature reaching 800 C. *Nuclear Engineering and Design*, 241(7), pp.2416-2424.
- Tam, C.M. and Tam, V.W.Y., 2012. Microstructural behaviour of reactive powder concrete under different heating regimes. *Magazine of concrete research*, 64(3), pp.259-267.
- Tam, C.M., Tam, V.W.Y. and Ng, K.M., 2010. Optimal conditions for producing reactive powder concrete. *Magazine of Concrete Research*, 62(10), pp.701-716.
- Tanyildizi, H., 2008. Effect of temperature, carbon fibers, and silica fume on the mechanical properties of lightweight concretes. *New carbon materials*, 23(4), pp.339-344.
- Taylor, G. D. 1991. *Construction materials* (Longman Scientific & Technical).
- Torayca. (NA). *T1700S data sheet*. Technical data sheet No. CFA-005
- Trägårdh J., 1999. Micro-structural features and related properties of self-compacting concrete. Skarendahl, A. and Petersson, O. (Eds). Proceedings of the First International RILEM Symposium on Self Compacting Concrete. Cachan Cedex: pp.175-86.
- Vicenzino, E., PERRY, V.H., CHOW, T.S., CULHAM, G. and ZAKARIASEN, D., 2005. First use of UHPFRC in thin precast concrete roof shell for Canadian LRT station. *PCI journal*, 50(5), pp.50-67.
- Vodak, F., Černý, R., Drchalova, J., Hošková, Š., Kapičková, O., Michalko, O., Semerak, P. and Toman, J., 1997. Thermophysical properties of concrete for nuclear-safety related structures. *Cement and concrete research*, 27(3), pp.415-426.
- Wang, J-Y., Chia, K-S., Liew, J-Y. R. and Zhang, M-H., 2013. Flexural performance of fiber-reinforced ultra-lightweight cement composites with low fiber content. *Cement and Concrete Composites*, 43, pp.39-47.

- Xu, Y., Wong, Y.L., Poon, C.S. and Anson, M., 2001. Impact of high temperature on PFA concrete. *Cement and Concrete Research*, 31(7), pp.1065-1073.
- y Leon, C.A.L., 1998. New perspectives in mercury porosimetry. *Advances in colloid and interface science*, 76, pp.341-372.
- Yazıcı, H., Yardımcı, M.Y., Aydın, S. and Karabulut, A.Ş., 2009. Mechanical properties of reactive powder concrete containing mineral admixtures under different curing regimes. *Construction and Building Materials*, 23(3), pp.1223-1231.
- Yazıcı, H., Yardımcı, M.Y., Yiğiter, H., Aydın, S. and Türkel, S., 2010. Mechanical properties of reactive powder concrete containing high volumes of ground granulated blast furnace slag. *Cement and Concrete Composites*, 32(8), pp.639-648.
- Yazıcı, H., Yiğiter, H., Karabulut, A.Ş. and Baradan, B., 2008. Utilization of fly ash and ground granulated blast furnace slag as an alternative silica source in reactive powder concrete. *Fuel*, 87(12), pp.2401-2407.
- Zanni, H., Cheyrezy, M., Maret, V., Philippot, S. and Nieto, P., 1996. Investigation of hydration and pozzolanic reaction in reactive powder concrete (RPC) using ^{29}Si NMR. *Cement and Concrete Research*, 26(1), pp.93-100.
- Zhang, Q. and Ye, G., 2012. Dehydration kinetics of Portland cement paste at high temperature. *Journal of thermal analysis and calorimetry*, 110(1), pp.153-158.
- Zhou, X.Q. and Hao, H., 2008. Mesoscale modelling of concrete tensile failure mechanism at high strain rates. *Computers & Structures*, 86(21), pp.2013-2026.

Appendixes

Appendix A: Physical and mechanical properties

Table A-1: Density and porosity at 7-d

Component	Treatment			
	A	B	C	D
<u>Density (kg/m³):</u>				
Sample 1	2170	2269	2229	2346
Sample 2	2176	2250	2281	2368
Sample 3	2160	2252	2241	2361
Average	2168	2257	2250	2358
SD	6.528	8.744	22.442	9.467
<u>Porosity (%)</u>				
Sample 1	4.59	4.07	1.77	1.35
Sample 2	4.35	3.33	1.96	1.43
Sample 3	4.69	3.85	1.76	1.44
Average	4.54	3.75	1.83	1.40
SD	0.14	0.31	0.09	0.04

Table A-2: Compressive strength in average of three samples (MPa)

Variables	Non pressure				With pressure			
	7-d		28-d		7-d		28-d	
	f'_c	SD	f'_c	SD	f'_c	SD	f'_c	SD
<u>Heating rate (°C/h):</u>								
10	78.94	1.86	88.73	1.71	99.81	11.08	111.00	1.47
50	111.60	10.18	119.38	3.68	147.94	7.89	126.85	2.36
100	75.96	2.19	91.79	3.65	104.31	2.48	107.27	4.73
<u>Heating duration (h)</u>								
12	79.02	1.85	100.54	0.77	83.20	4.55	105.15	1.34
24	76.34	2.53	102.35	2.49	84.62	2.63	105.56	3.49
48	111.60	5.08	119.38	3.68	147.94	4.04	126.85	2.36
<u>Heating start (d)</u>								
1	42.63	0.36	82.42	4.39	47.22	2.55	91.25	2.49
2	111.60	5.08	119.38	3.68	147.94	4.04	126.85	2.36
3	101.15	4.42	90.17	3.67	103.54	3.52	97.82	4.85

Table A-3: Compressive strength of RPC non-carbon fibre treated by 8 MPa static pressure and heat curing at 50 °C/h rate for 48 h after 2 days (MPa)

Age sample	Treatment			
	A	B	C	D
<u>7-d:</u>				
Sample 1	78.19	117.81	84.79	152.15
Sample 2	77.06	105.38	86.11	149.17
Sample 3	78.00	111.63	82.71	142.50
Average	77.75	111.60	84.54	147.94
SD	0.49	5.08	1.40	4.04
<u>28-d:</u>				
Sample 1	88.88	113.06	123.19	120.90
Sample 2	89.69	100.31	114.79	135.97
Sample 3	89.50	106.06	120.21	123.47
Average	89.35	106.48	119.40	126.78
SD	0.35	5.21	3.48	6.58

Table A-4: Flexural strength of RPC for all treatments (MPa)

Component	Treatment			
	A	B	C	D
<u>Non-carbon fibre:</u>				
Sample 1	14.79	16.64	13.02	16.80
Sample 2	12.09	13.59	13.83	15.76
Sample 3	12.66	13.54	13.44	15.10
Average	13.18	14.59	13.43	15.89
SD	1.42	1.77	0.40	0.85
<u>With carbon fibre</u>				
Sample 1	11.93	16.88	17.47	19.14
Sample 2	12.12	17.34	17.94	17.84
Sample 3	14.56	16.76	15.55	17.50
Average	12.87	16.99	16.99	18.16
SD	1.46	0.31	1.27	0.87

Table A-5: Compressive strength of RPC with carbon fibre which are treated by 8 MPa static pressure and heat curing at 50 °C/h rate for 48 h after 2 days

Sample	Treatment			
	A	B	C	D
Sample 1	88.50	109.63	131.11	132.43
Sample 2	93.25	102.19	121.88	136.88
Sample 3	96.88	113.43	126.67	136.11
Average	95.06	108.41	126.55	135.14
SD	3.43	4.67	3.77	1.94

Table A-6: Compressive strength of RPC after fixed high temperature exposure

Sample	Temperature (°C)			
	20	400	500	800
Sample 1	150.28	131.39	128.82	37.92
Sample 2	136.46	124.79	120.07	32.01
Sample 3	130.07	128.13	128.96	36.18
Average	138.94	128.10	125.95	35.37
SD	8.43	2.69	4.16	2.48

Table A-7: Compressive strength of RPC after cyclic exposure at 500 °C

Sample	Cyclic number			
	2	3	4	5
Sample 1	124.86	109.51	103.68	93.82
Sample 2	123.06	111.94	102.85	97.57
Sample 3	112.01	124.24	106.88	99.93
Average	119.98	115.23	104.47	97.11
SD	5.68	6.44	1.74	2.52

Table A-8: Compressive strength of RPC after air and water (quench) cooling following exposure at 500 °C

Sample	Cooling type			
	0 (initial)	1xA	1xW	2xW
Sample 1	150.28	128.82	104.93	93.13
Sample 2	136.46	120.07	108.47	96.46
Sample 3	130.07	128.96	100.56	89.93
Average	138.94	125.95	104.65	93.17
SD	8.43	4.16	3.24	2.67

Table A-9: Thermal conductivity and effusivity after exposure

Component	Temperature (°C)			
	20	400	500	800
<u>Thermal conductivity (W/m.K):</u>				
Sample 1	1,716.78	1,618.32	1,672.01	1,349.25
Sample 2	1,659.30	1,713.43	1,654.38	1,196.16
Sample 3	1,749.91	1,661.84	1,620.15	1,278.90
Average	1,708.66	1,664.53	1,648.85	1,274.77
SD	37.44	38.87	21.53	62.57
<u>Thermal effusivity (W.s^{1/2}/cm³.K):</u>				
Sample 1	1.54	1.36	1.46	0.90
Sample 2	1.43	1.53	1.43	0.65
Sample 3	1.59	1.44	1.37	0.79
Average	1.52	1.44	1.42	0.78
SD	0.07	0.07	0.04	0.10

Appendix B: Example element analysis from EDS

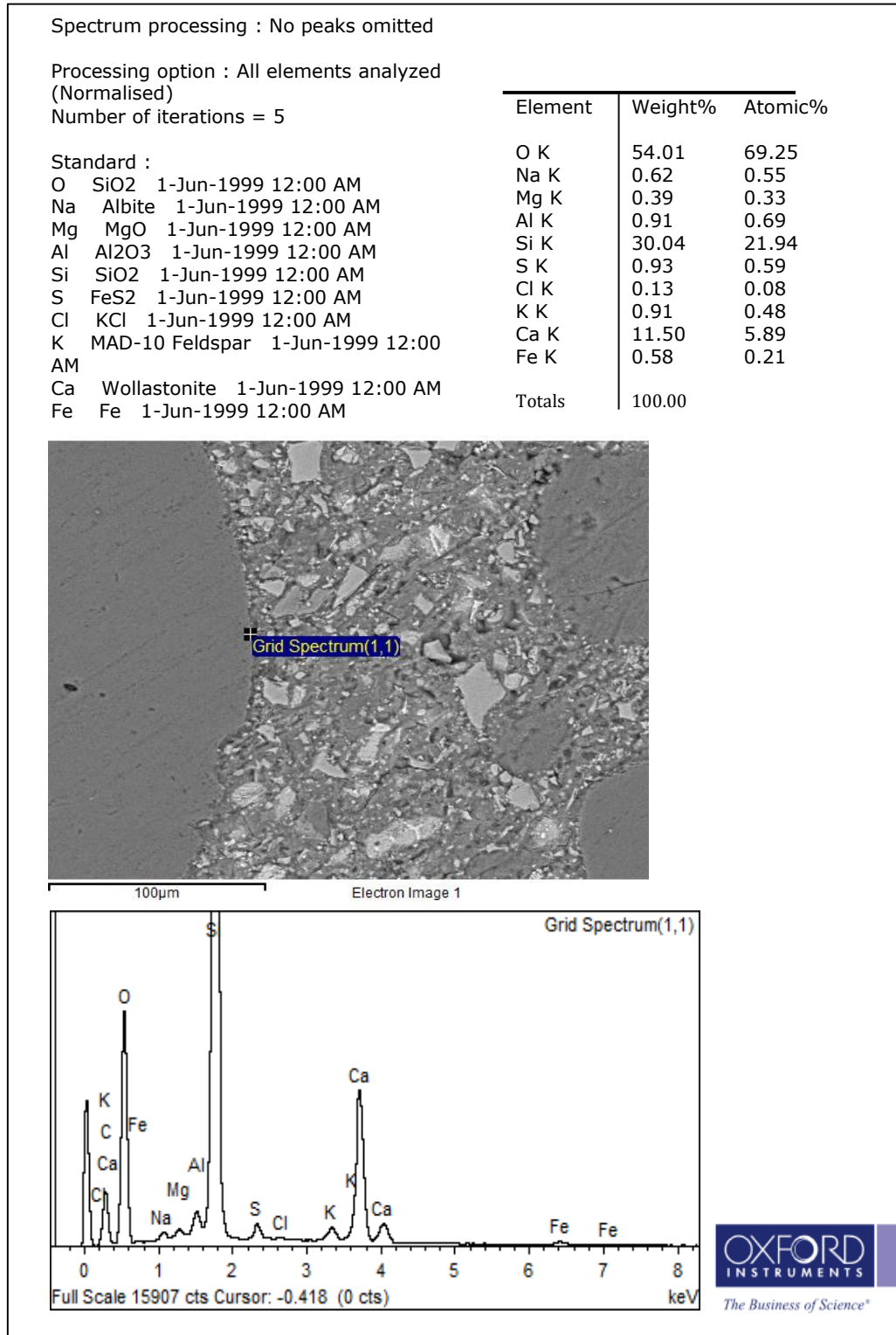


Figure B-1. A report of EDS containing information about atom weight of element, position of scanning and curve intensity of element.

Appendix C: Curve of TGA test (file: words format)

Appendix D: SEM images (file: tif format)

Appendix E: Analysis of pore distribution from MIP (file: excel format)

Appendix F: Analysis of element from EDS (file: excel format)